OFFICE OF CIVILIAN RADIOACTIVE WASTE MANAGEMENT
ANALYSIS/MODEL COVER SHEET

Complete Only Applicable Items

1. QA: QA

Page: 1 of: 126

2. ☒ Analysis — Check all that apply		3. ☐ Model — Check all that apply	
Type of Analysis	☐ Engineering ☐ Performance Assessment ☒ Scientific	Type of Model	☐ Conceptual Model ☐ Abstraction Model ☐ Mathematical Model ☐ System Model ☐ Process Model
Intended Use of Analysis	☐ Input to Calculation ☒ Input to another Analysis or Model ☒ Input to Technical Document	Intended Use of Model	☐ Input to Calculation ☐ Input to another Model or Analysis ☐ Input to Technical Document
Describe use:	Corroborative confidence building for models of UZ flow and transport.	Describe use:	

4. Title:

Natural Analogs for the Unsaturated Zone

5. Document Identifier (including Rev. No. and Change No., if applicable):

ANL-NBS-HS-000007 REV 00

6. Total Attachments:	7. Attachment Numbers - No. of Pages in Each:
5	I-44 II-3 III-8 IV-2 V-~~24~~40 JEH 4/5/00

	Printed Name	Signature	Date
8. Originator	Ardyth Simmons Ardyth Simmons	Ardyth Simmons	3/8/00
	Andre Unger Andre Unger	Andre Unger	3/8/00
	Michael Murrell Michael Murrell	Ardyth Simmons for Michael T. Murrell	3/8/00
9. Checker	Peter Persoff	Peter Persoff	3/8/00
	Mark Bandurraga	Peter Persoff for Mark Bandurraga	3/8/00
10. Lead/Supervisor	G.S. Bodvarsson		3/8/00
11. Responsible Manager	G.S. Bodvarsson		3/8/00

12. Remarks:

Initial Issue

Block 8: Other contributing authors: Boris Faybishenko, Steve Goldstein, Patricia Paviet-Hartmann, Robert Roback

Page count on Attachment V has been changed. Jane E Hamilworth for G.S. Bodvarsson 4/5/00

OFFICE OF CIVILIAN RADIOACTIVE WASTE MANAGEMENT
ANALYSIS/MODEL REVISION RECORD

Complete Only Applicable Items

2. Analysis or Model Title:

Natural Analogs for the Unsaturated Zone

3. Document Identifier (including Rev. No. and Change No., if applicable):

ANL-NBS-HS-000007 REV 00

4. Revision/Change No.	5. Description of Revision/Change
00	Initial Issue

CONTENTS

INTENTIONALLY LEFT BLANK

FIGURES

FIGURES (Continued)

Page

FIGURES (Continued)

INTENTIONALLY LEFT BLANK

TABLES

INTENTIONALLY LEFT BLANK

ACRONYMS

ACC	Accession Number
AMR	Analysis/Model Report
AP	Administrative Procedure (DOE)
CFu	Crater Flat Undifferentiated Unit
CHn	Calico Hills Nonwelded Hydrogeologic Unit
CHnv	Calico Hills nonwelded Vitric Hydrogeologic Unit
CHnz	Calico Hills Nonwelded Zeolitic Hydrogeologic Unit
CNWRA	Center for Nuclear Waste Regulatory Analyses
CRWMS	Civilian Radioactive Waste Management System
DIRS	Document Input Reference System
DOE	Department of Energy
DTN	Data Tracking Number
ER	Electrical Resistivity
ESF	Exploratory Studies Facility
FY	Fiscal Year
INEEL	Idaho National Engineering and Environmental Laboratory
ka	Thousand Years
LANL	Los Alamos National Laboratory
LBNL	Lawrence Berkeley National Laboratory
M	Molar
Ma	Million Years
M&O	Management and Operating Contractor
non-Q	Not Quality Affecting
NRC	Nuclear Regulatory Commission
NTS	Nevada Test Site
OCRWM	Office of Civilian Radioactive Waste Management
PA	Performance Assessment
PMR	Process Model Report
ppb	Parts Per Billion
ppt	Parts Per Trillion
PTn	Paintbrush Nonwelded Hydrogeological Unit
Qal	Quaternary Alluvium
QAP	Quality Administrative Procedure (M&O)

ACRONYMS (Continued)

QARD	Quality Assurance Requirements and Description
QIP	Quality Implementing Procedure
RIS	Records Information System
RMS	Root Mean Square
STN	Software Tracking Number
TBV	To Be Verified
TCw	Tiva Canyon Welded Hydrogeologic Unit
TDMS	Technical Data Management System
TDR	Time Domain Reflectometry
THC	Thermohydrologic-Chemical
THMC	Thermal-Hydrological-Mechanical-Chemical
TIC	Technical Information Center
TIMS	Thermal Ionization Mass Spectrometry
TSPA	Total System Performance Assessment
TSw	Topopah Spring Welded Hydrogeologic Unit
UZ	Unsaturated Zone
VA	Viability Assessment
YMP	Yucca Mountain Site Characterization Project

1. PURPOSE

The purpose of this Analysis/Model Report (AMR) is to document natural and anthropogenic (human-induced) analog sites and processes that are applicable to flow and transport processes expected to occur at the potential Yucca Mountain repository in order to build increased confidence in modeling processes of Unsaturated Zone (UZ) flow and transport. This AMR was prepared in accordance with *AMR Development Plan for U0135, Natural Analogs for the UZ* (CRWMS 1999a). Knowledge from analog sites and processes is used as corroborating information to test and build confidence in flow and transport models of Yucca Mountain, Nevada. This AMR supports the Unsaturated Zone (UZ) Flow and Transport Process Model Report (PMR) and the Yucca Mountain Site Description.

The objectives of this AMR are to test and build confidence in the representation of UZ processes in numerical models utilized in the UZ Flow and Transport Model. This is accomplished by:

- Applying data from Box Canyon, Idaho in simulations of UZ flow using the same methodologies incorporated in the Yucca Mountain UZ Flow and Transport Model to assess the fracture-matrix interaction conceptual model.

- Providing a preliminary basis for analysis of radionuclide transport at Peña Blanca, Mexico as an analog of radionuclide transport at Yucca Mountain.

- Synthesizing existing information from natural analog studies to provide corroborating evidence for representation of ambient and thermally coupled UZ flow and transport processes in the UZ Model.

Natural analogs do not provide an analysis or model in and of themselves, but can be used to test conceptual and numerical models over large spatial and temporal scales not accessible to laboratory or field experiments. In this sense they are uniquely suited to building confidence in process models and in this manner are used by other AMRs as a means of model "validation." However, natural analogs should be applied with caution, as they often have limitations; their boundary conditions and initial conditions may be unknown or they may have been inadequately characterized. The purpose of this work is, first, to catalog natural analog studies of unsaturated sites that were conducted by a variety of organizations in different countries and, second, to use information from carefully selected natural analog unsaturated sites to provide confidence in understanding how flow and transport in the unsaturated zone at Yucca Mountain would occur over thousands of years.

Analog sites discussed in relation to the Yucca Mountain unsaturated zone (UZ) flow and transport model include the following: (1) Rainier Mesa, Nevada, an area close to Yucca Mountain with similar climatic and geologic conditions; (2) Box Canyon, Idaho, a site to test numerical modeling methodology of flow in fractured porous media; (3) Peña Blanca, Mexico, a uranium ore deposit in fractured rhyolitic tuff for building confidence in understanding of radionuclide transport along preferential pathways; (4) volcanic rock-hosted uranium deposits that occur in the unsaturated zone in northern Nevada and southeastern Oregon; and (5) various active geothermal and fossil hydrothermal sites for building confidence in modeling coupled thermal-hydrologic-mechanical-chemical (THMC) processes. Results of the analog studies will

be used to corroborate estimates of the magnitude and limitation of operative processes in order to build realism into conceptual and numerical process models that are used as a foundation of performance assessment in the representative case of post-closure safety.

2. QUALITY ASSURANCE

This AMR was developed in accordance with AP-3.10Q, *Analyses and Models*. Other applicable Department of Energy (DOE) Office of Civilian Radioactive Waste Management (OCRWM) Administrative Procedures (APs) and YMP-LBNL Quality Implementing Procedures (QIPs) are identified in the *AMR Development Plan for U0135, Natural Analogs for the UZ* (CRWMS M&O 1999a).

This analysis was evaluated in accordance with QAP-2.0, *Conduct of Activities*, and determined to be non-Q. This is because the data that support it were collected as part of projects other than the Yucca Mountain Site Characterization Project (YMP) and are therefore non-Q. This AMR will be used to support performance assessment only in a confirmatory manner. Although the data utilized and results presented in this AMR are not required to be qualified, all work, documents, and data submittals comply with the current version of the U.S. DOE Office of Civilian Radioactive Waste Management (OCRWM) *Quality Assurance Requirements and Description* (QARD) DOE/RW-0333P (DOE 1998). This evaluation is documented in *Activity Evaluation of PSS Activity 6105 Science Support* (CRWMS M&O 1999b).

INTENTIONALLY LEFT BLANK

3. COMPUTER SOFTWARE AND MODEL USAGE

The software codes and routines used in this AMR are listed in Table 3-1. These were appropriate for the intended application and used only within their range of validation. The Q-status of these codes is provided in Attachment I and the Document Input Reference System (DIRS) database.

Table 3-1. Computer Software Codes and Routines

Software Name	Version	Software Tracking Number (STN)	Computer Platform
TOUGH2	1.3	10061-1.3-00	DEC or SUN Workstation with UNIX OS
Routine:		**ACC:**	
perm.for	1.0	MOL.19991011.0224	PC with DOS
plot.for	1.0	MOL.19991011.0225	PC with DOS
rocktype.for	1.0	MOL.19991011.0226	PC with DOS
save2tec.for	1.0	MOL.19991011.0227	PC with DOS
tough2tec.for	1.0	MOL.19991011.0228	PC with DOS
trans_cal.for	1.0	MOL.19991011.0229	PC with DOS
weight.for	1.0	MOL.19991011.0230	PC with DOS

The software program TOUGH2 (TOUGH2 V1.3, STN: 10061-1.3-00, Version 1.3) was obtained from configuration management per AP-SI.1Q *Software Management* and was reverified under AP-SI.1Q.

This AMR used the generalized conceptual model of UZ flow and transport at Yucca Mountain against which to compare the selected analogs. The numerical approach taken for the UZ Flow and Transport Model was utilized in Section 6.5.1.1 of this AMR to evaluate flow and transport processes. Input and output files for these model runs are listed in Attachment II.

The routines listed in Table 3-1 are for pre- and post-processing of input and output files for TOUGH2 V1.3. The documentation for these routines has been submitted to the Records Processing Center and is included as Attachment V.

Standard spreadsheet (Excel 97 SR-1) and graphics plotting programs (Tecplot, Version 7.5) were also used and are not subject to software quality assurance requirements.

The data for the isochron was fit in Section 6.5.2.1.4.2.3 with a commercially available, standard least squares fitting program. The fit was confirmed with an in-house Los Alamos National Laboratory (LANL) program that was adapted to run on the PC under the name Winfit.

INTENTIONALLY LEFT BLANK

4. INPUTS

4.1 DATA AND PARAMETERS

Inputs for this AMR include the following:

- Box Canyon, Idaho analog study in fractured, unsaturated basalt
- Peña Blanca, Mexico existing information and new analyses of uranium-series data
- Existing information from flow and seepage studies in the USA (e.g., Rainier Mesa, Apache Leap)
- Existing information from potential radionuclide transport sites and coupled process analog sites

The data described above were not generated for the Yucca Mountain Site Characterization Project (YMP) under an approved quality assurance program and are therefore non-Q (see Section 2). The reports are available for review through the Technical Information Center (TIC). All input data used for this AMR are listed in the DIRS included as Attachment I and the DIRS database.

4.2 CRITERIA

This AMR complies with the DOE interim guidance (Dyer 1999). The subparts of the interim guidance that apply to this analysis are those pertaining to the characterization of the Yucca Mountain site (Subpart B, Section 15), the compilation of information regarding the hydrology of the site in support of the License Application (Subpart B, Section 21(c)(1) (ii)), and the definition of hydrologic parameters used in performance assessment (Subpart E, Section 114(a)).

4.3 CODES AND STANDARDS

The use of codes (other than software codes) and standards is not applicable to this report.

INTENTIONALLY LEFT BLANK

5. ASSUMPTIONS

The fundamental assumption underlying this AMR is that natural analogs are one credible means of building confidence in understanding flow and transport processes at Yucca Mountain and the conceptual and numerical models used to describe them. The justification for this assumption is the widespread, documented and accepted use of natural analogs throughout the worldwide scientific community in addressing natural system behavior thought to occur at a nuclear waste repository over millennia. Statements made in the literature survey portion of this report (parts of Sections 6.5.1, 6.5.2; Section 6.5.3) are based on this fundamental assumption.

The same basic assumptions were used to analyze the Box Canyon site (Section 6.5.1.1) as were used to study variably saturated groundwater flow at Yucca Mountain. This is a direct consequence of applying the same model conceptualization of Box Canyon to that of Yucca Mountain, given the natural analog premises motivating this work.

Assumption 1. It is assumed that the dual-permeability representation of water- and gas-phase flow through both the fracture and matrix continua of the basalt is applicable to the Box Canyon site. This methodology was adopted to be consistent with the approach used at Yucca Mountain. This assumption is applied to all the analyses in Section 6.5.1.1. No further confirmation is needed for this assumption.

Assumption 2. In adopting the dual-permeability approach, water and gas flow through the variably saturated fracture and matrix continua are assumed to be governed by the mass conservation equations discretized using the EOS3 module of TOUGH2 codes. This assumption is fundamental to the numerical analysis of all Yucca Mountain simulations and is used here by analogy. This assumption is applied to all the analyses in Section 6.5.1.1. No further confirmation is needed for this assumption.

Assumption 3. Based on the observations of active water flow features given in Table 6-3, a conceptual fracture network was constructed and mapped onto a plan view of the mesh, as shown in Figure 6-5. Fractures above a dimensionless depth of 0.6 are assumed to extend vertically downward from the ground surface. Active water flow features observed below a dimensionless depth of 0.6 are assumed to result from fractures extending from the bottom of the model upward. Fractures are assumed not to cross the dimensionless depth of 0.6 where the two cooling fronts intersected. The orientation of the fractures is assumed north-south, east-west to coincide with the orientation of the mesh. This orientation was chosen because it is on an approximate 45-degree angle with the E and S series of slanted boreholes and represents the fracture orientation angle that would maximize the probability of these boreholes intersecting a fracture. The fracture pattern was also selected so that two neighboring fractures within the same dimensionless depth were on average separated by a distance equal to the fracture spacing. Furthermore, the length of a fracture extending to either side of the actual observation point was also equivalent to the fracture spacing at the dimensionless depth of the observation point. This

assumption was made in Section 6.5.1.1.3 and is applied throughout all the quantitative analyses in Section 6.5.1.1. Although other fracture patterns could be inferred from the data, their application would result in a comprehensive Monte-Carlo analysis which is beyond the scope of this work.

Assumption 4. In the context of fracture continuum parameters, β weighting factors were used to increase the permeability and porosity of nodes where flow was actually observed to occur relative to the unconditioned background nodes. In particular, the β weighting factor of these nodes was chosen so that a single fracture exists at the node in the orientation shown in Figure 6-5. To prevent biasing nodes from increasing the net infiltration through the model but rather promote preferential channel flow through observed fracture flow features, the weighting factor of neighboring nodes was decreased. Hence, conservation of net infiltration flux was enforced by constraining the cumulative sum of the weighting factor for all biased nodes resulting from the observed flow feature to be identical to that of unconditioned nodes. The value and distribution of the weighting factors for nodes neighboring observed flow features were assumed for the purposes of this study. This assumption was made in Section 6.5.1.1.3 and is applied throughout all the quantitative analyses in Section 6.5.1.1. Although other factors for decreasing weighting to neighboring nodes could be employed, insufficient data exist to justify any particular choice. Therefore, no further confirmation is needed for this assumption.

Assumption 5. Permeabilities for the fracture continuum determined from pneumatic tests are assumed to be representative of the permeability of the fracture continuum to the water phase. Furthermore, the injected gas phase is assumed to advect through the fracture continuum only, thereby allowing the matrix continuum nodes to be removed during calibration. This assumption is consistent with the permeability calibration methodology employed in the unsaturated zone at Yucca Mountain. This assumption is applied in Section 6.5.1.1.4. The simulated pressure response was recalculated using the final Box Canyon model (with matrix continuum nodes) and yielded similar values. Therefore, no further confirmation is needed for this assumption.

Assumption 6. Tsang (1992) provided a literature review to sort out the different definitions and denotations of the various "equivalent apertures" that arose due to field measurements regarding the relative magnitudes of "hydraulic aperture" and "tracer aperture". These definitions pertained to representing a rough-walled fracture by a pair of parallel plates separated by a constant aperture b. In this work, we assume that the equivalent aperture obtained from the pneumatic, infiltration and tracer tests are identical by using the bromide data to infer the arrival time of the infiltration front. This assumption was applied to all the analyses in Section 6.5.1.1.5. No further confirmation is needed for this assumption.

Assumption 7. Relative permeability and capillary pressure are described as continuous functions of effective liquid saturation following the expressions given by

Corey and van Genuchten, respectively, as implemented in TOUGH2 codes (Pruess 1991). These functions are chosen to represent both water- and gas-phase flow through the matrix and fracture continua. The van Genuchten capillary pressure is the standard function used at Yucca Mountain and was adopted by analogy. The Corey relative permeability function was chosen rather than the standard van Genuchten representation because it provided a significantly more robust alternative for simulating the advection of infiltration fronts in the Box Canyon model. (Both the Corey and van Genuchten functions are empirical and are obtained by regressing parameters to measured laboratory data). Therefore, the Corey function was assumed adequate given that no relative permeability-water saturation data has been obtained at the Box Canyon site to substantiate the choice of a particular function. Furthermore, we assumed that residual water satuation in the fracture and matrix continua are 0.01 and 0.1 respectively. These values were chosen to be identical to those used in the Yucca Mountain sitewide model because no data exists to identify their value at the Box Canyon site. However both the Box Canyon basalts and Yucca Mountain tufts are fractured volcanic rocks. This assumption was applied to all the analyses in Section 6.5.1.1.5. If uniqueness of calibration results were required, it would be necessary to confirm this assumption by collecting data regarding both water phase saturation and relative permeability at the Box Canyon site. However, for the evaluation of the appropriateness of the dual permeability approach, further confirmation is not required.

Assumption 8. A precipitation rate of 1.0 m/yr was assumed at the Box Canyon site. Furthermore, 0.1 m/yr was assumed to infiltrate to the water table with the remainder lost to surface runoff and evaporation. Calibration of the model was not sensitive to this infiltration rate because both the matrix and fracture continua were not fully saturated under these conditions and were able to respond to the infiltration tests by absorbing excess water. This assumption was made in Section 6.5.1.1 and applies to all analyses within the section. This assumption does not require further investigation.

Assumption 9. Background bromide concentrations resulting from the 96-1 infiltration test at Box Canyon (see Table 6-8) were assumed to be log-normally distributed based upon samples obtained prior to the 97-1 to 97-4 tests. This assumption was necessary to determine the ambient mean background concentration and to statistically determine a significant increase in bromide concentrations at a sampling point relative to ambient conditions. This assumption was applied to all the analyses in Section 6.5.1.1.5. No further confirmation is needed for this assumption.

Assumption 10. The first significant increase in bromide concentration at a sampling point was assumed to indicate the arrival of the infiltration front. Therefore, it was assumed that the bromide tracer was conservative and advected at the same velocity as the infiltration front in the fracture continuum. The bromide tracer within the fracture will experience dilution as it diffuses into the matrix and

disperses in the direction of flow. These processes were assumed not to attenuate the arrival of the bromide front below concentrations of 0.1 times the source concentration. The fractures are initially dry, so dispersion of the tracer relative to the water front should be negligible. In addition, the infiltration test is performed under unsaturated conditions. For the high-fracture-saturation water pulse, fracture/matrix exchange for both water and associated tracer is expected to be dominated by imbibition into the matrix. Under these conditions, matrix diffusion is expected to have negligible effects on the tracer concentrations along the infiltration front in the fracture water. This assumption was applied to all the analyses in Section 6.5.1.1.5. Calibrating hydrogeologic properties controlling infiltration front advection rate by using tracer (bromide) concentration measurements is a typical approach and, therefore, further confirmation of this assumption is not required.

Assumption 11. The first sampling event when the bromide concentration exceeded 240 mg/l was used to infer the infiltration front arrival at that sampling point. These times are listed as the maximum bromide arrival time on Table 6-9. The sampling time immediately prior to when bromide exceeded 240 mg/l is listed as the minimum bromide arrival time on Table 6-9. Together, the maximum and minimum provide a window on the expected arrival time of the infiltration front at the sampling point. In some cases, the first bromide sample exceeded a concentration of 240 mg/l, setting the maximum value on the time window, but no prior sample was taken to set the minimum value on the window. In this case, the minimum arrival time of the infiltration front was set as the start of the 97-1 infiltration test by default.

Assumption 12. A technical assumption made for the purposes of discussion in Section 6.5.3.2 in the discussion of fracture sealing under heated conditions is that all matrix pore water flashes to steam in the fracture. This assumption was made to satisfy one end-member scenario. If the opposite occurs, i.e., if a drying front propagates into the matrix and deposits silica in the matrix, then an upper bound is provided for the extent of fracture sealing (Lichtner et al. 1999, p. 19). This assumption does not need verification.

6. ANALYSIS/MODEL

Key scientific notebooks (with relevant page numbers) used for the analysis described in this AMR are listed in Table 6-1.

Table 6-1. Scientific Notebooks

LBNL Scientific Notebook ID	M&O Scientific Notebook ID	Accession Number	Page numbers
YMP-LBNL-AMS-NA-1 and Reference Binder YMP-LBNL-AMS-NA-1A	SN-LBNL-SCI-108-V1	MOL.19990927.0459	1-8, 18-27, 31-33, 53-61 and binder 1-97, A1-21
YMP-LBNL-AMS-NA-AU-1	SN-LBNL-SCI-158-V1	MOL.19990927.0460	20-103

6.1 INTRODUCTION

Natural analogs refer to natural or anthropogenic (human-produced) systems in which processes similar to those that are expected to occur in a nuclear waste repository are thought to have occurred over long time periods (decades to millennia) and large spatial scales (up to tens of kilometers). Analogs provide an important dimension to the understanding of processes that may take place in a nuclear waste repository and surrounding area. Analogs also provide an observable means of demonstrating whether the correct processes are represented in a total system performance assessment (TSPA). For some processes, such as those that are thermally coupled, natural analogs may be the only means of providing the required understanding of long-term and large-scale behavior that is needed to provide scientific confidence in process models that are used as input to total system performance assessment. Because the analogs are observable, they also perform the important illustrative function of bolstering public confidence in some aspects of nuclear waste disposal. However, analogs chosen for modeling must be selected carefully to exclude those for which initial and boundary conditions are poorly known and where important data, such as the source term, are poorly constrained. Even with these caveats in mind, it is important to examine natural analogs as a means of building confidence in understanding long-term behavior of both the natural and the engineered barrier systems. In this report we consider analogs for infiltration and flow processes (Section 6.5.1) as well as analogs to radionuclide transport processes (Section 6.5.2) and coupled THMC processes (Section 6.5.3) and discuss how each selected analog is used to test and build confidence in models of UZ flow and transport.

6.2 CONCEPTUAL MODEL OF UNSATURATED ZONE FLOW AND TRANSPORT AT YUCCA MOUNTAIN

The unsaturated zone (UZ) at Yucca Mountain is divided into five hydrogeologic units of alternating welded and nonwelded tuffs with contrasting hydrologic properties. Overlying these units are surficial deposits, designated Quaternary Alluvium (Qal), consisting of irregularly distributed deposits of alluvium and colluvium up to 30 m thick. These surficial alluvial deposits may be absent over large areas of the site, particularly on ridgetops and side slopes. The presence or absence of Qal and the slope aspect exert significant control over net infiltration at the site, with areas of thin or absent alluvium conducting moisture rapidly to the underlying tuff. Areas with thick alluvial cover accumulate moisture, where it is available for return to the atmosphere via evapotranspiration.

Underlying the Qal is the Tiva Canyon welded hydrogeologic unit (TCw) (Montazer and Wilson, 1984), a moderately to densely welded, devitrified ash flow tuff that may vary from 0 to 150 m in thickness. The fractured nature of the TCw and its relatively low porosity may facilitate moisture flux from the surface to below the zone of evapotranspiration. Below the TCw is the Paintbrush nonwelded unit (PTn), a 20 to 100 m thick sequence of partially welded to nonwelded, vitric and occasionally devitrified tuffs (Montazer and Wilson 1984, p. 14). Because it has significantly less fracturing and higher storativity than the welded units, the PTn may moderate moisture and gas phase fluxes between the surface and the repository horizon.

Underlying the PTn is the potential repository host rock, the Topopah Spring welded hydrogeologic unit (TSw). The TSw is composed of moderately to densely welded, devitrified ash flow tuffs, 290 to 360 m thick. Average porosity of the TSw units is low, except for the vitric caprock or basal vitrophyre. Below the TSw unit is the Calico Hills nonwelded unit (CHn), a 100 to 400 m thick sequence of nonwelded to partially welded ash flow tuffs. The CHn is divided into vitric (CHnv) and zeolitic (CHnz) facies. Perched water zones are generally found high in the CHn at the top of the CHnz, or at the TSw/CHn contact.

The deepest of the six UZ units is the Crater Flat undifferentiated unit (CFu), which consists of 0 to 200 m of undifferentiated welded and nonwelded, vitric, devitrified, and zeolitized ash flow and airfall tuffs. The CFu hydrofacies lies above the water table under the western margin and the southernmost half of the proposed repository block; toward the east and north, the unit lies above the water table, as does the CHn.

Matrix saturated hydraulic conductivities measured on laboratory samples are small for the welded units (10^{-10} to 10^{-12} m/s for TCw, 10^{-11} m/s for TSw) and higher for the moderately welded to nonwelded units (10^{-7} m/s for the PTn, 10^{-9} m/s for TC moderately welded) (Flint 1998, pp. 44-45). It is because of high bulk conductivities that fractures are thought to be well connected. Bulk conductivities are higher for the moderately to highly fractured welded units. Estimates of fracture densities for welded units are 10 to 20/m^3 (TCw), and 8 to 40/m^3 (TSw), while moderately welded units range from 1/m^3 in the PTn to 2 to 3/m^3 in the CHn (Montazer and Wilson 1984, p.1). High water potentials measured throughout much of the unsaturated zone indicate the absence of strong water potential gradients needed for matrix imbibition of fracture water (DOE 1998, p. 2-51).

Hydrologic properties of the potential repository block-bounding faults is poorly understood. Whether they act as pathways, barriers, or are neutral to moisture flow is currently unknown; however, Fridrich et al. (1994) interpreted linear thermal highs coincident with north-trending normal faults as evidence for fault-controlled hydrostructural pathways from the Paleozoic carbonates to the overlying tuff aquifer system. Based on results of finding bomb-pulse ^{36}Cl at the repository, fault zones may act as fast pathways through the repository horizon. Ahlers et al. (1999) showed pneumatic response data indicating that faults act as fast pathways for gas flow in the PTn and TSw.

Precipitation in the vicinity of Yucca Mountain is approximately 17 cm/yr (Hevesi et al. 1992, p. 677). Net infiltration is variable but averages approximately 8 mm/yr (DOE 1998, p. 2-5). Percolation flux estimates vary from 0.01 to 21.1 mm/yr, depending upon location and method of

estimation, but average around 7 mm/yr (DOE 1998, p. 2–5). At the repository horizon, percolation flux ranges from 1 to 20 mm/yr (DOE 1998, p. 2–5. Even though the average percolation flux may vary within this range over a scale of tens of meters, local fluxes at the centimeter scale of individual fractures could be many times the average values. The seepage into drifts depends on percolation flux. The key parameter is seepage threshold, the value below which seepage cannot occur. This value has been determined to be approximately 200 mm/yr (CRWMS M&O 1999d, p. 70).

Percolating water that could penetrate a waste package and contact waste materials may pick up and transport radionuclides either in solution, suspension, or as colloids. The radionuclide-carrying water would then migrate toward engineered barriers such as backfill, where it could be retarded before reaching the near-field heated region of the rock surrounding the drift. Gaseous transport is also part of the conceptual model for radionuclide transport, but is not discussed further in this report because it is difficult to evaluate through natural analogs. Transport of dissolved or colloidal species depends on factors that include the water chemical composition, pH, Eh, and temperature; the type and distribution of mineral fracture coatings (especially sorptive minerals such as zeolites, clays, and Fe-Mn oxides); and the nature and extent of fracture-matrix interaction.

Fracture flow has been shown to be the most likely mode of transport in the TSw, but water continuing downward would encounter different hydrologic conditions and flow properties when it reached the CHn (DOE 1998, p. 2-38). In some regions of the CHn it is expected that percolating water would contact both zeolitic and vitric tuffs. Flow in the zeolitic units would probably retard sorbing radionuclides such as Np, Cs, and Sr. In other areas, perched water zones resulting from low matrix permeabilities or hydrologic discontinuities may result in lateral diversion. Depending on the extent of the perched zone, water either may be laterally diverted for short distances before returning to the unsaturated zone or may continue laterally to the water table, bypassing the lower unsaturated zone.

6.3 CRITERIA FOR SELECTION OF ANALOGS USED IN MODEL VALIDATION

No single site will be a perfect analog to all ongoing and anticipated processes at Yucca Mountain. For this reason, focus is placed on sites having analogous processes rather than total system analogs. Given this caveat, however, it is still worthwhile to attempt to match as many features and characteristics as possible when identifying suitable analog sites. An ideal analog site to long-term radionuclide transport at Yucca Mountain would satisfy the following conditions: (1) have a known source term; (2) have a similar suite of radionuclides; (3) have a well-characterized data set; and (4) have similar geologic and hydrologic conditions. It is most useful if the analog has been in place for at least thousands of years, so that the results of long-term behavior are observable. The same criteria, slightly modified, can be used for geothermal analogs. There appears to be no perfect analog site for radionuclide transport at Yucca Mountain, partially because natural analog sites, with a few exceptions such as Oklo, in Gabon, provide little information about transport of neptunium and plutonium, two radionuclides of concern for Yucca Mountain. For this purpose, anthropogenic analogs are useful. However, in addition to using analogs for long-term predictions, models must be able to explain and match the transport times and pathways from contaminated sites that provide anthropogenic analogs, such as the Hanford Reservation, Washington; the Idaho National Engineering and Environmental Laboratory

(INEEL), and the Nevada Test Site (NTS). Anthropogenic analog sites will be a challenge to constrain in models, as they contain numerous contaminated sites with poorly identified source terms, a complex mixture of radionuclides and other contaminants, and often occur in highly heterogeneous formations.

6.4 METHODS

The overall scientific approach taken in this report is that of reasoning by analogy. Analogy relates the likeness of a process or set of properties to a similar process or property set, either in another location or a different time frame. Analogy temporarily accepts a probable theory without absolute proof. For example, by applying models to processes operating in the geosphere in natural analog locations, their accuracy can be tested by either finding a negative instance to disprove the model or finding the fit is good in a particular instance, thus increasing confidence in the model. Natural analogs are also used to determine the range of applicability of a model. This report applies natural analogs to the UZ flow and transport model in three ways. First, information and data from suitable selected analogs reported in the literature are used to "validate" processes ongoing or anticipated at Yucca Mountain and to suggest means by which data from the analog sites may be used in future modeling efforts to bound ambient and thermally coupled processes at Yucca Mountain. Second, data from a fractured, unsaturated site in basalt are used to test the validity of the approach for modeling flow and transport processes, including fracture-matrix interactions, in the Yucca Mountain site-scale UZ flow and transport model (Section 6.5.1.1). Third, uranium-series data from an analog site in unsaturated rhyolitic tuff are used to build confidence in assumptions about radionuclide transport in fractures and matrix over hundreds of thousands of years (Section 6.5.2). In these ways, performance assessment will incorporate knowledge gained from natural analogs into process models that provide input to Yucca Mountain performance.

Confidence may be built in models through a variety of different approaches, of which the comparison to natural analogs is only one. Other analysis/model reports may consider "validation" by application of field test data or by data set comparisons. These and other "validation" methods were not selected as approaches in this report because the specific purpose of this report was to investigate how the UZ flow and transport model may build increased confidence through application of natural analog information.

6.5 RESULTS

Although the Yucca Mountain data set is extensive, it is impossible to characterize deterministically flow and transport at all scales and under all anticipated environmental conditions. Analog sites, however, are able to provide data to indicate which flow and transport processes can be expected to be operative at Yucca Mountain over long periods of time and in some cases may bound those processes. Data from analog sites may also be used to build confidence in approaches to modeling flow and transport in fractured, unsaturated media. The following sections discuss some of the potential analog sites to Yucca Mountain for flow and transport processes. Section 6.5.1 discusses analogs to UZ infiltration, seepage and flow. Section 6.5.2 discusses analogs to radionuclide transport. Section 6.5.3 discusses analogs to thermally coupled UZ processes.

6.5.1 Analogs to UZ Infiltration, Seepage, and Flow

Section 6.5.1 examines analogs to UZ infiltration, seepage, and flow. Section 6.5.1.1 is a modeling study that uses data from Box Canyon, Idaho to build confidence in modeling approaches of UZ flow employed in Yucca Mountain models. Section 6.5.1.2 considers the analogous aspects of seepage and flow at Rainier Mesa to those at Yucca Mountain. Section 6.5.1.3 addresses aspects of the Apache Leap site that may be used as an analog to processes occurring at Yucca Mountain.

6.5.1.1 Box Canyon, Idaho

The variably saturated fractured basalt hydrogeological system at Box Canyon, Idaho was proposed for this study in order to examine the applicability of conceptual and numerical modeling methodologies utilized at Yucca Mountain to similar but separate UZ hydrogeological systems. Verification of the applicability of these approaches at natural analog sites serves to substantiate their use as design and predictive tools for the Yucca Mountain nuclear repository. Box Canyon was chosen for the study because a considerable body of hydrologic data was available from studies at INEEL of unsaturated flow in fractured basalts. The studies had been conducted at scales ranging from core sample measurements (cm-scale) and meter-scale laboratory tests to field tests that covered tens of meters to a kilometer-scale aquifer pumping test. The Box Canyon tests were in the intermediate-scale range.

All input and output files used during the numerical simulation of the Box Canyon site are listed in Attachment II.

6.5.1.1.1 Background

The Box Canyon site is located in the Eastern Snake River Plain near INEEL (see Figure 6-1) and is adjacent to the Big Lost River, which is a tributary of the Snake River. The Snake River Plain is primarily composed of fractured Quaternary basalt flows interbedded with sedimentary deposits. Sedimentary interbeds may separate basalt flow units that were formed at disparate times, and their thickness may range from a few centimeters to as much as 15 meters. Basalt flow units are comprised of a number of basalt flows arising from the same eruptive event. Individual basalt flows are from 3 m to 12 m thick and exhibit an extreme elongation in one direction giving them a finger or lenticular structure with a width ranging from 20 m to 60 m. The total basalt thickness in the Snake River Plain may exceed three kilometers (Whelan and Reed 1997; Knutson et al. 1993). The Box Canyon site is located on a basalt flow that is approximately 10 m to 12 m thick and also has a nearby cliff face exposure at the Big Lost River. Additional basalt flows underlie the upper basalt flow directly beneath the experimental site and the groundwater table is located at a depth of approximately 20 m.

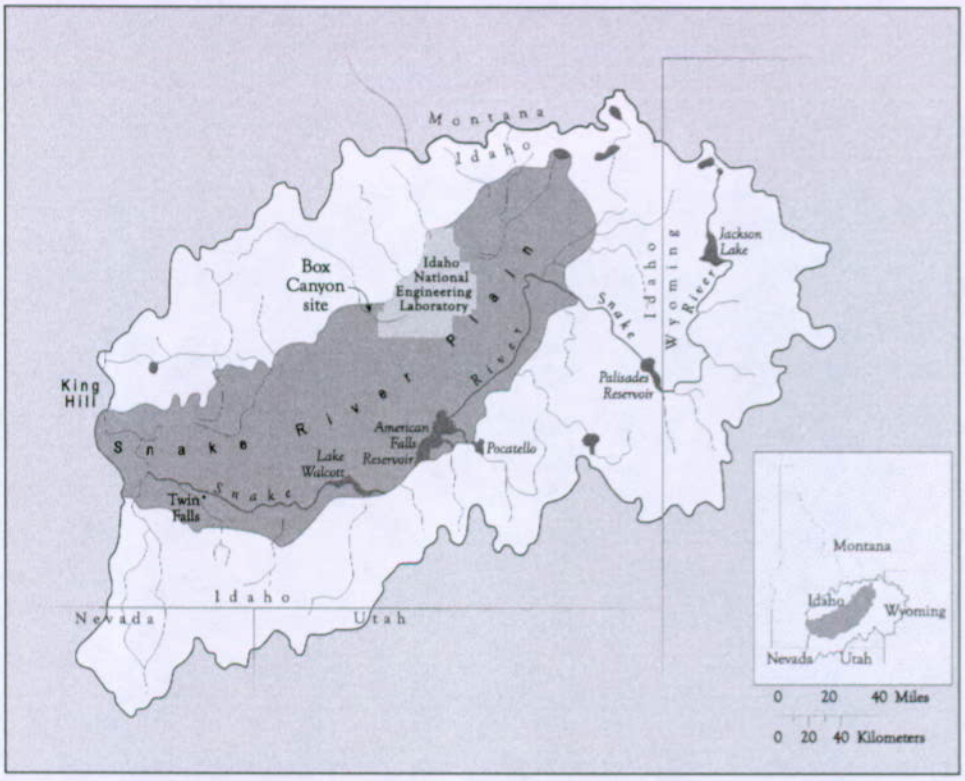

Figure 6-1. Map of East Snake River Plain Showing the Location of the Box Canyon Experimental Site (Faybishenko et al. 1999, Figure 2)

Several infiltration experiments were conducted at the Box Canyon site to study the flow of water in the variably saturated fractured basalt (Faybishenko et al. 1998a, 1999). The first is called 96-1 (two–week ponded infiltration test) while the second consists of four separate infiltration events called 97-1, 97-2, 97-3 and 97-4 (2-to-4 day infiltration events). Instrumentation was used to delineate the subset of fractures that actively conducted the infiltrating water. The purpose of this study was to construct and calibrate a numerical model to simulate the observed infiltration behavior of water at the Box Canyon site. The methodology adopted to simulate the Box Canyon site was based on the dual-permeability numerical approach used to characterize variably saturated flow at Yucca Mountain (Bandurraga and Bodvarsson 1999). Hydrogeological parameters used to calibrate the Box Canyon model could then be used to substantiate analogous parameters obtained during calibration of the Yucca Mountain site. Our investigation involved identifying physical processes and calibrating parameters controlling the observed infiltration of water at the Box Canyon site.

6.5.1.1.2 Geological Model Conceptualization

Conceptualization of the geological model for the Box Canyon site follows directly from Faybishenko et al. (1999). The site consists of layered basalt flows containing horizontal as well as vertical columnar fractures resulting from cooling of the basalt. The water table at the Box Canyon experimental site is approximately 20 m below the ground surface. Field data at the Box Canyon site consisted of monitoring pneumatic and infiltration tests almost entirely within the upper basalt flow. The elevation of the ground surface at the site is shown on Figure 6-2a, along

with the surface location of all instrumented vertical and slanted boreholes. The bottom of the upper basalt is identified by the presence of a first rubble zone observed in core logs and open borehole measurements (Faybishenko et al. 1998b). The top elevation of this rubble zone is shown on Figure 6-2b, resulting in an average thickness of the upper basalt flow of 12 m. The box outline indicates the perimeter of the infiltration pond used to contain the ponded water at the ground surface.

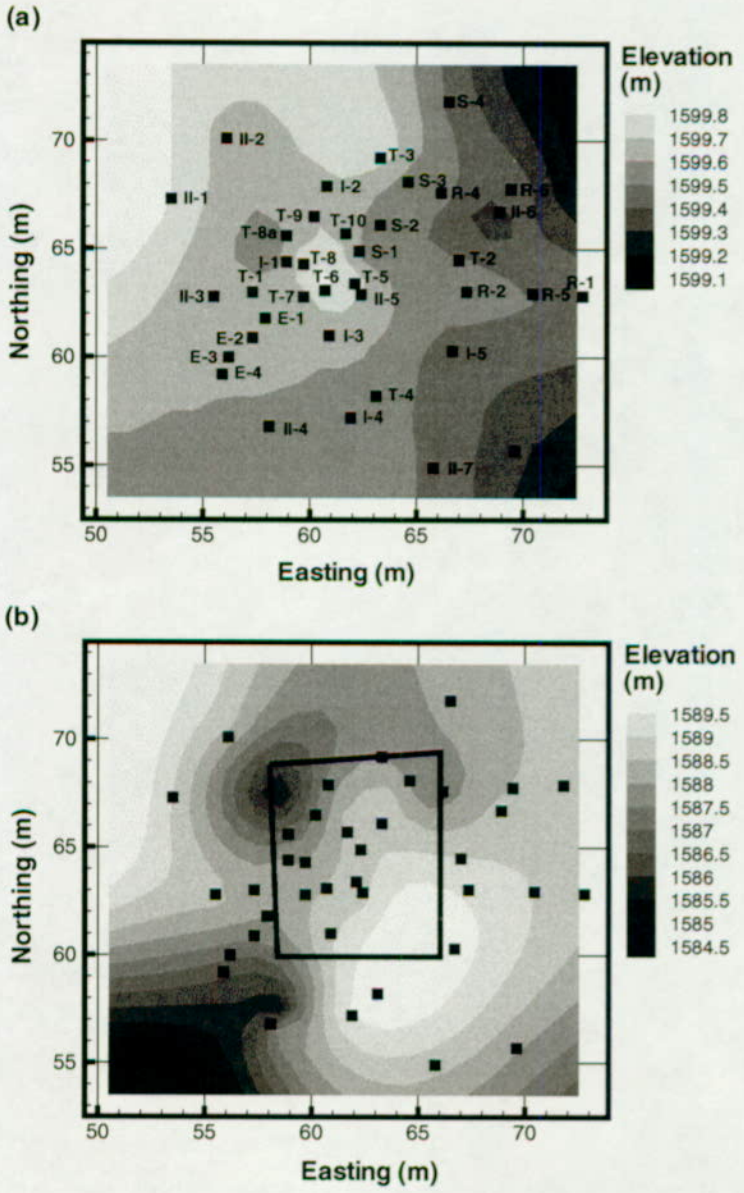

(Table 6-3 in DTN: LB990930123122.001)

Figure 6-2. Elevation of (a) Ground Surface and (b) Top of Rubble Zone with All Well Locations and Perimeter of the Infiltration Pond

Grossenbacher and Faybishenko (1995) mapped horizontal and vertical columnar basalt fractures along an outcrop near the Box Canyon experimental site. They observed that the vertical fracture spacing increased from ground surface to a dimensionless depth of 0.6. The dimensionless depth is defined as the depth from the ground surface divided by the thickness of the upper basalt flow. The vertical fracture spacing then decreased from the dimensionless depth of 0.6 to the bottom of the basalt flow. Basalt columns separated by vertical fractures were formed as the basalt cooled more rapidly from the ground surface downward than upward. The smaller fracture spacing in the upper part of the basalt flow resulted from larger temperature gradients near the surface than those at the lower part of the flow. Columnar fractures originating from the top and bottom of the basalt reached an identical spacing where the two cooling fronts met at the dimensionless depth of 0.6. The horizontal spacing of vertical fractures (D_H) as a function of dimensionless depth was used to subdivide the upper basalt flow into five zones extending from the ground surface to the bottom, in the following intervals: 0 to 0.2, 0.2 to 0.4, 0.4 to 0.6, 0.6 to 0.8 and 0.8 to 1.0. The horizontal and vertical fracture spacing, D_H and D_V, for each zone are provided in Table 6-2.

Table 6-2. Fracture and Matrix Properties Used in Box Canyon Study

Zonal Fracture Properties											
Zone	Fracture Spacing		Aperture	Permeability			Porosity	van Genuchten		ϕ scale	A_{fm} scale
	D_H (m)	D_V (m)	b (m)	k_x (m^2)	k_y (m^2)	k_z (m^2)	ϕ (-)	α (Pa^{-1})	m (-)	factor (-)	factor (-)
0.0 - 0.2	1.0	1.0	8.54E-05	1.04E-13	1.04E-13	1.04E-13	2.56E-04	5.00E-04	0.5	50.0	0.01
0.2 - 0.4	2.0	1.0	1.48E-04	4.05E-13	4.05E-13	2.70E-13	2.96E-04	5.00E-04	0.5	50.0	0.01
0.4 - 0.6	4.0	1.0	1.57E-04	4.03E-13	4.03E-13	1.61E-13	2.36E-04	5.00E-04	0.5	50.0	0.01
0.6 - 0.8	4.0	1.0	1.22E-04	1.89E-13	1.89E-13	7.57E-14	1.83E-04	5.00E-04	0.5	50.0	0.01
0.8 - 1.0	2.0	1.0	2.09E-04	1.14E-12	1.14E-12	7.61E-13	4.18E-04	5.00E-04	0.5	50.0	0.01
rubble zone	0.1	0.1	8.59E-04	1.06E-09	1.06E-09	1.06E-09	2.58E-02	5.00E-04	0.5	5.0	0.01
lower basalt	2.0	1.0	1.28E-03	2.62E-10	2.62E-10	1.75E-10	2.56E-03	5.00E-04	0.5	5.0	0.01
Zonal Matrix Properties											
0.0 - 0.2				1.00E-14	1.00E-14	1.00E-14	0.20	5.00E-05	0.25		
0.2 - 0.4				1.00E-14	1.00E-14	1.00E-14	0.20	5.00E-05	0.25		
0.4 - 0.6				1.00E-14	1.00E-14	1.00E-14	0.20	5.00E-05	0.25		
0.6 - 0.8				1.00E-14	1.00E-14	1.00E-14	0.20	5.00E-05	0.25		
0.8 - 1.0				1.00E-14	1.00E-14	1.00E-14	0.20	5.00E-05	0.25		
rubble zone				1.00E-14	1.00E-14	1.00E-14	0.20	5.00E-05	0.25		
lower basalt				1.00E-14	1.00E-14	1.00E-14	0.20	5.00E-05	0.25		

DTN: LB990930123122.001

Parameters which vary within each zone for the fracture continuum nodes include the horizontal and vertical fracture spacing (D_H and D_V, respectively), the components of the permeability tensor and the resulting aperture (k_x, k_y, k_z and b, respectively), porosity ϕ and a related scaling factor, van Genuchten capillary-pressure and relative permeability function parameters α and m, and the fracture-matrix interfacial area scaling factor A_{fm}. Similar parameters for the matrix continuum nodes include the permeability, porosity and van Genuchten parameters. The source, derivation or calibration method used to obtain these parameters is described in the following sections where relevant and are introduced in Table 6-2 for brevity.

The focus of the conceptual geological model is to address issues related to the geometry of fast preferential flow paths of infiltrating water in the basalt hydrogeological system. Therefore, we identified fractures that actively conducted water during the infiltration tests and then used these data to determine an interconnected fracture network. This involved examining hydrogeological data collected by Faybishenko et al. (1998a, 1999) for the 96-1 and 97-1 to 97-4 infiltration tests

to determine whether fractures that actively conducted water could be observed as they intersected a borehole. All such features are listed on Table 6-3 and were inferred from examination of bromide samples, lysimeter, tensiometer, time domain reflectometry (TDR) probe and electrical resistivity (ER) probe data collected during the 96-1 infiltration test as well as additional ER probe and bromide sample data collected during the 97-1 to 97-4 infiltration tests. The location in plan view of these observation points is provided on Figure 6-3. It is important to note that in terms of constructing the conceptual geological model, these data were used to infer only the structure of the fracture network and not any hydrogeological properties associated with it.

Table 6-3. Location of Borehole Intersections with Active Water-Conducting Fractures

observation point	vertical depth (ft)	vertical depth (m)	depth along borehole (m)	easting (m)	northing (m)	elevation (m)	elev. of rubble zone (m)	ground elev. (m)	dim. depth (-)	data source
S-1-1	2.00	0.61	0.70	62.12	64.60	1598.97	1588.75	1599.60	0.06	g
S-1-2	6.00	1.83	2.11	61.75	64.00	1597.75	1588.75	1599.70	0.18	a, g
S-1-3	10.00	3.05	3.52	61.39	63.39	1596.53	1588.75	1599.70	0.29	a
S-1-4	13.60	4.15	4.79	61.06	62.85	1595.43	1588.75	1599.70	0.39	a
S-2-1	3.00	0.91	1.06	62.98	65.68	1598.60	1588.75	1599.52	0.08	a
S-3-1	2.50	0.76	0.88	64.35	67.74	1598.80	1588.25	1599.50	0.06	a, c, g
S-3-2	6.50	1.98	2.29	63.94	67.16	1597.58	1588.50	1599.50	0.17	a
S-3-3	11.00	3.35	3.87	63.49	66.51	1596.21	1588.75	1599.50	0.31	a, g
S-3-4	26.50	8.08	9.33	61.92	64.28	1591.49	1588.75	1599.60	0.75	g
S-4-1	3.00	0.91	1.06	66.23	71.35	1598.56	1588.25	1599.48	0.08	a
S-4-2	48.00	14.63	16.89	62.11	64.58	1584.85	1588.75	1599.48	1.36	g
E-1-1	4.90	1.49	2.26	59.12	62.98	1598.18	1588.50	1599.67	0.13	b, d
E-1-2	8.50	2.59	3.93	60.02	63.85	1597.08	1588.25	1599.70	0.23	d
E-1-3	30.40	9.27	14.05	65.50	69.14	1590.40	1587.50	1599.50	0.76	d
E-1-4	38.20	11.64	17.66	67.45	71.02	1588.03	1588.25	1599.40	1.02	d
E-2-1	23.60	7.19	9.39	60.96	65.70	1592.50	1588.25	1599.60	0.63	d
E-2-2	38.10	11.61	15.16	63.21	68.65	1588.08	1588.25	1599.70	1.02	b, d
E-3-1	18.00	5.49	6.70	58.60	63.00	1594.15	1588.50	1599.60	0.49	b, d
E-3-2	24.00	7.32	8.93	59.40	64.00	1592.32	1588.00	1599.70	0.63	b, d
E-4-1	12.00	3.66	4.14	57.09	60.74	1595.97	1587.50	1599.60	0.30	b
E-4-2	20.00	6.10	6.90	57.88	61.77	1593.53	1588.00	1599.60	0.52	d
E-4-3	25.00	7.62	8.63	58.37	62.41	1592.01	1588.25	1599.60	0.67	d
I-1-1	1.00	0.30	0.30	58.90	64.40	1599.34	1588.06	1599.64	0.03	b, c, d
I-1-2	5.00	1.52	1.52	58.90	64.40	1598.12	1588.06	1599.64	0.13	b, c, d
I-1-3	10.00	3.05	3.05	58.90	64.40	1596.59	1588.06	1599.64	0.26	b, d
I-1-4	15.00	4.57	4.57	58.90	64.40	1595.07	1588.06	1599.64	0.39	d
I-1-5	20.00	6.10	6.10	58.90	64.40	1593.54	1588.06	1599.64	0.53	b, d
I-1-6	27.89	8.50	8.50	58.90	64.40	1591.14	1588.06	1599.64	0.73	b, d
I-1-7	33.00	10.06	10.06	58.90	64.40	1589.58	1588.06	1599.64	0.87	b, d
I-2-1	1.00	0.30	0.30	60.80	67.90	1599.40	1587.81	1599.70	0.03	b, d
I-2-2	5.00	1.52	1.52	60.80	67.90	1598.18	1587.81	1599.70	0.13	b, d
I-2-3	10.00	3.05	3.05	60.80	67.90	1596.65	1587.81	1599.70	0.26	b, c, d
I-2-4	14.00	4.27	4.27	60.80	67.90	1595.43	1587.81	1599.70	0.36	c, d
I-2-5	20.00	6.10	6.10	60.80	67.90	1593.60	1587.81	1599.70	0.51	b
I-3-1	1.00	0.30	0.30	60.90	61.00	1599.35	1588.98	1599.65	0.03	b, c, d
I-3-2	5.00	1.52	1.52	60.90	61.00	1598.13	1588.98	1599.65	0.14	b, d
T-2-1	2.00	0.61	0.61	67.00	64.50	1598.89	1589.00	1599.50	0.06	c, d, e
T-2-2	6.00	1.83	1.83	67.00	64.50	1597.67	1589.00	1599.50	0.17	b, c, d, e
T-2-3	10.00	3.05	3.05	67.00	64.50	1596.45	1589.00	1599.50	0.29	d, e
T-3-1	2.00	0.61	0.61	63.30	69.20	1599.14	1587.75	1599.75	0.05	d, e, f
T-3-2	6.00	1.83	1.83	63.30	69.20	1597.92	1587.75	1599.75	0.15	e
T-3-3	15.00	4.57	4.57	63.30	69.20	1595.18	1587.75	1599.75	0.38	b
T-4-1	2.00	0.61	0.61	63.10	58.20	1598.95	1589.75	1599.56	0.06	b, c, d, e, f
T-4-2	5.50	1.68	1.68	63.10	58.20	1597.88	1589.75	1599.56	0.17	e
T-4-3	9.00	2.74	2.74	63.10	58.20	1596.82	1589.75	1599.56	0.28	b, c, d, e
T-4-4	14.00	4.27	4.27	63.10	58.20	1595.29	1589.75	1599.56	0.43	b, c, d
T-4-5	19.00	5.79	5.79	63.10	58.20	1593.77	1589.75	1599.56	0.59	b, c, d

a 97 ER Probe
b 97 Bromide Sample
c 96 Bromide Sample
d 96 Lysimeter
e 96 Tensiometer
f 96 TDR Probe
g 96 ER Probe

DTN: LB990930123122.001

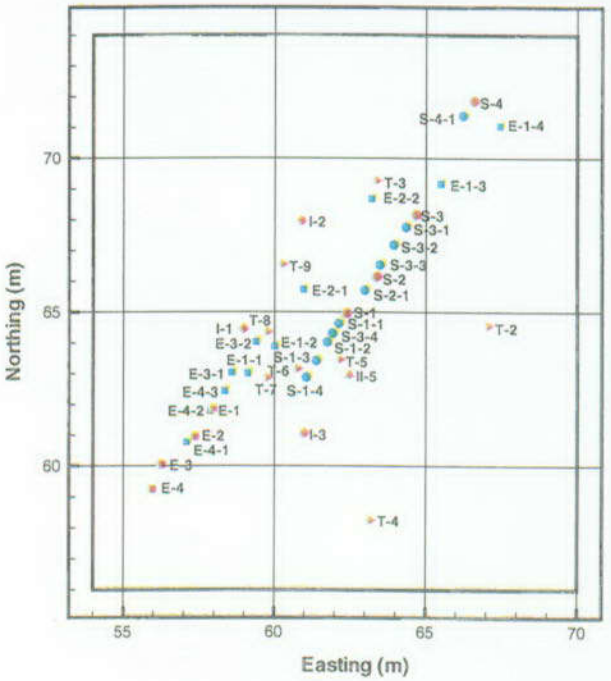

(Table 6-3 in DTN: LB990930123122.001)

Figure 6-3. Plan View of the Location of Borehole Intersections with Active Water-Conducting Fractures. The Red Symbols Indicate the Location of the Top of Each Borehole While the Green Symbols Indicate the Location, in Plan view, of the Observed Flow Features in the Slanted Boreholes. Symbol Shape is Used to Identify the Different Borehole Groups Identified by Their Name (Faybishenko et al, 1998a).

Hydrogeological characterization of the matrix was conducted by Knutson et al. (1990) who measured the permeability and porosity of core samples. These data are provided in Table 6-4. Samples with high porosities, obtained from vesicular regions of the matrix, yielded permeability values greater than 1×10^{-12} m^2 and were not included in this table. The arithmetic mean porosity of the core samples was 19.2% and the geometric mean permeability was 2.24×10^{-15} m^2. This permeability is expected to be biased towards the impermeable regions of the basalt because the permeability measurements from the vesicular zone were not included.

Table 6-4. Matrix Porosity and Permeability Measurements from Core Samples

sample	porosity (%)	permeability (m^2)
A-1	30.7	9.48E-14
A-2	23.5	3.50E-15
A-3	19.1	3.20E-15
A-4	15.3	8.00E-16
A-5	11.3	2.40E-15
A-6	23.1	2.00E-16
A-7	22.0	2.10E-15
A-10	23.5	7.40E-14
A-12	20.5	1.60E-15
A-18	26.0	-
A-19	12.0	5.30E-15
A-20	35.4	-
A-23	14.6	-
A-25	38.4	-
A-27	25.9	9.80E-15
A-30	16.2	5.00E-16
A-34	21.0	1.00E-16
B-1	10.6	1.28E-14
B-3	15.2	4.10E-15
B-5	14.9	3.14E-14
B-7	16.2	4.00E-16
B-9	26.6	2.60E-15
B-11	13.9	9.40E-15
B-12	25.5	1.00E-16
B-15	12.6	5.00E-16
C-5	14.8	1.10E-15
C-6	17.4	2.60E-15
C-15	9.9	7.00E-16
C-24	12.6	8.90E-15
C-38	12.4	4.30E-15
D-1	26.5	1.30E-15
D-2	12.8	1.80E-14
D-5	18.8	4.00E-15
D-6	5.2	3.00E-16
D-8	18.8	4.00E-15
D-13	19.0	1.80E-15
D-16	10.5	2.20E-15
D-17	26.3	-
D-26	11.8	5.40E-15
D-27	12.0	1.01E-14
D-29	17.5	1.00E-16
D-30	10.0	1.00E-16
D-31	18.6	4.00E-16
D-32	33.1	-
E-2	12.8	1.70E-15
E-4	24.0	3.20E-15
E-6	12.8	1.70E-15
E-9	22.4	9.00E-15
E-10	22.4	9.20E-15
E-30	43.2	-
mean	19.2	2.24E-15

DTN: LB990930123122.001

6.5.1.1.3 Numerical Model Conceptualization

Application of dual-permeability models to simulate fracture/matrix flow of infiltrating water in the variably saturated tuffs at Yucca Mountain has evolved through various conceptual stages. In general, they involve the application of various methodologies to reduce the interfacial area between the fracture and matrix continua and hence the degree to which they interact. Furthermore, the matrix continuum may be represented as a single node or as multiple interconnected nodes to spatially resolve the imbibition of water from the fracture continuum. Bandurraga and Bodvarsson (1999) describe the initial application of a dual-permeability model for Yucca Mountain where the matrix continuum is represented using a single node and the fracture/matrix interfacial area is reduced by a constant factor ranging from 0.0005 to 0.05. Doughty (1999) performed a sensitivity analysis using various procedures to scale the interfacial area between the fracture and matrix continua depending on the constant factor approach, the relative permeability of the liquid, and the saturation of the infiltrating liquid. Alternative representations of the matrix continuum were also included. Liu et al. (1998) developed an "active fracture" representation where a single parameter is used to estimate the fraction of fractures which actively conduct water, the spacing between these fractures, and the fracture/matrix interfacial area reduction factor. This methodology is based on relating the saturation of the infiltrating water to the fraction of active water-conducting fractures, the water capillary pressure and relative permeability-saturation relationships, and the flux of water between the fracture and matrix continua. All of this work has focused on calibrating the Yucca Mountain UZ flow and transport model to measured steady-state water saturation and capillary pressure profiles resulting from infiltration of long-term averaged precipitation over the site. We applied the dual-permeability approach at Box Canyon to simulate the transient migration of water from short-term infiltration events. Furthermore, extensive field work at the Box Canyon site focused on delineating fractures which actively conducted the infiltrating water. Given the significant decrease in scale from the Yucca Mountain to the Box Canyon model, the transient nature of the infiltration events, and the subsequent characterization of active water-conducting fractures, we adopted the initial implementation of the dual-permeability model from the Yucca Mountain studies. Validation of this preliminary approach at Box Canyon would provide the foundation for extending subsequent work from Yucca Mountain.

Calibration of the Box Canyon model was performed in two steps, using air-injection and infiltration test data. The conceptual geological model was used to develop a numerical model to simulate the physics of water- and gas-phase advection through the fractured basalt at Box Canyon. The numerical modeling effort was conducted using TOUGH2 codes (Pruess 1991) with the EOS3 module, which involves both mobile water and gas phases. This was necessary because calibration of the model involved the analysis of both pneumatic and infiltration test data.

The fracture-matrix system of the basalt was simulated using a dual-permeability grid in an analogous manner to that used to simulate the site-scale variably saturated groundwater flow field at Yucca Mountain. In the dual-permeability modeling approach, two separate nodes occupy the same geometric volume within the grid, with one node representing the matrix continuum and the other representing the fracture continuum. Both the matrix and fracture nodes are interconnected at each geometric volume within the grid where they overlap. Furthermore, the fracture continuum nodes are connected to adjacent fracture continuum nodes, while the matrix continuum nodes are connected to adjacent matrix continuum nodes. A three-dimensional visualization of the

structure of the model, including the zonation of the upper basalt and the inclusion of the rubble zone, as well as a portion of the lower basalt, is shown in Figure 6-4. Two separate views of the model are shown to illustrate the variable thickness of the upper basalt flow. In the figure, the arrows indicate the orientation of the views. The model was discretized using a grid of $23 \times 21 \times 21$ nodes of dimension 1.0 m × 1.0 m × 1.0 m in the x-, y- and z-dimensions, respectively, for each of the matrix and fracture continua nodes. Connections between nodes follow a simple seven-point lattice, with both fracture and matrix continua nodes connected to each other as well as to the six adjacent like nodes. The discretization was chosen to represent the zonal structure of the upper basalt flow and to resolve simulated water saturation profiles during the infiltration experiments. Furthermore, the lateral and vertical dimensions of the model were chosen to contain the full three-dimensional infiltration front extending from beneath the pond (see Figure 6-2) within the entire upper basalt flow without the interference from bounding conditions. This discretization yielded a combined total of 20286 matrix and fracture continua nodes which permitted reasonable simulation times of the model for calibration purposes.

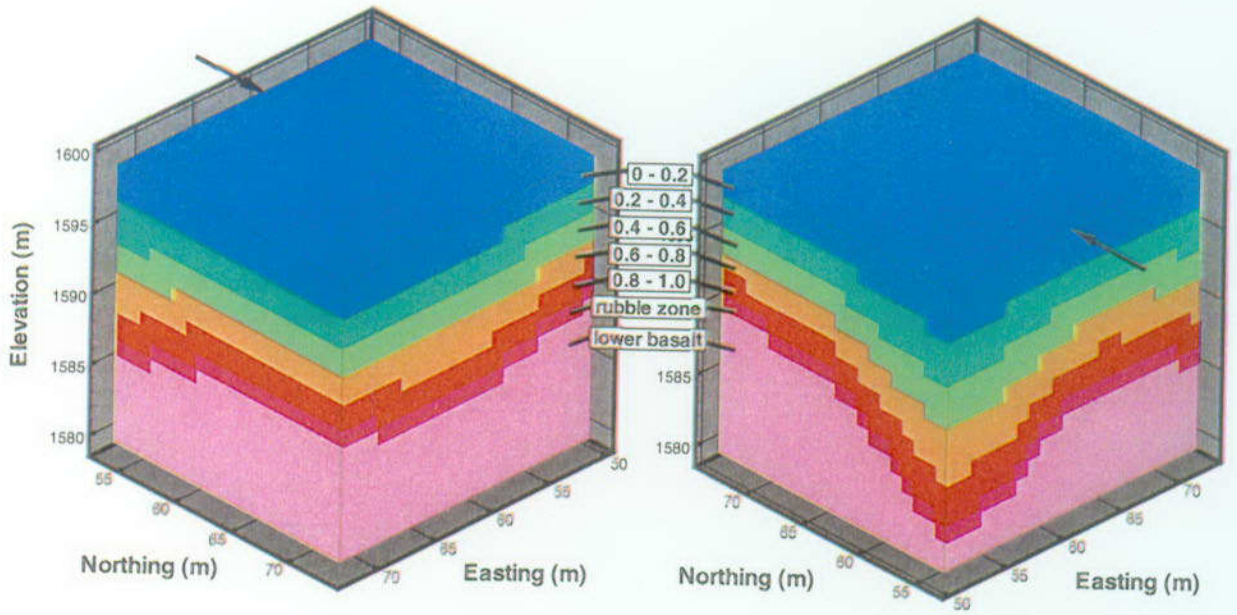

DTN: LB990930123122.002

Figure 6-4. Two Separate Views of the Numerical Model with Zonal Information

Based on the observations of active water flow features given in Table 6-3, a conceptual fracture network was constructed and mapped onto a plan view of the mesh, as shown in Figure 6-5. Fractures above a dimensionless depth of 0.6 are assumed to extend vertically downward from the ground surface. Active water flow features observed below a dimensionless depth of 0.6 are assumed to result from fractures extending from the bottom of the model upward. Fractures are assumed not to cross the dimensionless depth of 0.6 where the two cooling fronts intersected. The orientation of the fractures is assumed north-south, east-west to coincide with the orientation of the mesh. This orientation was chosen because it is on an approximate 45-degree angle with the E and S series of slanted boreholes and represents the fracture orientation angle that would maximize the probability of these boreholes intersecting a fracture. The fracture pattern was also selected so that two neighboring fractures within the same dimensionless depths were on average

separated by a distance equal to the fracture spacing. Furthermore, the length of a fracture extending to either side of the actual observation point was also equivalent to the fracture spacing at the dimensionless depth of the observation point.

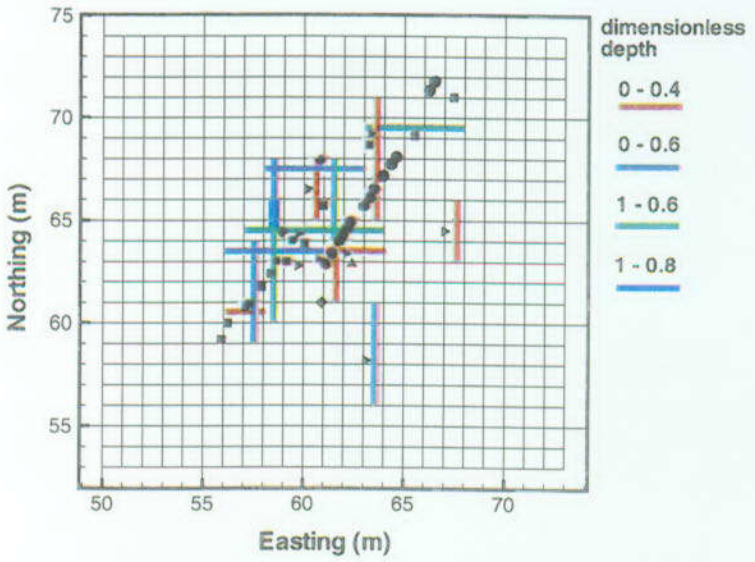

(Table 6-3 in DTN: LB990930123122.001)

Figure 6-5. Conceptual Distribution of Fractures Determined to Actively Conduct Infiltrating Water as a Function of Dimensionless Depth

The fracture network shown in Figure 6-5 was used to condition the permeability k_{fi} (m^2) and porosity ϕ_{fi} (–) of the fracture continuum nodes which are calculated from the fracture aperture b_i (m) of node i as:

$$k_{xfi} = \beta_{xi} \frac{b_i^3}{12 D_{Hi}} + \frac{b_i^3}{12 D_{Vi}} \quad \text{(Eq. 1)}$$

$$k_{yfi} = \beta_{yi} \frac{b_i^3}{12 D_{Hi}} + \frac{b_i^3}{12 D_{Vi}} \quad \text{(Eq. 2)}$$

$$k_{zfi} = \beta_{zi} \frac{b_i^3}{12 D_{Hi}} \quad \text{(Eq. 3)}$$

$$\phi_{fi} = \beta_{xi} \frac{b_i}{D_{Hi}} + \beta_{yi} \frac{b_i}{D_{Hi}} + \frac{b_i}{D_{Vi}} \quad \text{(Eq. 4)}$$

where k_{xfi}, k_{yfi} and k_{zfi} are diagonal components of the fracture continuum permeability tensor and β_{xi} (–), β_{yi} (–), and β_{zi} (–) are weighting factors for node i in the x-, y- and z- directions,

respectively. Derivation of the fracture continuum permeabilities is provided in Attachment IV. Weighting factors were only applied to terms depending on the horizontal fracture spacing and not on the vertical fracture spacing.

In the context of fracture continuum parameters, the β weighting factors were used to increase the permeability and porosity of nodes where flow was actually observed to occur relative to the unconditioned background nodes. In particular, the β weighting factor of these nodes was chosen so that a single fracture exists at the node in the orientation shown on Figure 6-5. The derivation of the appropriate β weighting factor to condition these nodes is given in Attachment IV. Conditioning these nodes in this manner is equivalent to replacing the fracture continuum permeability and porosity calculated using Equations 1 through 4 with that from a discrete fracture. All unconditioned nodes received weighting factors of $\beta_x = \beta_y = 1.0$ and $\beta_z = \beta_x + \beta_y$. The horizontal fracture spacing was always greater than the grid discretization except for a dimensionless depth of 0.0 – 0.2 where they were equal. Therefore, the fracture continuum permeability and porosity for the background unconditioned nodes was always less than that for nodes where observed water flow features occurred. This is equivalent to stating that background unconditioned nodes only conduct a fraction of infiltrating water from a single fracture that is proportional to the node discretization divided by the fracture spacing. To prevent biasing nodes from increasing the net infiltration through the model, but rather to promote preferential channel flow through observed fracture flow features, the weighting factor of neighboring nodes was decreased. Hence, conservation of net infiltration flux was enforced by constraining the cumulative sum of the weighting factor for all biased nodes resulting from the observed flow feature to be identical to that of unconditioned nodes. Figures 6-6 to 6-9 show β weighting factors for fractures extending to the various dimensionless depths. Weighting factors were not estimated for dimensionless depth interval 0.0 – 0.2 because the grid discretization was equal to the horizontal fracture spacing, implying that each fracture continuum node contained one discrete fracture.

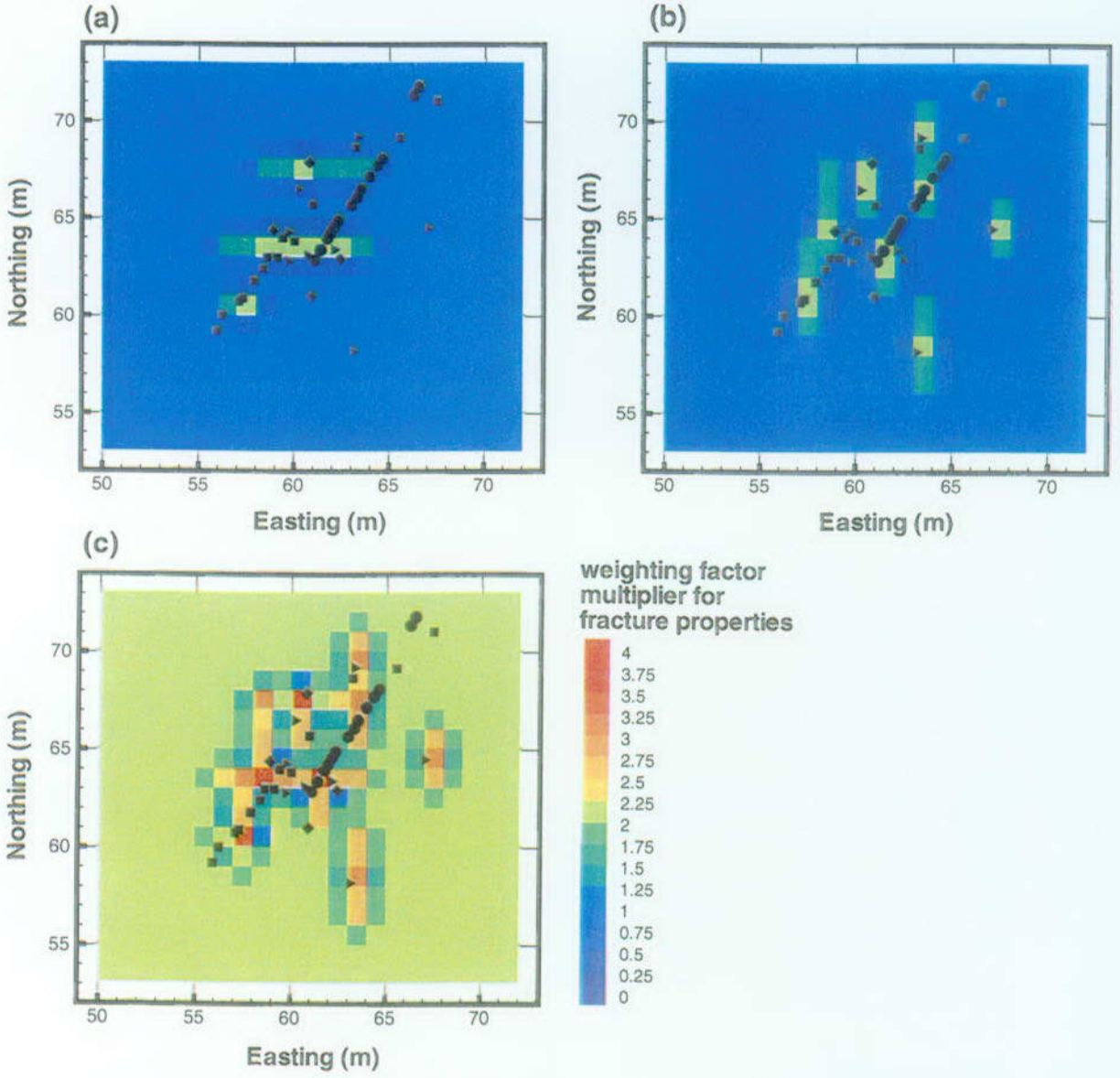

DTN: LB990930123122.002

Figure 6-6. Fracture Continuum Weighting Factors (a) β_x, (b) β_y, and (c) β_z for Dimensionless Depth Interval of 0.2 to 0.4

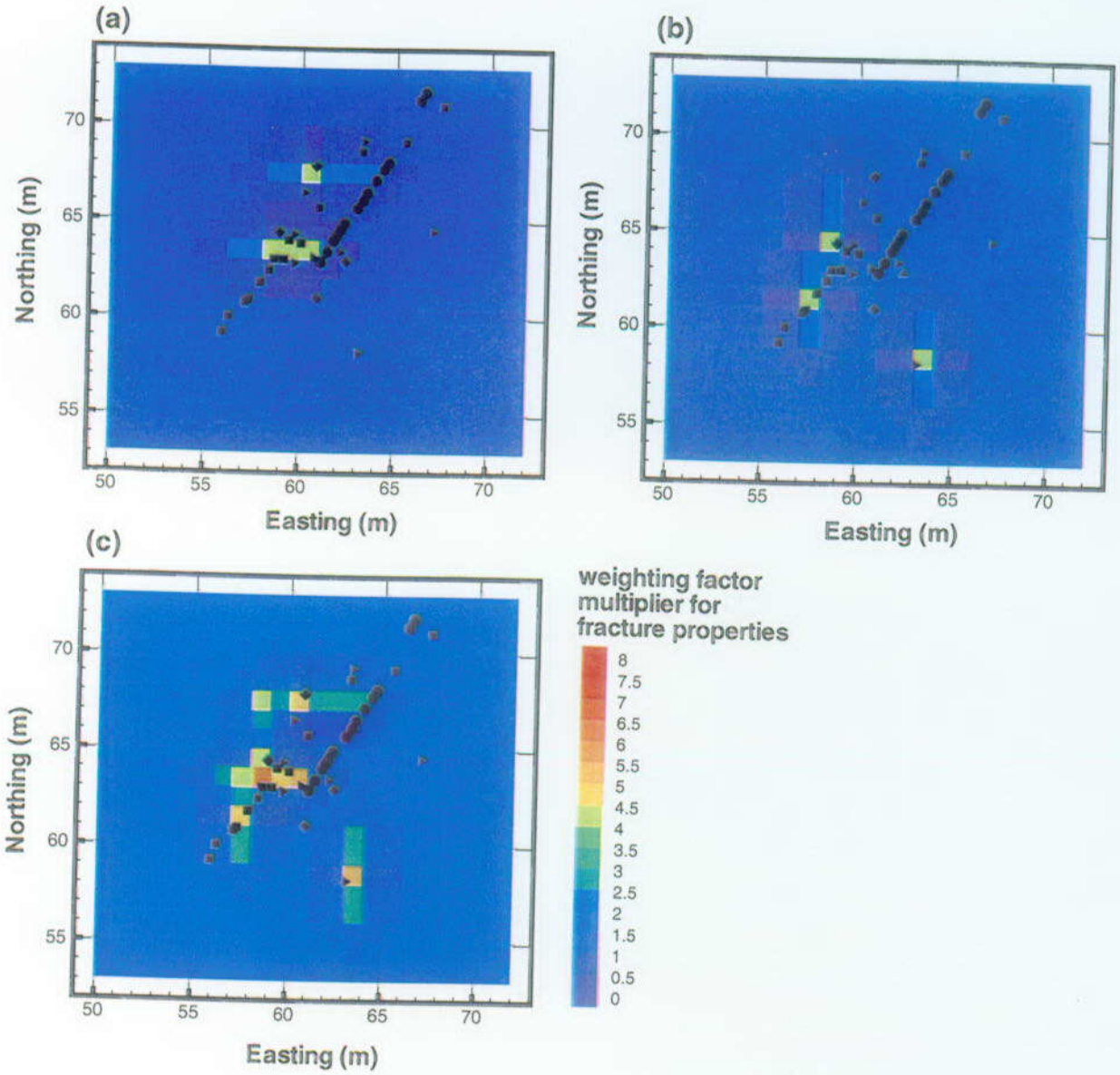

DTN: LB990930123122.002

Figure 6-7. Fracture Continuum Weighting Factors (a) β_x, (b) β_y, and (c) β_z for Dimensionless Depth Interval of 0.4 to 0.6

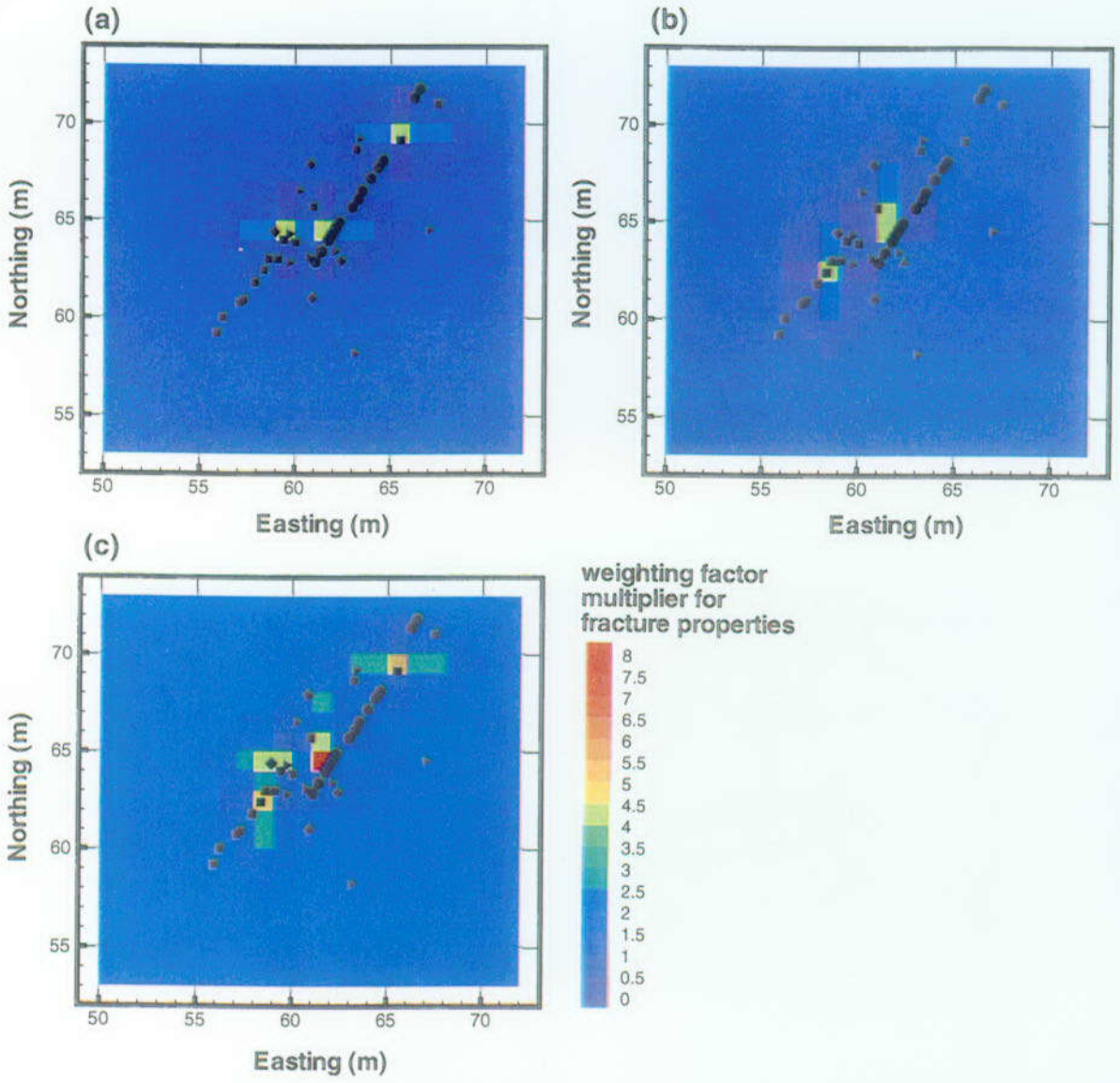

DTN: LB990930123122.002

Figure 6-8. Fracture Continuum Weighting Factors (a) β_x, (b) β_y, and (c) β_z for Dimensionless Depth Interval of 0.6 to 0.8

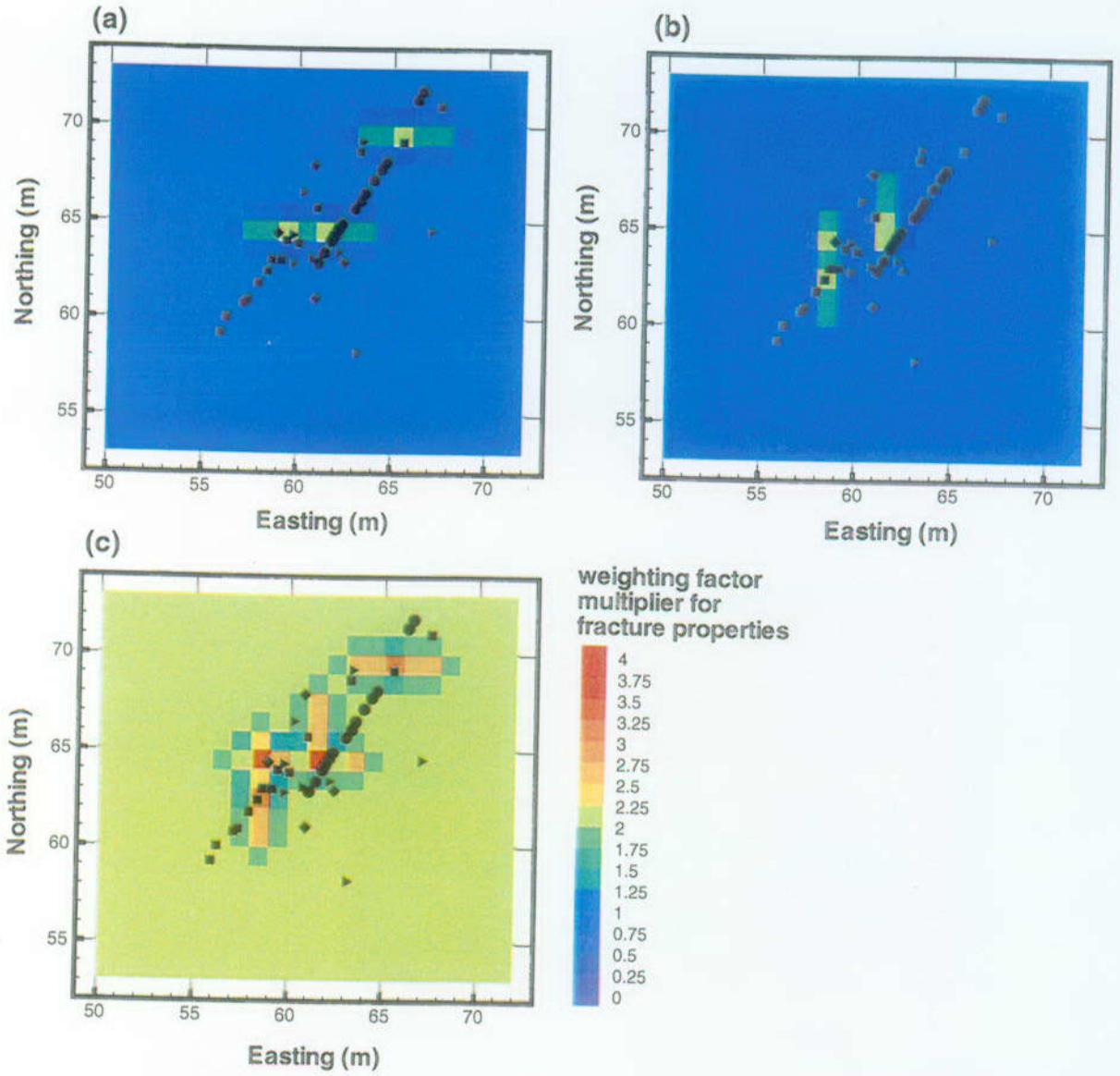

DTN: LB990930123122.002

Figure 6-9. Fracture Continuum Weighting Factors (a) β_x, (b) β_y, and (c) β_z for Dimensionless Depth Interval of 0.8 to 1.0

Flow of water and gas occurs between the fracture and matrix continua according to the mass conservation laws discretized by TOUGH2. Specifically, the interfacial area between the fracture and matrix continua through which the water and gas flow is given as:

$$A_{ifm} = 2\left(\beta_{xi}\Delta y_i \Delta z_i \frac{\Delta x_i}{D_{Hi}} + \beta_{yi}\Delta x_i \Delta z_i \frac{\Delta y_i}{D_{Hi}} + \Delta x_i \Delta y_i \frac{\Delta z_i}{D_{Vi}} \right) \quad \text{(Eq. 5)}$$

where $\Delta x_i = \Delta y_i = \Delta z_i = 1.0$ m, which represents the size of node i in the x-, y- and z-directions. This formulation is consistent with that used in the dual-permeability simulations of the UZ site-scale Yucca Mountain model.

6.5.1.1.4 Pneumatic Test Analysis

Pneumatic tests were conducted at the Box Canyon site to assess the permeability of the basalt. These tests consisted of air being injected into approximately three-meter packer intervals within slanted boreholes S-3 and S-4 as well as the vertical borehole II-5. These wells are all located within close lateral proximity of one another as shown on Figure 6-2a. The intent of these tests was to delineate vertical variations in the permeability of the upper basalt flow. The pneumatic tests consisted of injecting air at a constant rate within the packer interval and measuring the steady-state pressure response within the packer interval as well as in neighboring boreholes. This methodology has also been used extensively to characterize the permeability of the interconnected fracture network at Yucca Mountain (Huang et al. 1999). See Assumption #5 in Section 5 of this report. The injected air is assumed to flow entirely through the fracture network rather than through the matrix, given that air is a nonwetting phase in an air-water system and prefers to reside in the larger pore spaces of the fractures. In contrast, water preferentially resides in the matrix with saturations ranging from 0.55 to 0.8 within the model. This assumption was necessary to allow the pneumatic tests to estimate fracture continuum permeability as a single unknown property without any *a priori* assumptions regarding additional parameters involved in fracture/matrix flow to be calibrated using the infiltration arrival times. Although this assumption appears extreme, the complete and final Box Canyon model including matrix continuum nodes was used to resimulate selected pneumatic tests yielding similar pressure response results, implying that the assumption was justified. Details concerning the pneumatic tests conducted at Box Canyon can be found in Benito et al. (1998).

The pneumatic tests were simulated using the three-dimensional model in order to calibrate the permeability of the fracture continuum nodes. To calibrate the model, we used only steady-state pressure responses within the injection intervals. Matching pressure responses in adjacent boreholes could refine calibration of the fracture continuum permeabilities. The spatial location of each injection interval is given under the section "Centroid of Injection Interval" while the specific fracture continuum node within which injection was performed is given under section "Node" of Table 6-5. The applied injection rate and steady-state pressure response measured in the field are provided under section "Field Data" of Table 6-5. An initial estimate of fracture permeability surrounding the injection interval for each pneumatic test was obtained using an analytical solution derived by Baehr and Hult (1991) (see p. 2611, Eq. 56). These permeabilities are listed under the k_{test} column of Table 6-5.

INTENTIONALLY LEFT BLANK

Table 6-5. Fracture Permeability Calibration Results from the Analysis of the Pneumatic Test Data

Test ID	Zone	Centroid of Injection Interval Easting (m)	Northing (m)	Elevation (m)	Node ix	iy	iz	name	Field Data Q_{inj} (kg/s)	ΔP (Pa)	k_{field} (m^2)	Nodal Parameters k_{model} (m^2)	β_x	β_y	β_z	k_{mean} (m^2)	b (m)	Background Param. k_{mean} (m^2)	b (m)	Calibration P_{field} (Pa)	P_{model} (Pa)	$\Delta P_{residual}$ (Pa)	%error
1	0 - 0.2	63.76	66.90	1597.02	14	14	3	c1414	1.98E-03	35600	3.96E-14	1.58E-13	1.00	1.00	2.00	1.58E-13	9.83E-05			135387	136840	-1453	-1.07
2	0 - 0.2	65.79	70.63	1597.10	16	18	3	c1618	3.96E-03	114100	1.70E-14	6.78E-14	1.00	1.00	2.00	6.78E-14	7.41E-05	1.04E-13	8.54E-05	213887	202730	11157	5.22
3	0.2 - 0.4	62.40	62.90	1596.09	13	10	4	d1310	5.95E-03	52200	1.16E-13	4.66E-13	0.50	0.50	1.00	4.66E-13	1.65E-04			151998	149230	2768	1.82
4	0.2 - 0.4	65.53	70.21	1596.25	16	18	4	d1618	3.96E-03	171900	1.44E-14	5.76E-14	1.00	1.00	2.00	5.76E-14	7.73E-05			271698	209890	61808	22.75
5	0.2 - 0.4	62.40	62.90	1595.18	13	10	5	e1310	5.95E-03	223550	1.95E-14	7.79E-14	0.50	0.50	1.00	7.79E-14	9.08E-05			323360	227940	95420	29.51
6	0.2 - 0.4	63.32	66.28	1595.71	14	14	5	e1414	3.96E-03	49680	9.34E-14	3.74E-13	0.75	2.00	2.75	3.74E-13	1.39E-04			149490	135340	14150	9.47
7a	0.2 - 0.4	65.30	69.82	1595.47	16	17	5	e1617	3.96E-03	1438	4.40E-12	1.76E-11	1.00	1.00	2.00	1.40E-11	4.82E-04	4.06E-13	1.48E-04	101248	112740	-11492	-11.35
7b		65.30	69.82	1595.47	16	17	5		8.32E-03	4670	2.79E-12	1.12E-11								104480	125190	-20710	-19.82
8	0.4 - 0.6	62.40	62.90	1594.27	13	10	6	f1310	5.95E-03	5593	1.95E-12	3.91E-12	1.00	1.00	2.00	3.91E-12	3.35E-04			105414	126370	-20956	-19.88
9	0.4 - 0.6	62.88	65.65	1594.38	13	13	6	f1313	3.96E-03	69800	7.58E-14	1.52E-13	0.75	1.00	1.75	1.52E-13	1.14E-04			169621	169300	321	0.19
10	0.4 - 0.6	64.90	69.17	1594.14	15	17	6	f1517	3.57E-03	327000	7.09E-15	1.42E-14	1.00	1.00	2.00	1.42E-14	5.14E-05			426821	346040	80781	18.93
11	0.4 - 0.6	65.06	69.43	1594.67	16	17	6	f1617	3.96E-03	1728	4.18E-12	8.36E-12	1.00	1.00	2.00	8.36E-12	4.31E-04			101549	114900	-13351	-13.15
12a	0.4 - 0.6	62.40	62.90	1593.89	13	10	7	g1310	7.93E-03	9270	1.56E-12	3.11E-12	1.00	1.00	2.00	3.46E-12	3.22E-04			109103	132420	-23317	-21.37
12b		62.40	62.90	1593.31	13	10	7		5.95E-03	5705	1.92E-12	3.85E-12								105538	125220	-19682	-18.65
13a	0.4 - 0.6	62.44	65.02	1593.06	13	13	7	g1313	3.37E-03	320900	6.82E-15	1.36E-14	0.75	1.00	1.75	2.66E-14	6.40E-05			420733	269310	151423	35.99
13b		62.59	65.24	1593.51	13	13	7		7.93E-03	159800	4.88E-14	9.77E-14								259633	385320	-125687	-48.41
13c		62.59	65.24	1593.51	13	13	7		4.16E-03	360400	7.05E-15	1.41E-14								460233	293090	167143	36.32
14a	0.4 - 0.6	64.73	68.90	1593.59	15	16	7	g1516	7.93E-03	86400	1.17E-13	2.34E-13	0.75	1.00	1.75	2.69E-13	1.38E-04	4.04E-13	1.57E-04	186233	185340	893	0.48
14b		64.73	68.90	1593.59	15	16	7		7.93E-03	81300	1.27E-13	2.53E-13								181133	185340	-4207	-2.32
14c		64.66	68.78	1593.35	15	16	7		3.57E-03	34400	1.65E-13	3.30E-13								134233	146200	-11967	-8.92
15a	0.6 - 0.8	62.40	62.90	1592.97	13	10	8	h1310	8.92E-03	10470	1.50E-12	3.01E-12	0.75	1.00	1.75	6.45E-12	3.99E-04			110314	133120	-22806	-20.67
15b		62.40	62.90	1592.06	13	10	8		8.92E-03	2140	7.14E-12	1.43E-11								101984	133120	-31136	-30.53
15c		62.40	62.90	1592.06	13	10	8		6.94E-03	1466	8.14E-12	1.63E-11								101310	126650	-25340	-25.01
15d		62.40	62.90	1592.39	13	10	8		5.95E-03	8220	1.24E-12	2.47E-12								108064	123260	-15196	-14.06
16a	0.6 - 0.8	64.26	68.14	1592.07	15	16	8	h1516	5.95E-03	210000	2.19E-14	4.38E-14	0.75	1.00	1.75	9.45E-14	9.76E-05			309844	227740	82104	26.50
16b		64.42	68.39	1592.56	15	16	8		3.96E-03	53750	1.02E-13	2.04E-13								153594	196310	-42716	-27.81
17	0.6 - 0.8	62.40	62.90	1591.78	13	10	9	i1310	5.95E-03	960	1.04E-11	2.08E-11	0.75	1.00	1.75	2.08E-11	5.90E-04			100816	116430	-15614	-15.49
18a	0.6 - 0.8	61.88	64.23	1591.38	12	12	9	i1212	7.93E-03	164690	3.95E-14	7.90E-14	4.00	4.00	8.00	3.86E-14	6.14E-05			264546	307180	-42634	-16.12
18b		61.78	64.08	1591.06	12	12	9		5.15E-03	306000	9.43E-15	1.89E-14								405856	257760	148096	36.49
19a	0.6 - 0.8	62.00	64.41	1591.75	13	12	9	i1312	3.57E-03	79600	5.13E-14	1.03E-13	2.00	0.25	2.25	1.00E-13	9.84E-05			179456	186030	-6574	-3.66
19b		62.08	64.52	1591.99	13	12	9		6.94E-03	135200	4.90E-14	9.80E-14								235056	236290	-1234	-0.52
20	0.6 - 0.8	64.00	67.69	1591.14	14	15	9	i1415	3.96E-03	193600	1.51E-14	3.03E-14	0.75	0.75	1.50	3.03E-14	6.74E-05			293456	287860	5596	1.91
21	0.6 - 0.8	64.09	67.84	1591.46	15	15	9	i1515	5.95E-03	240000	1.67E-14	3.34E-14	0.75	1.00	1.75	3.34E-14	6.91E-05			339856	334740	5116	1.51
22	0.6 - 0.8	64.19	68.00	1591.78	15	16	9	i1516	3.96E-03	190700	1.65E-14	3.29E-14	0.75	1.00	1.75	3.29E-14	6.87E-05	1.89E-13	1.22E-04	290556	278340	12216	4.20
23	0.8 - 1.0	61.48	63.66	1590.16	12	11	10	j1211	3.96E-03	343350	5.71E-15	1.14E-14	0.50	1.00	1.50	1.14E-14	4.64E-05			443217	388130	55087	12.43
24a	0.8 - 1.0	63.73	67.24	1590.24	14	15	10	j1415	7.93E-03	37	3.24E-10	6.47E-10	1.00	1.00	2.00	5.02E-11	7.38E-04			99904	113430	-13526	-13.54
24b		63.95	67.61	1590.99	14	15	10		3.96E-03	218700	1.24E-14	2.48E-14								318567	106950	211617	66.43
24c		63.71	67.22	1590.19	14	15	10		6.94E-03	33	3.17E-10	6.34E-10								99900	111860	-11960	-11.97
24d		63.71	67.22	1590.19	14	15	10		9.31E-03	45	3.12E-10	6.25E-10								99912	115560	-15648	-15.66
25	0.8 - 1.0	61.34	63.46	1589.73	12	11	11	k1211	1.98E-03	449000	1.81E-15	3.61E-15	0.50	1.00	1.50	3.61E-15	3.16E-05			548879	463060	85819	15.64
26a	0.8 - 1.0	63.45	66.79	1589.33	14	14	11	k1414	7.93E-03	31	3.89E-10	7.77E-10	1.00	1.00	2.00	8.12E-10	1.87E-03	1.14E-12	2.09E-04	99910	100180	-270	-0.27
26b		63.48	66.83	1589.40	14	14	11		9.31E-03	41	3.44E-10	6.89E-10								99920	100230	-310	-0.31
26c		63.48	66.83	1589.40	14	14	11		6.94E-03	21	5.01E-10	1.00E-09								99900	100140	-240	-0.24
27	rubble zone	62.40	62.90	1588.43	13	10	12	l1310	7.93E-03	48	2.64E-10	1.06E-09	1.00	1.00	2.00	1.06E-09	8.59E-04	1.06E-09	8.59E-04	99938	99952	-14	-0.01
28a	lower basalt	62.96	65.98	1587.68	13	13	13	m1313	3.96E-03	16	4.20E-10	1.68E-09	1.00	1.00	2.00	1.19E-09	1.92E-03			99918	99941	-23	-0.02
28b		62.96	65.98	1587.68	13	13	13		6.94E-03	56	2.10E-10	8.39E-10								99958	99970	-12	-0.01
29a	lower basalt	62.72	65.59	1586.89	13	13	14	n1313	7.33E-03	78	1.67E-10	6.69E-10	1.00	1.00	2.00	1.29E-11	4.26E-04			99991	102130	-2139	-2.14
29b		62.48	65.20	1586.09	13	13	14		7.33E-03	124000	6.21E-14	2.48E-13								223913	102130	121783	54.39
30	lower basalt	62.33	64.94	1585.58	13	12	15	o1312	7.33E-03	50	2.68E-10	1.07E-09	1.00	1.00	2.00	1.07E-09	1.86E-03			99975	99945	30	0.03
31	lower basalt	61.93	64.28	1584.24	12	12	16	p1212	7.93E-03	3	4.31E-09	1.72E-08	1.00	1.00	2.00	1.72E-08	4.69E-03			99939	99981	-42	-0.04
32	lower basalt	61.36	63.36	1582.36	12	11	18	r1211	7.33E-03	2595	4.48E-12	1.79E-11	1.00	1.00	2.00	1.79E-11	4.76E-04	3.48E-10	1.28E-03	102555	101570	985	0.96
																					RMS error =	8647	Pa
																					residual bias =	15962	Pa

DTN: LB990930123122.001

INTENTIONALLY LEFT BLANK

To calibrate the permeability of the fracture continuum nodes, we removed the matrix continuum nodes to facilitate decreased simulation times. This procedure is consistent with the calibration methodology employed at Yucca Mountain (Huang et al. 1999) where the injected air is assumed to flow entirely through the fractures. Calibration of the model involved initially setting the gas-phase pressure equal to 100 kPa along the bottom boundary and decreasing it statically upwards to the top boundary. Constant pressure gas-phase boundary conditions were fixed at all sides of the model. Calibration then proceeded by adjusting the permeability of each fracture continuum node within which the centroid of an injection interval was located, until the model closely matched the observed field pressure response at steady state for the applied injection rate. The background permeability of each zone within the upper basalt flow (in addition to the rubble zone and lower basalt) was calculated by taking the geometric mean permeability of all nodes (see k_{mean} of "Nodal Parameters" section on Table 6-5) within which air injection took place for each specific zone. This calibration methodology is only meant to estimate the mean permeability of each of the various zones and does little to determine the spatial continuity in the permeability field around boreholes S-3, S-4 and II-5. This objective was considered sufficient for the purpose of this calibration, given that an estimate for the site-wide permeability was needed in order to simulate the infiltration tests.

The steady-state water saturation profile was established by applying an infiltration rate of 0.01 m/yr to the fracture continuum nodes along the surface of the model. This resulted in a maximum water saturation of 0.23 along the top of the model that decreased to 0.05 at the bottom. Permeability calibration by air injection was found to be insensitive to these low water saturations because the injected air always reduced the water saturation at the injection node and immediately surrounding nodes to a residual value of 0.01 at steady state.

The permeability values used to calibrate the model for each injection node are given in column k_{model} of Table 6-5. These values are all two or four times larger than those estimated by Baehr and Hult (1991). This difference is considered satisfactory given that the analytical model does not take into account the 3-dimensional structure of air flow in the fracture network. Multiple tests often had the centroids of their packer intervals within the same node. A single permeability value was then estimated for each node by taking the geometric mean value of all the individual tests within the particular node. The fracture aperture, b, of the node was then estimated by assuming the permeability tensor was isotropic, $k_x = k_y = k_z$ = mean of k_{model}, so that b was the arithmetic mean value calculated from Equations 1 through 3. The background fracture aperture was calculated in an identical manner. The background permeability and porosity values for the various zones of the upper basalt, rubble zone and lower basalt are provided under section "Background Param." of Table 6-5.

The results of the model calibration are described on Table 6-5 under the "calibration" subsection. The residual, $\Delta P_{residual}$, is calculated as the change in pressure observed in the field minus the change in pressure simulated in the model at the node in which injection took place. The values of P_{field} and P_{model} include the static gas phase pressure at the injection node. The percent error, % error is the residual, $\Delta P_{residual}$, divided by P_{field}. The RMS error, which is the square-root of the mean of the sum of the squares of the residuals, is 8647 Pa, which is larger than 22 of the 51 pneumatic pressure responses. This is caused by the difficulty in matching the large pressure

increase in the low permeability injection nodes by adjusting only the permeability of the injection node along with the mean background value. Injection node permeability values that were similar to or higher than the mean background value were more accurately simulated by the model. The residual bias, calculated as the arithmetic mean of $\Delta P_{residual}$, is 15962 Pa, also indicating that the fit was poorest for injection nodes within the lowest permeabilities that subsequently induced the largest pressure response. The RMS and residual bias errors indicate that the calibration methodology used is only suitable for estimating the average background permeability and should not be interpreted as a precise fit to the data from each test. Using an inverse model capable of estimating spatial continuity of the permeability field could significantly reduce the RMS and residual bias calibration errors. At the same time, these data show the validity of the volume-averaged approach of estimating the air permeability of rocks as performed at Yucca Mountain.

The permeability of the rubble zone is at least three orders of magnitude higher than that of the upper basalt. Although the permeability was estimated using only one measurement, it is consistent with field observations indicating that it is a highly permeable layer that provides a distinct hydrogeological separation between the upper and lower basalt flows. The bottom of the rubble zone is difficult to delineate from core data and may extend further into the lower basalt than shown on Figure 6-4. This would explain the higher permeabilities measured in the lower basalt relative to the upper basalt flow.

6.5.1.1.5 Infiltration Test Analysis

Two sequential sets of infiltration experiments were conducted at Box Canyon. The first is labeled 96-1 (two-week ponded infiltration test) while the second consists of four separate infiltration events called 97-1, 97-2, 97-3 and 97-4 (2-to-4 day infiltration tests). All tests were conducted within the infiltration pond shown on Figure 6-2b. Details concerning the infiltration experiments can be found in Faybishenko et al. (1998a, 1999). The starting time and duration of all ponding events is provided in Table 6-6, while the infiltration rates measured during the ponding events are provided in Table 6-7.

Table 6-6 . Ponding Test Initiation and Duration Times

Test	Start of Ponding	End of Ponding	Test Duration (days)	Time Since Datum (days)
96-1	8/27/96 12:27	9/9/96 11:00	12.94	0.00
97-1	9/11/97 12:15	9/13/97 12:45	2.02	379.99
97-2	9/18/97 14:56	9/20/97 16:46	2.08	387.10
97-3	10/2/97 15:40	10/4/97 16:00	2.01	401.13
97-4	10/31/97 13:51	11/3/97 15:00	3.05	430.06

DTN: LB990930123122.001

Table 6-7. Ponding Test Infiltration Rates

Infiltration Test	Time since 96-1 (days)	Infiltration Rate (m/day)
96-1	0.00	0.110
	0.50	0.100
	1.00	0.095
	1.50	0.085
	2.00	0.080
	2.50	0.075
	3.00	0.065
	3.50	0.060
	4.00	0.054
	4.50	0.050
	12.94	0.030
97-1	379.99	0.100
	380.24	0.075
	380.49	0.060
	380.99	0.040
	381.49	0.030
	382.01	0.025
97-2	387.10	0.175
	387.23	0.120
	387.35	0.800
	387.48	0.060
	387.60	0.045
	387.85	0.035
	388.10	0.030
	389.18	0.025
97-3	401.13	0.065
	401.63	0.045
	402.13	0.030
	403.15	0.025
97-4	430.06	0.040
	432.06	0.030
	433.11	0.025

DTN: LB990930123122.001

Analysis of the infiltration experiments involved calibrating hydrogeological parameters in the dual-permeability model of the Box Canyon site to match the arrival times of the infiltration front at various monitoring points. Simulations were also performed to determine whether the fracture pattern inferred from active water flow features in the subsurface acts to preferentially redistribute the infiltrating water within the computational domain. Furthermore, the model was used to examine the influence of the zonation pattern in fracture densities within the basalt flow and rubble zone on flow patterns of the infiltrating water. The permeability of the fracture continuum

nodes for the dual-permeability model was taken directly from the pneumatic test calibration. Other relevant parameters are provided in Table 6-2; their source is discussed below.

Boundary conditions applied to the numerical model for simulating the infiltration experiments consisted of a constant gas phase pressure of 100 kPa along the bottom of the model which then decreased statically upwards. All sides of the model were constrained as constant gas-phase pressure boundary conditions. An infiltration rate of 0.1 m/yr resulting from recharge was used to establish the steady-state water saturation profile. The gas-phase pressure distribution and steady-state water saturation profiles were used as initial conditions for all subsequent transient simulations. For the infiltration test simulations, the slightly irregular nature of the infiltration pond was approximated to fit within coordinates (58 m E, 60 m N) to (67 m E, 69 m N) in order to conform to the regular nature of the grid. Infiltration of the ponded water was simulated by injecting water at the rate observed during each event (Faybishenko et al. 1999) as specified on Table 6-7 to every fracture continuum node at the top of the model within the perimeter of the infiltration pond. No attempt was made to redistribute the infiltrating water with respect to the inferred fracture network shown on Figure 6-5 or based on variations in ground surface elevation within the pond. The constant pressure gas-phase boundary condition was removed from the surface nodes within the perimeter of the pond.

6.5.1.1.5.1 Calibration Using Infiltration Front Arrival Times

Calibration of hydrogeological parameters controlling the infiltration rate of water in the fracture-matrix basalt system involved adjusting the porosity of the fracture continuum, the permeability of the matrix continuum, and the interfacial area between the fracture and matrix continua. These parameters were modified until the infiltration front arrival times simulated by the numerical model matched field data obtained at sampling intervals during the infiltration events. The arrival times of the infiltration front were inferred from the first significant increase in bromide concentration in water samples taken as part of the tracer tests conducted during each infiltration test. Therefore, it was assumed, as stated in Section 5, Assumption #10, that the bromide tracer was conservative and advected at the same velocity as the infiltration front in the fracture continuum. It is important to note that the bromide data were used to constrain parameters controlling variably saturated groundwater flow. Transport of bromide was not simulated within the variably saturated flow field.

Tsang (1992) provided a literature review to sort out the different definitions and denotations of the various "equivalent apertures" that arose due to field measurements regarding the relative magnitudes of "hydraulic aperture" and "tracer aperture." These definitions pertained to representing a rough-walled fracture by a pair of parallel plates separated by a constant aperture *b*. Under fully saturated conditions, hydraulic tests provided an equivalent parallel plate aperture given by the geometric mean of the aperture distribution between the rough-walled fracture surfaces, while tracer tests indicated an arithmetic mean aperture. Therefore, advection of a tracer in rough-walled fractures should occur more rapidly than hydraulic testing would indicate. Extension of this "rule-of-thumb" to the Box Canyon site is made difficult by the variably saturated nature of the fractures. In this case, the infiltration front is channeled by the largest apertures while some water is drawn into the smaller apertures by capillary forces due to the wetting nature of the water phase on the fracture surfaces (Pruess, 1998). The equivalent fracture required by the fracture continuum nodes to conduct the infiltrating water may then be closer to

the arithmetic mean of the aperture distribution. In this work, we assume, as stated in Section 5, Assumption #6, that the equivalent aperture obtained from the pneumatic, infiltration, and tracer tests are identical by using the bromide data to infer the arrival time of the infiltration front.

Tracer tests conducted during the 97-1 to 97-4 series of infiltration tests provided the most comprehensive set of bromide measurements and consequently were used during the calibration. Given that the 96-1 bromide tracer test had been conducted previously, there was a preexisting background concentration of bromide prior to the start of the 97-1 test. Table 6-8 provides the background bromide concentrations measured prior to the 97 series of infiltration tests. Statistical analysis of the data indicated that they were log-normally distributed with a mean of 4.35 ln(mg/l) (or 77.48 mg/l) and a standard deviation of 0.94 ln(mg/l). Given these statistics, a bromide concentration of 240 mg/l provided a 88.5% confidence interval for the bromide concentration being significantly greater than the mean background concentration. This concentration was approximatgely 0.08 of the source pond bromide concentration used in 96-1 and 0.1 of the source pond bromide concentration used in 97-1 to 97-4 which is demonstrated by the maximum bromide concentration shown on Table 6-8. The maximum bromide concentration is reached at late time and is quite variable in magnitude due to variability within the pond itself. Therefore, the first sampling event when the bromide concentration exceeded 240 mg/l was used to infer the infiltration front arrival at that sampling point. This inference assumes, as stated in Section 5, Assumption #10, that dilution of the bromide tracer in the fracture continuum at the infiltration front, because of dispersion and losses into the matrix continuum, did not attenuate a bromide concentration of 0.1 of the source value. These times are listed as the maximum bromide arrival times on Table 6-9. The sampling time immediately prior to when bromide exceeded 240 mg/l is listed as the minimum bromide arrival time on Table 6-9. Together, the maximum and minimum provide a window on the expected arrival time of the infiltration front at the sampling point. In some cases, the first bromide sample exceeded a concentration of 240 mg/l, setting the maximum value on the time window, but no prior sample was taken to set the minimum value on the window. In this case, the minimum arrival time of the infiltration front was set as the start of the 97-1 infiltration test by default.

Table 6-8. Background Bromide Concentrations Prior to the 97-1 to 97-4 Infiltration Tests.

Well ID	Vertical Depth (m)	Max. Br^- Conc. (mg/l)	Background Br^- Conc.			
			mean (mg/l)	# samples	sample 1 (mg/l)	sample 2 (mg/l)
E1	1.50	2256.76	-	0		
E2	7.20	55.98	-	0		
	11.70	231.78	63.38	1	63.38	
E3	5.50	143.55	34.96	2	34.96	34.96
	7.30	103.99	68.80	1	68.80	
E4	3.50	308.50	-	0		
	7.50	81.67	56.90	1	56.90	
	13.40	56.62	-	0		
I1	0.30	106.69	45.39	2	43.70	47.07
	1.50	2048.92	-	0		
	3.00	353.15	-	0		
	6.10	41.91	46.56	2	38.05	55.07
	8.50	378.41	124.46	1	124.46	
	10.10	429.72	43.66	2	44.24	43.08
I2	0.30	2736.95	53.96	2	56.60	51.32
	1.50	1438.37	-	0		
	3.00	1703.16	-	0		
	6.10	2661.59	-	0		
I3	0.30	3460.86	42.09	2	41.32	42.86
	1.50	926.81	53.35	1	53.35	
T2	1.80	1490.44	845.23	1	845.23	
	4.40	213.56	117.57	1	117.57	
T3	4.60	2110.00	-	0		
T4	0.60	2060.86	54.01	1	54.01	
	2.70	1024.37	-	0		
	4.30	1046.65	204.00	1	204.00	
	5.80	1068.52	-	0		
T5	1.50	-	47.98	1	47.98	
	3.00	507.62	-	0		
T6	0.60	2909.92	-	0		
	4.60	1809.34	-	0		
T7	0.60	4040.73	66.39	1	66.39	
	1.80	1042.95	829.34	2	778.14	880.53
	3.00	964.10	-			
	5.80	-	89.73	1	89.73	
T8	0.30	2268.61	-			
T9	0.30	2609.84	54.55	1	54.55	
	1.50	2648.43	-			

DTN: LB9909301123122.001

Table 6-9. Bromide Arrival Times During the 97-1 to 97-4 Infiltration Test.

Time datum for Br^- arrival times (start of 97-1): 9/11/97 12:15 PM

Well ID	Vertical Depth (m)	Max. Br^- Arrival Time Br^- > 240 mg/l (date)	(days)	Min. Br^- Arrival Time Br^- < 240 mg/l (date)	(days)
E1	1.50	9/12/97 10:29 AM	0.93	-	-
E4	3.50	9/25/97 5:32 PM	14.22	9/20/97 1:10 PM	9.04
I1	1.50	9/12/97 9:04 AM	0.87	9/11/97 7:21 PM	0.30
	3.00	10/16/97 12:28 PM	35.01	-	-
	8.50	10/31/97 12:12 PM	50.00	9/8/97 10:20 AM	-3.08
	10.10	9/25/97 6:12 PM	14.25	9/19/97 5:31 PM	8.22
I2	0.30	9/11/97 7:37 PM	0.31	9/10/97 3:13 PM	-0.88
	1.50	9/12/97 3:17 PM	1.13	-	-
	3.00	9/20/97 12:22 PM	9.00	-	-
	6.10	9/18/97 7:29 PM	7.30	9/11/97 7:20 PM	0.30
I3	0.30	9/11/97 6:59 PM	0.28	9/10/97 3:49 PM	-0.85
	1.50	10/4/97 12:48 PM	23.02	9/8/97 10:40 AM	-3.07
T3	4.60	9/26/97 2:34 PM	15.10	-	-
T4	0.60	9/21/97 10:00 AM	9.91	9/19/97 4:35 PM	8.18
	2.70	9/20/97 1:26 PM	9.05	-	-
	4.30	9/17/97 6:50 PM	6.27	-	-
	5.80	9/21/97 10:00 AM	9.91	9/20/97 1:23 PM	9.05
T5	3.00	10/16/97 1:41 PM	35.06	10/4/97 12:58 PM	23.03
T6	0.60	9/11/97 7:10 PM	0.29	-	-
	4.60	11/3/97 3:30 PM	53.14	-	-
T7	0.60	9/11/97 7:04 PM	0.28	9/10/97 3:42 PM	-0.86
	3.00	9/20/97 12:45 PM	9.02	-	-
T8	0.30	9/12/97 8:55 AM	0.86	-	-
T9	0.30	9/11/97 7:34 PM	0.30	9/10/97 3:27 PM	-0.87
	1.50	9/11/97 7:32 PM	0.30	-	-

DTN: LB990930123122.001

Calibration of the model was performed by extracting one-dimensional vertical columns from beneath the infiltration pond where the 97-1 bromide data indicated borehole intersections with fractures that actively conducted water. Therefore, it was assumed that the infiltration front in the full three-dimensional model progressed downwards in a one-dimensional manner along vertical columnar fractures to each sampling point. Calibration involved the use of the one-dimensional columns rather than the full three-dimensional model to significantly reduce simulation times. Discretization of the one-dimensional columns consisted of the same 1.0 m^3 blocks used to discretize the site model. Although numerical accuracy in terms of resolving the water saturation at the infiltration front could be significantly improved with a finer discretization, discretization of the columns was identical to the site model. This allowed calibration parameters to be transferred directly to the site model and avoided concerns regarding scaling issues.

Parameter estimation was performed manually. Consequently, only a qualitative analysis of a given parameter's sensitivity to the overall calibration process is provided. A systematic calibration methodology using an inverse model such as ITOUGH2 (Finsterle 1999) would

provide a better understanding of the interrelationship of parameters assumed to control preferential flow paths of infiltrating water in the fractured basalt at Box Canyon. This approach would require detailed coordination between the field and modeling efforts to obtain data sets of sufficient quality to withstand the rigorous statistical analysis performed during inverse modeling.

Calibration was initially performed by matching infiltration front arrival times at borehole I-1 at vertical depths of 1.5 m and 10.1 m below the ground surface. Calibration proceeded by manually adjusting the fracture continuum porosity as calculated from the fracture aperture given by Equation 4, the matrix continuum permeability, and fracture-matrix interfacial area given by Equation 5. Justification for scaling the fracture continuum porosity is based on fractures having rough walls that create an irregular aperture distribution. Fractures may have many dead-end channels that contribute to tortuous flow of water through the fracture plane. Increasing the fracture porosity acts to slow down the rate at which the infiltration front advects through the fracture continuum. Matrix permeability was adjusted using the core sample values provided on Table 6-4 because large-scale vesicular zones are distributed throughout the basalt matrix. These act to increase permeability of the matrix continuum at the 1 m^3 scale of the nodes relative to the core scale. Increasing matrix permeability acts to slow down the rate at which the infiltration front advects through the fracture continuum because the matrix continuum is also able to conduct a portion of the infiltrating water. Increasing matrix permeability also acts to dampen the increase in water saturation at the infiltration front, attenuating its migration rate, because the matrix then responds more rapidly to the flow of water from the fracture continuum. This flow of water occurs because the capillary pressure within the fracture continuum decreases substantially at the infiltration front where the water saturation approaches unity. The capillary pressure, along with the water saturation, changes much more slowly in the matrix continuum than in the fracture continuum because of the large matrix storage capacity. The difference in water potentials caused by the disequilibrium in the fracture and matrix continua then causes the flow of water from the fracture into the matrix continuum.

The fracture-matrix interfacial area given by Equation 5 was scaled downward to decrease the exchange of water between the fracture and matrix continua nodes at the infiltration front resulting from the influence of the capillary forces. This parameter is expected to be small given that channelized flow of water is observed to occur in fractures (Pruess 1998; Su et al. 1999). This implies significantly less contact area for water between the fracture and matrix continua than if sheet flow were to occur in the fracture plane. Reduction in interfacial area acts to decrease the influence of the matrix continuum on the fracture continuum, thereby increasing the rate at which the infiltration front advects in the fracture continuum.

Calibration results for borehole I-1 are shown in Figure 6-10, which shows the change in water saturation in the fracture and matrix continuum nodes as a function of time where the time datum is the start of the 96-1 infiltration test. Sampling point I-1 at a depth of 1.5 m shows a rapid water saturation change within the time window specified by the bromide data. This response occurred immediately after the 97-1 test, indicating that the infiltration front advected rapidly through the fracture continuum near the ground surface. Sampling point I-1 at a depth of 10.1 m also responds within the time window specified by the bromide data, although the response does not occur until during the 97-2 infiltration test. All of the water that had infiltrated from the 97-1 test was completely absorbed from the fracture into the matrix continuum nodes before the infiltration

front could reach a depth of 10.1 m. It was not until the 97-2 test that a sufficient increase in water saturation relative to steady-state conditions existed in the matrix to allow the infiltration front to propagate to a greater depth.

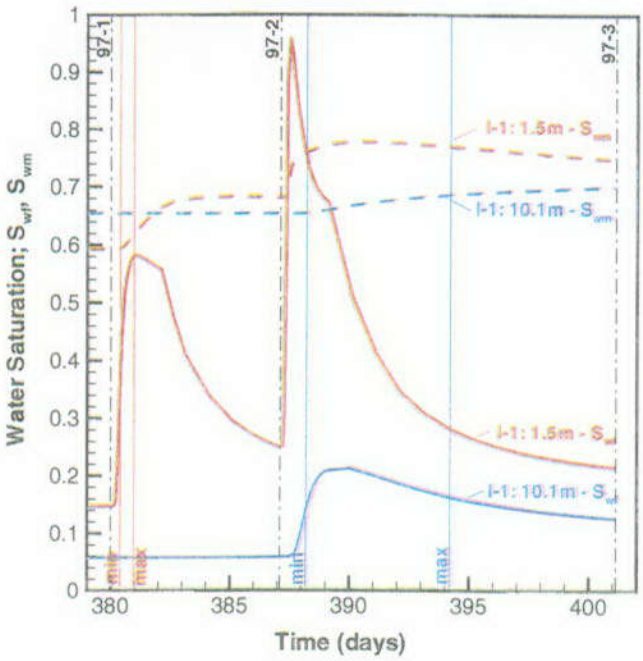

DTN: LB990930123122.002

Figure 6-10. Simulated Infiltration Front Arrival Times at Sampling Points in Borehole I-1 Given by Water Saturation in the Fracture (S_{wf}) and Matrix (S_{wm}) Continua

Fracture and matrix continuum properties obtained during the calibration for borehole I-1 are given in Table 6-2. Of particular note is that the fracture porosity was scaled upward by a factor of 50 relative to the fracture porosity from the permeability calibration exercise. Porosity was an extremely sensitive parameter controlling the infiltration rate of water in the fracture continuum. The resulting fracture continuum porosity for the upper basalt ranged from 0.01 to 0.02. The matrix permeability was increased by a factor of 4.5 to reflect the presence of vesicular zones distributed throughout the upper basalt. The fracture-matrix interfacial area was scaled by a factor of 0.01 to allow the matrix to completely absorb the 97-1 infiltration front between a depth of 1.5 m and 10.1 m while allowing the 97-2 infiltration front to propagate to a depth of 10.1 m.

Capillary pressure in both the variably saturated matrix and fracture continua nodes was represented using van Genuchten functions as implemented in TOUGH2 codes (Pruess 1991) with α and m parameters provided in Table 6-2. Although no formal capillary pressure-water saturation data have been obtained to characterize either the fractures or basalt matrix at Box Canyon, this choice of parameters yielded capillary pressures in the range of 10 kPa to 50 kPa, which was consistent with tensiometer measurements from the site (Faybishenko et al. 1998a, 1999). Residual water saturations of 0.01 and 0.1 were used in the fracture and matrix continua, respectively.

The relative permeability of the water and gas phases in both the matrix and fracture continuum nodes were represented using the Corey function, as implemented in TOUGH2, rather than the van Genuchten function as conventionally used for the Yucca Mountain simulations. Figure 6-11 shows the relative permeability of the infiltrating water phase using both van Genuchten and Corey functions in the fracture and matrix continua. The van Genuchten curves exhibit a very steep slope as the water saturation approaches unity, whereas the slope of the Corey curves when the water saturation is unity equals three. The steep slope of the van Genuchten curve substantially increased the numerical difficulty for the Newton iteration relative to the Corey curve. Use of the van Genuchten function increases the water saturation in the fracture and matrix continua relative to that simulated using the Corey curve. This requires a corresponding increase in the fracture-matrix interfacial area scaling factor to imbibe the water from the 97-1 infiltration test. The sensitivity of the calibration results to uncertainty in the form of the relative permeability curve implies that water saturation as well as relative permeability data are necessary in order to constrain the uniqueness of the calibration results. Given that these data do not exist for the Box Canyon site, the Corey relative permeability curve was used due to numerical efficiency

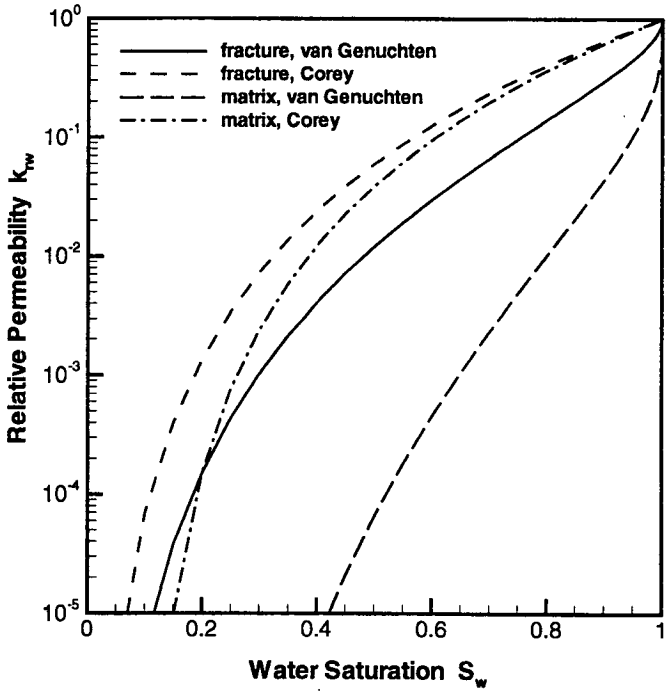

DTN: LB990930123122.002

Figure 6-11. Van Genuchten and Corey Relative Permeability Curves for the Fracture and Matrix Continua

The possibility of non-uniqueness existed during the calibration of the I-1 column because three parameters were adjusted to calibrate the model to the arrival time of an infiltration front at two different depths. The possibility of non-uniqueness is addressed by determining whether parameters used to calibrate I-1 are capable of predicting infiltration front arrival times at other sampling locations where bromide data are available.

Figure 6-12 shows calibration results for sampling intervals within borehole I-2 using hydrogeological parameters estimated from the I-1 calibration. The only sampling point in

borehole I-2 that has both a minimum and maximum expected arrival time occurs at a depth of 6.1 m. The minimum arrival time occurs 0.3 days after the start of the 97-1 test and the maximum occurs only 0.2 days after the start of the 97-2 test. Examination of Figure 6-12 shows that the majority of the simulated infiltration water from the 97-1 test is absorbed into the matrix before the start of the 97-2 test, although a small 0.08 increase in water saturation does reach a depth of 6.1 m. This is the remnant of a severely attenuated infiltration front from the 97-1 test. At the start of the 97-2 test, the water saturation rapidly increases after 0.2 days, although the peak saturation of the infiltration front arrives 0.5 days after the maximum expected arrival time. In general, these parameters do capture the rapid arrival of water after the start of the 97-2 test, although the arrival time could be increased by decreasing the porosity multiplier given in Table 6-2. As the sampling depth decreases from 6.1 m to 3.0 m, 1.5 m and finally 0.3 m, the arrival time of the infiltration front increases dramatically. Both sampling depths of 0.3 m and 1.5 m show peak water saturations before the maximum expected arrival time of the infiltration front. Simulation of the infiltration front at a depth of 3.0 m yielded an arrival time shortly after the 97-1 test, although the maximum expected time as inferred from the bromide data did not occur until after the start of the 97-2 test. The significance of this is impossible to infer given that no minimum expected arrival time could be obtained from the bromide data.

Given the relatively coarse discretization, permeability differences within the upper basalt flow that were within an order-of-magnitude of one another, and the fact that the infiltration rate from the pond was applied uniformly to all nodes within the perimeter of the infiltration pond, the arrival time of the infiltration front at shallow depths such as 1.5 m at I-2 is expected to be similar to that for I-1 at the same depth. Confirmation of the non-uniqueness of the parameters chosen to simulate I-1 is given by the simulated behavior of the infiltration front at a depth of 6.1 m in I-2.

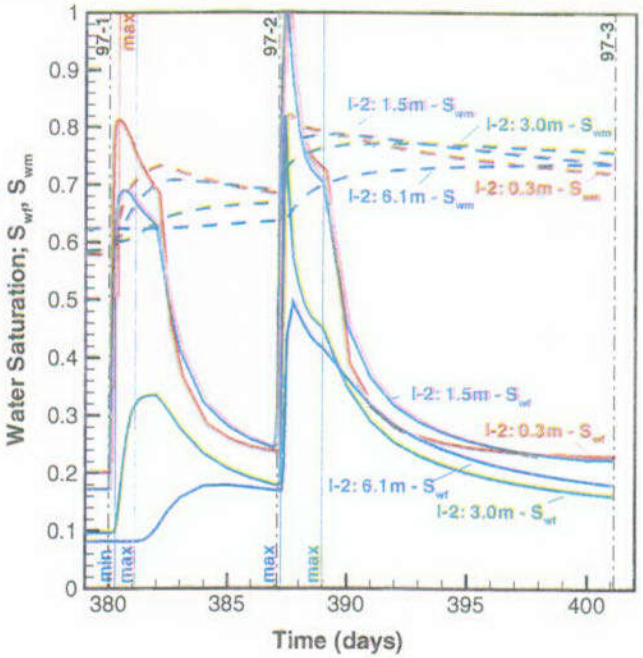

DTN: LB990930123122.002

Figure 6-12. Simulated Infiltration Front Arrival Times at Sampling Points in Borehole I-2 Given by Water Saturation in the Fracture (S_{wf}) and Matrix (S_{wm}) Continua

Figure 6-13 shows the arrival time of the infiltration front for borehole T-5 at a depth of 3.0 m. Bromide data indicated that the maximum and minimum expected arrival times of the infiltration front did not occur until after the start of the 97-3 test. Examination of the simulated arrival times indicates that the model predicts that the infiltration front should arrive after the 97-2 test. This implies that the fracture-matrix interfacial area may have been significantly higher for the columnar fracture extending downward to borehole T-5 at a sampling depth of 3.0 m, causing both the 97-1 and 97-2 test infiltration fronts to be absorbed into the matrix. Alternatively, the fracture pathway may not have been an active conduit for water during one or both of the 97-1 and 97-2 tests. These results indicate that the ability to simulate preferential flow of infiltrating water in a specific columnar fracture relative to another can only be performed using the full three-dimensional site model.

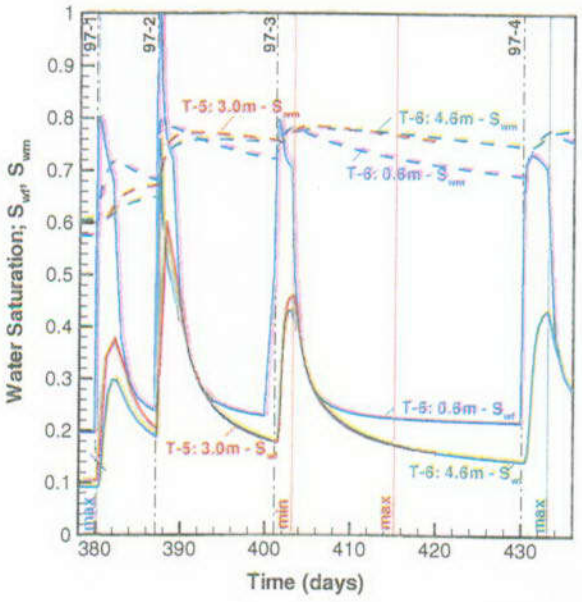

DTN: LB990930123122.002

Figure 6-13. Simulated Infiltration Front Arrival Times at Sampling Points in Boreholes T-5 and T-6 Given by Water Saturation in the Fracture (S_{wf}) and Matrix (S_{wm}) Continua

Figures 6-13 to 6-15 show simulated infiltration front arrival times for boreholes T-6, T-7, T-8, T-9, E-1 and I-3. All of these sampling points are relatively shallow and do not include a minimum expected infiltration front arrival time from the bromide data. Therefore, no interpretation is provided for these sampling intervals.

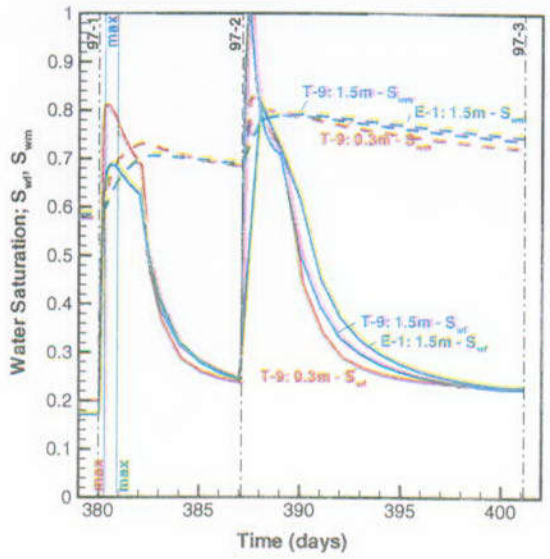

DTN: LB990930123122.002

Figure 6-14. Simulated Infiltration Front Arrival Times at Sampling Points in Boreholes T-9 and E-1 Given by Water Saturation in the Fracture (S_{wf}) and Matrix (S_{wm}) Continua

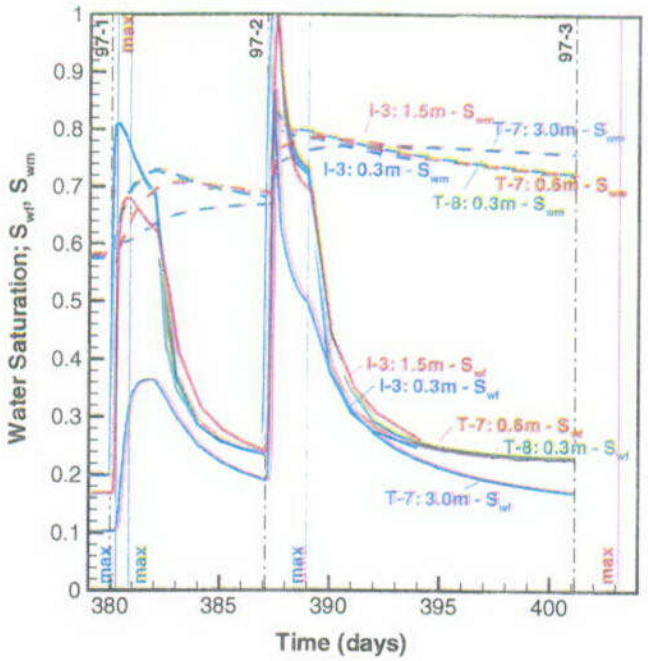

DTN: LB990930123122.002

Figure 6-15. Simulated Infiltration Front Arrival Times at Sampling Points in Borehole I-3, T-7 and T-8 Given by Water Saturation in the Fracture (S_{wf}) and Matrix (S_{wm}) Continua

6.5.1.1.5.2 Three-Dimensional Model Simulation

Following the calibration of the one-dimensional columns extracted from the site model, the full three-dimensional site model was used to examine infiltration front arrival times in boreholes E-4 and T-4. These boreholes had sampling points with both minimum and maximum times and were outside the perimeter of the infiltration pond. Hence, the full three-dimensional infiltration front extending from beneath the pond was simulated in order to capture the lateral migration of the infiltrating water to these observation points. Use of the full three-dimensional model serves as confirmation regarding the applicability of parameters obtained during the calibration with the one-dimensional columns.

Figure 6-16 shows the water saturation distribution in the fracture continuum of the three-dimensional dual-permeability model at the start of the 97-2 infiltration test. Within the dimensionless depth interval of 0.0 to 0.2, the water saturation directly beneath the pond is approximately 0.24, while the ambient background water saturation is 0.18. The elevated water saturation distribution resulting from the 97-1 test diminishes as depth increases. Of particular note is the fact that the water saturation distribution has a relatively uniform lateral distribution at each depth interval and is not closely associated with the observed fracture continuum nodes indicated on Figure 6-5. The cause of this last observation will be explained shortly.

Figure 6-17 shows the water saturation distribution in the fracture continuum at 0.9 days into the 97-2 infiltration test (388 days since 96-1). This time was chosen because it roughly coincided with the arrival time of the infiltration front for sampling depths between 3.0 m and 6.0 m from the one-dimensional analysis. These depths are in the range of sampling depths in boreholes E-4 and T-4. The simulated region of elevated water saturation due to the infiltrating water is quite uniform both laterally and vertically. The uniform vertical shape is consistent with the one-dimensional simulations where there was very little time lag between the arrivals of the infiltration front with depth, indicating that the infiltration front traveled rapidly through the fracture continuum. The uniform lateral shape of the infiltration front indicates that the inferred fracture pattern shown on Figure 6-5, along with the zonal distribution of hydrogeological parameters in the upper basalt, had little influence on preferential flow of infiltrating water through the fracture continuum. This may be a consequence of insufficiently large permeability contrasts as a result of the choice of weighting factors for the fracture continuum. Alternatively, application of the measured infiltration rate equally to all nodes within the infiltration pond, regardless of the inferred fracture pattern or ground elevation within the pond, may have biased the model to create the uniform infiltration pattern.

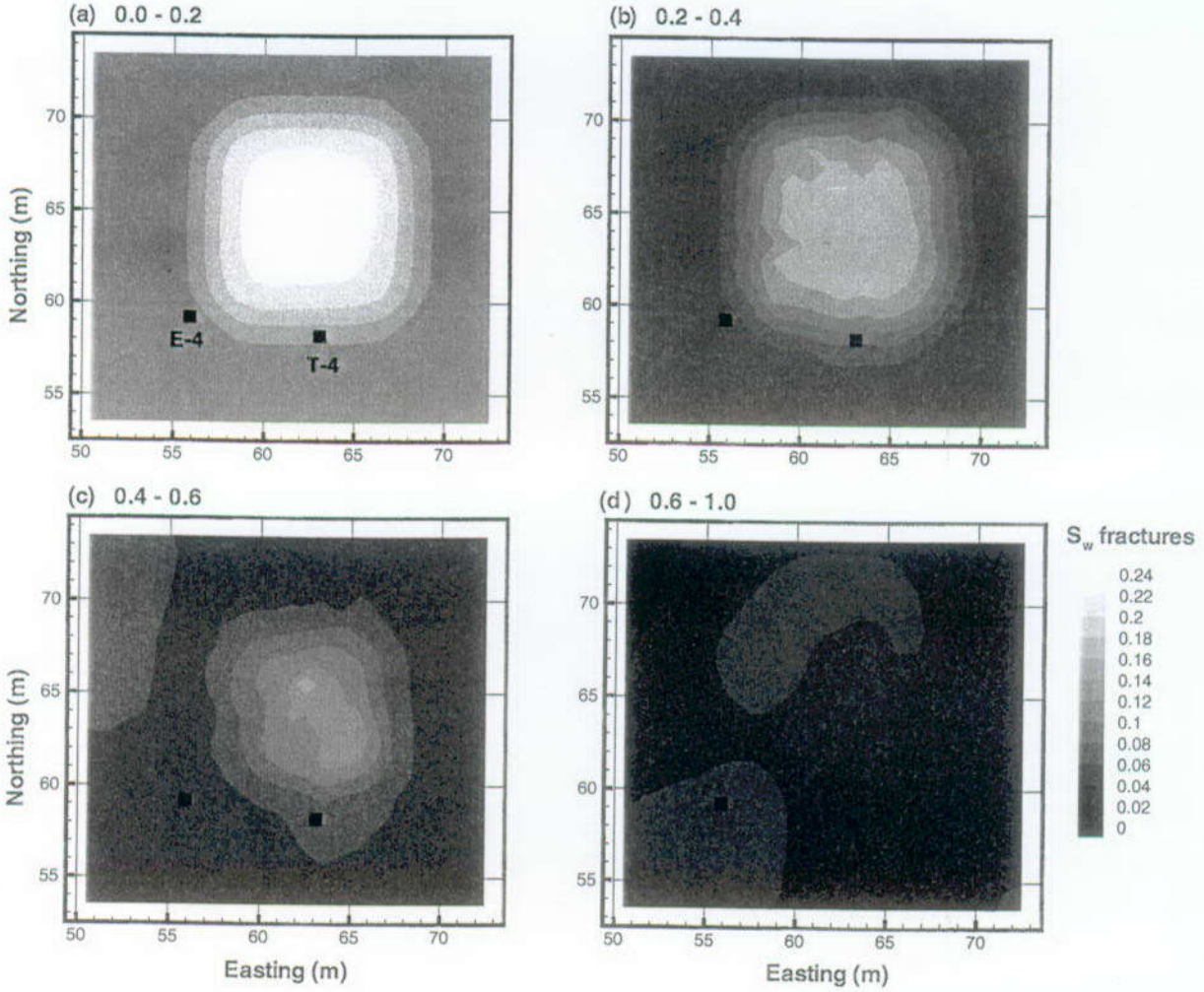

DTN: LB990930123122.002

Figure 6-16. Water Saturation Distribution in the Fracture Continuum at the Start of the 97-2 Infiltration Test – 387.1 Days Since the Start of 96-1

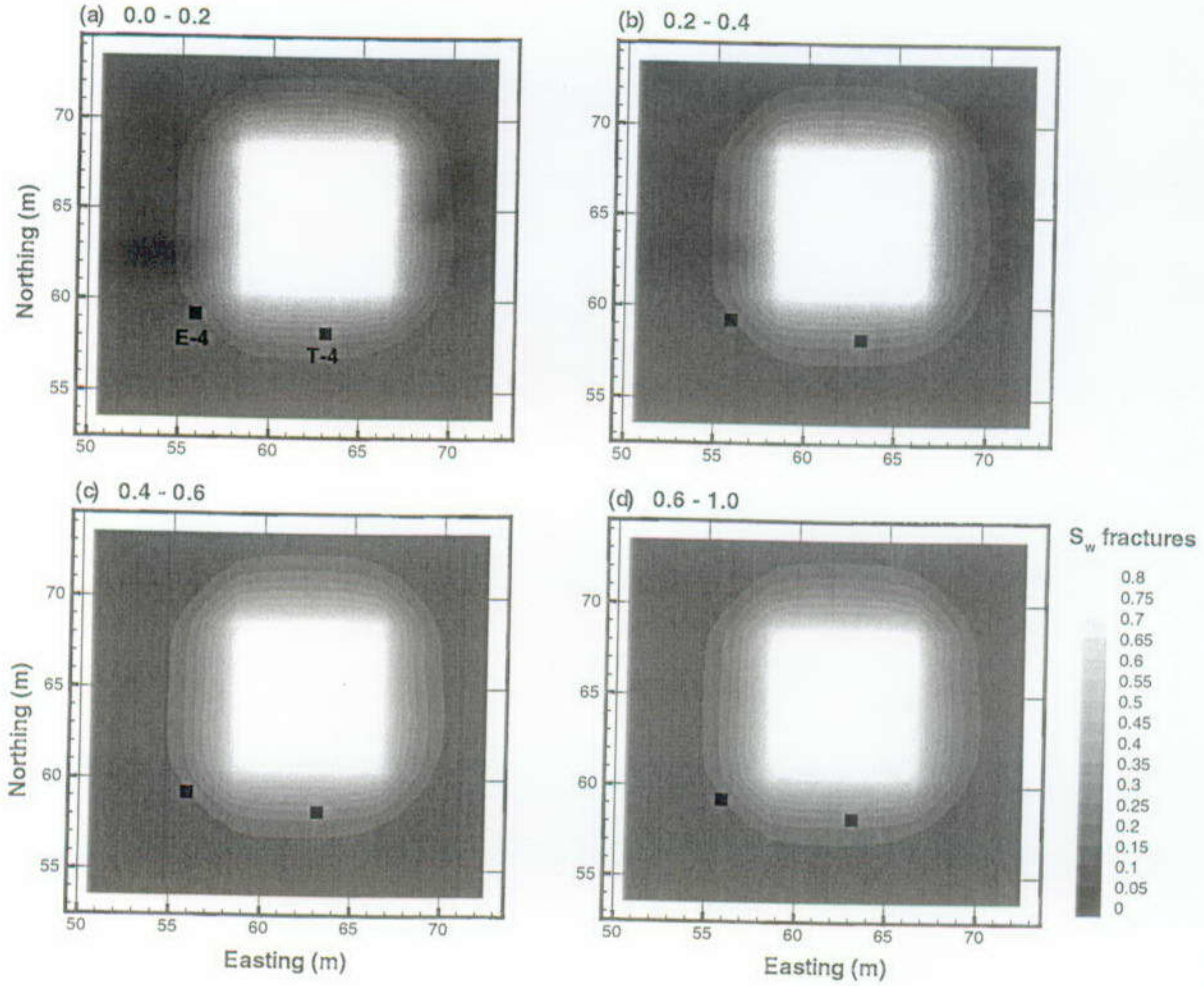

DTN: LB990930123122.002

Figure 6-17. Water Saturation Distribution in the Fracture Continuum 0.9 Days into the 97-2 Infiltration Test – 388.0 Days Since the Start of 96-1

Figure 6-18 shows the water saturation distribution 2.9 days (390 days since 96-1) into the 97-2 infiltration test. This time was chosen because it roughly coincides with rapid decline in water saturation at the end of the 97-2 infiltration test, which occurred over a 2.08 day period. Once again, the lateral extent of the saturation distribution appears uniform with depth, with no preference given to the observed fracture network. Figure 6-17 shows the water saturation distribution before the minimum expected time of the infiltration front for E-1 at a vertical depth of 1.5 m and T-4 at vertical depths of 0.6 m and 5.8 m. Figure 6-18 shows the water saturation just after the maximum expected arrival time of the infiltration front for both T-4 sampling intervals and within the time window for the arrival at E-1. Figure 6-17 shows that the initial rapid advection of the infiltration front is restricted to a one-dimensional flow path directly beneath the pond and misses boreholes T-4 and E-1. Capillary forces do cause lateral migration of the infiltration front by 2.9 days after 97-2, which is consistent with bromide tracer samples obtained from the site.

6.5.1.1.6 Summary and Conclusions of Box Canyon Study

The hydrogeological system at Box Canyon was simulated using TOUGH2 (TOUGH2 V1.3, STN: 10061-1.3-00, Version 1.3). This involved the application of the dual-permeability formulation to represent both water and air flow through the variably saturated, fractured basalt present at the site. The modeling approach was adapted from the methodology used to simulate flow and transport processes in unsaturated rocks at Yucca Mountain (Bandurraga and Bodvarsson, 1999; Doughty, 1999). Construction of the conceptual model involved subdividing the upper basalt flow into zones based upon the vertical columnar fracture spacing. We used sampling points within the boreholes that indicated active flow of water during the infiltration tests to infer a network of active water-conducting fractures. This network was used to bias hydrogeological properties of the fracture continuum nodes of the model to channel infiltrating water to places where it was observed to flow.

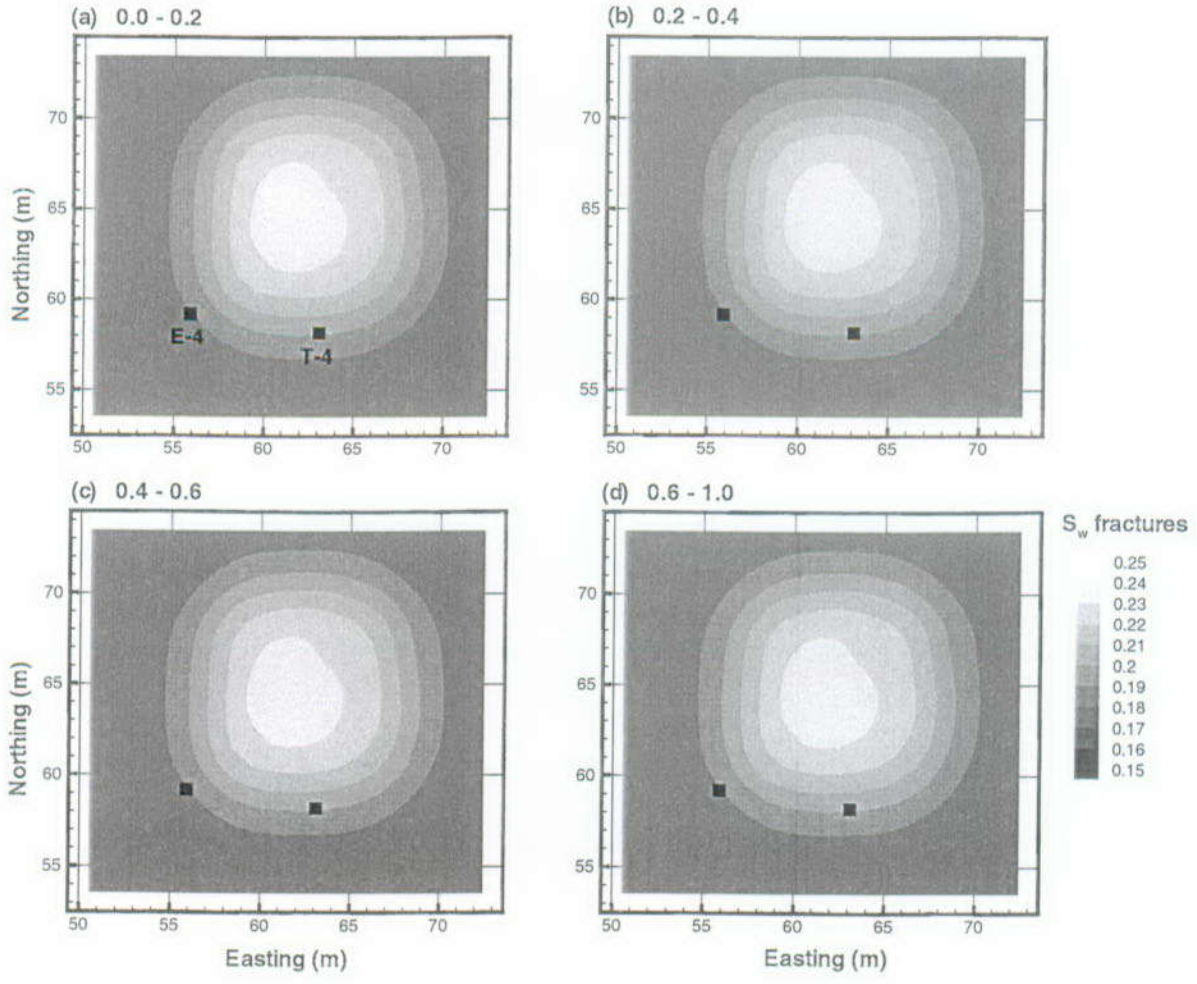

DTN: LB990930123122.002

Figure 6-18. Water Saturation Distribution in the Fracture Continuum 2.9 Days into the 97-2 Infiltration Test – 390.0 Days Since the Start of 96-1

Calibration of the model proceeded in two stages. First, the permeability of the fracture continuum nodes was adjusted to reflect the pressure response from pneumatic tests conducted at the site. Second, arrival times of the infiltration front as inferred from the bromide tracer data were used to calibrate the fracture continuum porosity, matrix continuum permeability, and fracture-matrix continua interfacial area. Calibration results indicated that the fracture continuum porosity was a very sensitive parameter controlling the arrival time of the infiltration front. The fracture continuum porosity of the upper basalt flow was scaled by a factor of 50 relative to that calculated using the aperture from the permeability calibration. The matrix continuum permeability was increased by a factor of 4.5 relative to the core measurements to reflect the influence of the highly permeable vesicular zones on the field scale. Finally, the fracture-matrix continua interfacial areas were multiplied by a factor of 0.01. This caused the 97-1 infiltration pulse to be completely absorbed from the fracture into the matrix continuum at a shallow depth while permitting the 97-2 infiltration pulse to advect rapidly to a greater depth. The 97-1 and 97-2 infiltration tests were the first two in the 97 series of infiltration tests. Physically, the choice of interfacial scaling area scaling factor is justified by the decreased contact area of the water phase between the fracture and matrix resulting from the channelized flow of the infiltrating water through the variably saturated fractures. The physical rationale for increasing the porosity given the channelized flow of water in the fracture continuum may be a consequence of multiple factors resulting from the rough-walled nature of the fracture surfaces, such as flow of water into dead-end fracture channels, and the tortuous flow paths of water rivulets within the rough-walled fracture plane.

Simulation of the three-dimensional infiltration front indicates that it is relatively uniform both laterally and vertically. It shows little if any influence from either the zoned distribution of hydrogeological parameters in the upper basalt or the fracture network that was meant to channel the flow of infiltrating water. This may be a consequence of distributing the water that was observed to infiltrate from the pond during the various infiltration tests equally to all surface nodes within the perimeter of the pond. Alternatively, the bias applied to the fracture nodes may have provided an insufficient permeability contrast to preferentially channel the infiltrating water as expected.

Parameter estimation for both the pneumatic and infiltration tests was conducted manually. This calibration method was adopted to provide a preliminary interpretation of the expected range in these parameters. The scaling factors employed during calibration imply a bias indicating inaccuracies in applying the conceptual model as discretized to represent flow processes controlling water infiltration in variably saturated fractures. In general, a consistent set of parameters was obtained which allowed the dual-permeability model to replicate the field data. Although the dual-permeability approach is also applied to explain groundwater flow at Yucca Mountain, the vastly different scales of Box Canyon and Yucca Mountain imply that upscaling is an issue when comparing parameter values.

6.5.1.2 Rainier Mesa

Rainier Mesa is located approximately 20 miles to the northeast of Yucca Mountain, Nevada. The area contains a number of tunnels that were excavated for the underground nuclear weapons testing program. Before construction of the Exploratory Studies Facility (ESF), the hydrogeologic

data collected at Rainier Mesa provided the only extensive underground observations in tuff units similar to those of Yucca Mountain.

Rainier Mesa is situated at a higher elevation than Yucca Mountain and has a mean annual precipitation of ~320 mm/yr, approximately double the Yucca Mountain mean (Wang et al. 1993, p. 676). About eight percent of the measured Rainier Mesa mean precipitation was observed to be infiltrating into one of the tunnels constructed in zeolitic tuffs at the Rainer Mesa site. The seepage was associated with a small number of faults and fractures (Wang 1991, p. 79). These structural features are thought to be a pathway for flow from perched water above the zeolitic horizon (Wang 1991, p. 82). The seepage is geochemically similar to meteoric water (Wang et al. 1993, p. 677). Tracer tests and tritium samples indicate that the likely rate of fast pathway flow is from one to six years to reach from the surface to the water table at a depth of 1000 m. The travel time is orders of magnitude less than the matrix travel time calculated using measured matrix sample conductivities. This observation is supported by measurements of 'bomb-pulse' ^{36}Cl in several samples from one of the tunnels (Wang et al. 1993, p. 677).

The stratigraphy of both Rainier Mesa and Yucca Mountain consists of alternating welded and nonwelded tuffs. The zeolitic Tunnel Bed tuffs at Rainier Mesa show a range of mineral compositions similar to those in the Calico Hills nonwelded (CHnz) tuff at Yucca Mountain (Wang et al. 1993, p. 676). Also, the higher Rainier Mesa mean precipitation is similar to the long-term average predicted for Yucca Mountain (DOE 1998, p. 2-28). However, the relative thicknesses of the welded and nonwelded tuff units at the two sites differ significantly (Figure 6-19). Below the welded tuff caprock at Rainier Mesa lies the approximately 150-meter-thick nonwelded Paintbrush Tuff (PTn). The bottom third of this unit is extensively zeolitized due to hydrothermal alteration of the tuff shortly after its emplacement. At Yucca Mountain, the PTn is mostly vitric, with thin localized lenses of clays and zeolites. Seepage at Rainier Mesa occurs only in tunnels constructed in the zeolites; for the tunnel constructed in nonwelded, non-zeolitized tuff, no seepage is observed.

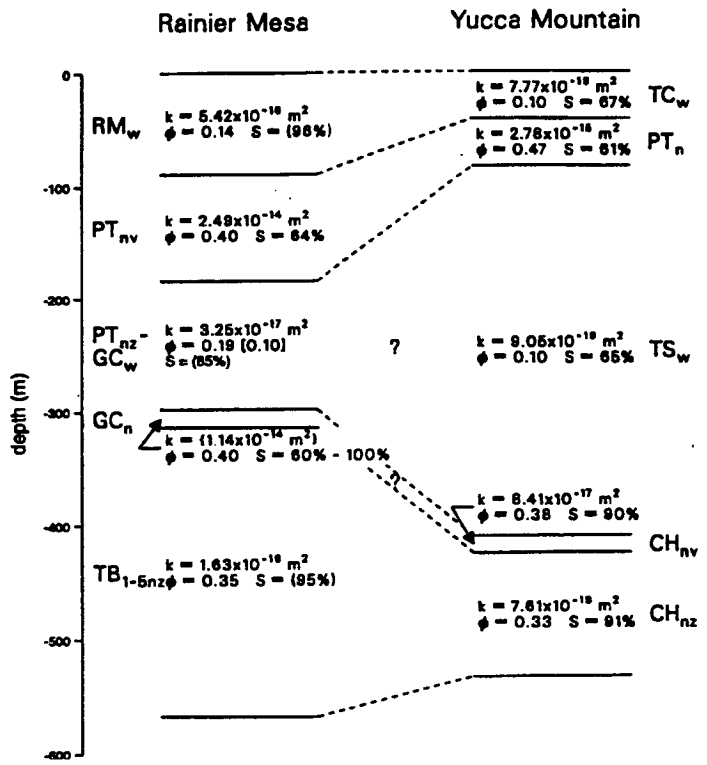

Figure 6-19. Comparison of Hydrogeologic Stratigraphic Sections of Rainier Mesa and Yucca Mountain (Wang et al. 1993, p. 675)

Tuff matrix permeabilities at Rainier Mesa are reported (Wang et al. 1993) to be several orders of magnitude higher than those of corresponding units at Yucca Mountain. Since the tuffs at the two sites have similar origins, mineralogy, and porosity, there is no apparent reason why their permeabilities should be different. Wang et al. (1993, p. 676) suggested that the differences could be an artifact of different measurement methods. Now that extensive matrix permeability data are available for Yucca Mountain tuffs, this issue could be readily resolved by repeating the permeability measurement procedure on Rainier Mesa samples.

In spite of differences in thickness of stratigraphic units and reported permeabilities, Rainier Mesa provides one of the best opportunities to study a number of processes analogous to Yucca Mountain. These include episodic pulses, such as those that affect the PTn; flow patterns and percolation fluxes based on geochemical signatures; seepage into drifts; and sorption in vitric and zeolitic units. A substantial body of data already exists that could be applied in the Yucca Mountain UZ flow and transport model to evaluate seepage and percolation under wetter climate scenarios. Additional tests would have to be conducted to evaluate sorption and retardation processes. An aspect of the Rainier Mesa site that affects its suitability as an analog is the perturbation by nearby underground nuclear weapons testing that may have affected the PTn and increased the number of structural features that act as fast flow pathways. This effect would need to be evaluated before the Rainier Mesa data are used to develop important conclusions about long-term predictions of Yucca Mountain's response to thermal and climate perturbations.

6.5.1.3 Other Flow and Seepage Analogs

In addition to the Box Canyon and Rainer Mesa sites, other locations may be suitable as analogs to infiltration and flow processes at Yucca Mountain. One that has already been used in Yucca Mountain analyses is the U.S. Nuclear Regulatory Commission's (NRC) Apache Leap site in Arizona. Saturated and unsaturated flow parameters from tuff at the site were compared to Yucca Mountain data (Wang 1992). Based on the differences between the flow parameters of the tuffs for the Yucca Mountain and Apache Leap sites, a relationship between pore-size distribution index and saturated permeability was developed. The relationship could be applied to test its utility in scaling hydrologic parameters of faults or fractures at Yucca Mountain, based on measured data from other sites.

6.5.2 Analogs to UZ Transport of Radionuclides

Section 6.5.2.1 discusses previous and new work at Peña Blanca, Mexico as an analog to UZ transport of radionuclides. Section 6.5.2.2 considers a variety of sites in northwestern Nevada and their potential application as analogs to UZ flow and transport at Yucca Mountain.

6.5.2.1 Natural Analog Studies at Peña Blanca, Mexico

6.5.2.1.1 Introduction

Section 6.5.2.1 provides a summary of the analysis of data from previous Peña Blanca studies relevant to source term issues and to radionuclide retention in the UZ. This analysis includes a bibliography (Attachment III) of existing studies regarding alteration of uraninite, flow pathways for radionuclides, periods of radionuclide migration, and their degree of retention in the Peña Blanca flow system. Subsections 6.5.2.1.2 and 6.5.2.1.3 provide the geologic setting of Peña Blanca and the historical context of previous analog studies. Subsection 6.5.2.1.4 discusses both previous studies that utilized the uranium-series disequilibrium approach and new analyses conducted by the Yucca Mountain Project in 1999, as well as conclusions based on the new work. Subsection 6.5.2.1.5 summarizes supplemental hydrologic studies that were conducted previously and that could be built upon through recommendations made in Subsection 6.5.2.1.6 to obtain a more complete three-dimensional picture of actinide transport at Peña Blanca for the purpose of building confidence in understanding similar potential transport processes at Yucca Mountain.

6.5.2.1.2 Background

The Yucca Mountain site is located in silicic tuffs of Miocene age, in an arid, oxidizing environment with the potential emplacement horizon hundreds of meters above the saturated zone. In the 1980s, Goodell and others recognized the significance of the Peña Blanca uranium deposits in the Mexican State of Chihuahua as natural analogs for the potential repository at Yucca Mountain (Goodell 1985; Murphy 1995). In the 1970s, the Peña Blanca region was a major target of uranium exploration and exploitation by the Mexican government. Since that time the Nopal I uranium deposit has been extensively studied by researchers in the U.S. and Europe because it is a good analog for evaluating the fate of spent fuel, associated actinides, and fission products at a geologic repository. A bibliography of studies associated with Peña Blanca is part of this report (Attachment III).

The Nopal I uranium deposit at Peña Blanca represents an environment that closely approximates that of the potential high-level radioactive waste repository at Yucca Mountain, Nevada in the following ways:

- Climatologically: both are located in semi-arid to arid regions.
- Structurally: both are part of a basin and range horst structure composed of Tertiary rhyolitic tuffs overlying carbonate rocks.
- Hydrologically: both are located in a chemically oxidizing, unsaturated zone 100 meters or more above the water table.
- Chemically: the alteration of uraninite to secondary uranium minerals at Nopal I may be similar to the eventual fate of uranium fuel rods in a potential geologic repository like Yucca Mountain.

6.5.2.1.3 Geology

The Peña Blanca uranium district is located approximately 50 km north of Chihuahua City, Mexico, in the northern part of the Sierra Peña Blanca (Figure 6-20). The region is part of the Chihuahua tectonic belt, which is characterized by Laramide-age northwesterly vergent folds and thrust faults in Mesozoic and lower Tertiary rocks. A regionally extensive sequence of Tertiary volcanic rock unconformably overlies the older units. The region was affected by north-south-trending normal faulting that is thought to be the southern manifestation of the Rio Grande Rift tectonism. North-south oriented basin and range topography now characterizes the region (Goodell 1985).

6.5.2.1.3.1 The Peña Blanca District

The Sierra Peña Blanca is a north-south trending, westerly-tilted basin and range-style horst block. The uranium deposits are located close to the eastern edge of the block (Pearcy et al. 1995).

The oldest rocks in the vicinity of the Peña Blanca district are Early to Late Cretaceous reef, back-reef and basinal, thinly bedded to massive limestone. The limestone is unconformably overlain by a sequence of Tertiary volcanic and lesser sedimentary rocks. From older to younger, these Tertiary units are the Pozos conglomerate and rhyolitic ignimbrite of the Corrales, Coloradas, Nopal, and Escuadra Formations. The Piloncillos fanglomerate locally separates the Nopal and Escuadra Formations. The Nopal Formation was dated at 44 Ma (million years). (K-Ar age, Alba and Chavez 1974; Pearcy et al. 1995).

The Peña Blanca uranium district consists of three exploration camps: El Nopal, Margaritas, and El Cuervo. Many of the uranium deposits in the district have been drilled or developed by underground or open-pit mining over a period of 20 years, but there has been no mining activity at Peña Blanca since 1985. Combined, these deposits contained more than 2,000 metric tons of U_3O_8 and constitute the bulk of Mexican uranium sources. The deposits occur close to the eastern edge of the Sierra Peña Blanca range and, in general, are concentrated in the lower part of the

Tertiary volcanic section. Uranium mineralization locally extends downward into the upper part of the Cretaceous limestone (see Figure 6-21).

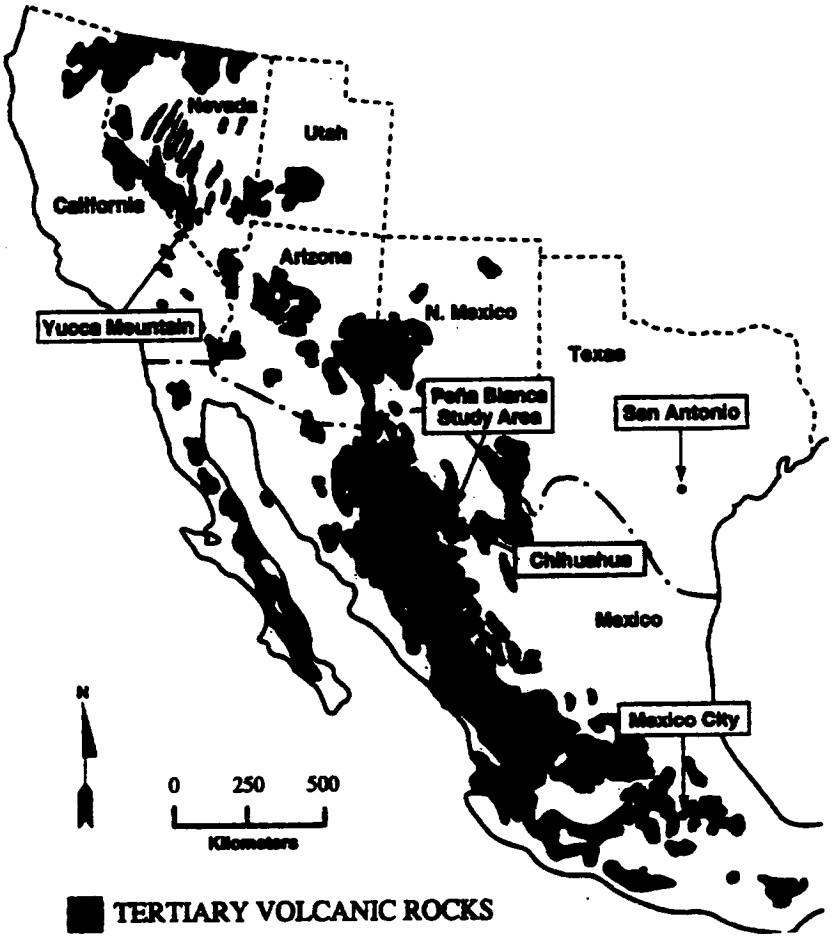

Figure 6-20. The Nopal I Uranium Deposit in the Peña Blanca Mining District, Chihuahua, Mexico. Yucca Mountain is located northwest of the Peña Blanca district along a general trend of Tertiary volcanic rocks in the Basin and Range province (from Pearcy et al. 1994, p. 715)

6.5.2.1.3.2 The Nopal I Deposit

Nopal I is a small, high-grade uranium deposit located in a highly brecciated zone that occurs at the intersection of two steep faults (Figure 6-21). The Nopal I deposit is interpreted to have formed by hydrothermal solutions that precipitated uraninite (nominally UO_{2+x}) as they moved through a subvertical, highly fractured zone within welded silicic tuff (Pearcy et al. 1994, p. 714). The Nopal I deposit is nearly cylindrical, having rough horizontal dimensions of 18 m by 30 m with a nominal ore zone extending approximately 100 m vertically (Pearcy et al. 1995, p. 685) (Figure 6-21). Currently, about 300 metric tons of oxidized uranium remains on site. The upper, highest-grade portion of the deposit is hosted by heavily fractured, silicic tuffs of the Nopal and Coloradas Formations. The deposit extends into the underlying Pozos Formation, although the grade decreases significantly. In the vicinity of the ore body, the Nopal Formation is a densely welded crystal-lithic rhyolitic tuff with phenocrysts of quartz, sanidine, and biotite. A highly

altered vitrophyre occurs at the base of the formation. The Coloradas Formation is a lithic-crystal, densely welded tuff with phenocrysts of quartz, sanidine, plagioclase, and biotite.

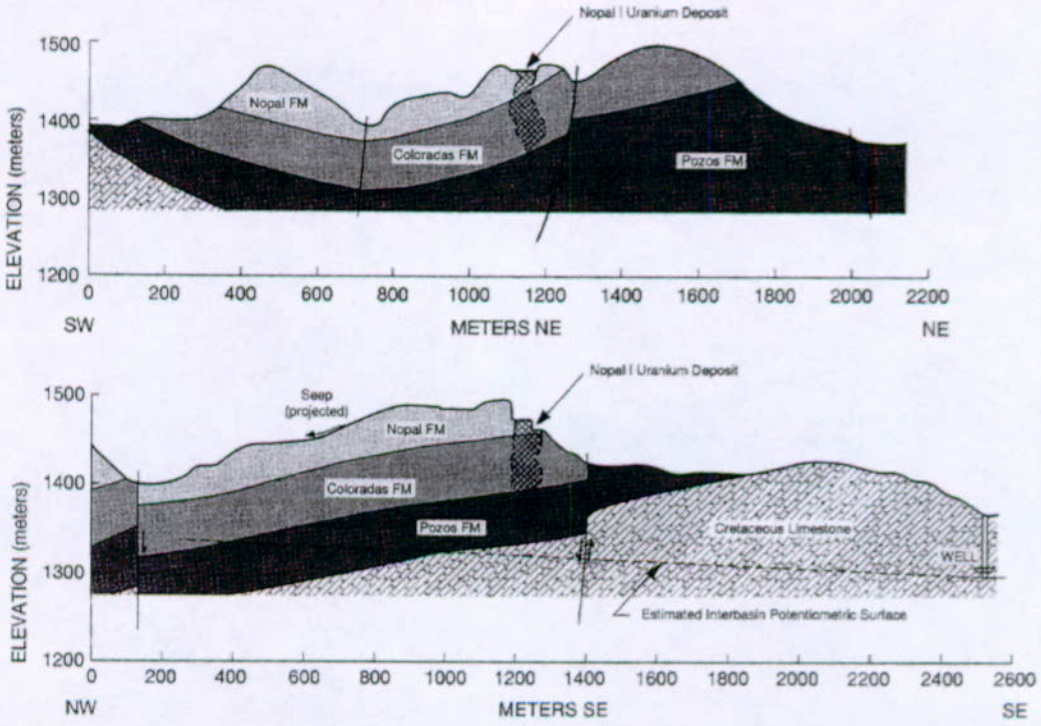

Figure 6-21. Orthogonal, Vertical Cross Sections of the Nopal I Deposit Illustrating Its Location above the Water Table and Within Silicic Tuffs of the Nopal and Coloradas Formations and the Basal Conglomerate of the Pozos Formation (from Pearcy et al. 1994, p. 716)

Uraninite occurs only very locally in highly silicified pods near the center of the ore body. The uraninite is interpreted to be part of a relict ore assemblage that was altered by oxidizing fluids that produced a secondary suite of uranyl oxy-hydroxides (schoepite) and uranyl silicates (uranophane) (Pearcy et al. 1994). Uranophane is the most abundant ore mineral but at least seven other uranium-bearing minerals have been identified (Pearcy et al. 1994, Table 2). Uranophane occurs as euhedral needles as well as granular masses in highly oxidized zones that are also enriched in kaolinite, limonite and chalcedony. The sequence of U-bearing oxidation products observed at Nopal I (uraninite- schoepite- uranophane) is very similar to those produced in laboratory experiments with uranium oxide exposed to oxidizing conditions in the presence of simulated groundwater (Wronkiewicz et al. 1996).

Finally, uranium-rich caliche located at the elevation of the deposit and about 3 m outside the limit of U mineral occurrence has been dated by U-series isochron techniques at 53.6 ± 0.8 ka (thousand years), suggesting that weathering of the deposit has been the dominant mode of alteration for at least that period (Pearcy et al. 1994, p. 714).

6.5.2.1.4 Characterization of Radionuclide Transport Using U-Series Disequilibria

6.5.2.1.4.1 Previous Work

Studies of U-series disequilibria within and around uranium deposits can provide valuable information on the timing of actinide mobility and hence the undisturbed stability of a potential repository over the geologic time scales associated with the required lifetime of the facility. The theory underlying this technique is discussed in Section 6.5.2.1.6.3. This section summarizes studies that have examined uranium transport through fractures within and outside the Nopal I deposit. The interested reader is referred to Attachment III, which contains a bibliography, for a more extensive list of radionuclide migration studies of Peña Blanca.

6.5.2.1.4.1.1 Center for Nuclear Waste Regulatory Analyses Work

The Center for Nuclear Waste Regulatory Analyses (CNWRA) at the Southwest Research Institute, with support of the NRC, has conducted numerous and varied studies with the goal of using Peña Blanca as an analog to Yucca Mountain.

Leslie et al. (1993) and Pearcy et al. (1994) compared the alteration of uraninite from Nopal I to laboratory experiments of degradation of spent nuclear fuel at Yucca Mountain, Nevada. They found that uraninite from the Nopal I deposit should be a good natural analog to spent nuclear fuel because long term experiments on spent fuel show alteration parageneses, intergrowths, and morphologies that are remarkably similar to those observed at Nopal I. Oxidation of the uraninite at Nopal I has produced an ordered suite of minerals, first forming uranyl oxide hydrates followed by uranyl silicates. Consistent with a high calcium abundance in Nopal I, the dominant secondary uranium phase is uranophane, a calcium uranyl silicate. In comparison, laboratory experiments find that the general trend is to form mixed uranium oxides, then uranyl oxhydroxides, then finally uranium silicates, mostly uranophane with lesser amounts of soddyite (Wronkiewicz et al. 1996). Finally, uraninite at Nopal I has a low trace element component (average of 3 wt %) that compares well with that of spent nuclear fuel (typically < 5 wt %).

In an effort to determine the relative mobility of uranium along mesofractures (>1 mm and longer than 10 m – Pearcy et al. 1995, p. 693), microfractures (< 1 mm), and matrix at Nopal I, Pearcy et al. (1994, 1995) mapped and sampled portions of Levels +10 (originally 5 –10 meters below surface before mining operations) and +00 (10 m lower than level +10) of the Nopal I deposit. Approximately 1200 m^2 for level +10 and 200 m^2 for level +00 were painstakingly cleared of loose rocks, soil, and debris. A 1 m × 1 m grid with axes oriented NS and EW was constructed over the two cleared areas and referenced to this framework (see Figure 6-22). Fracture mapping was carried out at a scale of 1:25 and includes 11,374 individual fractures. On Figure 6-22, the visible uranophane line indicates the limit of visible U mineralization and marks the nominal edge of the deposit. The intent of this figure is to note the fine degree of detail in which fracture locations have been mapped. Examination of the distribution of U in the host tuff at scales ranging from 10^{-6} to 10 m indicates that, outside the primary deposit, U occurs mainly along fractures in secondary minerals (and iron hydroxides, oxides, and silicates). Major conclusions from this work (Pearcy et al. 1995), based on both field study and ^{234}U analyses, include:

- Transport of U away from the deposit occurred mainly along fracture paths.
- Transport along mesofractures occurred at 20 times greater distance (up to 30 m) than along microfractures.
- Mobilization of U from the deposit occurred within the last 1 Ma (million years).
- Matrix transport was limited to distances of <1 mm.

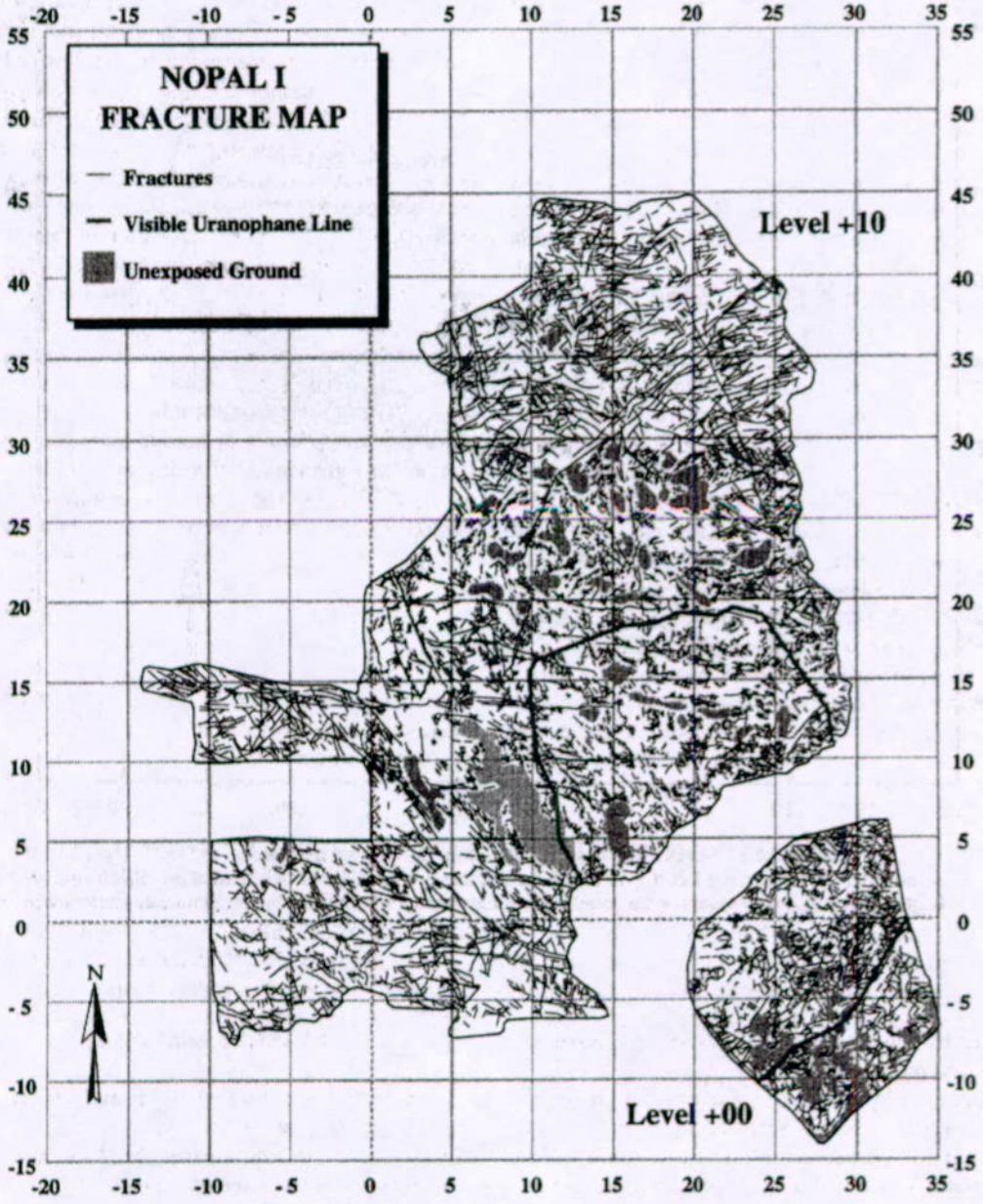

Figure 6-22. Fracture Map of the Nopal I Deposit (from Pearcy et al. 1995, Figure 3). Perimeter Scale is in Meters

Prikryl et al. (1997) reported electron microprobe analyses of U concentration in fracture filling minerals, as well as ^{238}U-^{234}U-^{230}Th alpha spectrometry data on bulk fracture samples from the major E-W trending fracture at 13.5 m N (fracture B). The microprobe results for goethite, hematite, and amorphous Fe-oxyhydroxide minerals and bulk samples indicate that there are strong mineralogic and spatial controls on the distribution of U in this fracture. Uranium concentrations in bulk fracture materials and in goethite and hematite minerals show a decreasing trend away from the ore body. This trend suggests that U was mobilized and transported away from the deposit, most likely by episodic infiltration of meteoric water. Analysis of uranium content at any sample location along the fracture reveals that goethite has a higher U concentration than hematite. This indicates that either uranium has a greater affinity for goethite or that uranium was more enriched in solutions during goethite formation. Uranium and thorium isotopic data on the 13.5 m N fracture (Fracture B) also revealed a $^{234}U/^{238}U$ ratio greater than unity, both within and outside the deposit. This suggests that U mobilization was relatively recent (< 1 Ma) and is related to uptake of U from fracture fluids that carried excess ^{234}U. Variations in $^{234}U/^{238}U$ were interpreted as due to a multistage mobilization process. $^{230}Th/^{234}U$ activity ratios greater than unity were interpreted as due to either 1) ^{234}U loss after ^{230}Th ingrowth, or 2) preferential sorption of ^{230}Th by fracture-filling minerals from solution.

Pickett and Murphy (1997) obtained additional ^{238}U-^{234}U-^{230}Th data for other fractures at Nopal I. Both bulk analyses and results of sequential extractions on fracture-filling materials were reported. They found that most of the data for fracture-filling materials lie in the "forbidden zone," which is the region on a Concordia plot where there is no finite single-stage age solution (see Section 6.5.2.1.4.2.2). This observation led these authors to invoke multiple U mobilization events involving both enrichment and removal over the past few hundred ka to explain these data. The sequential extraction data were also complex. Data for crystalline iron-oxides and resistates were similar to the bulk rock systematics. However, amorphous iron oxyhydroxides were interpreted to be older than bulk rock, and adsorbed or ion exchangeable surface sites were suggested to be younger than bulk rock. They interpreted the ^{238}U-series as well as U/Pb isotopic systematics in terms of U mineral history and the nature and timing of U transport at Pena Blanca. They analyzed three samples of uranophane which gave $^{238}U/^{206}Pb$ and $^{235}U/^{207}Pb$ internal and external isochron ages of 3.4 and 3.2 Ma, respectively. The isotopic and chemical data indicate the following history:

- Primary uraninite mineralization occurred approximately 8 Ma.
- Deposition of uranyl silicates occurred during a single period around 3 Ma.
- Complex episodic U mobilization and remobilization, including dispersion of uranium via aqueous transport into the surrounding fractured tuff, took place over the past few hundred thousand years.

6.5.2.1.4.1.2 University of Texas, El Paso Work

Wong (1998) completed a study of uranium-series disequilibria utilizing gamma spectrometry for fracture-infilling materials at Nopal I. Samples were collected from various fractures both within and outside the deposit including the large fracture (B) at 13.5 m N. Mineralogy of these samples was also determined by x-ray diffraction. The $^{230}Th/^{238}U$ and $^{226}Ra/^{230}Th$ activity ratios ranged from 0.58-1.74 and 0.85-1.54, respectively (Wong, 1998, pp. 87, 93). Samples with higher U concentrations within the deposit had more limited ranges in $^{230}Th/^{238}U$ and $^{226}Ra/^{230}Th$ with activity ratios of ~1.0-1.1 and 0.8-1.1, respectively. Because these are gamma spectrometry data, estimated errors are fairly large, +/- 10% or more. Consequently, it is difficult to draw strong conclusions from these data. However, the observations of disequilibria for both $^{230}Th/^{238}U$ and $^{226}Ra/^{230}Th$ led Wong to conclude that there had been open system behavior for these nuclides, within the past 8 ka for Ra/Th and within the past 300 ka for Th/U.

6.5.2.1.4.1.3 University of Paris Work

Electron paramagnetic resonance has been used at Peña Blanca to detect radionuclide migration. An example of one such study is Allard and Muller (1998), who tested the potential use of point defect centers (essentially radiation damage from absorbed dose) in kaolinite to detect U mobilization. They compared integrated defects to current uranium distribution to infer the past distributions of uranium at Peña Blanca. This investigation indicated two major migration events:

- Past accumulation of U outside the mineralized zone followed by leaching;
- A late-stage accumulation of uranium in the area of the primary uranium deposit.

6.5.2.1.4.2 Recent Work by YMP

Studies of U-series disequilibrium within and around uranium deposits can provide valuable information on the timing of actinide mobility over the geologic time scales associated with the required lifetime of a potential repository. Prior studies at Peña Blanca, summarized in Section 6.5.2.1.4.1, have focused on the extent and timing of uranium-series mobility or transport at this site and concluded open system behavior suggesting mobility of uranium and its daughter products. Previous U-series thermal ionization mass spectrometry (TIMS) work at the Nopal I deposit in Peña Blanca done by Los Alamos National Laboratory (LANL) for the YMP (Murrell et al., 1997) found closed system behavior suggesting very limited mobility in fracture-filling material for U, Th, and Pa for the last 100 to 400 ka. However, these results and conclusions were in contrast to decay-counting data for the same samples obtained by the CNWRA and their conclusion of open-system U behavior (Pickett and Murphy, 1997).

In an effort to settle these apparent discrepancies and to learn the true extent of uranium mobility at Peña Blanca, the YMP analyzed 18 additional samples for ^{238}U-^{234}U-^{230}Th-^{266}Ra and ^{235}U-^{231}Pa in four prominent uranium mineralized fractures. The relevant decay series are as follows:

$^{238}U(t_{1/2}=4.47\times10^{9}\ y) \rightarrow {}^{234}U(t_{1/2}=2.45\times10^{5}\ y) \rightarrow {}^{230}Th(t_{1/2}=7.54\times10^{4}\ y) \rightarrow {}^{226}Ra(t_{1/2}=1600\ y) \rightarrow {}^{206}Pb$

$^{235}U(t_{1/2}=7.04\times10^{8}\ y) \rightarrow {}^{231}Pa(t_{1/2}=3.28\times10^{4}\ y) \rightarrow {}^{207}Pb$

$^{232}Th(t_{1/2}=1.41\times10^{10}\ y) \rightarrow {}^{228}Ra(t_{1/2}=5.77\ y) \rightarrow {}^{208}Pb$

6.5.2.1.4.2.1 Analytical Method

We measured ^{238}U-^{234}U-^{230}Th-^{226}Ra and ^{235}U-^{231}Pa in 18 samples from fractures that emanate from the primary U-bearing zone of the deposit. These samples were obtained from the CNWRA. Sample locations are shown in Figure 6-23. A photograph showing the E-W fracture (Fracture B, 13.5 m N) is shown in Figure 6-24.

The samples consisted of splits of powders (labeled whole rock (WR) or powdered (PWD) on Table 6-10) prepared by the CNWRA, or hand specimens provided by the CNWRA. Hand specimens are labeled "hand sample" or "previous" (if reported by Murrell et al. (1997)) on Table 6-10. Fracture-filling materials were removed from the hand samples in the LANL laboratory for analysis. For the samples prepared in the laboratory, approximately 100 grams of material from each hand specimen were subdivided with a chisel into tuff and fracture-filling mineral fractions of <1 cm size. The fracture-filling mineral fractions of 5-10 g were then homogenized and powdered with a mortar and pestle, and aliquots of 0.5-1 g were taken for U-series analysis. Sample replicates, standard reference ore BL-4 supplied by the Canadian Certified Reference Material Program, geologic reference Table Mountain Latite (TML) supplied by the University of California at Santa Cruz, and blanks were also analyzed.

The aliquots were dissolved in Teflon vials with hydrochloric, hydrofluoric, nitric, and perchloric acids. After treating insoluble fluorides with boric acid, samples were redissolved in 1M (molar) nitric acid and centrifuged to verify complete dissolution. Samples were then quantitatively transferred, and 1M nitric acid stock solutions were prepared in 1-liter polyethylene bottles. Aliquots were spiked with $^{233,236}U$ tracer and ^{229}Th tracer. Uranium and Th were separated by standard anion exchange methods. The U fractions were loaded onto Ta-Re-Ta triple filaments and the Th fractions were loaded onto Re-Re double filaments. These were analyzed in a Sector 54-WARP thermal ionization mass spectrometer (TIMS).

For measurements of ^{226}Ra and ^{231}Pa, separate aliquots equal in mass to the Th and U aliquot were taken and spiked with ^{228}Ra tracer and ^{233}Pa tracer. The Ra fraction was separated by standard cation exchange methods, including a large column for Ra-Ba isolation and small EDTA columns for Ra/Ba separation. The Pa fraction was separated using Eichrom TRUSpec resin, followed by anion exchange columns for Pa/U separation. The Ra fraction was loaded on a Re filament with silica gel and analyzed in the Sector 54-WARP instrument. The Pa fraction was

loaded on a carburized Re filament and analyzed in a NBS 12-90 TIMS. Results for replicates and geologic standards agreed within the quoted uncertainties (see Table 6-10). Most importantly, the results for the geologic standards returned secular equilibrium activity ratios for U-Th and U-Pa (Th-Ra for standards and some samples have yet to be analyzed) indicating that the needed analytical accuracy was obtained (see Table 6-10). Blanks are negligible in comparison with the amounts of these elements in the samples.

Table 6-10. Summary of Results for Fracture and Reference Materials.

Sample	Fracture	Th	(+/-)	U	(+/-)	Th/U	(+/-)	$(^{238}U)/(^{232}Th)$	(+/-)	$^{230}Th/^{232}Th$ x10^{-6}	(+/-)	$(^{230}Th)/(^{232}Th)$	(+/-)	$^{234}U/^{238}U$ x10^{-6}	(+/-)	$(^{234}U)/(^{238}U)$	(+/-)	$(^{230}Th)/(^{234}U)$	(+/-)	$(^{234}U)/(^{232}Th)$	(+/-)	$(^{230}Th)/(^{238}U)$	(+/-)	$(^{231}Pa)/(^{235}U)$	(+/-)	$(^{226}Ra)/(^{230}Th)$	(+/-)
		(ppm)	(%)	(ppm)	(%)	(wt.)	(%)		(%)	(ppm)	(%)		(%)	(ppm)	(%)		(%)		(%)		(%)		(%)		(%)		(%)
TML-97B-1	std	30.461	0.36	10.899	0.09	2.795	0.37	1.089	0.37	5.862	0.36	1.093	0.36	54.959	0.14	1.000	0.14	1.003	0.53	1.089	0.39	1.003	0.51	NA	NA	NA	NA
TML-97B-2	std	30.623	0.31	10.885	0.09	2.813	0.32	1.082	0.32	5.810	0.46	1.083	0.46	54.980	0.14	1.001	0.14	1.001	0.58	1.082	0.35	1.001	0.56	1.006	0.76	NA	NA
BL4	std	12.222	0.34	1714.801	0.09	0.007	0.35	426.992	0.35	2290.600	0.90	426.943	0.90	54.963	0.10	1.000	0.10	1.000	0.97	427.121	0.36	1.000	0.97	0.997	0.70	NA	NA
NOPI-309-WR1	F	34.766	0.31	1266.389	0.09	0.027	0.32	110.858	0.32	623.141	0.20	116.147	0.20	59.257	0.13	1.078	0.13	0.971	0.41	119.555	0.35	1.048	0.38	0.984	0.71	0.987	1.29
NOPI-320-WR1	F	27.595	0.36	424.337	0.12	0.065	0.38	46.799	0.38	140.478	0.29	26.184	0.29	53.839	0.14	0.980	0.14	0.571	0.50	45.856	0.40	0.559	0.47	0.643	0.82	NA	NA
NOPI-376-WR1	C	32.042	0.30	255.831	0.12	0.125	0.32	24.299	0.32	163.315	0.36	30.440	0.36	64.857	0.19	1.180	0.19	1.061	0.52	28.682	0.38	1.253	0.48	NA	NA	0.870	1.16
NOPI-403-WR1	E	38.495	0.34	299.822	0.11	0.128	0.35	23.703	0.35	143.507	0.38	26.748	0.38	57.723	0.16	1.051	0.16	1.074	0.54	24.901	0.39	1.128	0.52	0.993	0.83	NA	NA
NOPI-404-WR1	E	36.379	0.33	131.977	0.08	0.276	0.34	11.041	0.34	73.211	0.80	13.646	0.80	63.990	0.10	1.165	0.10	1.061	0.87	12.658	0.35	1.236	0.87	NA	NA	NA	NA
NOPI-407-WR1	E	36.687	0.33	444.205	0.14	0.083	0.36	36.849	0.36	189.204	0.24	35.265	0.24	51.806	0.18	0.943	0.18	1.015	0.47	34.743	0.40	0.957	0.43	1.005	0.83	0.754	1.13
NOPI-410-WR1	E	42.343	0.31	12.659	0.17	3.345	0.35	0.910	0.35	5.839	0.40	1.088	0.40	63.774	0.18	1.161	0.18	1.031	0.56	1.056	0.40	1.196	0.53	0.998	0.77	NA	NA
NOPI-411-WR1	E	36.446	0.36	14.809	0.14	2.461	0.38	1.237	0.38	9.183	0.43	1.712	0.43	73.332	0.16	1.335	0.16	1.037	0.60	1.650	0.41	1.384	0.58	1.003	0.91	NA	NA
NOPI-418 prev	B	15.955	0.34	5508.559	0.39	0.003	0.52	1050.733	0.52	6917.074	0.18	1289.266	0.18	65.339	0.20	1.190	0.20	1.031	0.62	1250.501	0.56	1.227	0.59	0.990	0.82	0.989	0.75
NOPI-419-hand sample	B	28.896	0.36	238.679	0.11	0.121	0.37	25.138	0.37	210.186	0.53	39.176	0.53	81.740	0.14	1.488	0.14	1.048	0.66	37.396	0.40	1.558	0.64	1.001	0.80	0.924	1.24
NOPI-420-PWD	B	26.895	0.32	1303.204	0.14	0.021	0.35	147.468	0.35	930.444	0.16	173.425	0.16	62.339	0.19	1.136	0.19	1.036	0.43	167.470	0.40	1.176	0.38	0.984	0.83	0.839	1.09
NOPI-421-hand sample (LANL)	B	36.501	0.34	893.188	0.17	0.041	0.38	74.471	0.38	512.600	0.37	95.543	0.37	66.899	0.17	1.218	0.17	1.054	0.56	90.671	0.41	1.283	0.53	NA	NA	NA	NA
NOPI-421 prev	B	36.010	0.34	871.040	0.47	0.041	0.58	73.615	0.58	503.606	0.28	93.867	0.28	66.818	0.20	1.216	0.20	1.049	0.67	89.520	0.61	1.275	0.64	0.993	0.79	0.764	0.65
NOPI-423-PWD	B	49.477	0.35	583.132	0.12	0.085	0.37	35.869	0.37	228.380	0.25	42.567	0.25	63.005	0.19	1.147	0.19	1.035	0.48	41.129	0.42	1.187	0.45	1.002	0.90	NA	NA
NOPI-423-hand sample	B	37.028	0.34	299.824	0.09	0.123	0.35	24.643	0.35	165.206	0.29	30.793	0.29	64.818	0.16	1.180	0.16	1.059	0.48	29.070	0.39	1.250	0.46	0.988	0.73	1.003	1.13
NOPI-424-hand sample	B	34.996	0.32	61.854	0.09	0.565	0.33	5.389	0.33	34.030	0.51	6.343	0.51	62.753	0.12	1.142	0.12	1.031	0.62	6.148	0.36	1.177	0.61	1.002	0.91	0.975	0.87
NOPI-425 prev	B	34.731	0.32	295.600	0.49	0.117	0.59	25.903	0.59	162.739	0.28	30.333	0.28	62.126	0.20	1.131	0.20	1.036	0.68	29.287	0.62	1.171	0.65	0.997	0.89	0.834	0.84
NOPI-425-hand sample (LANL)	B	38.048	0.34	127.948	0.11	0.297	0.36	10.234	0.36	63.681	0.30	11.870	0.30	61.357	0.19	1.117	0.19	1.039	0.50	11.428	0.41	1.160	0.47	0.996	0.88	1.121	0.68

Submitted with this AMR under DTN: LA9909MM122122.001

Note: This table summarizes the concentration and isotopic data obtained for samples from fractures at the Peña Blanca uranium deposit in Mexico. The data for the isotopes in parentheses are radioactivity ratios.
NA=not analyzed

INTENTIONALLY LEFT BLANK

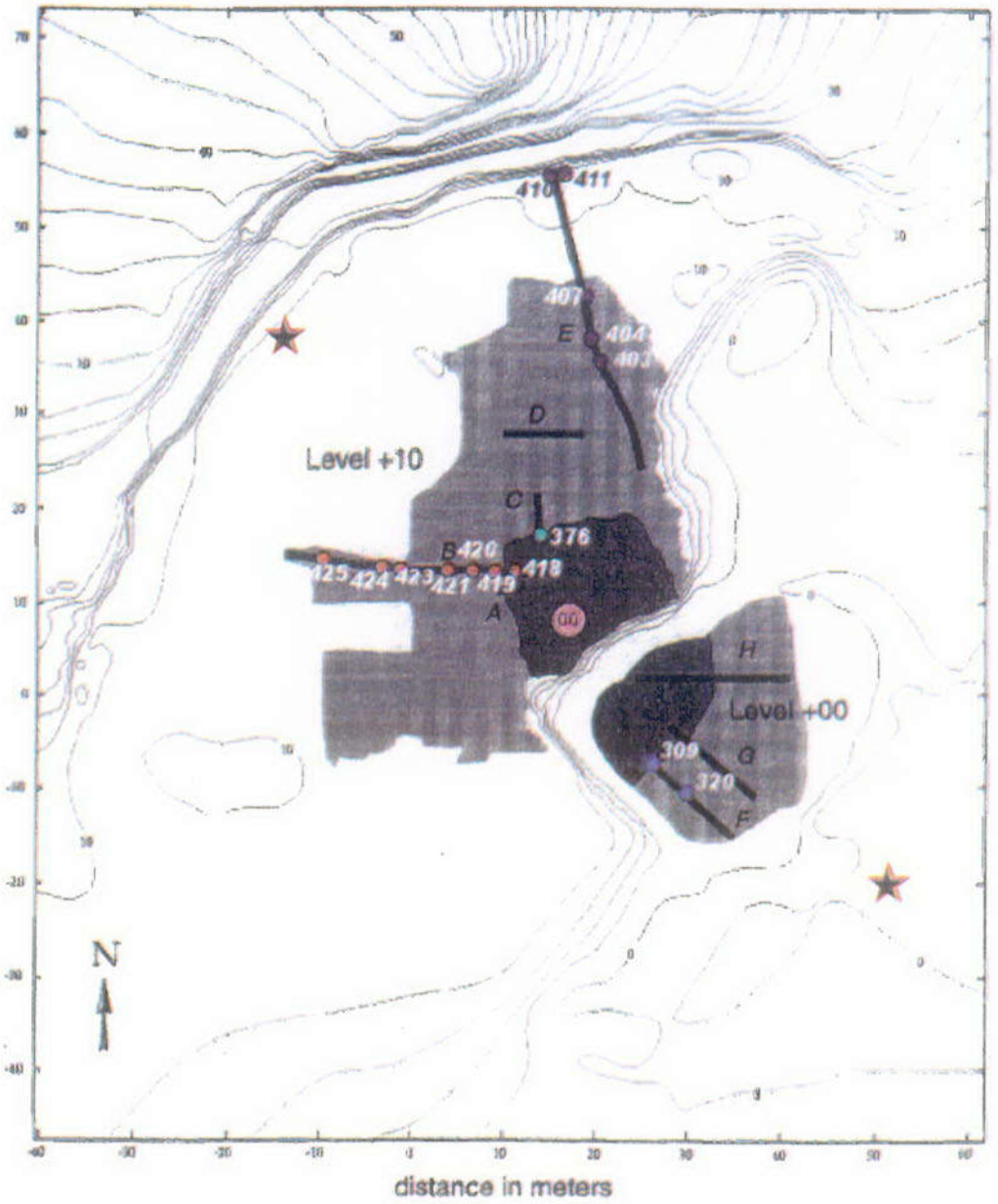

Figure 6-23. Topographic Map for Nopal I Area (modified from Pickett and Murphy 1997, Fig. 1). The figure illustrates the extent of visible uranium mineralization (black shaded area), major fractures A-H located near the deposit, sample locations from this study, and proposed locations for drilling of near-field groundwater monitoring wells (stars and location marked 00)

Figure 6-24. Photo of the +10 Level of Nopal I. The arrows illustrate the location of the major east-west trending fracture B, looking to the east. Most of the samples in this study are from this fracture

6.5.2.1.4.2.2 Uranium and Thorium Isotopic Results

Results for uranium and thorium isotopes for the samples and standards are shown in Table 6-10. Uranium concentrations for the samples generally decrease from the outer margin of the deposit to the far end of the fractures, in general agreement with prior studies (Pearcy et al. 1995; Wong 1998). The absolute concentrations for the powders agree well with the results obtained by Pickett and Murphy (1997). However, the U concentration results for the hand samples that we prepared are often lower than powders prepared by the CNWRA from the same location. This difference indicates less fracture material and more matrix in our samples.

$^{234}U/^{238}U$ activity ratios are shown in Figure 6-25 and range from 0.94 to 1.49 with a mean of about 1.2. There is no obvious systematic spatial trend for these data within the fractures. These results are also similar to values reported by Pickett and Murphy (1997). The $^{234}U/^{238}U$ results are generally consistent with an old ^{234}U enrichment (~100-1000 ka; calculated model ^{234}U ages from Ivanovich and Harmon 1992, pp. 55-58) produced during dissolution processes and preserved in precipitated minerals. However, as can be seen from Figure 6-25, there appears to be small-scale post-depositional loss and gain of ^{234}U to the fracture materials that have spread the distribution about the mean.

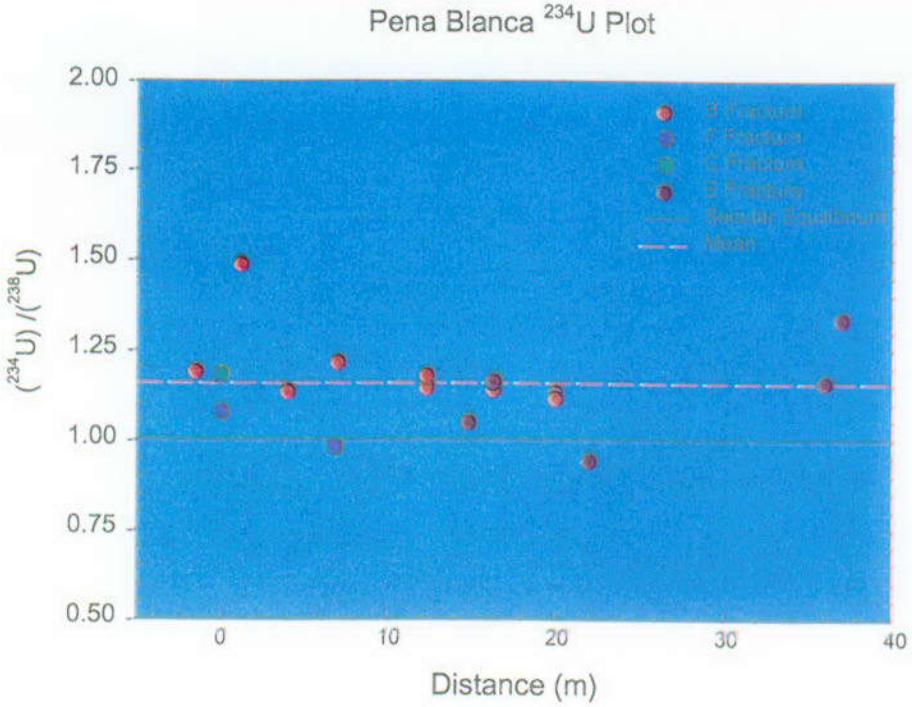

(Data in Table 6-10, DTN: LA9909MM122122.001)

Figure 6-25. Plot of $^{234}U/^{238}U$ Activity Ratio versus Distance from the Edge of the Deposit for the Fracture Samples in This Study (see Table 6-10)

Figure 6-26 has been modified from Pickett and Murphy (1997) by addition of typical error bars and data from Murrell et al. (1997). In this type of plot, known as a Concordia plot, the evolution of a closed system through time is shown by the curved arrow labeled "time." Most of the data of Pickett and Murphy (1997) fall in the "forbidden zone," the region of no finite single-stage age solution. These values have led Pickett and Murphy (1997) and Wong (1998) to invoke multiple U mobilization events involving both U enrichment and removal over the past few hundred thousand years to explain their data. The values are a consequence of their higher $^{230}Th/^{234}U$ and variable $^{226}Ra/^{230}Th$ measurements, which cannot be explained by a simple model of closed system evolution. The $^{230}Th/^{234}U$ activity ratios we observe are generally close to 1 (see Table 6-10). These values differ significantly from those obtained by Pickett and Murphy (1997). These latter values are difficult to discern from secular equilibrium using the decay-counting methods employed by previous studies. This difficulty may be the reason for the difference between the more precise TIMS data and Pickett and Murphy's (1997) results and conclusions.

6.5.2.1.4.2.3 Uranium-Thorium Ages

Because the fracture minerals were deposited by aqueous solutions, the ages of the mineral phases are related to the timing of the primary fluid flow. Subsequent alteration of these mineral phases during more recent fluid movement can also be evaluated using uranium-series disequilibria data. As shown in Figure 6-27 (analytical errors are smaller than the points and are <1%), we found that the majority of the U-Th data provide finite solutions to the age equation, and while most points plot very near the "forbidden zone," only two points (NOPI 403 and NOPI 407) actually fall in

this area. The data for these two samples are consistent with small amounts of ^{234}U loss. Model U-Th ages for the other samples indicate ages of greater than 300 ka (with the exception of a discordant sample (NOPI 320) also indicating ^{234}U loss). These model ages are summarized in Table 6-11.

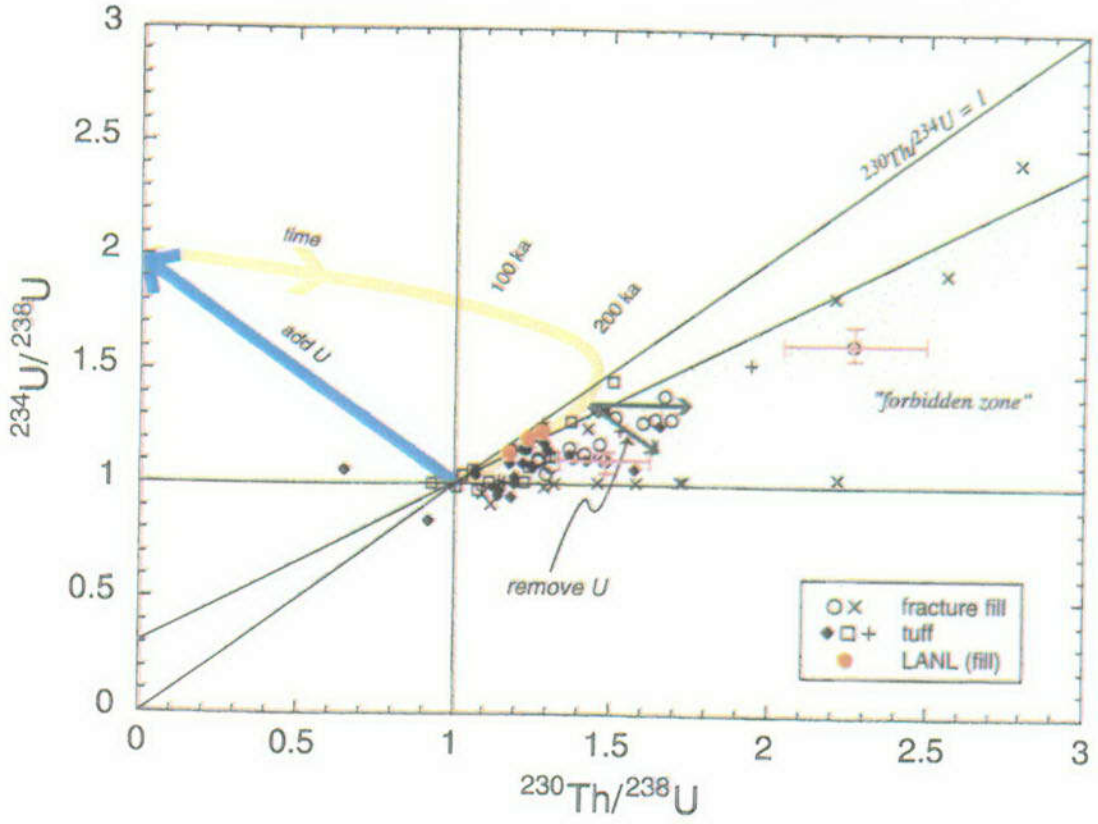

NOTE: Error bars for data of Pickett and Murphy (1997) are typical and have been added to the figure.

Figure 6-26. Plot of Measurements of $^{234}U/^{238}U$ versus $^{230}Th/^{238}U$ for Fracture Filling Materials Obtained by the CNWRA (from Pickett and Murphy 1997, Figure 4), with Added Data (Identified as LANL) from Murrell et al. (1997).

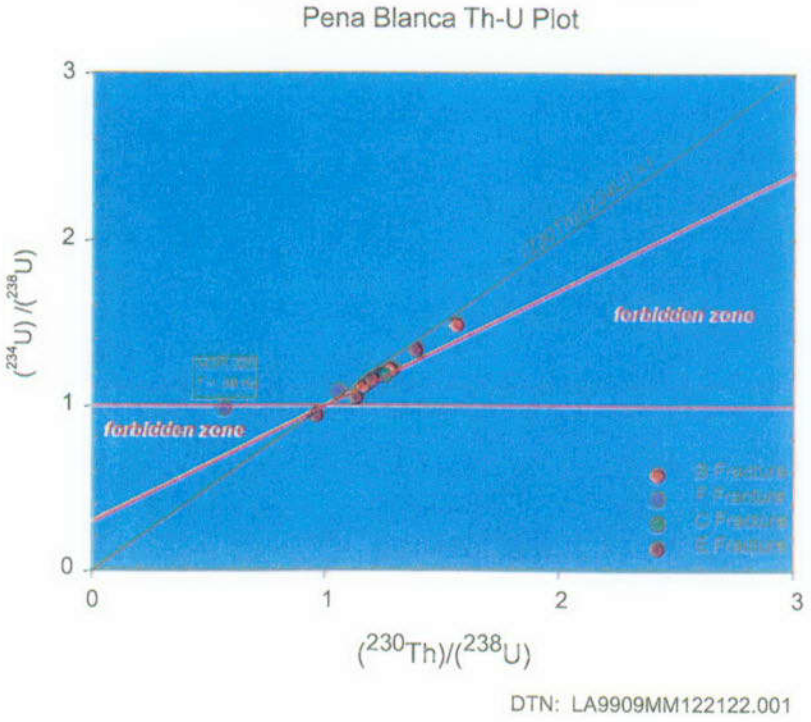

Figure 6-27. Plot of Measurements of $(^{234}U)/(^{238}U)$ versus $(^{230}Th)/(^{238}U)$ for Fracture Filling Materials from This Study (Table 6-10)

The ages in Table 6-11 are calculated using zero initial ^{230}Th in the samples. Because such a model is not strictly correct, such ages are upper limits on the true age. This is generally a small effect given the high U concentrations in these samples. However, there is a clear correlation noted for Fracture B that is related to the Th/U of the sample, with highest ages for samples with the lowest authigenic component and greatest Th/U. Since the model ages appear to be noticeably affected by the relative abundances of authigenic and non-authigenic components in the samples, a correction is needed to obtain an age for only the authigenic component (i.e. true age of deposition) (Ivanovich and Harmon 1992, pp. 55-57). Hence, we use the measured Th/U ratios to correct the measured $^{230}Th/^{234}U$ and $^{234}U/^{238}U$ ratios for the non-authigenic component within these samples. This is accomplished by plotting the data in two diagrams consisting of $^{234}U/^{238}U$ versus $^{232}Th/^{238}U$, and $^{230}Th/^{238}U$ versus $^{232}Th/^{238}U$ (Figure 6-28) (Ludwig and Titterington 1994). If the samples along the fracture are isochronous, are derived as mixtures of two components, and behaved as a closed system, then these plots will yield a linear trend or isochron. The y-intercepts of the weighted least square fit of the points correspond to the $^{230}Th/^{234}U$ and $^{234}U/^{238}U$ ratios in the authigenic components of the samples. The program Winfit finds a least squares fit with weighting in two dimensions. This is required for the isochron fit. Based on these ratios, the calculated age for the authigenic component is 425 ± 80 ka (7 points). Based on this age, initial $^{234}U/^{238}U$ activity ratios are ~2, in reasonable agreement with typical values for modern water samples near Nopal I (Pickett and Murphy 1999, Table 2). While this isochron age for Fracture B agrees with the uncorrected data from NOPI-418 (398±20 ka), the sample with the

highest U concentration, the fit is not exact and one point (NOPI 419) is far off the best-fit lines. This means that at least one of the model requirements has been violated.

Table 6-11. U-Th Model Ages

Sample	U-Th Age ka	+/-
NOPI-309-WR1	324	9
NOPI-320-WR1	88	4
NOPI-376-WR1	630	120
NOPI-404-WR1	>780	
NOPI-410-WR1	424	24
NOPI-411-WR1	342	11
NOPI-418 previous	398	20
NOPI-419-hand sample	320	9
NOPI-420-PWD	485	27
NOPI-421-hand sample (LANL)	461	20
NOPI-421 previous	438	28
NOPI-423-PWD	464	17
NOPI-423-hand sample	589	100
NOPI-424-hand sample	454	34
NOPI-425 previous	500	50
NOPI-425-hand sample (LANL)	578	100

Submitted with this AMR under DTN: LA9909MM122122.001

NOTE: Model assumes zero intial Th and closed system behavior since deposition.
Such assumptions may not be valid for all samples.
Blank intended.

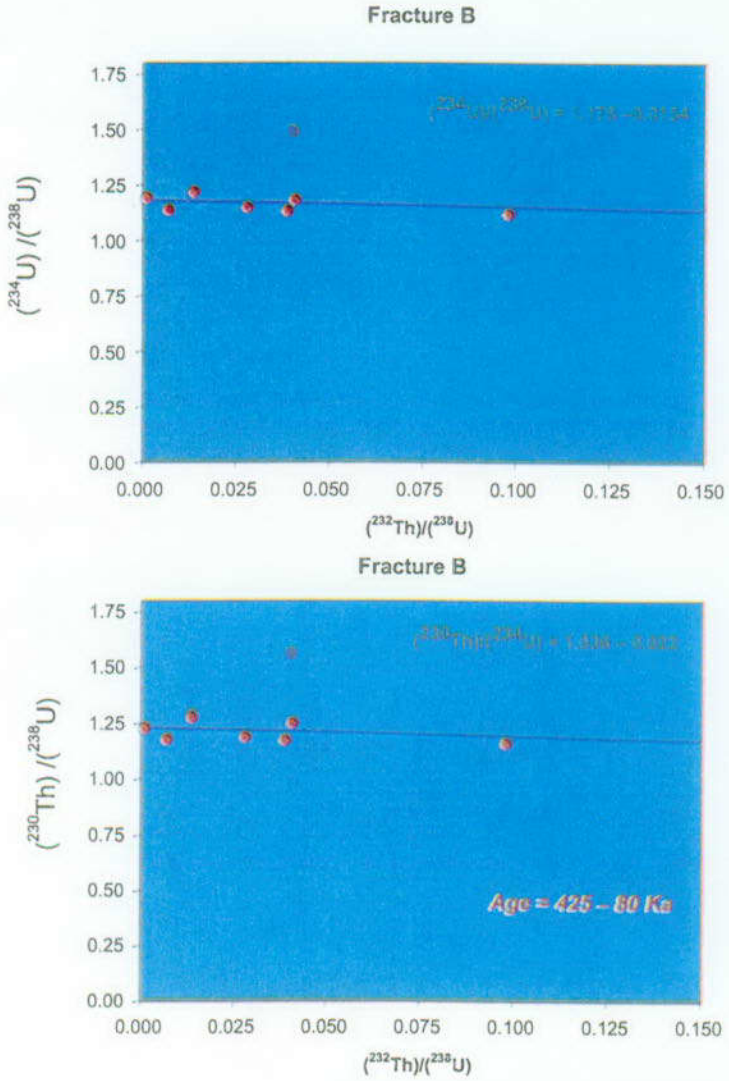

DTN: LA9909MM122122.001

NOTE: $(^{234}U)/(^{238}U)$ and $(^{230}Th)/(^{238}U)$ activity ratios for the authigenic components are the y-intercepts of the weighted least squares fits. The isochron is calculated from the quotient, $(^{230}Th)/(^{234}U)$.

Figure 6-28. Diagrams of $(^{234}U)/(^{238}U)$ versus $(^{232}Th)/(^{238}U)$, and $(^{230}Th)/(^{238}U)$ versus $(^{232}Th)/(^{238}U)$ for Samples from Fracture B.

6.5.2.1.4.2.4 Protactinium Isotopic Results

Results for ^{231}Pa for the samples and standards are shown in Figure 6-29. Analytical errors are smaller than the data points and are typically <1%. The $^{231}Pa/^{235}U$ activity ratios are either at or very near secular equilibrium (sample mean = 0.996 ± 0.007). This means that ^{231}Pa-^{235}U (and ^{238}U since the 238/235 ratios are natural) have behaved as a closed system in the fractures over the last 200 ka. From these observations we can conclude that uranium (235, 238) has remained in the fractures over the last 200 ka. Based on these results, the mobility of uranium discussed above seems limited to the ^{234}U.

As can been seen from Figure 6-29, NOPI 320 is younger, with a U-Pa model age of 47 ± 2 ka. This sample also has an anomalously low U-Th model age of 88 ± 4 ka. The U-Pa model age is similar to U-Th ages for caliche and opal (Pearcy et al. 1995, p. 714) of about 50 ka and may indicate enhanced fluid flow at this time. This event caused resetting of sample NOPI 320 but had no measurable effect on U (235,238), Th, or Pa mobility in the vast majority of fracture samples. The difference in U-Pa and U-Th ages for this sample may be a result of post-depositional loss of ^{234}U from this sample (but not $^{235,238}U$).

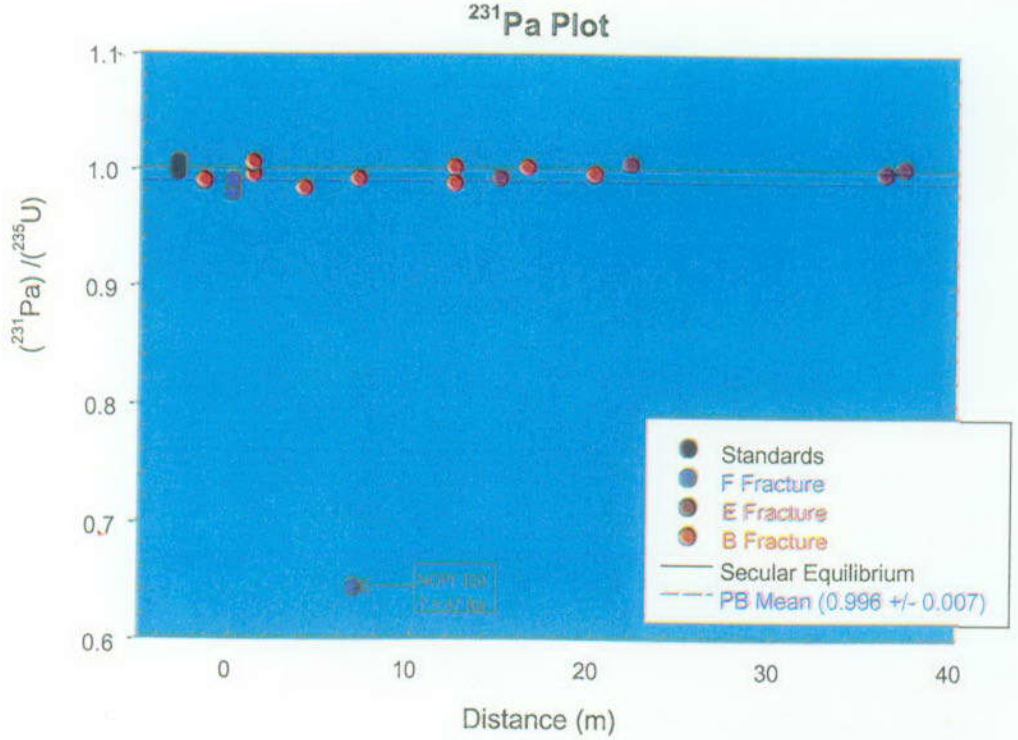

(Table 6-10, DTN: LA9909MM122122.001)

Figure 6-29. Plot of $^{231}Pa/^{235}U$ Activity Ratio versus Distance from the Edge of the Deposit for the Fracture Samples in This Study

6.5.2.1.4.2.5 Radium Isotopic Results

Results for $^{226}Ra/^{230}Th$ for the fracture samples are shown in Figure 6-30. The $^{226}Ra/^{230}Th$ activity ratios range from 0.7 to 1.1. These results are similar to values reported by Wong (1998, pp. 87, 93). The $^{226}Ra/^{230}Th$ results are consistent with open system Ra behavior over the last 5 ka. It is useful to point out that the Ra results demonstrate that fluids have occupied the fractures over the last 5 ka, which implies that U has had ample opportunity for fluid interactions. It is also interesting to note that a variety of plant (*Phacelia robusta*) growing in the vicinity has very high radium contents (Leslie et al. 1999).

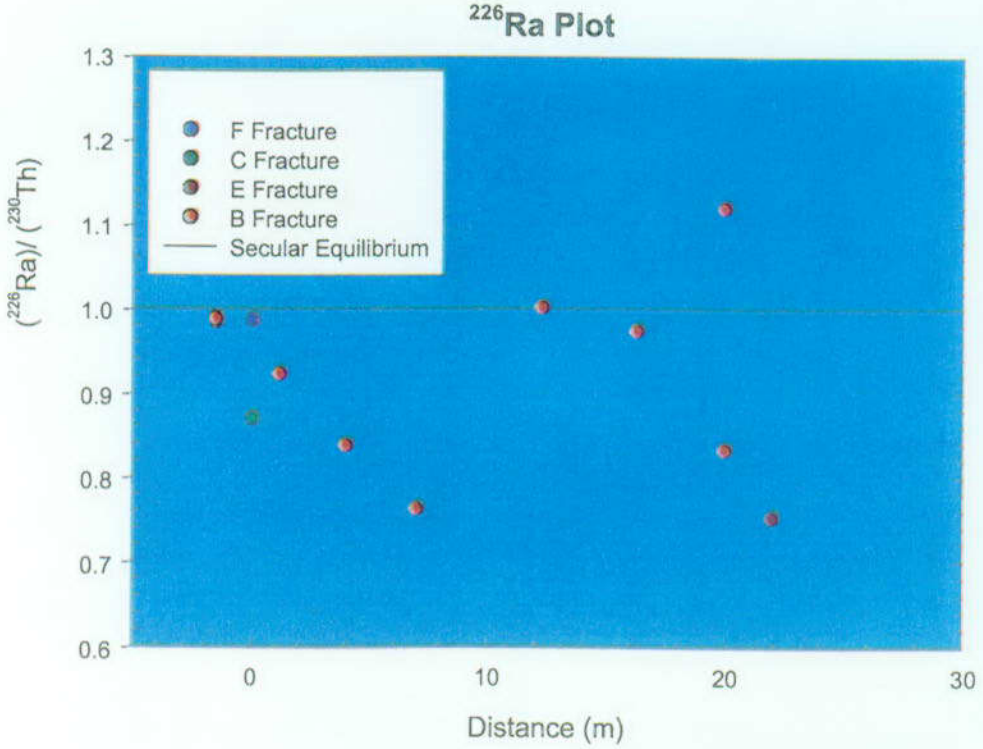

(Table 6-10, DTN: LA9909MM122122.001)

Figure 6-30. Results for $^{226}Ra/^{230}Th$ versus Distance from the Edge of the Deposit for the Fracture Samples

6.5.2.1.4.2.6 Discussion and Conclusions of U-series Analyses

Transport of some U-series nuclides at Peña Blanca has occurred over a range of time scales. From the U-Th age data it appears that the primary transport of U to the fractures occurred more than 300 ka ago. Subsequently, there has not been significant ^{238}U or ^{235}U redistribution. The $^{231}Pa/^{235}U$ activity ratios for the fracture samples support this conclusion. Results for one anomalous sample along with U-Th ages for opal and caliche (Pickett and Murphy 1997, p. 121) suggest enhanced aqueous fluxes at ~50-90 ka and local U mobility. The enhanced flux had no effect on U (235,238), Th, or Pa distribution in the remainder of the fracture samples. The $^{226}Ra/^{230}Th$ activity ratios indicate redistribution of radium within the last 5 ka due to secondary fluid events. These sorts of interactions appear to have also produced small redistributions of ^{234}U. Presumably, this reflects the preferential mobility of ^{234}U resulting from selective leaching and direct-recoil effects. Such effects are well-documented in rock-water systems (e.g., Ivanovich and Harmon 1992) and are manifested by aqueous phases with elevated $^{234}U/^{238}U$. The fine-grained nature of the fracture filling materials makes this mechanism especially effective at Peña Blanca. Therefore, while we were unable to reproduce Pickett and Murphy's (1997) results in detail, we did confirm a recent but limited redistribution of ^{234}U along fractures. In an analog sense, this stability should extend to transuranics and the rare earth elements. The high mobility of Ra is also noteworthy and should be considered in modeling transport of Sr and Cs.

Our results indicate that the uranium (235, 238), thorium, and protactinium in the fracture-filling minerals have remained stable for more than 300 ka. This stability has apparently survived even recent hydrologic disturbances from surface water infiltration of the fracture due to mining activities, as well as the infiltration of rainwater since the fractured rock was uplifted above the water table (Pearcy et al. 1994, p. 714). Results for one anomalous sample and opal/caliche dating suggest that hydrologic disturbances occurred ~50 ka ago. In addition, the radium disequilibria data suggest that hydrologic disturbance(s) also occurred over the past 5 ka. Hence, it appears that uranium, thorium, and protactinium in secondary fracture materials are unaffected by surface water infiltration and perhaps saturated ground-water flow over ~100 ka time scales. This research provides one important indication of the probable immobility of those radionuclides in a high-level nuclear waste repository over its required lifetime.

The two data sets discussed above (Figure 6-26 versus Figures 6-27 through 6-30) directly contrast with each other in their final interpretations. The major implication of the Pickett and Murphy (1997) and Wong (1998) data is that the host rhyolitic tuffs around Nopal I have not effectively retained the uranium mobilized from uraninite alteration. Their results suggest that the rocks at Yucca Mountain may not be effective barriers to actinide migration. In contrast, the more precise TIMS data (this work) indicate that the geochemical system at Nopal I restricts actinide mobility in the unsaturated environment. By analogy with our results, the tuffs at Yucca Mountain should have similar retentive properties to impede oxidized uranium mobility. The accumulation of natural analog data from Peña Blanca and similar sites would be of particular importance if it demonstrates the general validity (or the converse) of low actinide mobility in unsaturated siliceous tuffs under semi-arid climate conditions.

6.5.2.1.5 Aqueous Transport of Uranium at Peña Blanca

Complementary to studies of fracture-filling materials, Pickett and Murphy (1999) recently presented measurements of U-Th isotopic composition and concentration in various water samples collected near the Nopal I uranium deposit. They analyzed samples of three different types: perched water trapped in an old borehole about 20 m outside the deposit, seep water obtained from an old adit approximately 8 m below the +10 m surface, and a groundwater sample located in the regional carbonate aquifer 1.3 km southeast of the deposit. They also measured the major element chemistry of these samples including major anions, cations, pH, pO_2, and conductivity. Samples were generally filtered (0.20 μm filter) and acidified in the field, with the exception of the seep waters, which were filtered and acidified 11 months after collection.

Uranium concentrations range from 170 ppt for the groundwater, to 200-900 ppt for the seep water, to 5 ppb for the perched water. Thorium concentrations range from 0.14 ppt (parts per trillion) for the groundwater, to 0.5 – 1.2 ppt for the seep water, to 16 - 27 ppb (parts per billion) for the perched water (Pickett and Murphy 1999). The U and Th concentrations generally correlate with concentrations of major cations and anions and total conductivity, which may reflect evaporation-dilution or rock dissolution effects on all of these species. Th and U concentrations also correlate strongly with each other, which is surprising given the expected differences in solution chemistry and potential solubility controls for these two elements.

Pickett and Murphy (1999) interpret these concentrations in the context of solubility control by various uranium silicate minerals (haiweeite, soddyite) and thorianite. They find that the perched

water is close to solubility for haiweeite, a calcium uranyl silicate mineral. All of the other waters are undersaturated with respect to uranium mineral phases. However, all of the waters are supersaturated with respect to thorianite, which is attributed to the presence of colloidal Th in the <0.2 um fraction of these samples. The overall correlation between Th and U is left unexplained, but seemingly points to greater control on concentrations by evaporation followed by dilution or rock dissolution effects. Kinetic factors present in natural systems will also complicate the interpretations based on thermodynamic solubility.

Reaction path modeling suggests that uraninite dissolution under oxidizing conditions without continuous water replenishment will lead to a secondary U assemblage dominated by schoepite, allowing higher aqueous U contents ($4x10^{-5}$ molal) than if controlled by uranyl silicates (Pickett and Murphy 1999). However, their data also show that the secondary U assemblage at Nopal I is dominated by uranyl silicates, which indicates geochemical processes other than those they modeled.

$^{234}U/^{238}U$ activity ratios are highest for the seep water (2.85-5.07), lower for the perched water (2.19), and still lower for the groundwater (1.39). A positive correlation between 1/U concentration and $^{234}U/^{238}U$ for the perched and seep waters is consistent with selective leaching of ^{234}U in dilute seep waters versus greater dissolution for the perched waters. This interpretation is also consistent with results for the major element concentrations and Th discussed above. Pickett and Murphy interpret the lower $^{234}U/^{238}U$ ratio in the carbonate aquifer as resulting from prolonged interaction with old calcites, allowing U exchange and masking preferential leaching/recoil effects for ^{234}U.

$^{230}Th/^{232}Th$ activity ratios are also highest for the seep water, which, along with the higher $^{234}U/^{238}U$, may reflect greater influence of selective leaching/recoil effects. $^{230}Th/^{234}U$ activity ratios are quite low (< 0.01) relative to typical values in the rock of 1-1.5, indicating that Th is significantly less mobile than U.

6.5.2.1.6 Ongoing Work at Nopal I

During the summer of 1999, a group of investigators from the Yucca Mountain Site Characterization Project (YMP) went to the Peña Blanca district to see the deposits first-hand and to evaluate the need for future work. Based on discussions held during this trip, we recommend the following areas for future work.

6.5.2.1.6.1 Three-Dimensional Studies

Previous work at Peña Blanca has primarily been in two dimensions with data for only exposed planar surfaces. Some of the fractures that are exposed on the surface actually extend through the deposit in the vertical plane. Little has been done regarding boreholes, and we do not know if there has been preferential flow/drainage downward through such fractures. For this reason, there is a need to extend geochemical studies to the third dimension. This extension will be accomplished with a borehole through the deposit. The proposed location for this borehole is shown in Figure 6-23 (position 00) and in Figure 6-31. Analyses of recovered core would provide

samples by which to evaluate the downward path of radionclide migration. Analyses would consist of major elements, U-series, Sr, and oxygen isotopes.

Figure 6-31. Photo of the +10 Level, Illustrating the Location of a Proposed Drill Site to Recover Rock Core as Well as Groundwater. The location is within the zone of uranium mineralization at the feet of the person in the photo.

6.5.2.1.6.2 Groundwater Studies at Nopal I

Although the Pickett and Murphy (1999) study provides some useful preliminary data for waters at Nopal I, they were limited by availability of samples. Thus, numerous outstanding questions remain with respect to uranium and uranium-series transport. The extent and spatial dependence of uranium transport from the deposit via groundwater cannot be thoroughly evaluated without higher resolution sampling of any potential groundwater uranium plume in the vicinity of the deposit. In addition, colloidal transport of Th (and Pa or possibly U) is suggested by their preliminary work, but cannot be verified without concentration versus size fraction studies on filtered or ultrafiltered water samples. Measurements of radium isotopes serve as an analog for Cs or Sr transport at Yucca Mountain, but have yet to be obtained for aqueous samples. Solubility effects on both uranium and thorium concentrations have been considered by Pickett and Murphy, but generally don't appear to be of primary importance. Collection of additional samples and further analyses to address other possible mechanisms such as pH dependent sorption, solution complexation, evaporation-dilution, and rock dissolution should be useful to discern the important mechanisms controlling U concentration and transport.

To address these issues, a series of water-producing wells are proposed for the site. These wells would be located at 00 (see Figures 6-23 and 6-32) and +50 m and –50 m (Figure 6-23) and –500 m and +500 m. The proposed locations of the +50 and + 500 wells are marked in Figure 6-32. The depth to the water table is not known but is thought to be about 200 m, based on

depths of nearby wells. In addition to these wells, perched water samples and samples from seepage tests are being collected. Sampling of the wells and seep are being conducted seasonally to monitor variability over time. Analyses consist of major cations and anions, U-series, Sr, and oxygen isotopes.

Figure 6-32. Photo from the +10 Level, Illustrating Possible Locations of Near-Field (50 m) and Far-Field (500 m) Groundwater Monitoring Wells (Stars). These locations are expected to be down-gradient in the regional aquifer and useful for characterization of any potential uranium plume from the deposit

6.5.2.1.6.3 Modeling Radionuclide Transport at Peña Blanca

With the availability of solid and fluid samples for analyses as described above, there should be sufficient data to model radionclude transport at Peña Blanca using a natural analog approach. Such an approach is based on the parent-daughter relationships for the U and Th decay series. For example, in an undisturbed rock that is sufficiently old for the daughters to have grown into secular equilibrium, the activity of a parent radioisotope is identical to that of all its daughters. However, in environments where water passes through and interacts with solid phases, the different geochemical behavior of the nuclide leads to significant radioactive disequilibria between parents and daughters in the fluids and associated solids (e.g. 234/238 ratios for the fracture materials and water at Peña Blanca). Both thermodynamic and kinetic factors play a role in creating and maintaining the disequilibria. By modeling the local mass-balance of the various radioisotopes, with constraints placed by their different decay rates and the parent-daughter relationships, one can derive information on the rates of adsorption-desorption and transport of contaminants under a given geochemical and hydrologic environment, on time scales of days to 1,000,000 years (Ku et al. 1992).

We have just completed such a study at INEEL that provides quantitative data on:

- Regional flow patterns and preferential flow paths
- Retardation factors for U, Th and Ra
- The migration velocity of specific types of contaminants through the aquifer
- Rock dissolution rates

The information obtained from the natural analog study at Peña Blanca could be used to understand and predict the mobility (or retardation) of radioactive contaminants at Yucca Mountain. For example, uranium is itself of concern and is also geochemically similar to some transuranic elements, e.g., neptunium; Th (IV) can be used as a proxy for Pu (IV), Pa (V) for Pu (V), etc. The transport rate of ^{137}Cs, ^{90}Sr and ^{133}Ba can be inferred from that of ^{226}Ra, provided that the geochemical fractionation between Cs, Sr, Ba and Ra can be reasonably determined by measuring their concentrations in fluid and rock samples. The natural analog approach has advantages over laboratory studies and theoretical calculations in that the natural analog approach takes into account the combined effects of variable speciation, geologic heterogeneity and geologic time scales. These parameters are commonly difficult to accurately duplicate in laboratory and theoretical studies, but could be determined *in situ* at Peña Blanca using samples from the proposed sampling effort.

6.5.2.1.6.4 The Timing of Recent U Mobilization at Peña Blanca

As discussed in Section 6.5.2.1.4, much of the TIMS evidence supports the conclusion that the system has been closed to many U-series radionuclides for 300 ka. However, some evidence, consisting of U-Th dates of ~50 ka for caliche and opal (Pickett and Murphy (1997)) and a U-Pa age for fracture sample NOPI 320 (this study), indicates a younger mobilization event for at least some radionuclides. The timing, nature, and extent of such events need to be evaluated further for Peña Blanca in order to judge their importance at Yucca Mountain. We obtained initial samples of opal and calcite during our field trip to the site and will determine U-series and stable isotope data for these samples.

6.5.2.2 Uranium Deposits in Northern Nevada

Most natural analogs to radionuclide transport are located in saturated environments (e.g., Oklo, Gabon; Cigar Lake, Canada) or in shallow, weathered saturated/unsaturated sites (e.g., Alligator Rivers, Australia; Bangombe, Gabon). With regard to unsaturated zone analogs, in addition to Peña Blanca, the McDermitt Caldera uranium deposits and other uranium deposits in northern Nevada and southeastern Oregon have been mentioned as possible analogs to potential UZ radionuclide transport processes at Yucca Mountain (Alexander and Van Luik 1991). YMP representatives, including the AMR originator, visited a number of the deposits in 1995 to observe the geologic setting and characteristics of mineralization first-hand. As a follow-up to Project interest, Castor et al. (1996) compared features of sixteen of the deposits, five of which are located in settings with a thin vadose zone. These are the Moonlight, Bretz, and Opalite mines of the McDermitt caldera, Virgin Valley deposits of northwestern Nevada, and Painted Hills deposits near Reno, Nevada (Figure 6-33). Mines in the Lakeview District and Steens Mountain areas of southeastern Oregon all occur in saturated rhyolite flows, bedded tuff or mafic volcanic rock. Mineralization of the McDermitt caldera is discussed in Wallace and Roper (1981). For more

detail on all of the deposits, the interested reader may consult the extensive reference list in Castor et al. (1996).

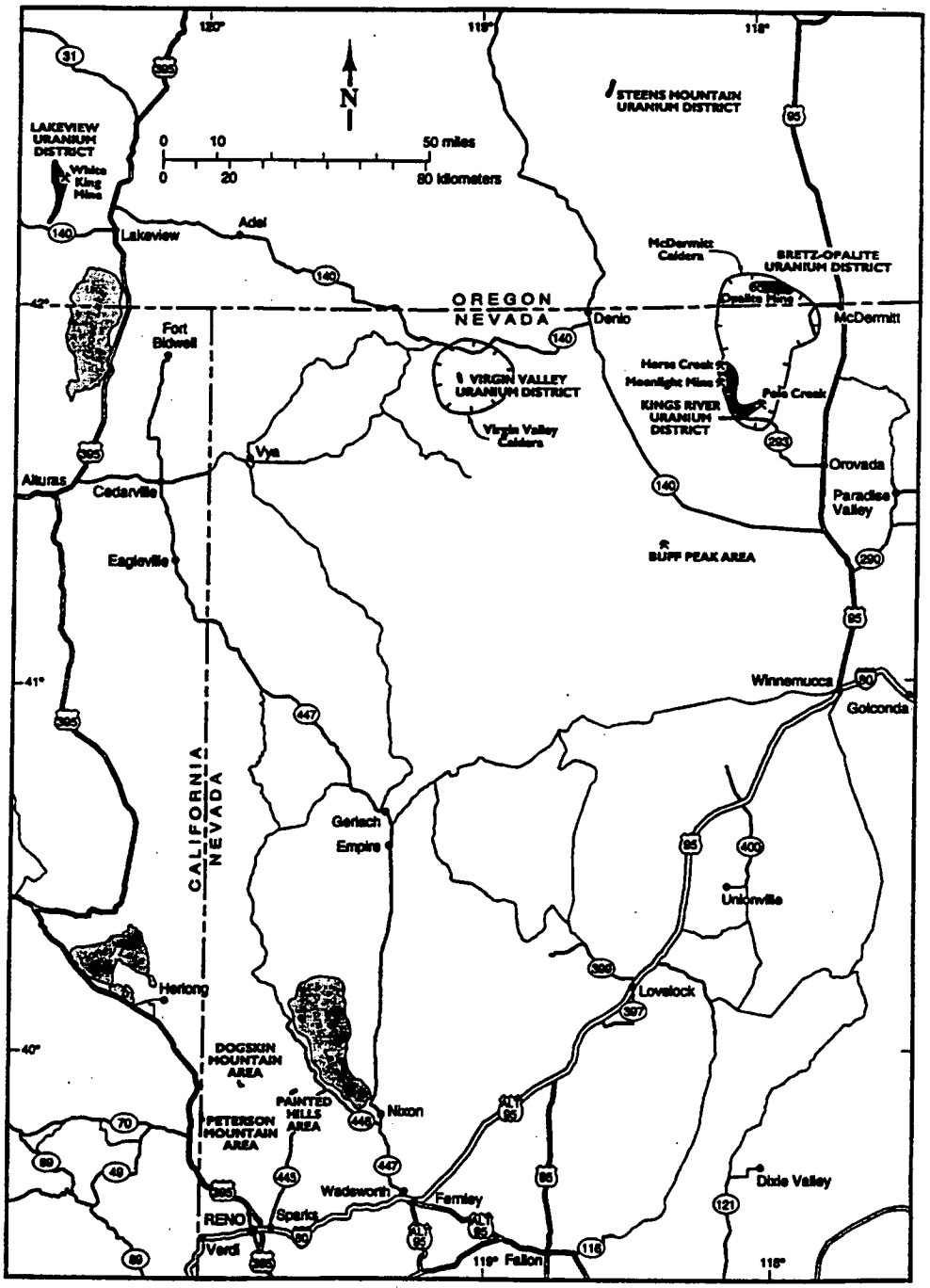

Figure 6-33. Location Map of Uranium Districts in Northern Nevada and Southeastern Oregon (Castor et al. 1996, Figure 1)

The age of tuffs in the McDermitt caldera and Virgin Valley is 15.7 to 16.5 Ma (Castor et al., 1996). Depth to the water table is 38 to 50 m. At the Moonlight mine, uranium deposition has occurred along faults; host rocks are dacite flows and rhyolite ash flow tuffs in the footwall and biotite rhyolite breccias in the hanging wall. Ore deposition was associated with epithermal fluids and occurs mainly in the rhyolite breccias. The Moonlight mine is the only area at McDemitt with recorded uranium production (approximately 700 kg of U_3O_8 with an average grade of approximately 0.13% U_3O_8). The ore at Moonlight is exposed by an inclined adit about 80 m deep that is presently flooded at a depth of about 50 m.

At the Bretz and Opalite mines, mineralization is associated with mercury (1.6% Hg) in hot springs and caldera ring fracture faults in silicified breccia. Uranium deposition is genetically related to magmatic systematics in the Virgin Valley caldera and is associated with airfall and minor ash flow tuffs, and lacustrine sediments including diatomite and lignite. Stratiform opal deposits contain uranium and uranium is also found along fractures in rhyolitic breccia. In the Painted Hills district near Reno, uranium mineralization is associated with late-stage mineralization within a caldera, and notable concentration is found at the contact between rhyolitic ash flow tuff and a basalt dike and as fracture filling in the tuffs. Of the sites discussed above, zeolites were observed only in the Virgin Valley area but have been reported at the Bretz and Moonlight mines. In all of the deposits mentioned, uranium is found as U(VI); only at the Moonlight mine is it also found as U(IV) in association with zircon.

Some of the uranium mineralization at McDermitt caldera and the other northern Nevada deposits may constitute good analogs to aspects of radionuclide transport at Yucca Mountain, but this is questionable for several reasons. One reason is that the host volcanic rocks for these deposits are somewhat different (i.e., peralkaline rhyolite and trachyandesite flows, bedded tuffs, lacustrine sediments, and basalt dikes). Another reason is that the uranium mineralization is fine-grained and low in concentration in these deposits. Age of deposition is poorly constrained for most of the deposits. Drilling has taken place in only two of the areas, which could provide solid samples for analyses; hydrologic data are sparse. Previous characterization has included the geologic setting of uranium deposition, uranium oxidation state, primary and secondary mineral assemblages, and a little water chemistry (Table 6-12).

Table 6-12. Water Chemistry Characteristics of Northern Nevada/Southeastern Oregon Uranium Districts (modified from Castor et al. 1996, Table 12).

Study site	Water Type	Temperature (°C)	pH	TDS** (mg/L)	Depth to water (m)
McDermitt caldera area	Ca-Na-HCO_3-SO_4	0-28	6.8-9.4	66-724	50
Virgin Valley, nonthermal	Na-HCO_3-SO_4	7-24	6.4-9.7	95-184	<60
Virgin Valley, thermal	Na-SO_4-HCO_3	26.5-92	7.5-9.05	600-630	<60
Lakeview	Ca-Na-HCO_3	7.8	6.3-8.1	-	0
Bottle Creek	Ca-Na-HCO_3-SO_4	7-90	6.4-10.1	42-1216	-
Dogskin Mountain	Ca-Na-HCO_3	-	-	86-121	-
Yucca Mountain	Na-HCO_3-SO_4	33.8-44	6.8-8.7	245-530	28-752*

* Higher values (>300 m) are most representative of the water level depth beneath Yucca Mountain.

**TDS - Total dissolved solids

DTN: LB990930123122.001

Furthermore, the origin of the Virgin Valley and Painted Hills deposits is uncertain. Deposition by ascending fluids along dike barriers is suggested since mineralization occurs almost exclusively along footwalls of mafic dikes. At both the Painted Hills deposits and at Virgin Valley, evidence suggests remobilization and redeposition of uranyl minerals to account for local enrichment. Source term information needed for models is lacking.

In summary, answers to the following questions are needed for all of the northern Nevada deposits discussed before analogies could be made regarding potential transport at Yucca Mountain: (1) timing and mechanism for emplacement of primary uranium mineralization; (2) distribution of diagenetic minerals and their relation to uranium mineralization; (3) age, source, and trapping mechanism of fracture-controlled uranium mineralization; (4) physical and chemical hydrologic attributes of the system. In spite of their appealing proximity to Yucca Mountain for ease of study, the northern Nevada uranium deposits would require extensive additional characterization before data could be used in any sense for building confidence in flow and transport process models.

6.5.3 Analogs to Coupled Thermal-Hydrologic-Mechanical-Chemical (THMC) Processes

6.5.3.1 Introduction

The emplacement of heat-generating waste in a geologic repository located in an unsaturated zone will cause perturbations to the natural environment through heat transfer resulting from convection and conduction and by associated geochemical and geomechanical changes taking place in the repository near-field and altered rock zones. Although data collected from heater tests have significantly advanced the Project's understanding of thermohydrologic processes and coupled behavior, it will be difficult to measure repository thermohydrologic behavior deterministically, because of both the expense of carrying out these types of laboratory and *in situ* experiments, and the experiments being too limited for the time frame over which the processes take place. Natural analogs provide opportunites for testing models and building understanding in thermally coupled processes by assessing data from fossil hydrothermal systems, by observing ongoing processes in geothermal fields, and by using data from geothermal systems to test and build confidence in numerical modeling codes and in thermodynamic and kinetic databases. The following subsection discusses the three opportunities for application of natural analogs in that order.

6.5.3.2 Fossil Hydrothermal and Intrusive Contacts

The effects of shallow (<500 m) magmatic intrusions into unsaturated rocks can be quite different from effects associated with deeper hydrothermal systems. This section examines the thermally coupled hydrologic-chemical (THC) processes that are relevant to THC interactions during the repository post-closure period and provides natural analog cases where the effects of magmatic intrusion and attendant heating have been studied in both saturated and unsaturated systems.

Processes that are relevant to THC interactions during the repository post-closure period include the following: zeolitization of volcanic glass, affecting transport pathways and sorption; potential dehydration of zeolites and vitrophyre, causing water release and affecting heat and fluid flow; effect of heat on sorption properties; changes in water chemistry resulting from interactions between engineered barriers and groundwater, which may affect seepage and flow; and fracture

permeability changes caused by dissolution or precipitation of minerals, including formation of mineral caps.

A good analogy for understanding future repository behavior is the fossil hydrothermal system at Yucca Mountain itself (Bish and Aronson 1993). Detailed mineralogical examination of Yucca Mountain tuffs showed that most zeolitic alteration occurred 13 to 11.6 Ma, at about the same time as tuff emplacement. After formation of the major zeolitic horizons, deep-seated hydrothermal activity persisted until about 10 Ma. This activity was limited to temperatures of 90 to 100°C, the zeolite stability limit; at prolonged exposure to temperatures greater than 90°C, the sorptive zeolites clinoptilolite and mordenite are altered to analcime plus quartz and/or calcite.

Conceptual models for mineral evolution at Yucca Mountain (Carey et al. 1997) suggest that the most likely mineralogical reactions caused by repository heating would include dissolution of volcanic glass and precipitation of clinoptilolite, clay and opal-CT; dissolution and precipitation of silica polymorphs (cristobalite, opal-CT, tridymite, and quartz); alteration of feldspars to clays; and, finally, reactions involving calcite and zeolites. Figure 6-34a illustrates paleotemperatures that were inferred from mineralogical data in several drillholes at Yucca Mountain. Measured present-day temperature profiles are shown for comparison. It can be seen from the figure that present-day temperatures in the drillhole G-3, which is within the repository block, compare closely to inferred paleotemperatures. In contrast, increasingly higher paleotemperatures are inferred for drillholes G-1 and G-2 which are closer to the center of the Timber Mountain caldera source of eruption (G-2 being the farthest north). Figure 6-34b shows mineral and glass abundances and clay mineralogy from GU-3/G-3 drill core that were used to infer the paleotemperatures. Similar mineral abundance diagrams for G-1 and G-2 drill core indicate a northward progression of an increasing abundance of clays and zeolites along with decreased abundance of glass. This is in keeping with the reactions stated above.

Thermodynamic modeling results indicate that the stability of various zeolites is a function of silica activity, temperature, aqueous sodium concentration, and the mineralogy of silica polymorphs. Increasing temperature or sodium concentration causes the alteration of zeolites to other phases. Kinetic effects are, however, important in assessing the significance of thermodynamic and natural analog study conclusions. Kinetic data suggest that saturated conditions are necessary for notable progress in these reactions, as discussed by Carey et al. (1997). Therefore, under ambient conditions the reactions are likely to proceed more slowly in the Yucca Mountain unsaturated zone (excluding perched water zones) than below the water table. Similarly, the persistence of opal-CT below the water table indicates that silica reaction kinetics at Yucca Mountain are slower than laboratory studies would suggest (Carey et al. 1997). However, if prolonged boiling occurred in saturated tuffs, significant progress in all these reactions could occur. The thermal design of the repository would limit the occurence of temperatures above 100°C to the Topopah Spring welded unit, and in any case, the current Enhanced Design Alternative (EDA-II) design scenario calls for sufficient drift spacing so that temperatures between drifts remain below boiling (CRWMS M&O 1999c).

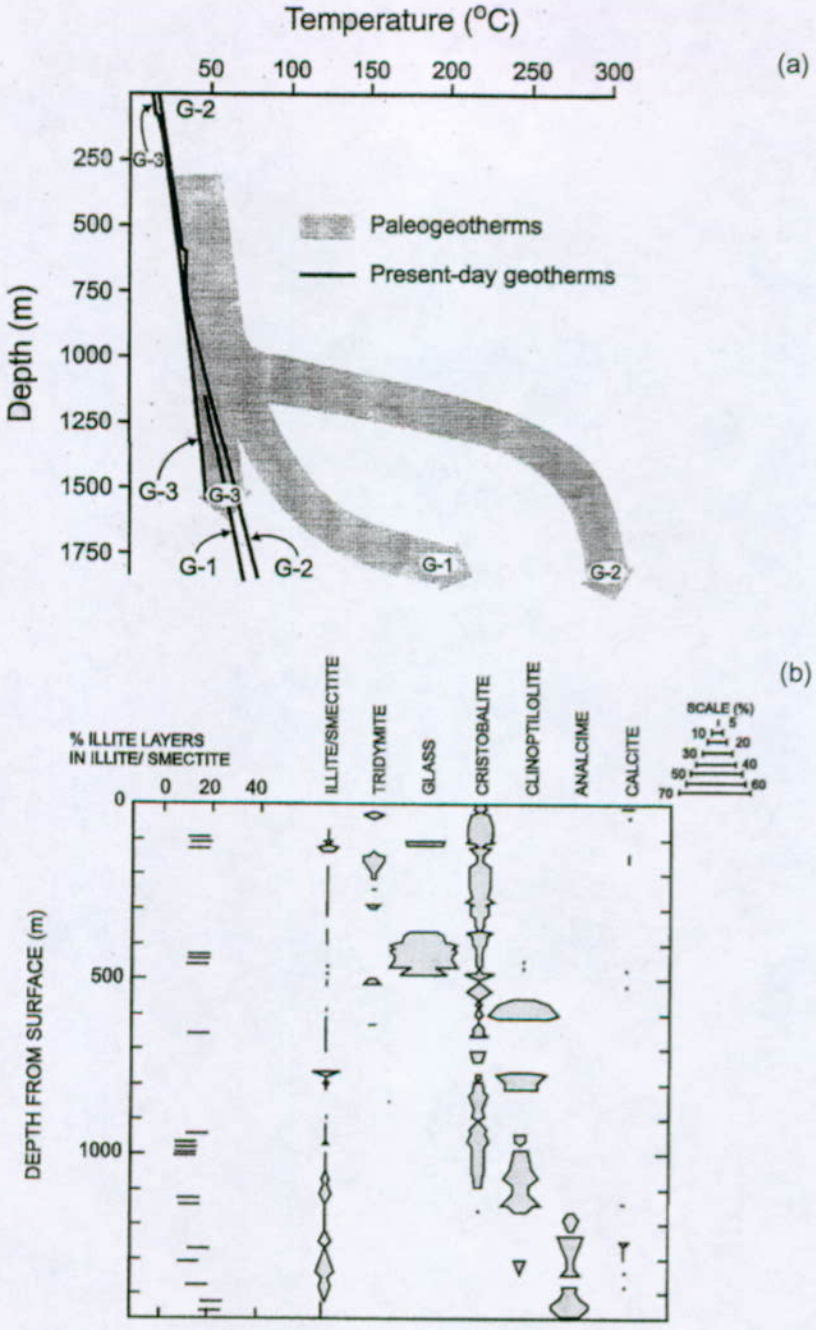

Figure 6-34. Anticipated Mineral Alteration at Yucca Mountain. (a) illustrates paleotemperatures inferred from mineralogical data in drill holes USW G-3, G-2, and G-1 along with present-day temperature profiles. (b) compares mineral and glass abundances in drill core USW GU-3/G-3 determined by x-ray powder diffraction (CRWMS/M&O 1998a, pp. F6.1-75, 76).

In addition to considering Yucca Mountain as a self-analog, contacts between igneous intrusions and host rock may provide useful information as coupled process analogs. Numerous igneous intrusion contact zones have been examined with the objectives of understanding chemical reactions and migration of elements away from the heated contact zone as well as understanding THC effects, both in saturated and unsaturated systems. In early studies, elemental migration across the 2-m-wide contact zone around the Eldora Stock in Colorado was investigated as an analog to elemental transfer in a crystalline repository during heating by waste canisters (Brookins 1986; Wollenberg and Flexser 1986). Oxygen isotope data showed a distinct contrast between the 60 Ma quartz monzonite stock and the Precambrian metamorphic country rock, which Wollenberg and Flexser (1986) interpreted to indicate a lack of hydrothermal convective cooling. No systematic uranium enrichment or depletion that could be related to distance from the contact was detected (Wollenberg and Flexser 1986), but data were insufficient to ascertain whether uranium mineralization occurred before or after emplacement of the stock.

In contrast to the Eldora stock, intrusion of the Alamosa River, Colorado stock, a monzonite body that intruded tuffaceous and andesitic volcanic rocks about 30 Ma ago (Brookins 1984), appears to have established a large-scale convecting hydrothermal system (Brookins 1986). Alteration of the tuffs is observable to 60 m from the contact with the occurrence of calcite intergrown with the rock matrix, chlorite and sericite, quartz overgrowths, and epidote (Wollenberg and Flexser 1986). The contact itself contains a dense intergrowth of epidote, sphene, and fine hematite-filled fractures. Uranium occurs in sphene but is otherwise absent from the contact (Wollenberg and Flexser 1986). Concentration gradients of Cs, Th, and Co in the tuff increase toward the contact, but other trace elements show no indication of migration between the stock and the tuff (Wollenberg and Flexser 1986).

The effects of shallow (<500 m) magmatic intrusions into unsaturated host rocks can be quite different from effects associated with deeper hydrothermal systems, which have been studied more extensively, and of which the two previously mentioned studies are examples. One study in an unsaturated environment was the contact between the Banco Bonito obsidian flow and underlying Battleship Rock tuff in a steep-walled canyon on the southwest rim of the Valles Caldera, New Mexico. This site has been the focus of a number of analog studies (Krumhansl and Stockman 1988; Stockman et al. 1994). The Banco Bonito flow filled a steep-walled canyon cut in the Battleship Rock tuff about 400 ka ago. Present hydrologic conditions are unsaturated. The obsidian, initially at temperatures of 850°C, heated the porous tuff in the canyon walls to 150-350°C for decades, and, according to models, vaporized much of the pore water, and caused refluxing of water. Contact effects include a reddish "baked" zone extending tens of feet into the tuffs. Krumhansl and Stockman (1988) found that Cs and Rb showed little variation with distance from the contact whereas Th, Ta, Hf, Co and rare earth elements showed slight concentration trends; however, it is possible that these trends may have predated the obsidian flow. Stockman et al. (1994) observed no evidence of trends in trace element migration at the contact; however, water and Cl are depleted near the contact, whereas F is slightly enriched toward the contact. No evidence of hydrothermal alteration was noted, suggesting that the area was unsaturated at the time of contact.

The Valles analog site presents several interesting features. First, the Battleship Rock Tuff is very homogeneous in major and trace element composition, such that it would be possible to detect

distinct elemental differences caused by heating at the contact. Second, there is no hydrothermal overprint that could blur the effect caused by deposition of the obsidian flow. Based on a detailed mineralogical, chemical, and isotopic study, Stockman et al. (1994) concluded that, overall, the effects of heating in this unsaturated environment appeared to have been slight and were limited to the tuff nearest the contact. Some evidence existed for devitrification and migration of volatile elements in the tuff within 10 meters of the contact, but variations in major and trace element chemistry were small and difficult to distinguish from the natural variability of these elements in the rock. Apart from devitrification, the principal mineralogic change in tuff near the contact was the development of feldspar-silica linings on voids in the pumiceous tuff matrix; no significant development of zeolites was found. It was not possible to map paleoisotherms from the heating event, but Stockman et al. (1994) developed a model to predict the temperatures in the obsidian and tuff as a function of time. The model predicts the movement of a boiling front several tens of meters into the tuff over several hundred years and is relatively insensitive to assumed saturation.

The influence of a shallow basaltic intrusion into pyroclastic deposits at Grants Ridge, New Mexico, was studied by WoldeGabriel et al. (1999). At this location, a 2.6 Ma basalt plug intruded into 3.3-Ma nonwelded, pumice-rich, compositionally homogeneous, rhyolitic tuff and volcaniclastic sediments. A 10-m-wide aureole characterized by color variation, contact welding, brecciation, partial melting, and stoping developed around the 150-m wide basalt plug. Despite the high-temperature basaltic intrusion, there was no evidence in the country rock of pervasive hydrothermal circulation and alteration that could have been caused by extensive fluid-driven convective heat transfer. WoldeGabriel et al. (1999) found that the proportion of volcanic glass, volatile species, Fe, and some trace element and rare earth element contents in the host rocks were somewhat depleted at the contact of the intrusion. In contrast, the degree of devitrification and potassium content were higher along the contact. The authors postulated that vapor-phase expulsion of elemental species could have been responsible for the minor depletion of elements during devitrification of the silicic glass at near-solidus temperature related to the basaltic intrusion.

The Woldegabriel et al. (1999) study performed finite-difference numerical modeling to model the Grants Ridge intrusion as a dry, conduction-dominated system and compared its results with those of an analytical solution and with the heat and mass transfer code FEHM (Zyvoloski et al. 1992, 1997). Modeling results, which agreed well with geochemical and mineralogical data, indicated that contact welding of the host rocks apparently occurred at temperatures > 700°C under a density-driven lateral load of approximately 1 Mpa, corresponding to the observed depth below the former ground surface of ~100m. Other physical changes in the host rock, represented by partial devitrification and color changes, apparently occurred at temperatures of 500 to 600°C, which probably persisted for up to 55 years after emplacement of the basaltic plug (WoldeGabriel et al. 1999). Because devitrification is generally enhanced by the presence of aqueous fluids, the abundance of volcanic glass within a short distance (~10 m) from the plug is consistent with the authors' inference that the plug intruded into an unsaturated environment. Although no apparent hydrothermal alteration was recognized in the contact zone, this field study and others like it provide an upper temperature bound natural analog to evaluate the effects of heat from decay of radioactive waste. Results of these types of studies are also important for performance assessment of basaltic magma intrusions into or close to a potential repository environment. Field and

laboratory data from the analog study can also be used to build confidence and to calibrate models of such processes within similar physical and chemical environments.

In the Paiute Ridge area of the Nevada Test Site, late Miocene basaltic magma intruded a sequence of 22 to 11 Ma tuffs in a single magmatic pulse (Lichtner et al. 1999). The intrusions formed as dikes, sills, and lopoliths. The original depth of the intrusions was on the order of 150 to 250 m (Crowe et al. 1983). A contact aureole ~3 m wide surrounds the intrusions. Matyskiela (1997) studied alteration surrounding one intrusion, the 50-m-wide Papoose Lake sill, in proposing the Paiute Ridge intrusive complex as a natural analog for THC processes at Yucca Mountain. Matyskiela's (1997) analysis was based on a pure heat conduction model. Matyskiela's (1997) model results indicated maximum temperatures in the tuff host rock of 550°C and cooling times ranging from 10 to 400 years. Matyskiela's (1997) major finding was alteration of glass shards to cristobalite and clinoptilolite within 60 m of the intrusion. He interpreted the alteration as hydrothermal in origin, resulting from emplacement of the intrusion (although he never conclusively demonstrated that the alteration post-dated the intrusion). Most significant was Matyskiela's (1997) observation of complete filling of pore spaces with silica at fracture-matrix interfaces, thus creating open conduits for infiltrating fluid flow along fractures.

Matyskiela (1997) estimated enhanced fracture flow to be as much as five times ambient conditions. This is the opposite behavior to formation of a silica cap, as predicted by recent simulations conducted for Yucca Mountain (Hardin 1998, pp. 5.57-5.58) in which fractures would become filled with quartz or chalcedony, thus inhibiting further flow. Here a contradiction exists between modeling results and limited field observations that needs to be resolved. An issue is the extent to which a fracture can be filled by the silica contained in matrix pore water. Figure 6-35 shows that for a given matrix porosity, the degree of sealing of the fracture depends on the fracture volume fraction and the particular silica polymorph that precipitates (Lichtner et al. 1999). This analysis is predicated upon the assumption that as pore fluid in the matrix is brought into equilibrium with respect to a particular silica polymorph (e.g., amorphous silica) at boiling conditions, the matrix fluid boils and escapes into the surrounding fracture network. As the fluid vaporizes, its released silica content precipitates in fractures. Lichtner et al.'s (1999) two-phase numerical simulation results suggest that at distances of tens of meters from the larger of the Paiute Ridge intrusions that they studied (width $\geq$ 39 m), prolonged boiling conditions were established for times on the order of several thousands of years. The analysis shown in Figure 6-35 represents a limiting case and is dependent on all pore water flashing to steam in the fracture, as assumed in Section 5, Assumption #11. Amorphous silica, with its higher solubility, gives the largest fracture filling, followed by chacedony and quartz. For complete sealing of the fracture, a very small fracture volume fraction is necessary. Moderate filling could represent fracture coatings that armor the fracture.

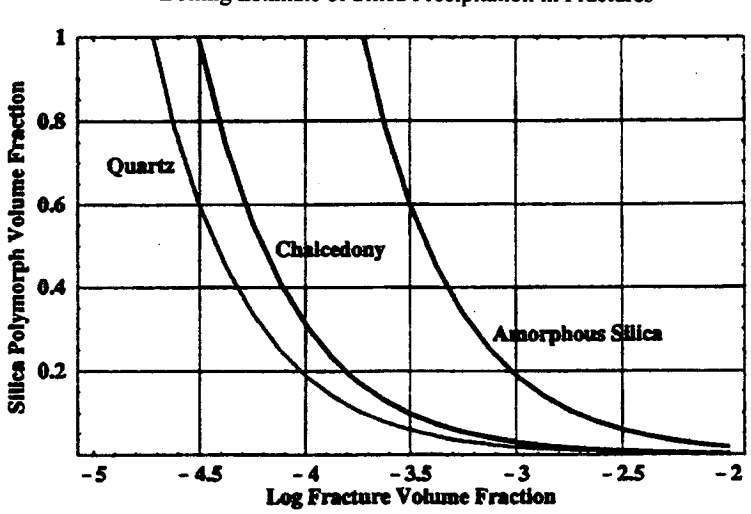

Figure 6-35. Volume of Silica Polymorphs Precipitated in Fracture as a Function of Volume Fraction for a Matrix Porosity ϕ_m = 0.1 (from Lichtner et al. 1999, Figure 10). A volume fraction of one represents complete filling of the fracture, assuming that the fracture was initially open.

THC processes can be better constrained through analysis of selected intrusive complexes hosted in unsaturated tuffaceous rock. The ideal intrusion to serve as a natural analog to THC processes anticipated at a Yucca Mountain repository should have been emplaced above the water table, should be of sufficient size to produce enough heat to sustain boiling conditions for times on the order of several thousand years (~30 m width), and should occur in host rock of similar composition and characteristics to the Topopah Spring Tuff. The Paiute Ridge intrusive complex satisfies the first two criteria, but the tuff host rock into which it has intruded is a nonwelded vitric tuff. Nevertheless, this does not exclude it as a meaningful analog. Field observations at the Paiute Ridge complex could help to determine key mineral reactions and possible reaction rates.

In summary, in both the Banco Bonito study and the Grants Ridge basalt intrusion study, the effects of high-temperature intrusions into unsaturated environments appeared to have been slight, to have been limited to within 10 m or so of the contact, and to show no evidence of fluid driven convective heat transfer or pervasive hydrothermal alteration of the country rock. These field studies, along with the Paiute Ridge field studies, provide data for assessment of magmatic intrusions into or near a potential repository. But just as importantly, they provide a limiting case natural analog for evaluating effects of heat from decay of radioactive waste in an unsaturated environment.

6.5.3.3 Geothermal Systems

Many processes that are expected to take place under repository conditions are the same as those that occur in geothermal fields. These include evaporation, boiling, condensation, single- and two-phase fluid flow, mineral alteration and reaction, mineral precipitation and dissolution, and consequent potential changes in fracture-matrix interaction. Behavior of coupled processes related to geothermal systems has been observed, measured, and simulated for more than two decades in the geothermal industry. Data and analyses from geothermal analogs yield important

information about expected thermohydrologic conditions at Yucca Mountain and about perturbations caused by thermally induced geochemical and mechanical changes in the rock mass. Geothermal analogs are one of the major ways of building confidence in understanding the thermohydrologic behavior of the repository system as it is coupled to chemical processes over long time periods. Data from geothermal fields can be used to test coupled process modeling codes used by the YMP in order to match observations (e.g., chemical reactions, occurrence of heat pipes) in geothermal fields with those predicted by the code.

Many active geothermal fields throughout the world could serve as potential analog sites to some hydrothermal conditions expected to occur at Yucca Mountain. An appropriate candidate site would include features such as temperatures ranging from 25 to 300°C, a broad range of phenomena and features available for study, a range of water chemistries that would bound those expected to occur at Yucca Mountain, a range of hydrologic properties (e.g., porosity, permeability, fracture characteristics) similar to Yucca Mountain, water-saturated and unsaturated environments, a suite of hydrothermal alteration minerals similar to those expected to form at Yucca Mountain (e.g., zeolites and clays), evidence of fracture-matrix interactions, an active monitoring system, and access to extensive data sets from the recorded history of the field.

Because many of the same thermohydrologic processes operating in geothermal systems are applicable to behavior of a nuclear waste repository, the same numerical tools may be utilized to study thermohydrologic evolution in both environments. Geothermal reservoir simulators have been used to model laboratory experiments, to study fundamental aspects of geothermal reservoir dynamics, and to perform simulation studies, such as parameter matching and field history studies in their various natural, exploited, and predicted states for dozens of specific geothermal fields. For all of these applications, it is essential that users have a high level of confidence in the ability of their numerical tools to simulate processes and predict thermohydrologic conditions over extended time periods.

The versatility of geothermal reservoir simulators has made possible their application to a wide range of fluid and heat flow problems. Some of the main areas in which numerical simulation studies have produced significant advances in understanding geothermal systems include: (1) pressure decline in the depletion of boiling reservoirs, (2) evaluation of boiling and condensation zones, (3) reservoir exploitation strategies, (4) vapor-dominated and liquid-dominated heat pipes, (5) transition from liquid-dominated to vapor-dominated systems, (6) natural evolution of hydrothermal convection systems, (7) fluid and heat transfer in fractured porous media, (8) nonisothermal and two-phase well testing, (9) effects of reinjection and natural recharge, and (10) noncondensable gas effects.

Numerical simulators in geothermal studies are used to determine the characteristic parameters of reservoirs, especially the reserves of heat and fluid, and to simulate the performance of reservoirs upon production and injection. To produce an adequate model, numerical codes must be able to handle processes of heat transfer, two-phase flow under nonisothermal conditions in one, two, and three dimensions with varying degrees of non-linearity, coupling of fluid and heat flows, and complex boundary conditions. Solution of two-phase fluid flow problems with heat transport in a fractured porous medium is a challenging task that adds complexity when modeled in three dimensions, as is being done for the Yucca Mountain performance assessment. Modeling of

geothermal systems has provided major advances toward this goal, which adds confidence to numerical models of Yucca Mountain.

Table 6-13 provides a comparison between issues important to assessing coupled processes that may occur at Yucca Mountain and processes taking place in geothermal reservoir systems. Some issues that are important for assessing Yucca Mountain, such as water saturation near the heater and localized seepage, have been omitted from the list because they are not of concern in geothermal reservoir engineering. The table shows geothermal fields that could be used as potential analogs to study THC processes. Corresponding to each issue, geothermal sites are listed that may, upon further evaluation, provide added confidence in modeling thermally coupled processes at Yucca Mountain using approaches suggested in column 4 of the table.

Conflicting conclusions regarding the effect of mineral precipitation on fracture permeability, reported in Section 6.5.3.2 and identified as having uncertainty by PA (see Section 7.2), point toward THC processes (three of the four last issues in column 1 of table 6-13) as having high priority for additional study in active geothermal systems. Logically fields with high similarity factors to Yucca Mountain would be the first to investigate. These would include fields such as Larderello, Long Valley, Yellowstone, and several of the New Zealand fields and Reykjanes.

Table 6-13. Application of Geothermal Field Information as Analogs to Coupled Processes Anticipated at a Potential Yucca Mountain Repository

Yucca Mountain Issue	Geothermal Analog	Potential Sites	Possible Approach
Multiphase Flow (liquid, vapor, gas)	Multiphase Flow (liquid, vapor, gas)	All	Numerical Modeling, Conduct and Review Geothermal Post Audits
Hydrologic Properties	Hydrologic Properties	Kamojang (Indonesia), Tianjin (China), Wairakei (New Zealand), Oguni (Japan), Sumikawa (Japan)	Numerical Modeling
Preferential Flow	Preferential Flow	Wairakei (New Zealand), The Geysers (CA), Dixie Valley (NV), East Mesa (CA), Cerro Prieto (Mexico)	Numerical Stochastic Modeling, Evaluate Geothermal Tracer Study Results
Fracture Network Permeability	Fracture Network Permeability	All Modeled Fractured Sites, e.g. Cerro Prieto (Mexico), Krafla (Iceland), Matsukawa (Japan), Sumikawa (Japan), Olkaria (Kenya), Krafla (Iceland), Wairakei (New Zealand), Geysers (CA), Kamojang (Indonesia), Larderello (Italy)	Reservoir Model Calibrations Used
Fracture-Matrix Interaction	Fracture-Matrix Interaction	Yellowstone (WY), Long Valley (CA), Olkaria (Kenya), Fenton Hill (NM), Dixie Valley (NV)	Field and Laboratory Experiments, Evaluate Geothermal Tracer Study Results
Heat Pipes, Boiling and Condensation	Heat Pipes, Boiling and Condensation	The Geysers (CA), Kamojang (Indonesia), Matsukawa (Japan), Larderello (Italy)	Numerical Modeling to Extend Measurements
Mineral Precipitation and Dissolution	Mineral Precipitation and Dissolution	Larderello (Italy), Dixie Valley (NV), Wairakei (New Zealand), Broadlands (New Zealand), Long Valley (CA), Yellowstone (WY)	Laboratory Experiments, Analog Site Investigation, Numerical Modeling
Self-Sealing	Caprocks	The Geysers (CA), Kamojang (Indonesia), Matsukawa (Japan), Larderello (Italy), Cerro Prieto (Mexico), Reykjanes (Iceland)	Core Sample Evaluation, Water Chemistry Evaluation, Numerical Modeling
Mineral Alteration	Mineral Alteration	Wairakei (New Zealand), Broadlands (New Zealand), Dixie Valley (NV), Yellowstone (WY)	Core Sample Evaluation, Numerical Modeling
Thermo-Hydro-Mechanical Effects	Subsidence, Flow Changes	Wairakei (New Zealand), Bulalo (Philippines), Krafla (Iceland)	Numerical Modeling
Similarity Factor for comparison to Yucca Mountain: a - similar water chemistry, b - similary geology, c - similar alteration mineralogy.		Larderello (Italy) - b, possibly c: Yellowstone (WY) - a,b,c; Fenton Hill (NM) - b; Dixie Valley (NV) - c; Wairakei (New Zealand) - a,b.c; Broadlands (New Zealand) - a,b,c; Long Valley (CA) - a,b, possibly c.	

The capabilities and limitations of geochemical modeling codes such as the solubility/speciation and reaction path code EQ3/6 (Wolery and Daveler 1992) and thermodynamic databases have been tested by analyzing natural hydrothermal systems that have some mineralogical and environmental similarities to Yucca Mountain. The Yellowstone caldera closely duplicates characteristics of the volcanic sequence at Yucca Mountain and temperatures anticipated at the candidate repository horizon. The Yellowstone volcanic sequence is dominated by Quaternary silicic welded ash flow tuffs and rhyolite flows. Geothermal activity is reflected in hundreds of hot springs and geysers which emit waters that have circulated through the volcanic rocks and have formed a variety of hydrothermal mineral assemblages. Using data from 13 USGS drill cores as a basis for deriving paragenetic sequences of mineral deposition in the Yellowstone geothermal systems, Meijer (1987) conducted preliminary thermodynamic simulations using an early version of EQ3/6. His evaluation suggested that the most significant effects of the thermal pulse on the chemical environment at the repository horizon would be the transport and redeposition of silica along hydrologic and thermal gradients and the precipitation of clays in the groundmass of the devitrified repository host rock. Secondary effects could include the deposition of clays and zeolites in fractures and cavities adjacent to the repository and in the underlying vitrophyre. These horizons should remain stable unless acidic groundwater conditions are generated in association with the repository. Results of Carey et al.'s (1997) model of mineral evolution at Yucca Mountain compared favorably with Meijer's (1987) simulations.

Bruton et al. (1995) catalogued a survey of literature and data for many geothermal fields as a means of selecting a field analog site for thermohydrologic-chemical studies at Yucca Mountain. The sites included in their survey numbered among them many of the better-known geothermal fields: The Geysers, California; Krafla and other geothermal areas in Iceland; Cerro Prieto, Mexico; Valles Caldera, New Mexico; Larderello, Italy; Long Valley Caldera, California; Yellowstone, Wyoming; and the Wairakei and Ohaaki-Broadlands fields of New Zealand. Some of these fields were considered unsuitable because they occurred in rock types dissimilar to Yucca Mountain, a few lacked sufficient data or had access problems, and others were entirely liquid- or vapor-dominated fields. The geothermal system at Wairakei was selected by the Yucca Mountain Project as the site most amenable to study of THC processes because it possessed the greatest number of features similar to Yucca Mountain (Bruton et al. 1995, p. 8), because of logistic practicalities, and the potential for collaborative research.

EQ3/6 was used to simulate mineral-fluid relations in the Wairakei geothermal field and other New Zealand geothermal fields (Glassley and Christensen 1992; Bruton et al. 1993). Comparisons between observed mineral assemblages and model simulations of equilibria were used to evaluate the thermodynamic database for various environmental conditions encompassing the possible range of temperatures and water conditions anticipated in a Yucca Mountain repository system. The results of these modeling studies are generally consistent with observed vein and matrix mineral equilibria at Wairakei for fluids at temperatures greater than 240°C. Both field data and model results indicate that stable mineral assemblages can be significantly impacted by small differences in fluid chemistry, temperature, or pressure. Comparison of laboratory data with field data from natural hydrothermal waters at Wairakei for amorphous silica precipitation has shown that significant discrepancies exist between results obtained with different test conditions (Carroll et al. 1995). Rates measured in the field were 400 times faster than those obtained in laboratory measurements. Silica precipitation under repository conditions

at Yucca Mountain could exhibit rate behavior somewhere in the range between the laboratory and field experiments.

The results of these studies emphasize two points necessary for use of natural systems in model validation. First, the natural systems must be thoroughly understood and quantitatively characterized, if rigorous testing of simulations is to be completed. Second, simulations must be capable of providing predictive results that can be tested in an active field setting. The chemical and hydrological features associated with actively evolving systems must be amenable to measurement and study, if kinetically controlled systems are to be rigorously simulated.

7. CONCLUSIONS AND ONGOING STUDIES

7.1 CONCLUSIONS

Carefully selected natural analogs are important tools for understanding flow and transport processes anticipated to occur at a potential nuclear waste repository. The instrumental use of natural analogs in building confidence in conceptual and numerical models has been demonstrated by a literature study and analyses related to the key unsaturated zone flow and transport processes relevant at Yucca Mountain. The analyses were the Box Canyon study of flow in fractured media (Section 6.5.1.1) and the Peña Blanca study of radionuclide sequestration in fractured rhyolitic tuff (Section 6.5.2.1). Specific conclusions drawn from the literature study and analyses follow.

Using numerical simulation of the extensive data set from tracer infiltration tests, the Box Canyon study demonstrated that conceptual models and large-scale, volume-averaged numerical modeling approaches used for the UZ flow and transport model at Yucca Mountain can be applied with confidence. A consistent set of parameters was obtained to calibrate the site-wide model to both pneumatic and infiltration tests using the dual-permeability approach.

From the Peña Blanca U-Th age data, it appears that the primary transport of uranium (U) to the fractures occurred more than 300 ka ago. The $^{231}Pa/^{235}U$ activity ratios for the fracture samples support this conclusion. The $^{226}Ra/^{230}Th$ activity ratios indicate redistribution of radium (Ra) within the last 5 ka as a result of secondary fluid events caused by hydrologic disturbance(s). Hence, it appears that uranium (235, 238), thorium, and protactinium (Pa) in secondary fracture materials are unaffected by surface water infiltration and perhaps saturated groundwater flow over ~100 ka time scales. Therefore, the data demonstrate a high degree of stability for uranium (235,238), thorium, and protactinium in fracture-filling materials. In an analog sense, this stability should extend to transuranics and the rare earth elements. The high mobility of Ra is also noteworthy and should be considered in modeling transport of strontium (Sr) and cesium (Cs). By analogy with our results, the tuffs at Yucca Mountain should have similar retentive properties to impede oxidized uranium mobility.

The effects of shallow (<500 m) magmatic intrusions into unsaturated rocks can be quite different from effects associated with deeper hydrothermal systems. In the Banco Bonito study, the effects of heating in this unsaturated environment appeared to have been slight and to have been limited to within 10 m of the contact, although the boiling front predicted by modeling advanced several tens of meters into the tuff over several hundred years. Similarly, in the Grants Ridge basalt intrusion study, despite the high temperature intrusion, there was no evidence of fluid-driven convective heat transfer or pervasive hydrothermal alteration of the country rock. These field studies, along with the Paiute Ridge field studies, provide data for assessment of magmatic intrusions into or near a potential repository. But just as importantly, they provide a limiting case natural analog for evaluating effects of heat from decay of radioactive waste in an unsaturated environment.

Our literature study noted the utility of applying thermodynamic/kinetic modeling codes to hydrothermal data in carefully selected systems for building confidence in mineral reactions and rates. Analyses utilizing codes capable of handling reactive transport associated with thermally

coupled processes, such as those used in geothermal studies, are needed to represent the potential changes in hydrologic properties caused by mineral precipitation or dissolution. The changes in hydrologic properties and the extent of reaction of host rock to heat, as noted above, will be quite different in dry and saturated systems.

The modeling studies that used data from hydrothermal waters and minerals at New Zealand emphasize two points necessary for use of natural systems in model validation. First, the natural systems must be thoroughly understood and quantitatively characterized if rigorous testing of simulations is to be completed. Second, simulations must be capable of providing predictive results that can be tested in an active field setting. Codes utilized in geothermal reservoir simulations provide the necessary tools for such a task while data sets from geothermal fields such as those listed in Table 6-13 provide the field data for exercising the codes.

7.2 BASIS FOR ONGOING ANALOG STUDIES

7.2.1 Confidence-Building in Total System Performance Assessment (TSPA) and the License Application Through Natural Analogs

The fourth of five elements of the post-closure safety case for the Site Recommendation-License Application (DOE 1999), calls for an assessment of insights gained from the study of natural analogs. "Relevant information about the possible system performance of the site can be gleaned from analysis of natural processes that share characteristics with the repository system...These data may provide a degree of independent validation of the reasonableness of selected aspects of the assessments of repository performance" (DOE 1999, p. 15). As the safety case evolves, it seems likely that natural analog information will be used in the confirmatory sense for the "reasonable case," rather than supporting the safety arguments. However, the principal factors upon which the safety case is based, as well as the "other factors" that will be bounded, may be strengthened from confidence-building through natural analogs.

The TSPA Viability Assessment (VA) made no specific recommendations for use of natural analogs, but did discuss processes that were sensitive in TSPA calculations and that need to be understood with greater certainty. The TSPA-VA indicated that for peak dose rates, the fraction of waste packages contacted by seepage water was the most important parameter in each of the three simulation periods (10,000, 100,000, and 1,000,000 year) (CRWMS M&O 1998d, p. 11-58). Its effect becomes more dominant over time because an increase in the number of waste packages contacted by water leads to an increase in radionuclide releases from the repository.

The seepage model for TSPA assumed steady-state conditions and neglected the effect of the rock matrix. Drift collapse and thermal alteration of hydrologic properties were not considered. TSPA-VA stated that the possibility of episodic flow at the repository and its effect on seepage needs further study as well as the effect of discrete fracture flow (CRWMS M&O 1998d, p. 11-58). Natural analogs may be used to investigate the effects of drift collapse and thermal alteration of hydrologic properties on drift seepage.

The TSPA-VA model of UZ transport did not account for a number of processes, including alteration of the UZ caused by thermal alteration of minerals, chemical interactions of repository materials, mineral dissolution, and precipitation. Thermal-chemical alteration could cause

reduced matrix sorption and fracture-matrix interaction, thereby causing increased release rates from the UZ. Another process not accounted for was the ability of host rock to filter out colloids. A third process not accounted for was fracture sorption. However, the assumptions of no colloid filtration and no radionuclide sorption onto fracture surfaces are conservative for transport in the UZ. Although sensitivity studies conducted to date have found that transport is not highly sensitive to fracture sorption, this result requires further investigation to better define the appropriate range of parameters for fracture sorption. Radionuclide transport in the UZ is sensitive to changes in matrix diffusion, which suggests that further effort is needed to bound the magnitude of matrix diffusion (CRWMS M&O 1998c, p. 7-92).

According to TSPA-VA, process-level modeling of chemical alteration to fracture properties should be considered in the license application time frame. Formation of a mineral cap surrounding the emplacement drift has been suggested in modeling studies (Hardin 1998 p. 5.57 and 5.58) as a result of phase-change processes during thermal loading. Matyskiela's (1997) natural analog study also suggested that boiling of fracture fluids may cause deposition of minerals that alter the flow through the fracture system, although Lichtner's (1999) analysis challenges this conclusion. This issue should be investigated further through geothermal and fossil hydrothermal analogs because the fracture-matrix interaction parameter is potentially a key factor in describing the processes altered by chemistry and subsequently the manner in which fractures and matrix rock communicate with each other. The TSPA (CRWMS M&O 1998b, p. 3-164) noted that it is essential that the flow processes be accurately represented so that an assessment can be made as to whether or not the development of mineral deposits is physically realistic. A major question to be addressed is whether water will remain in the system long enough to allow for precipitation in fractures or whether it will flow through the fracture network during the condensate drainage period such that precipitation in fractures is minimal. Natural analogs of carefully selected systems may help to place bounds and add realism to the conceptualization of coupled thermohydrologic-chemical effects.

Thermohydrologic-mechanical (THM) processes were not considered in the TSPA. Although not as long-lasting as the chemically driven processes, THM processes may alter fracture properties and hence flow fields during thermal compression and expansion in the heating period. Although most of the mechanical effects tend to be reversible, and at most would permanently change the natural permeability by an order of magnitude (CRWMS M&O 1998b, p. 3-164), the mechanical influence on the fracture network may require further analysis with respect to large-scale gas-phase flow effects while the repository is at its hottest. An anthropogenic analog, such as an underground facility with decades of monitoring data, may be useful for building confidence in THM issues.

7.2.2 Ongoing Investigations

In FY99, the Yucca Mountain Project began to address areas that could benefit from improved confidence through natural analog studies. A synthesis was prepared of knowledge gained from natural analog studies by the international community and anthropogenic analog sites in the United States regarding not only flow and transport processes in the UZ, but all relevant natural and engineered barrier system processes. The synthesis will be published in the *Yucca Mountain Site Description for the Site Recommendation*. This will help to identify areas of existing analog information that can be used to build confidence in understanding long-term behavior of a waste

repository and areas where no appropriate analogs can be identified. It will help to focus the future direction of the YMP natural analog program with regard to study of particular sites.

The existing uncertainties and limitations of UZ flow and transport models that can be addressed through natural analogs have been discussed in Section 7.2.1. The purpose of conducting the specific additional analog studies is to ascertain that, for areas of uncertainty, the bounds placed on flow, transport, and thermally coupled processes are reasonable and the approaches taken in modeling them capture the processes correctly. As a result of our natural analog study of UZ flow and transport processes for this AMR, the following ongoing investigations are being conducted.

Rainier Mesa data will be revisited to evaluate data gaps and determine where additional limited data collection may be helpful. These data will be used in drift seepage models to compare to seepage under long-term average climate conditions. The data will be used to evaluate episodic pulses, such as those that affect the PTn, flow patterns and percolation fluxes from geochemical signatures, and sorption in vitric and zeolitic units.

For confidence in radionuclide transport, it is necessary to use information from both natural and anthropogenic systems. Natural analog systems provide information where long-term behavior is well understood but where the suite of radionuclides may differ from Yucca Mountain and where initial conditions are poorly understood. Anthropogenic systems are studied for a different reason; i.e., numerical models of Yucca Mountain flow and transport must be able to match predictions for anthropogenic sites over the short-term or they will not be able to sustain confidence in their predictions for Yucca Mountain over the long term. Here, data from Hanford, INEEL, NTS, and perhaps other sites with known leakage along fast pathways are being utilized, but with caution. The matter of plugging data from these sites into Yucca Mountain models is neither trivial nor straightforward.

Because previous work at Peña Blanca was primarily associated with two-dimensional fracture exposures on planar surfaces, we do not know whether there has been preferential flow/drainage downward through fractures. Therefore, geochemical studies are being extended to the third dimension. This will be accomplished with a cored borehole in FY00. Analyses of recovered core will provide samples by which to evaluate the downward path of radionuclide migration. Second, the extent and spatial dependence of uranium transport from the deposit through groundwater cannot be thoroughly evaluated without higher resolution sampling of any potential groundwater uranium plume in the vicinity of the deposit. To address this issue and others related to mechanisms controlling U concentration and transport, we will drill a series of water-producing wells, supplemented by collecting samples from perched water and a seepage test.

With the availability of solid and fluid samples, it is expected that there will be sufficient data to model radionuclide transport at Peña Blanca using a natural analog approach based on parent-daughter relationships for the U and Th decay series. The natural analog approach takes into account the combined effects of variable speciation, geologic heterogeneity, and geologic time scales. These parameters are commonly difficult to accurately duplicate in laboratory and theoretical studies, but will be determined *in situ* at Peña Blanca using samples from the proposed sampling effort. Finally, are using U-series and stable isotope data for samples of opal and calcite to determine the timing, nature, and extent of mobilization events in the 50-ka range and to judge their importance for predictive models for Yucca Mountain.

For understanding potential thermohydrologic processes at Yucca Mountain, the type of data that can be collected in a practical sense (e.g., field test point measurements) limits the ability to confirm models directly. For this reason, knowledge of long-term geothermal system behavior provides an appealing potential analog to understanding processes that may occur at a Yucca Mountain repository over millenia. We are investigating systems identified on Table 6-13 as having similar thermohydrologic-chemical characteristics to those predicted at Yucca Mountain for building confidence in numerical models of thermally coupled processes. We are building on previous THC thermodynamic and kinetic modeling studies described in this report to include the testing of reactive transport codes and models (e.g., TOUGHREACT, FEHM) using natural analog data. TOUGHREACT (Xu and Pruess 1998) has been applied to ESF heater test data and FEHM has been applied to study reactions at the Grants Ridge and Paiute Ridge igneous contact sites, but we know of no case in which a reactive transport code has been tested with geothermal analog data to consider the back-coupling effects of mineral reactions on hydrologic properties of a system. This type of coupling should be represented correctly in numerical models to match long-term, large-scale geothermal data before it can be modeled with confidence at Yucca Mountain.

Field studies provide a testing ground for THC codes and for building confidence in thermodynamic and kinetic models used to calculate mineral reactions. Observations of fracture-matrix margins may provide a means for testing and validating porosity-permeability and fracture-matrix interaction models employed in THC codes. For this reason, we are improving confidence in THC processes and models through analysis of selected intrusions hosted in unsaturated tuffaceous rock, such as portions of the Paiute Ridge intrusive complex. A detailed petrologic study of devitrified and vitric host rocks as a function of distance from the intrusive contact is being conducted to determine key mineral reactions and hydrologic effects. Field observations at the Paiute Ridge complex will help to estimate kinetically and thermodynamically possible mineral reaction rates and to determine whether mineral reactions act to increase or decrease matrix or fracture permeability.

INTENTIONALLY LEFT BLANK

8. INPUTS AND REFERENCES

8.1 DOCUMENTS CITED

Ahlers, C.F.; Finsterle, S.; and Bodvarsson, G.S. 1999. "Characterization and Prediction of Subsurface Pneumatic Response at Yucca Mountain, Nevada." *Journal of Contaminant Hydrology 38* (1-3), 47–68. Amsterdam, The Netherlands: Elsevier Science. TIC: 244160.

Alba, L.A. and Chavez, R. 1974. "K-Ar Ages of Volcanic Rocks from the Sierra Pena Blanca, Chihuahua, Mexico." *Isochron/West, 10,* 21–23. Socorro, New Mexico: Bureau of Mines and Mineral Resources. TIC: 246110.

Alexander, D.H. and Van Luik, A.E. 1991. "Natural Analogue Studies Useful in Validating Regulatory Compliance Analyses." *Validation of Geosphere Flow and Transport Models (GEOVAL), Proceedings of a NEA/SKI Symposium, Stockholm, Sweden, May 14–17, 1990,* 589–597. Paris, France: Organization for Economic Cooperation and Development. TIC: 246109.

Allard, T. and Muller, J.P. 1998. "Kaolinite as an In Situ Dosimeter for Past Radionuclide Migration at the Earth's Surface." *Applied Geochemistry, 13* (6), 751–765. Oxford, UK: Elsevier Science. TIC: 246131.

Baehr, A.L. and Hult, M.F. 1991. "Evaluation of Unsaturated Zone Air Permeability through Pneumatic Tests." *Water Resources Research 27* (10), 2605–2617. Washington, D.C.: American Geophysical Union. TIC: 245788.

Bandurraga, T.M. and Bodvarsson, G.S. 1999. "Calibrating Hydrogeologic Parameters for the 3-D Site-Scale Unsaturated Zone Model of Yucca Mountain, Nevada." *Journal Of Contaminant Hydrology 38* (1–3), 25-46. Amsterdam, The Netherlands: Elsevier Science Publishers. TIC: 244160.

Benito, P.H.; Cook, P.; Faybishenko, B.; Freifeld, B.; and Doughty, C. 1998. *Box Canyon Pneumatic Connectivity Study: Preliminary Data Analysis.* LBNL-38060. Berkeley, California: Lawrence Berkeley National Laboratory. TIC: on order.

Bish, D.L. and Aronson, J.L. 1993. "Paleogeothermal and Paleohydrologic Conditions in Silicic Tuff from Yucca Mountain, Nevada." *Clays and Clay Minerals, 41* (2), 148–161. Long Island City, New York: Pergamon Press. TIC: 224613.

Brookins, D.G. 1984. "Natural Analogs." *Geochemical Aspects of Radioactive Waste Disposal,* 197-231. New York, New York: Springer-Verlag. TIC: 206675.

Brookins, D.G.1986. "Natural Analogues for Radwaste Disposal: Elemental Migration in Igneous Contact Zones." *Chemical Geology, 55,* 337–344. Amsterdam, The Netherlands: Elsevier Science Publishers. TIC: 246170.

Bruton, C.J.; Glassley, W.E.; and Bourcier, W.L. 1993. "Testing Geochemical Modeling Codes using New Zealand Hydrothermal Systems." *Proceedings of the Topical Meeting on Site*

Characterization and Model Validation: FOCUS '93, September 26-29, 1993, Las Vegas, Nevada, 240–245. La Grange Park, Illinois: American Nuclear Society. TIC: 102245.

Bruton, C.J.; Glassley, W.E.; and Meike, A. 1995. *Geothermal Areas as Analogs to Chemical Processes in the Near-Field and Altered Zone of the Potential Yucca Mountain, Nevada Repository.* UCRL-ID-119842. Livermore, California: Lawrence Livermore National Laboratory. ACC: MOL.19960408.0126.

Carey, J.W.; Chipera, S.J.; Vaniman, D.T.; and Bish, D.L. 1997. *Three-Dimensional Mineralogic Model of Yucca Mountain, Nevada, Rev. 1.1, Draft R0.* Milestone Report SP32B5M4. Los Alamos, New Mexico: Los Alamos National Laboratory. ACC: MOL.19980520.0170.

Carroll, S.; Mroczek, E.; Bourcier, B.; Alai, M.; and Ebert, M. 1995. *Comparison of Field and Laboratory Precipitation Rates of Amorphous Silica from Geothermal Waters at 100°C.* Milestone Report MOL207. Livermore, California: Lawrence Livermore National Laboratory. ACC: MOL.19960415.0465.

Castor, S.B.; Henry, C.D.; and Shevenell, L.A. 1996. *Volcanic Rock-Hosted Uranium Deposits in Northwestern Nevada and Southeastern Oregon–Possible Sites for Studies of Natural Analogues for the Potential High-Level Nuclear Waste Repository at Yucca Mountain, Nevada.* Report from Mackey School of Mines. Reno, Nevada: University of Nevada. ACC: MOL.19960927.0026.

Crowe, B.; Self, S.; Vaniman, D.; Amos, R.; and Perry, F. 1983. "Aspects of Potential Magmatic Disruption of a High-Level Radioactive Waste Repository in Southern Nevada." *Journal of Geology, 91,* 259–276. Chicago, Illinois: University of Chicago Press. TIC: 216959.

CRWMS M&O (Civilian Radioactive Waste Management System Management and Operating Contractor) 1998a. *Yucca Mountain Site Description.* Book 3-Section 6, 7. B00000000-01717-5700-00019-00. Las Vegas, Nevada: CRWMS M&O. ACC: MOL.19981021.0043.

CRWMS M&O 1998b. *Thermal Hydrology.* Chapter 3 of *Total System Performance Assessment-Viability Assessment (TSPA-VA) Analyses Technical Basis Document.* B00000000-01717-4301-00003-00. Washington D.C.: DOE OCRWM. ACC: MOL.19980724.0392.

CRWMS M&O 1998c. *Unsaturated Zone Radionuclide Transport.* Chapter 7 of *Total System Performance Assessment-Viability Assessment (TSPA-VA) Analyses Technical Basis Document.* B00000000-01717-4301-00003-00. Washington D.C.: DOE OCRWM. ACC: MOL.19980724.0396.

CRWMS M&O 1998d. *Summary and Conclusions.* Chapter 11 of *Total System Performance Assessment-Viability Assessment (TSPA-VA) Analyses Technical Basis Document.* B00000000-01717-4301-00003-00. Washington D.C.: DOE OCRWM. ACC: MOL.19980724.0400.

CRWMS M&O 1999a. *Analysis and Modeling Development Plan (DP) for U0135, Natural Analogues for the UZ, Rev. 00.* TDP-NBS-HS-000008. Las Vegas, Nevada: CRWMS M&O. ACC: MOL.19990826.0108.

CRWMS M&O 1999b. *PSS Activity 6105 "Science Support" (non-Q).* Activity Evaluation. Las Vegas, Nevada: CRWMS M&O. ACC: MOL.19990326.0063.

CRWMS M&O 1999c. *License Application Design Selection Report.* B00000000-01717-4600-00123 Rev.01. Las Vegas, Nevada: CRWMS M&O. ACC: MOL.19990917.0120.

CRWMS M&O 2000. *Seepage Calibration Model and Seepage Testing Data.* MDL-NBS-HS-000004. Las Vegas, Nevada: CRWMS M&O. ACC: MOL.19990721.0521. URN-0024.

DOE 1998. *Introduction and Site Characteristics.* Volume I of *Viability Assessment of a Repository at Yucca Mountain.* DOE/RW-0508/VI. Washington D.C.: DOE OCRWM. ACC: MOL.19981007.0028.

Doughty, C. 1999. "Investigation of Conceptual and Numerical Approaches for Evaluating Moisture, Gas, Chemical, and Heat Transport in Fractured Unsaturated Rock." *Journal of Contaminant Hydrology 38* (1–3), 69–106. New York, New York: Elsevier Science Publishers. TIC: 244160.

Dyer, J.R. 1999. "Revised Interim Guidance Pending Issuance of New U.S. Nuclear Regulatory Commission (NRC) Regulations (Revision 01, July 22, 1999), for Yucca Mountain, Nevada." Letter from J.R. Dyer (DOE) to D.R. Wilkins (CRWMS M&O), September 9, 1999, OL&RC:SB-1714, with enclosure, "Interim Guidance Pending Issuance of New U.S. Nuclear Regulatory Commission (NRC) Regulations (Revision 01)." ACC: MOL.19990910.0079.

Faybishenko, B.; Holland, P.; Mesa, M.; Burgess, D.; Knutson, C.; and Sisson, B. 1998a. *Lithological Conditions at the Box Canyon Site: Results of Drilling, Coring and Open Borehole Measurements–1995–1997 Data Report.* Report LBNL-40182. Berkeley, California: Lawrence Berkeley National Laboratory. TIC: 245839.

Faybishenko, B.A.; Salve, R.; Zawislanski, P.; Lee, K.H.; Cook, P.; Freifeld, B.; Williams, K.; and Doughty, C. 1998b. *Ponded Infiltration Test at the Box Canyon Site: Data Report and Preliminary Analysis.* Report LBNL-40183. Berkeley, California: Lawrence Berkeley National Laboratory. ACC: MOL.19981002.0035.

Faybishenko, B.; Doughty, C.; Steiger, M.; Long, J.C.S.; Wood, T.R.; Jacobsen, J.S.; Lore, J.; and Zawislanski, P.T. 1999. *Conceptual Model of the Geometry and Physics of Water Flow in a Fractured Basalt Vadose Zone: Box Canyon Site, Idaho.* LBNL-42925. Berkeley, California: Lawrence Berkeley National Laboratory. TIC: 245840.

Finsterle, S. 1999. *ITOUGH2 User's Guide.* Report LBNL-40040. Berkeley, California: Lawrence Berkeley National Laboratory. TIC: 243018.

Flint, L.E. 1998. *Characterization of Hydrogeologic Units Using Matrix Properties, Yucca Mountain, Nevada.* Water-Resources Investigations Report 97–4243. Denver, Colorado: U.S. Geological Survey. ACC: MOL.19980429.0512.

Fridrich, C.J.; Dudley, W.W., Jr.; and Stuckless, J.S. 1994. "Hydrogeologic Analysis of the Saturated-Zone Ground-water System, under Yucca Mountain, Nevada." *Journal of Hydrology, 154*, 133-168. Amsterdam, The Netherlands: Elsevier Science. TIC: 224606.

Glassley, W.E. and Christensen, B.W. 1992. "Water-Rock Interaction in New Zealand Hydrothermal Systems: Comparison of Some Simulated and Observed Geochemical Processes." *High Level Waste Management, Proceedings of the Third International Conference, Las Vegas, Nevada, April 12–16, 1992*, 352–356. La Grange Park, Illinois: American Nuclear Society. TIC: 204231.

Goodell P. 1985. "Chihuahua City Uranium Province, Chihuahua, Mexico." *Uranium Deposits in Volcanic Rocks, Proceedings of a Technical Committee Meeting on Uranium Deposits in Volcanic Rocks, El Paso, Texas, April 2–5, 1984*, 97–124. El Paso, Texas: International Atomic Energy Association. TIC: 246156.

Grossenbacher, K. and Faybishenko, B. 1995. *Spacing of Thermally Induced Columnar Joints in Basalt: Variation with Depth.* LBNL-38060. Berkeley, California: Lawrence Berkeley National Laboratory. TIC: on order.

Hardin, E.L. 1998. *Near-Field/Altered Zone Models.* Milestone Report SP3100M4. Livermore, California: Lawrence Livermore National Laboratory. ACC: MOL.19980504.0577.

Hevesi, J.A.; Flint, A.L.; and Istock, J.D. 1992. "Precipitation Estimation in Mountainous Terrain Using Multivariate Geostatistics, Part II: Isohyetal Maps." *Journal of Applied Meteorology, 31*, 677–688. Boston, Massachusetts: American Meteorological Society. TIC: 225247.

Huang, K.; Tsang, Y.W.; and Bodvarsson, G.S. 1999. "Simultaneous Inversion of Air Injection Tests in Fractured Unsaturated Tuff at Yucca Mountain." *Water Resources Research, 35* (8), 2375–2386. Washington, D.C.: American Geophysical Union. TIC: 245633.

Ivanovich, M. and Harmon, R.S., eds. 1992. *Uranium Series Disequilibrium: Applications to Earth, Marine, and Environmental Sciences,* 2nd Ed. Oxford, England: Clarendon Press. TIC: 234680.

Knutson, C.F.; McCormick, K.A.; Smith, R.P.; Hackett, W.R.; O'Brien, J.P.; and Crocker, J.C. 1990. *Fiscal Year 89 Report RWMC Vadose Zone Basalt Characterization.* Report EG&G-WM-8949. Idaho Falls, Idaho: EG & G Idaho. TIC: 245912.

Knutson, C.F.; Cox, D.O.; Dooley, K.J.; and Sisson, J.B. 1993. "Characterization of Low Permeability Media Using Outcrop Measurements." *68th Annual Technical Conference and Exhibition of the Society of Petroleum Engineers, October 3-6, 1993, Houston Texas.* SPE Paper 26487. Richardson, Texas: Society of Petroleum Engineers. TIC: 247011.

Krumhansl, J.L. and Stockman, H.W. 1988. "Site Selection Criteria and Preliminary Results from the Valles Caldera Natural Analog Study." *Proceedings of Workshop IV on Flow and Transport Through Unsaturated Fractured Rock-Related to High Level Radioactive Waste Disposal, Tucson, Arizona, 1988,* 249–276. Tucson, Arizona: University of Arizona. TIC: on order.

Ku, T.L.; Luo, S.; Leslie, B.W.; and Hammond, D.E. 1992. "Decay-Series Disequilibria Applied to the Study of Rock-Water Interaction and Geothermal Systems." *Uranium Series Disequilibrium: Applications to Earth, Marine, and Environmental Sciences, 2nd Ed.* Ivanovich, M. and Harmon, R.S., eds., 631-668. New York, New York: Oxford University Press. TIC: 234680.

Leslie, B.; Pearcy, E.; and Prikryl, J. 1993. "Oxidative Alteration of Uraninite at the Nopal I Deposit, Mexico." *Scientific Basis for Nuclear Waste Management XVI, Materials Resources Symposium Proceedings, Boston, Massachusetts, November 30–December 4, 1992,* 294, 505-512. Pittsburgh, Pennsylvania: Materials Research Society. TIC: 208880.

Leslie, B.W.; Pickett, D.A.; and Pearcy, E.C. 1999. "Vegetation-Derived Insights on the Mobilization and Potential Transport of Radionuclides from the Nopal I Natural Analog Site, Mexico." *Scientific Basis for Nuclear Waste Management, XXII Symposium Proceedings, Boston, Massachusetts, November 30–December 4, 1998.* Warrendale, Pennsylvania: Materials Research Society. (in press). TIC: 246246.

Lichtner, P.C.; Keating, G.; and Carey, B. 1999. *A Natural Analogue for Thermal-Hydrological-Chemical Coupled Processes at the Proposed Nuclear Waste Repository at Yucca Mountain, Nevada.* Report LA-13610-MS. Los Alamos, New Mexico: Los Alamos National Laboratory. TIC: 246032.

Liu, H.H.; Doughty, C.; and Bodvarsson, G.S. 1998. "An Active Fracture Model for Unsaturated Flow and Transport in Fractured Rocks." *Water Resources Res*earch *34* (10), 2633-2646. Washington, D.C.: American Geophysical Union. TIC: 243012.

Ludwig, K.R. and Titterington, D.M. 1994. "Calculation of $^{230}Th/^{238}U$ Isochrons, Ages, and Errors." *Geochimica et Cosmochimica Acta, 22,* 5031–5042. New York, New York: Pergamon Press. TIC: 245769.

Matyskiela, W. 1997. "Silica Redistribution and Hydrologic Changes in Heated Fractured Tuff." *Geology 25* (12), 1115–1118. Boulder, Colorado: Geological Society of America. TIC: 236809.

Meijer, A. 1987. *Investigations of Natural Geologic and Geochemical Analogs in Relation to a Potential Nuclear Waste Repository at Yucca Mountain, Nevada.* Milestone Report R398. Albuquerque, New Mexico: Los Alamos National Laboratory. ACC: NNA.19900112.0350.

Montazer, P. and Wilson, W.E. 1984. *Conceptual Hydrologic Model of Flow in the Unsaturated Zone, Yucca Mountain, Nevada.* Water-Resources Investigations Report 84–4345. Denver, Colorado: U.S. Geological Survey. ACC: NNA.19890327.0051.

Murphy, W. 1995. "Natural Analogs for Yucca Mountain." *Radwaste Magazine, 2* (6), 44-50. LaGrange Park, Illinois: American Nuclear Society. TIC: 237929.

Murrell, M.T.; Goldstein, S.; and Dixon, P.R. 1997. "Uranium Decay Series Mobility from a Uranium Ore Deposit: Implications for Nuclear Repository Stability." *EOS Transactions, 78* (46), F788. Washington, D.C.: American Geophysical Union. TIC: 246604

Pearcy, E.C.; Prikryl, J.D.; Murphy, W.M.; and Leslie, B.W. 1994. "Alteration of Uraninite from the Nopal I Deposit, Peña Blanca District, Chihuahua, Mexico, Compared to Degradation of Spent Nuclear Fuel in the Proposed U.S. High-Level Nuclear Waste Repository at Yucca Mountain, Nevada." *Applied Geochemistry, 9,* 713-732. New York, New York: Elsevier Science. TIC: 236934.

Pearcy, E.C.; Prikryl, J.D.; and Leslie, B.W. 1995. "Uranium Transport Through Fractured Silicic Tuff and Relative Retention in Areas with Distinct Fracture Characteristics." *Applied Geochemistry, 10,* 685-704. Oxford, UK: Elsevier Science. TIC: 246848.

Pickett, D.A. and Murphy, W.M. 1997. "Isotopic Constraints on Radionuclide Transport at Peña Blanca." *Seventh EC Natural Analogue Working Group Meeting, Proceedings of an International Workshop, Stein am Rhein, Switzerland, October 28–30, 1996,* van Maravic, H. and Smellie, J., eds., 113–122. Stein am Rhein, Switzerland: European Commission. TIC: on order.

Pickett, D.A. and Murphy, W.M. 1999. "Unsaturated Zone Waters from the Nopal I Natural Analog, Chihuahua, Mexico–Implications for Radionuclide Mobility at Yucca Mountain." *Scientific Basis for Nuclear Waste Management, XXII Symposium Proceedings, Boston, Massachusetts, November 30–December 4, 1998 556, 809–816.* Warrendale, Pennsylvania: Materials Research Society. TIC: 246426.

Prikryl, J.D.; Pickett, D.A.; Murphy, W.M.; and Pearcy, E.C. 1997. "Migration Behavior of Naturally Occurring Radionuclides at the Nopal I Uranium Deposit, Chihuahua, Mexico." *Journal of Contaminant Hydrology, 26,* 61–69. New York, New York: Elsevier Science. TIC: 242381.

Pruess, K. 1991. *TOUGH2–A General Purpose Numerical Simulator for Multiphase Fluid and Heat Flow.* Report LBL-29400. Berkeley, California: Lawrence Berkeley National Laboratory. ACC: NNA.19940202.0088.

Pruess, K. 1998. "On Water Seepage and Fast Preferential Flow in Heterogeneous, Unsaturated Rock Fractures." *Journal of Contaminant Hydrology, 30* (3–4), 333–362. Amsterdam, The Netherlands: Elsevier Science. TIC: 238921.

Stockman, H.; Krumhansl, J.; Ho, C.; and McConnell, V. 1994. *The Valles Natural Analogue Project.* Report NUREG/CR-6221. Washington, D.C.: U.S. Nuclear Regulatory Commission. TIC: 246123.

Su, G.W.; Geller, J.T.; Pruess, K.; and Wen, F. 1999. "Experimental Studies of Water Seepage and Intermittent Flow in Unsaturated, Rough-Walled Fractures." *Water Resources Research, 35* (4), 1019–1037. Washington, D.C.: American Geophysical Union. TIC: 245798.

Tsang, Y.W. 1992. "Usage of "Equivalent Apertures" for Rock Fractures as Derived from Hydraulic and Tracer Tests." *Water Resources Research, 28* (5), 1451-1455. Washington, D.C.: American Geophysical Union. TIC: 245891.

Wallace, A.B. and Roper, M.W. 1981. "Geology and Ore Deposits Along the Northeastern Margin, McDermitt Caldera Complex, Oregon." *Uranium in Volcanic and Volcaniclastic Rocks: AAPG Studies in Geology, 13,* 73-80. Goodell, P.C. and Waters, A.C., eds. Tulsa, Oklahoma: American Association of Petroleum Geologists. TIC: 245898.

Wang, J.S.Y. 1991. "Propagation of Infiltration Pulses through Unsaturated Tuff Units." in *A Review of Rainier Mesa Tunnel and Borehole Data and Their Possible Implications to Yucca Mountain Site Study Plans.* LBL-32068. Berkeley, California: Lawrence Berkeley National Laboratory. ACC: NNA.19920506.0020.

Wang, J.S.Y. 1992. "Variations of Hydrological Parameters of Tuff and Soil." *High Level Radioactive Waste Management, Proceedings of the 3rd Annual International Conference, Las Vegas, Nevada, April 12–14, 1992,* 727–731. LaGrange Park, Illinois: American Nuclear Society. TIC: 208542.

Wang, J.S.Y.; Cook, N.G.W.; Wollenberg, H.A.; Carnahan, C.L.; Javandel, I.; and Tsang, C.F. 1993. "Geohydrologic Data and Models of Rainier Mesa and Their Implications to Yucca Mountain." *High Level Radioactive Waste Management, Proceedings of the 4th* Annual International Conference, Las Vegas, Nevada, April 26–30, 1993, 675–681. LaGrange Park, Illinois: American Nuclear Society. TIC: 208542.

Whelan, J.A. and Reed, M.F. 1997. "Geostatistical Analysis of Regional Hydraulic Conductivity Variations in the Snake River Plain Aquifer, Eastern Idaho." *GSA Bulletin, 109* (7), 855-868. Boulder, Colorado: Geological Society of America. TIC: 246133.

WoldeGabriel, G.; Keating, G.N.; and Valentine, G.A. 1999. "Effects of Shallow Basaltic Intrusion into Pyroclastic Deposits, Grants Ridge, New Mexico, USA." *Journal of Volcanology and Geothermal Research, 92,* 389–411. Amsterdam, The Netherlands: Elsevier Science. TIC: 246037.

Wolery, T.J. and Daveler, S.A. 1992. *EQ6, A Computer Program for Reaction Path Modeling of Aqueous Geochemical Systems: Theoretical Manual, User's Guide, and Related Documentation (Version 7.0).* Report UCRL-MFA-110662, Pt. IV. Livermore, California: Lawrence Livermore National Laboratory. TIC: 205002.

Wollenberg, H.A. and Flexser, S. 1986. "Contact Zones and Hydrothermal Systems as Analogues to Repository Conditions." *Chemical Geology 55,* 345–359. Amsterdam, The Netherlands: Elsevier Science Publishers. TIC: 246171.

Wong, V. 1998. *Gamma-Ray Characterization of Uranium-Series Nuclides and its Application to the Study of the Peña Blanca Natural Analog Site, Chihuahua, Mexico.* Ph.D. dissertation. El Paso, Texas: University of Texas at El Paso. TIC: 245933.

Wronkiewicz, D.J.; Bates, J.K.; Wolf, S.F.; and Buck, E.C. 1996. "Ten-Year Results from Unsaturated Drip Tests With UO_2 at 90°C: Implications for the Corrosion of Spent Nuclear Fuel." *Journal of Nuclear Materials, 238,* 78–95. Amsterdam, The Netherlands: Elsevier Science. TIC: 243361.

Xu, T. and Pruess, K. 1998. *Coupled Modeling of Non-Isothermal Multi-Phase Flow, Solute Transport and Reactive Chemistry in Porous and Fractured Media: 1. Model Development and Validation.* LBNL-42050. Berkeley, California: Lawrence Berkeley National Laboratory. TIC: 243735.

YMP 1998. *Repository Safety Strategy: U.S. Department of Energy's Strategy to Protect Public Health and Safety after Closure of a Yucca Mountain Repository.* YMP/96-01, Rev. 2. Washington D.C.: DOE OCRWM. ACC: MOL.19980727.0001.

Zyvoloski, G.A; Dash, Z.V.; and Kelkar, S. 1996. *FEHMN 1.0, Finite Element Heat and Mass Transfer Code.* Technical Report LA-12062-MS, Rev. 1. Albuquerque, New Mexico: Los Alamos National Laboratory. ACC: NNA.19910625.0038.

SOFTWARE CITED

Software code: TOUGH2 V1.3. STN: 10061-1.3-00.

Software macro: perm.for V1.0. ACC: MOL.19991011.0224.

Software macro: plot.for V1.0. ACC: MOL.19991011.0225.

Software macro: rocktype.for V1.0. ACC: MOL.19991011.0226.

Software macro: save2tec.for V1.0 ACC: MOL.19991011.0227.

Software macro: tough2tec.for V1.0. ACC: MOL.19991011.0228.

Software macro: trans_cal.for V1.0. ACC: MOL.19991011.0229.

Software macro: weight.for V1.0. ACC: MOL.19991011.0230.

8.2 CODES, STANDARDS, REGULATIONS AND PROCEDURES

AP-3.10Q. Analyses And Models. Las Vegas, Nevada: CRWMS M&O. ACC: MOL.19990702.0314.

AP-SI.1Q. *Software Management.* Las Vegas, Nevada: CRWMS M&O. ACC: MOL.19990630.0395.

DOE (U.S. Department of Energy)1998. *Quality Assurance Requirements and Description.* DOE/RW-0333P, Rev 8. Washington D.C.: DOE OCRWM. ACC: MOL.19980601.0022.

QAP-2-0. *Conduct of Activities.* Las Vegas, Nevada: CRWMS M&O. ACC: MOL.19980826.0209.

YMP-LBNL-QIP-SI.0, Rev. 4, Mod. 0. *Computer Software Qualification.* Berkeley, California: Lawrence Berkeley National Laboratory. ACC: MOL.19990503.0120.

8.3 SOURCE DATA, LISTED BY DATA TRACKING NUMBER

LB990930123122.001. Box Canyon Datasets, Including Fracture/Matrix Properties, Infiltration Rates, and Bromide Concentrations. Submittal date: 01/11/2000.

LB990930123122.002. Model input and output files used to generate figures in AMR U0135. Submittal date: 01/11/2000.

8.4 OUTPUT DATA, LISTED BY DATA TRACKING NUMBER

LA9909MM122122.001. U-Series Natural Analog Studies at Peña Blanca, Mexico. Submittal date: Will be submitted with AMR.

8.5 SUPPORTING BIBLIOGRAPHY

Bodvarsson, G.S. and Bandurraga, T.M. 1997. "Conceptual Model of Flow and Transport at Yucca Mountain." Chapter 2 of *The Site-Scale Unsaturated Zone Model of Yucca Mountain, Nevada, for the Viability Assessment.* Bodvarsson, G.S.; Bandurraga, T.M. and Wu, Y.S., eds. Milestone Report SD24UFM4. Berkeley, California: Lawrence Berkeley National Laboratory. ACC: MOL.19971014.0232.

Zyvoloski, G.A.; Robinson, B.A.; Dash, Z.; and.Trease, L.L. 1997. *Summary of Models and Methods for the FEHM Application, a Finite-Element-Heat and Mass-Transfer Code.* Report LA-13307-MS. Albuquerque, New Mexico: Los Alamos National Laboratory.

INTENTIONALLY LEFT BLANK

9. ATTACHMENTS

Attachment I - Document Input Reference Sheet

Attachment II - List of Input/Output files for Box Canyon Study (Section 6.5.1.1)

Attachment III - Peña Blanca Natural Analog Bibliography

Attachment IV - Derivation of Fracture Continuum Properties

Attachment V - Software Routines

INTENTIONALLY LEFT BLANK

ATTACHMENT I–DOCUMENT INPUT REFERENCE SHEET

DIRS as of the issue date of this AMR. Refer to the DIRS database for the current status of these inputs.

OFFICE OF CIVILIAN RADIOACTIVE WASTE MANAGEMENT
DOCUMENT INPUT REFERENCE SHEET

1. Document Identifier No./Rev.: ANL-NBS-HS-000007/Rev. 00			Change:	Title: Natural Analogs for the Unsaturated Zone					
Input Document			4. Input Status	5. Section Used in	6. Input Description	7. TBV/TBD Priority	8. TBV Due To		
2. Technical Product Input Source Title and Identifier(s) with Version		3. Section					Unqual.	From Uncontrolled Source	Un-confirmed
2a									
1.	DTN: LB990930123122.001. Box Canyon Datasets, including Fracture/Matrix Properties, Infiltration Rates, and Bromide Concentrations. Submittal date: 01/11/2000.	Table 6.2.xls – all columns except for 'model calibration data'. Table 6.3.xls – entire Table 6.4.xls – Entire, except for 'mean'. Table 6.5.xls – 'centroid of injection interval' and 'Field Data' Table 6.6.xls – Entire Table 6.7.xls – Entire BromideData .xls – Entire	N/A – N/Q	6.5.1.1	Fracture and matrix properties of the Box Canyon model. Location of borehole intersections with active water conducting fractures. Matrix porosity and permeability measurements from core samples. Fracture permeability calibration results from the analyzing of the pneumatic test data. Ponding test infiltration and duration times. Ponding test infiltration rates Bromide concentration during the 97-1 to 97-4 infiltration tests	N/A	N/A	N/A	N/A

OFFICE OF CIVILIAN RADIOACTIVE WASTE MANAGEMENT
DOCUMENT INPUT REFERENCE SHEET

1. Document Identifier No./Rev.: ANL-NBS-HS-000007/Rev. 00			Change:	Title: Natural Analogs for the Unsaturated Zone					
Input Document			4. Input Status	5. Section Used in	6. Input Description	7. TBV/TBD Priority	8. TBV Due To		
2. Technical Product Input Source Title and Identifier(s) with Version		3. Section					Unqual.	From Uncontrolled Source	Un-confirmed
2.	LB990930123122.002. Model input and output files used to generate figures in AMR U0135. Submittal date: 01/11/2000.	Input Files	N/A-N/Q	6.5.1.1	Input files for modeling results at Box Canyon	N/A	N/A	N/A	N/A
3.	Ahlers, C.F.; Finsterle, S.; and Bodvarsson, G.S. 1999. "Characterization and Prediction of Subsurface Pneumatic Response at Yucca Mountain, Nevada." *Journal of Contaminant Hydrology 38* (1-3), 47–68. Amsterdam, The Netherlands: Elsevier Science. TIC: 244160.	8.2 and 9	N/A – Reference only	6.2	Pneumatic data showing faults as fast flow pathways in PTn and TSw	N/A	N/A	N/A	N/A
4.	Alba, L.A. and Chavez, R. 1974. "K-Ar Ages of Volcanic Rocks from the Sierra Pena Blanca, Chihuahua, Mexico." *Isochron/West, 10,* 21–23. Socorro, New Mexico: Bureau of Mines and Mineral Resources. TIC: 246110.	Entire	N/A – Reference only	6.5.2.1.3.1	K-Ar ages of Nopal and Escuadra Formations	N/A	N/A	N/A	N/A

OFFICE OF CIVILIAN RADIOACTIVE WASTE MANAGEMENT
DOCUMENT INPUT REFERENCE SHEET

1. Document Identifier No./Rev.: ANL-NBS-HS-000007/Rev. 00			Change:	Title: Natural Analogs for the Unsaturated Zone					
Input Document			4. Input Status	5. Section Used in	6. Input Description	7. TBV/TBD Priority	8. TBV Due To		
2. Technical Product Input Source Title and Identifier(s) with Version		3. Section					Unqual.	From Uncontrolled Source	Un-confirmed
5.	Alexander, D.H. and Van Luik, A.E. 1991. "Natural Analogue Studies Useful in Validating Regulatory Compliance Analyses." *Validation of Geosphere Flow and Transport Models (GEOVAL), Proceedings of a NEA/SKI Symposium, Stockholm, Sweden, May 14–17, 1990,* 589–597. Paris, France: Organization for Economic Cooperation and Development. TIC: 246109.	Entire	N/A – Reference only	6.5.2.2	McDermitt caldera U deposits proposed as potential YM analogs	N/A	N/A	N/A	N/A
6.	Allard, T. and Muller, J.P. 1998. "Kaolinite as an In Situ Dosimeter for Past Radionuclide Migration at the Earth's Surface." *Applied Geochemistry, 13* (6), 751–765. Oxford, United Kingdom: Elsevier Science. TIC: 246131.	pp. 759-764	N/A – Reference only	6.5.2.1.4.1.3	Use of electron paramagnetic resonance to show transport and accumulation of U at Pena Blanca	N/A	N/A	N/A	N/A

OFFICE OF CIVILIAN RADIOACTIVE WASTE MANAGEMENT
DOCUMENT INPUT REFERENCE SHEET

1. Document Identifier No./Rev.: ANL-NBS-HS-000007/Rev. 00			Change:	Title: Natural Analogs for the Unsaturated Zone					
Input Document			4. Input Status	5. Section Used in	6. Input Description	7. TBV/TBD Priority	8. TBV Due To		
2. Technical Product Input Source Title and Identifier(s) with Version		3. Section					Unqual.	From Uncontrolled Source	Un-confirmed
7.	Baehr, A.L. and Hult, M.F. 1991. "Evaluation of Unsaturated Zone Air Permeability Through Pneumatic Tests." *Water Resources Research, 27* (10), 2605-26127. Washington, D.C.: American Geophysical Union. TIC: 245788.	Entire	N/A – Reference only	6.5.1.1.4	Reference to analytical solution for interpreting pneumatic test.	N/A	N/A	N/A	N/A
8.	Bandurraga, T.M. and Bodvarsson, G.S. 1999. "Calibrating Hydrogeologic Parameters for the 3-D Site-Scale Unsaturated Zone Model of Yucca Mountain, Nevada." *Journal Of Contaminant Hydrology 38* (1–3), 25-46. Amsterdam, The Netherlands: Elsevier Science Publishers. TIC: 244160.	Entire	N/A-Reference only	6.5.1.1.1	Description of conceptual model used at Yucca Mountain.	N/A	N/A	N/A	N/A

OFFICE OF CIVILIAN RADIOACTIVE WASTE MANAGEMENT
DOCUMENT INPUT REFERENCE SHEET

1. Document Identifier No./Rev.: ANL-NBS-HS-000007/Rev. 00			Change:	Title: Natural Analogs for the Unsaturated Zone					
Input Document			4. Input Status	5. Section Used in	6. Input Description	7. TBV/TBD Priority	8. TBV Due To		
2. Technical Product Input Source Title and Identifier(s) with Version		3. Section					Unqual.	From Uncontrolled Source	Un-confirmed
9.	Benito, P.H.; Cook, P.; Faybishenko, B.; Freifeld, B.; and Doughty, C. 1998. *Box Canyon Pneumatic Connectivity Study: Preliminary Data Analysis.* LBNL-38060. Berkeley, California: Lawrence Berkeley National Laboratory. TIC: on order.	Entire	N/A – Reference only	6.5.1.1.4	Detailed description of all pneumatic tests conducted at Box Canyon.	N/A	N/A	N/A	N/A
10.	Bish, D.L. and Aronson, J.L. 1993. "Paleogeothermal and Paleohydrologic Conditions in Silicic Tuff from Yucca Mountain, Nevada." *Clays and Clay Minerals, 41* (2), 148-161. Long Island City, New York: Pergamon Press. TIC: 224613.	Entire	N/A – Reference only	6.5.3.2	Study of YM as self-analog using mineralogy and temperature data	N/A	N/A	N/A	N/A
11.	Brookins, D.G. 1984. "Natural Analogs." *Geochemical Aspects of Radioactive Waste Disposal,* 197–231. New York, New York: Springer-Verlag. TIC: 206675.	197-231	N/A – Reference only	6.5.3.2	Description of Alamosa River stock as hydrothermal analog for geologic repository	N/A	N/A	N/A	N/A

OFFICE OF CIVILIAN RADIOACTIVE WASTE MANAGEMENT
DOCUMENT INPUT REFERENCE SHEET

1. Document Identifier No./Rev.: ANL-NBS-HS-000007/Rev. 00			Change:	Title: Natural Analogs for the Unsaturated Zone					
Input Document			4. Input Status	5. Section Used in	6. Input Description	7. TBV/TBD Priority	8. TBV Due To		
2. Technical Product Input Source Title and Identifier(s) with Version		3. Section					Unqual.	From Uncontrolled Source	Un-confirmed
12.	Brookins, D.G.1986. "Natural Analogues for Radwaste Disposal: Elemental Migration in Igneous Contact Zones." *Chemical Geology, 55*, 337-344. Amsterdam, The Netherlands: Elsevier Science Publishers. TIC: 246170.	Entire	N/A – Reference only	6.5.3.2	Various igneous contact zones as possible analogs to radionuclide transport at a geologic repository	N/A	N/A	N/A	N/A
13.	Bruton, C.J.; Glassley, W.E.; and Bourcier, W.L. 1993. "Testing Geochemical Modeling Codes using New Zealand Hydrothermal Systems." *Proceedings of the Topical Meeting on Site Characterization and Model Validation: FOCUS '93, September 26-29, 1993, Las Vegas, Nevada*, 240–245. La Grange Park, Illinois: American Nuclear Society. TIC: 102245.	Entire	N/A – Reference Only	6.5.3.3	Use of mineral data from New Zealand geothermal field to test EQ3/6 code and database	N/A	N/A	N/A	N/A

OFFICE OF CIVILIAN RADIOACTIVE WASTE MANAGEMENT
DOCUMENT INPUT REFERENCE SHEET

1. Document Identifier No./Rev.: ANL-NBS-HS-000007/Rev. 00			Change:	Title: Natural Analogs for the Unsaturated Zone					
Input Document			4. Input Status	5. Section Used in	6. Input Description	7. TBV/TBD Priority	8. TBV Due To		
2. Technical Product Input Source Title and Identifier(s) with Version		3. Section					Unqual.	From Uncontrolled Source	Un-confirmed
14.	Bruton, C.J.; Glassley, W.E.; and Meike, A. 1995. *Geothermal Areas as Analogs to Chemical Processes in the Near-Field and Altered Zone of the Potential Yucca Mountain, Nevada Repository.* UCRL-ID-119842. Livermore, California: Lawrence Livermore National Laboratory. ACC: MOL.19960408.0126.	Entire	N/A – Reference only	6.5.3.3	Selection criteria for choice of geothermal analog for YM repository	N/A	N/A	N/A	N/A
15.	Carey, J.W.; Chipera, S.J.; Vaniman, D.T.; and Bish, D.L. 1997. *Three-Dimensional Mineralogic Model of Yucca Mountain, Nevada, Rev. 1.1, Draft R0.* Milestone Report SP32B5M4. Los Alamos, New Mexico: Los Alamos National Laboratory. ACC: MOL.19980520.0170.	Entire	N/A – Reference only	6.5.3.2	Likely mineral phases to form at YM under repository heating	N/A	N/A	N/A	N/A

OFFICE OF CIVILIAN RADIOACTIVE WASTE MANAGEMENT
DOCUMENT INPUT REFERENCE SHEET

1. Document Identifier No./Rev.: ANL-NBS-HS-000007/Rev. 00			Change:	Title: Natural Analogs for the Unsaturated Zone					
Input Document			4. Input Status	5. Section Used in	6. Input Description	7. TBV/TBD Priority	8. TBV Due To		
2. Technical Product Input Source Title and Identifier(s) with Version		3. Section					Unqual.	From Uncontrolled Source	Un-confirmed
16.	Carroll, S.; Mroczek, E.; Bourcier, B.; Alai, M.; and Ebert, M. 1995. *Comparison of Field and Laboratory Precipitation Rates of Amorphous Silica from Geothermal Waters at 100°C.* Milestone Report MOL207. Livermore, California: Lawrence Livermore National Laboratory. ACC: MOL.19960415.0465.	Entire	N/A – Reference only	6.5.3.3	Comparison of field and laboratory rates of amorphous silica precipitation from geothermal waters at 100 degrees Celsius.	N/A	N/A	N/A	N/A

OFFICE OF CIVILIAN RADIOACTIVE WASTE MANAGEMENT
DOCUMENT INPUT REFERENCE SHEET

1. Document Identifier No./Rev.: ANL-NBS-HS-000007/Rev. 00			Change:	Title: Natural Analogs for the Unsaturated Zone					
Input Document			4. Input Status	5. Section Used in	6. Input Description	7. TBV/TBD Priority	8. TBV Due To		
	2. Technical Product Input Source Title and Identifier(s) with Version	3. Section					Unqual.	From Uncontrolled Source	Un-confirmed
17.	Castor, S.B.; Henry, C.D.; and Shevenell, L.A. 1996. *Volcanic Rock-Hosted Uranium Deposits in Northwestern Nevada and Southeastern Oregon– Possible Sites for Studies of Natural Analogues for the Potential High-Level Nuclear Waste Repository at Yucca Mountain, Nevada.* Report from Mackey School of Mines. Reno, Nevada: University of Nevada. ACC: MOL.19960927.0026.	Entire	N/A – Reference only	6.5.2.2	Summary of available data on uranium deposits in northwestern Nevada and southeastern Oregon	N/A	N/A	N/A	N/A
18.	Crowe, B.; Self, S.; Vaniman, D.; Amos, R.; and Perry, F. 1983. "Aspects of Potential Magmatic Disruption of a High-Level Radioactive Waste Repository in Southern Nevada." *Journal of Geology, 91*, 259-276. Chicago, Illinois: University of Chicago Press. TIC: 216959.	Section on characteri-zation of NTS intrusive bodies	N/A – Reference only	6.5.3.2	Depth of emplacement of NTS igneous intrusive bodies	N/A	N/A	N/A	N/A

OFFICE OF CIVILIAN RADIOACTIVE WASTE MANAGEMENT
DOCUMENT INPUT REFERENCE SHEET

1. Document Identifier No./Rev.: ANL-NBS-HS-000007/Rev. 00			Change:	Title: Natural Analogs for the Unsaturated Zone					
Input Document			4. Input Status	5. Section Used in	6. Input Description	7. TBV/TBD Priority	8. TBV Due To		
	2. Technical Product Input Source Title and Identifier(s) with Version	3. Section					Unqual.	From Uncontrolled Source	Un-confirmed
19.	CRWMS M&O (Civilian Radioactive Waste Management System Management and Operating Contractor) 1998a. *Yucca Mountain Site Description.* Book 3-Section 6, 7. B00000000-01717-5700-00019-00. Las Vegas, Nevada: CRWMS M&O. ACC: MOL.19981021.0043.	p. F6.1-75 to F6.1-76	N/A – Reference only	6.5.3.2	Figure showing potential mineral alteration zones at Yucca Mt.	N/A	N/A	N/A	N/A
20.	CRWMS M&O 1998b. *Thermal Hydrology.* Chapter 3 of *Total System Performance Assessment-Viability Assessment (TSPA-VA) Analyses Technical Basis Document.* B00000000-01717-4301-00003-00. Washington D.C.: DOE OCRWM. ACC: MOL.19980724.0392.	Ch. 3, p. 189-191	N/A - Reference only	7.1.1	Handling of coupled processes in TSPA-VA calculations	N/A	N/A	N/A	N/A

OFFICE OF CIVILIAN RADIOACTIVE WASTE MANAGEMENT
DOCUMENT INPUT REFERENCE SHEET

1. Document Identifier No./Rev.: ANL-NBS-HS-000007/Rev. 00			Change:	Title: Natural Analogs for the Unsaturated Zone					
Input Document			4. Input Status	5. Section Used in	6. Input Description	7. TBV/TBD Priority	8. TBV Due To		
2. Technical Product Input Source Title and Identifier(s) with Version		3. Section					Unqual.	From Uncontrolled Source	Un-confirmed
21.	CRWMS M&O 1998c. *Unsaturated Zone Radionuclide Transport.* Chapter 7 of *Total System Performance Assessment-Viability Assessment (TSPA-VA) Analyses Technical Basis Document.* B00000000-01717-4301-00003-00. Washington D.C.: DOE OCRWM. ACC: MOL.19980724.0396.	Ch. 7, p. 102	N/A - Reference only	7.1.1	Radionuclide transport processes that were not covered in TSPA-VA	N/A	N/A	N/A	N/A
22.	CRWMS M&O 1998d. *Summary and Conclusions.* Chapter 11 of *Total System Performance Assessment-Viability Assessment (TSPA-VA) Analyses Technical Basis Document.* B00000000-01717-4301-00003-00. Washington D.C.: DOE OCRWM. ACC: MOL.19981008.0011.	Ch. 11, p. 58	N/A – Reference only	7.1.1	Role of seepage in TSPA-VA calculations.	N/A	N/A	N/A	N/A

OFFICE OF CIVILIAN RADIOACTIVE WASTE MANAGEMENT
DOCUMENT INPUT REFERENCE SHEET

1. Document Identifier No./Rev.: ANL-NBS-HS-000007/Rev. 00			Change:	Title: Natural Analogs for the Unsaturated Zone					
Input Document			4. Input Status	5. Section Used in	6. Input Description	7. TBV/TBD Priority	8. TBV Due To		
	2. Technical Product Input Source Title and Identifier(s) with Version	3. Section					Unqual.	From Uncontrolled Source	Un-confirmed
23.	CRWMS M&O 1999a. *Analysis and Modeling Development Plan (DP) for U0135, Natural Analogues for the UZ, Rev. 00."* TDP-NBS-HS-000008. Las Vegas, Nevada: CRWMS M&O. ACC: MOL.19990826.0108.	Entire	N/A – Reference only	2	Plan	N/A	N/A	N/A	N/A
24.	CRWMS M&O 1999b. *PSS Activity 6105 "Science Support" (non-Q).* Activity Evaluation. Las Vegas, Nevada: CRWMS M&O. ACC: MOL.19990326.0063.	Entire	N/A – Reference Only	2	Activity Evaluation	N/A	N/A	N/A	N/A
25.	CRWMS M&O 1999c. *License Application Design Selection Report.* B00000000-01717-4600-00123 Rev.01. Las Vegas, Nevada: CRWMS M&O. ACC: MOL.19990917.0120.	Entire	N/A – Reference Only	6.5.3.2	Thermal loading considered for EDA-II design	N/A	N/A	N/A	N/A

OFFICE OF CIVILIAN RADIOACTIVE WASTE MANAGEMENT
DOCUMENT INPUT REFERENCE SHEET

1. Document Identifier No./Rev.: ANL-NBS-HS-000007/Rev. 00			Change:	Title: Natural Analogs for the Unsaturated Zone					
Input Document			4. Input Status	5. Section Used in	6. Input Description	7. TBV/TBD Priority	8. TBV Due To		
	2. Technical Product Input Source Title and Identifier(s) with Version	3. Section					Unqual.	From Uncontrolled Source	Un-confirmed
26.	CRWMS M&O 2000. *Seepage Calibration Model and Seepage Testing Data.* MDL-NBS-HS-000004. Las Vegas, Nevada: CRWMS M&O. ACC: MOL.19990721.0521. URN-0024.	70	N/A – Reference Only	6.2	Seepage threshold value for YM	N/A	N/A	N/A	N/A
27.	DOE 1998. *Introduction and Site Characteristics.* Volume I of *Viability Assessment of a Repository at Yucca Mountain.* DOE/RW-0508/VI. Washington D.C.: DOE OCRWM. ACC: MOL.19981007.0028.	Chapter 2	N/A – Reference Only	6.2 6.5.1.2	Conceptual model of UZ flow processes.	N/A	N/A	N/A	N/A

OFFICE OF CIVILIAN RADIOACTIVE WASTE MANAGEMENT
DOCUMENT INPUT REFERENCE SHEET

1. Document Identifier No./Rev.: ANL-NBS-HS-000007/Rev. 00			Change:	Title: Natural Analogs for the Unsaturated Zone					
Input Document			4. Input Status	5. Section Used in	6. Input Description	7. TBV/TBD Priority	8. TBV Due To		
	2. Technical Product Input Source Title and Identifier(s) with Version	3. Section					Unqual.	From Uncontrolled Source	Un-confirmed
28.	Doughty, C. 1999. "Investigation of Conceptual and Numerical Approaches for Evaluating Moisture, Gas, Chemical, and Heat Transport in Fractured Unsaturated Rock." *Journal of Contaminant Hydrology, 38* (1-3), 69-106. New York, New York: Elsevier Science Publishers. TIC: 244160.	Entire	N/A – Reference Only	6.5.1.1.3	Sensitivity analysis for scaling of fracture-matrix interfacial area.	N/A	N/A	N/A	N/A

OFFICE OF CIVILIAN RADIOACTIVE WASTE MANAGEMENT
DOCUMENT INPUT REFERENCE SHEET

1. Document Identifier No./Rev.: ANL-NBS-HS-000007/Rev. 00			Change:	Title: Natural Analogs for the Unsaturated Zone					
Input Document			4. Input Status	5. Section Used in	6. Input Description	7. TBV/TBD Priority	8. TBV Due To		
2. Technical Product Input Source Title and Identifier(s) with Version		3. Section					Unqual.	From Uncontrolled Source	Un-confirmed
29.	Dyer, J.R. 1999. "Revised Interim Guidance Pending Issuance of New U.S. Nuclear Regulatory Commission (NRC) Regulations (Revision 01, July 22, 1999), for Yucca Mountain, Nevada." Letter from J.R. Dyer (DOE) to D.R. Wilkins (CRWMS M&O), September 9, 1999, OL&RC:SB-1714, with enclosure, "Interim Guidance Pending Issuance of New U.S. Nuclear Regulatory Commission (NRC) Regulations (Revision 01)." ACC: MOL.19990910.0079.	Entire	N/A-Reference only	4.2	Interim Guidance	N/A	N/A	N/A	N/A

OFFICE OF CIVILIAN RADIOACTIVE WASTE MANAGEMENT
DOCUMENT INPUT REFERENCE SHEET

1. Document Identifier No./Rev.: ANL-NBS-HS-000007/Rev. 00			Change:	Title: Natural Analogs for the Unsaturated Zone					
Input Document			4. Input Status	5. Section Used in	6. Input Description	7. TBV/TBD Priority	8. TBV Due To		
2. Technical Product Input Source Title and Identifier(s) with Version		3. Section					Unqual.	From Uncontrolled Source	Un-confirmed
30.	Faybishenko, B.; Holland, P.; Mesa, M.; Burgess, D.; Knutson, C.; and Sisson, B. 1998a. *Lithological Conditions at the Box Canyon Site: Results of Drilling, Coring and Open Borehole Measurements—1995–1997 Data Report.* Report LBNL-40182. Berkeley, California: Lawrence Berkeley National Laboratory. TIC: 245839.	Entire	N/A-Reference only	6.5.1.1.2	Description of core logs and other details pertaining to Box Canyon site	N/A	N/A	N/A	N/A
31.	Faybishenko, B.A.; Salve, R.; Zawislanski, P.; Lee, K.H.; Cook, P.; Freifeld, B.; Williams, K.; and Doughty, C. 1998b. *Ponded Infiltration Test at the Box Canyon Site: Data Report and Preliminary Analysis.* Report LBNL-40183. Berkeley, California: Lawrence Berkeley National Laboratory. ACC: MOL.19981002.0035.	Entire	N/A – Reference only	6.5.1.1.5	Data source for the 96-1 data set in DTN: LB990930123122.001.	N/A	N/A	N/A	N/A

OFFICE OF CIVILIAN RADIOACTIVE WASTE MANAGEMENT
DOCUMENT INPUT REFERENCE SHEET

1. Document Identifier No./Rev.: ANL-NBS-HS-000007/Rev. 00			Change:	Title: Natural Analogs for the Unsaturated Zone					
Input Document			4. Input Status	5. Section Used in	6. Input Description	7. TBV/TBD Priority	8. TBV Due To		
2. Technical Product Input Source Title and Identifier(s) with Version		3. Section					Unqual.	From Uncontrolled Source	Un-confirmed
32.	Faybishenko, B.; Doughty, C.; Steiger, M.; Long, J.C.S.; Wood, T.R.; Jacobsen, J.S.; Lore, J.; and Zawislanski, P.T. 1999. *Conceptual Model of the Geometry and Physics of Water Flow in a Fractured Basalt Vadose Zone: Box Canyon Site, Idaho.* LBNL-42925. Berkeley, California: Lawrence Berkeley National Laboratory. TIC: 245840.	Entire	N/A – Reference only	6.5.1.1	Outlines the general conceptual model developed prior to this study to explain field data collected at the Box Canyon site. It is also source for the 97-1 to 97-4 data set, in DTN: LB990930123122.001.	N/A	N/A	N/A	N/A
33.	Finsterle, S. 1999. *ITOUGH2 User's Guide.* Report LBNL-40040. Berkeley, California: Lawrence Berkeley National Laboratory. ACC: MOL.19980429.0512.	Entire	N/A – Reference only	6.5.1.1	Inverse modeling methodology	N/A	N/A	N/A	N/A

OFFICE OF CIVILIAN RADIOACTIVE WASTE MANAGEMENT
DOCUMENT INPUT REFERENCE SHEET

1. Document Identifier No./Rev.: ANL-NBS-HS-000007/Rev. 00			Change:	Title: Natural Analogs for the Unsaturated Zone					
Input Document			4. Input Status	5. Section Used in	6. Input Description	7. TBV/TBD Priority	8. TBV Due To		
2. Technical Product Input Source Title and Identifier(s) with Version		3. Section					Unqual.	From Uncontrolled Source	Un-confirmed
34.	Flint, L.E. 1998. *Characterization of Hydrogeologic Units Using Matrix Properties, Yucca Mountain, Nevada.* Water-Resources Investigations Report 97–4243. Denver, Colorado: U.S. Geological Survey. ACC: MOL.19980429.0512.	Entire	N/A-Reference only	6.2	UZ matrix properties, Yucca Mt.	N/A	N/A	N/A	N/A
35.	Fridrich, C.J.; Dudley, W.W., Jr.; and Stuckless, J.S. 1994. "Hydrogeologic Analysis of the Saturated-Zone Ground-water System, under Yucca Mountain, Nevada." *Journal of Hydrology, 154*, 133-168. Amsterdam, The Netherlands: Elsevier Science. TIC: 224606.	Entire	N/A – Reference only	6.2	Conceptual model of SZ transport; role of faults as barriers or pathways to flow between UZ and SZ	N/A	N/A	N/A	N/A

OFFICE OF CIVILIAN RADIOACTIVE WASTE MANAGEMENT
DOCUMENT INPUT REFERENCE SHEET

1. Document Identifier No./Rev.: ANL-NBS-HS-000007/Rev. 00			Change:	Title: Natural Analogs for the Unsaturated Zone					
Input Document			4. Input Status	5. Section Used in	6. Input Description	7. TBV/TBD Priority	8. TBV Due To		
2. Technical Product Input Source Title and Identifier(s) with Version		3. Section					Unqual.	From Uncontrolled Source	Un-confirmed
36.	Glassley, W.E. and Christensen, B.W. 1992. "Water-Rock Interaction in New Zealand Hydrothermal Systems: Comparison of Some Simulated and Observed Geochemical Processes." *High Level Waste Management, Proceedings of the Third International Conference, Las Vegas, Nevada, April 12–16, 1992*, 352–356. La Grange Park, Illinois: American Nuclear Society. TIC: 204231.	Entire	N/A – Reference only	6.5.3.3	Application of New Zealand geothermal data to testing EQ3/6 code and database	N/A	N/A	N/A	N/A

OFFICE OF CIVILIAN RADIOACTIVE WASTE MANAGEMENT
DOCUMENT INPUT REFERENCE SHEET

1. Document Identifier No./Rev.: ANL-NBS-HS-000007/Rev. 00			Change:	Title: Natural Analogs for the Unsaturated Zone					
Input Document			4. Input Status	5. Section Used in	6. Input Description	7. TBV/TBD Priority	8. TBV Due To		
	2. Technical Product Input Source Title and Identifier(s) with Version	3. Section					Unqual.	From Uncontrolled Source	Un-confirmed
37.	Goodell P. 1985. "Chihuahua City Uranium Province, Chihuahua, Mexico." *Uranium Deposits in Volcanic Rocks, Proceedings of a Technical Committee Meeting on Uranium Deposits in Volcanic Rocks, El Paso, Texas, April 2–5, 1984*, 97–124. El Paso, Texas: International Atomic Energy Association. TIC: 246156.	Entire	N/A – Reference only	6.5.2.2	Proposal of Pena Blanca as a good analog to Yucca Mountain	N/A	N/A	N/A	N/A
38.	Grossenbacher, K. and Faybishenko, B. 1995. *Spacing of Thermally Induced Columnar Joints in Basalt: Variation with Depth*. LBNL-38060. Berkeley, California: Lawrence Berkeley National Laboratory. TIC: on order.	Entire	N/A – Reference only	6.5.1.1.2	Data source for vertical and horizontal fracture spacings.	N/A	N/A	N/A	N/A

OFFICE OF CIVILIAN RADIOACTIVE WASTE MANAGEMENT
DOCUMENT INPUT REFERENCE SHEET

1. Document Identifier No./Rev.: ANL-NBS-HS-000007/Rev. 00			Change:	Title: Natural Analogs for the Unsaturated Zone					
Input Document			4. Input Status	5. Section Used in	6. Input Description	7. TBV/TBD Priority	8. TBV Due To		
2. Technical Product Input Source Title and Identifier(s) with Version		3. Section					Unqual.	From Uncontrolled Source	Un-confirmed
39.	Hardin, E.L. 1998. *Near-Field/Altered Zone Models.* Milestone Report SP3100M4. Livermore, California: Lawrence Livermore National Laboratory. ACC: MOL.19980504.0577.	p. 5.57-5.67	N/A – Reference only	6.5.3.2	Potential formation of silica cap at YM	N/A	N/A	N/A	N/A
40.	Hevesi, J.A.; Flint, A.L.; and Istock, J.D. 1992. "Precipitation Estimation in Mountainous Terrain Using Multivariate Geostatistics, Part II: Isohyetal Maps." *Journal of Applied Meteorology, 31*, 677-688. Boston, Massachusetts: American Meteorological Society. TIC: 225247.	Entire	N/A – Reference only	6.2	Calculation of precipitation at YM	N/A	N/A	N/A	N/A

OFFICE OF CIVILIAN RADIOACTIVE WASTE MANAGEMENT
DOCUMENT INPUT REFERENCE SHEET

1. Document Identifier No./Rev.: ANL-NBS-HS-000007/Rev. 00			Change:	Title: Natural Analogs for the Unsaturated Zone					
Input Document			4. Input Status	5. Section Used in	6. Input Description	7. TBV/TBD Priority	8. TBV Due To		
2. Technical Product Input Source Title and Identifier(s) with Version		3. Section					Unqual.	From Uncontrolled Source	Un-confirmed
41.	Huang, K.; Tsang, Y.W.; and Bodvarsson, G.S. 1999. "Simultaneous Inversion of Air Injection Tests in Fractured Unsaturated Tuff at Yucca Mountain." *Water Resources Research, 35* (8), 2375-2386. Washington, D.C.: American Geophysical Union. TIC: 245633.	Entire	N/A – Reference only	6.5.1.1.4	Outlines the methodology used at Yucca Mountain for using pneumatic tests to determine fracture permeabilities.	N/A	N/A	N/A	N/A
42.	Ivanovich, M. and Harmon, R.S., eds. 1992. *Uranium Series Disequilibrium: Applications to Earth, Marine, and Environmental Sciences, 2nd Ed.* Oxford, England: Clarendon Press. TIC: 234680.	55–58, 77–78, 460–461, 631–668	N/A – Reference only	6.5.2.1.4.2.3	Calculated model of U-234 ages	N/A	N/A	N/A	N/A

OFFICE OF CIVILIAN RADIOACTIVE WASTE MANAGEMENT
DOCUMENT INPUT REFERENCE SHEET

1. Document Identifier No./Rev.: ANL-NBS-HS-000007/Rev. 00			Change:	Title: Natural Analogs for the Unsaturated Zone					
Input Document			4. Input Status	5. Section Used in	6. Input Description	7. TBV/TBD Priority	8. TBV Due To		
2. Technical Product Input Source Title and Identifier(s) with Version		3. Section					Unqual.	From Uncontrolled Source	Un-confirmed
43.	Knutson, C.F.; McCormick, K.A.; Smith, R.P.; Hackett, W.R.; O'Brien, J.P.; and Crocker, J.C. 1990. *Fiscal Year 89 Report RWMC Vadose Zone Basalt Characterization.* Report EG&G-WM-8949. Idaho Falls, Idaho: EG & G Idaho. TIC: 245912.	Entire	N/A – Reference only	6.5.1.1.2	Data source for matrix porosity and permeability.	N/A	N/A	N/A	N/A
44.	Knutson, C.F.; Cox, D.O.; Dooley, K.J.; and Sisson, J.B. 1993. "Characterization of Low Permeability Media Using Outcrop Measurements." *68th Annual Technical Conference and Exhibition of the Society of Petroleum Engineers, October 3-6, 1993, Houston Texas.* SPE Paper 26487. Richardson, Texas: Society of Petroleum Engineers. TIC: 247011.	Entire	N/A – Reference only	6.5.1.1.1	Geological description of Box Canyon site.	N/A	N/A	N/A	N/A

OFFICE OF CIVILIAN RADIOACTIVE WASTE MANAGEMENT
DOCUMENT INPUT REFERENCE SHEET

1. Document Identifier No./Rev.: ANL-NBS-HS-000007/Rev. 00			Change:	Title: Natural Analogs for the Unsaturated Zone					
Input Document			4. Input Status	5. Section Used in	6. Input Description	7. TBV/TBD Priority	8. TBV Due To		
	2. Technical Product Input Source Title and Identifier(s) with Version	3. Section					Unqual.	From Uncontrolled Source	Un-confirmed
45.	Krumhansl, J.L. and Stockman, H.W. 1988. "Site Selection Criteria and Preliminary Results from the Valles Caldera Natural Analog Study." *Proceedings of Workshop IV on Flow and Transport Through Unsaturated Fractured Rock–Related to High Level Radioactive Waste Disposal, Tucson, Arizona, 1988,* 249-276. Tucson, Arizona: University of Arizona. TIC: on order.	Entire	N/A – Reference only	6.5.3.2	Alteration effects at contact between tuff and obsidian, Valles Caldera	N/A	N/A	N/A	N/A

OFFICE OF CIVILIAN RADIOACTIVE WASTE MANAGEMENT
DOCUMENT INPUT REFERENCE SHEET

1. Document Identifier No./Rev.: ANL-NBS-HS-000007/Rev. 00			Change:	Title: Natural Analogs for the Unsaturated Zone					
Input Document			4. Input Status	5. Section Used in	6. Input Description	7. TBV/TBD Priority	8. TBV Due To		
	2. Technical Product Input Source Title and Identifier(s) with Version	3. Section					Unqual.	From Uncontrolled Source	Un-confirmed
46.	Ku, T.L.; Luo, S.; Leslie, B.W.; and Hammond, D.E. 1992. "Decay-Series Disequilibria Applied to the Study of Rock-Water Interaction and Geothermal Systems." *Uranium Series Disequilibrium: Applications to Earth, Marine, and Environmental Sciences, 2nd Ed.* Ivanovich, M. and Harmon, R.S., eds. New York, New York: Oxford University Press. TIC: 234680.	Entire	N/A – Reference only	6.5.2.1.6.2	Use of U-series disequilibrium in natural analog approach to study of rock-water systems	N/A	N/A	N/A	N/A

OFFICE OF CIVILIAN RADIOACTIVE WASTE MANAGEMENT
DOCUMENT INPUT REFERENCE SHEET

1. Document Identifier No./Rev.: ANL-NBS-HS-000007/Rev. 00			Change:	Title: Natural Analogs for the Unsaturated Zone					
Input Document			4. Input Status	5. Section Used in	6. Input Description	7. TBV/TBD Priority	8. TBV Due To		
	2. Technical Product Input Source Title and Identifier(s) with Version	3. Section					Unqual.	From Uncontrolled Source	Un-confirmed
47.	Leslie, B.; Pickett, D.; and Pearcy, E. 1999. "Vegetation-Derived Insights on the Mobilization and Potential Transport of Radionuclides from the Nopal I Natural Analog Site, Mexico." *Scientific Basis for Nuclear Waste Management, XXII Symposium Proceedings, Boston, Massachusetts, November 30 – December 4, 1998.* Warrendale, Pennsylvania: Materials Research Society. TIC: 246246.	Entire	N/A – Reference only	6.5.2.1.4.2.6	U-enriched plants at Nopal I	N/A	N/A	N/A	N/A

OFFICE OF CIVILIAN RADIOACTIVE WASTE MANAGEMENT
DOCUMENT INPUT REFERENCE SHEET

1. Document Identifier No./Rev.: ANL-NBS-HS-000007/Rev. 00			Change:	Title: Natural Analogs for the Unsaturated Zone					
Input Document			4. Input Status	5. Section Used in	6. Input Description	7. TBV/TBD Priority	8. TBV Due To		
2. Technical Product Input Source Title and Identifier(s) with Version		3. Section					Unqual.	From Uncontrolled Source	Un-confirmed
48.	Leslie, B.W.; Pearcy, E.A.; and Prikryl, J.C. 1993. "Oxidative Alteration of Uraninite at the Nopal I Deposit, Mexico." *Scientific Basis for Nuclear Waste Management XVI, Materials Resources Symposium Proceedings, Boston, Massachusetts, November 30 – December 4, 1992, 294*, 505. Pittsburgh, Pennsylvania: Materials Research Society. TIC: 208880.	Entire	N/A – Reference only	6.5.2.1.4.1.1	Comparison of alteration sequence at Nopal I with that from laboratory experiments	N/A	N/A	N/A	N/A
49.	Lichtner, P.C.; Keating, G.; and Carey, B. 1999. *A Natural Analogue for Thermal-Hydrological-Chemical Coupled Processes at the Proposed Nuclear Waste Repository at Yucca Mountain, Nevada. LA-13610-MS.* Los Alamos, New Mexico: Los Alamos National Laboratory. TIC: 246032.	Entire	N/A – Reference only	5 6.5.3.2 7.2.1	Calculated volumes of minerals precipitated from boiling water in fractures	N/A	N/A	N/A	N/A

OFFICE OF CIVILIAN RADIOACTIVE WASTE MANAGEMENT
DOCUMENT INPUT REFERENCE SHEET

1. Document Identifier No./Rev.: ANL-NBS-HS-000007/Rev. 00			Change:	Title: Natural Analogs for the Unsaturated Zone					
Input Document			4. Input Status	5. Section Used in	6. Input Description	7. TBV/TBD Priority	8. TBV Due To		
2. Technical Product Input Source Title and Identifier(s) with Version		3. Section					Unqual.	From Uncontrolled Source	Un-confirmed
50.	Liu, H.H.; Doughty, C.; and Bodvarsson, G.S. 1998. "An Active Fracture Model for Unsaturated Flow and Transport in Fractured Rocks." Water Resources Research, 34, (10), 2633-2646. Washington, D.C.: American Geophysical Union. TIC: 243012.	Entire	N/A – Reference only	6.5.1.1.3	"Active fracture" model	N/A	N/A	N/A	N/A
51.	Ludwig, K.R. and Titterington, D.M. 1994. "Calculation of ^{230}Th /U Isochrons, Ages, and Errors." *Geochimica et Cosmochimica Acta*, 22, 5031-5042. New York, New York: Pergamon Press. TIC: 245769.	Entire	N/A – Reference only	6.5.2.1.4.2.3	Methodology for calculation of ^{230}Th/^{234}U isochrons and source of errors	N/A	N/A	N/A	N/A

OFFICE OF CIVILIAN RADIOACTIVE WASTE MANAGEMENT
DOCUMENT INPUT REFERENCE SHEET

1. Document Identifier No./Rev.: ANL-NBS-HS-000007/Rev. 00			Change:	Title: Natural Analogs for the Unsaturated Zone					
Input Document			4. Input Status	5. Section Used in	6. Input Description	7. TBV/TBD Priority	8. TBV Due To		
2. Technical Product Input Source Title and Identifier(s) with Version		3. Section					Unqual.	From Uncontrolled Source	Un-confirmed
52.	Matyskiela, W. 1997. "Silica Redistribution and Hydrologic Changes in Heated Fractured Tuff." *Geology 25* (12),1115-1118. Boulder, Colorado: Geological Society of America. TIC: 236809.	Entire	N/A – Reference only	6.5.3.2	Analog study of fossil hydrothermal systems at Paiute Ridge, NV	N/A	N/A	N/A	N/A
53.	Meijer, A. 1987. *Investigations of Natural Geologic and Geochemical Analogs in Relation to a Potential Nuclear Waste Repository at Yucca Mountain, Nevada.* Milestone Report R398. Albuquerque, New Mexico: Los Alamos National Laboratory. ACC: NNA.19900112.0350.	Entire	N/A – Reference only	6.5.3.3	Attributes of Yellowstone hydrothermal system that compare with potential conditions at a YM repository	N/A	N/A	N/A	N/A

OFFICE OF CIVILIAN RADIOACTIVE WASTE MANAGEMENT
DOCUMENT INPUT REFERENCE SHEET

1. Document Identifier No./Rev.: ANL-NBS-HS-000007/Rev. 00			Change:	Title: Natural Analogs for the Unsaturated Zone					
Input Document			4. Input Status	5. Section Used in	6. Input Description	7. TBV/TBD Priority	8. TBV Due To		
2. Technical Product Input Source Title and Identifier(s) with Version		3. Section					Unqual.	From Uncontrolled Source	Un-confirmed
54.	Montazer, P. and Wilson, W.E. 1984. *Conceptual Hydrologic Model of Flow in the Unsaturated Zone, Yucca Mountain, Nevada.* Water-Resources Investigations Report 84–4345. Denver, Colorado: U.S. Geological Survey. ACC: NNA.19890327.0051.	Entire	N/A-Reference only	6.2	Conceptual hydrologic model of UZ flow, Yucca Mt.	N/A	N/A	N/A	N/A
55.	Murphy, W. 1995. "Natural Analogs for Yucca Mountain." *Radwaste Magazine*, 2 (6), 44-50. LaGrange Park, Illinois: American Nuclear Society. TIC: 237929.	Entire	N/A – Reference only	6.5.2.1.2	Pena Blanca as a good analog to YM - rationale	N/A	N/A	N/A	N/A

OFFICE OF CIVILIAN RADIOACTIVE WASTE MANAGEMENT
DOCUMENT INPUT REFERENCE SHEET

1. Document Identifier No./Rev.: ANL-NBS-HS-000007/Rev. 00			Change:	Title: Natural Analogs for the Unsaturated Zone					
Input Document			4. Input Status	5. Section Used in	6. Input Description	7. TBV/TBD Priority	8. TBV Due To		
2. Technical Product Input Source Title and Identifier(s) with Version		3. Section					Unqual.	From Uncontrolled Source	Un-confirmed
56.	Murrell, M.T.; Goldstein, S.; and Dixon, P.R. 1997. "Uranium Decay Series Mobility from a Uranium Ore Deposit: Implications for Nuclear Repository Stability." *EOS Transactions, 78* (46), F788. Washington, D.C.: American Geophysical Union. TIC: 246604.	Entire	N/A-Reference only	6.5.2.1	1997 U-series results	N/A	N/A	N/A	N/A
57.	Pearcy, E.C.; Prikryl, J.D.; Murphy, W.M.; and Leslie, B.W. 1994. "Alteration of Uraninite from the Nopal I Deposit, Peña Blanca District, Chihuahua, Mexico, Compared to Degradation of Spent Nuclear Fuel in the Proposed U.S. High-Level Nuclear Waste Repository at Yucca Mountain, Nevada." *Applied Geochemistry, 9*, 713-732. New York, New York: Elsevier Science. TIC: 236934.	Entire	N/A – Reference only	6.5.2.1.4.2.3 6.5.2.1 4.2.4	Ages of hydrologic disturbance at Nopal I based on U-Th data	N/A	N/A	N/A	N/A

OFFICE OF CIVILIAN RADIOACTIVE WASTE MANAGEMENT
DOCUMENT INPUT REFERENCE SHEET

1. Document Identifier No./Rev.: ANL-NBS-HS-000007/Rev. 00			Change:	Title: Natural Analogs for the Unsaturated Zone					
Input Document			4. Input Status	5. Section Used in	6. Input Description	7. TBV/TBD Priority	8. TBV Due To		
2. Technical Product Input Source Title and Identifier(s) with Version		3. Section					Unqual.	From Uncontrolled Source	Un-confirmed
58.	Pearcy, E.C.; Prikryl, J.D.; and Leslie, B.W. 1995. "Uranium Transport Through Fractured Silicic Tuff and Relative Retention in Areas with Distinct Fracture Characteristics." *Applied Geochemistry, 10,* 685-704. Oxford, United Kingdom: Elsevier Science. TIC: 246848.	Entire	N/A – Reference only	6.5.2.1.4.2.3	U and Th isotopic compositions for Nopal I samples	N/A	N/A	N/A	N/A
59.	Pickett, D.A. and Murphy, W.M. 1997. "Isotopic Constraints on Radionuclide Transport at Peña Blanca." *Seventh EC Natural Analogue Working Group Meeting, Proceedings of an International Workshop, Stein am Rhein, Switzerland, October 38–30, 1996,* 113–122. Stein am Rhein, Switzerland: European Commission. TIC: on order.	Entire, Table 2	N/A – Reference only	6.5.2.1.4.1.1	U-series data collected at Nopal I	N/A	N/A	N/A	N/A

OFFICE OF CIVILIAN RADIOACTIVE WASTE MANAGEMENT
DOCUMENT INPUT REFERENCE SHEET

1. Document Identifier No./Rev.: ANL-NBS-HS-000007/Rev. 00			Change:	Title: Natural Analogs for the Unsaturated Zone					
Input Document			4. Input Status	5. Section Used in	6. Input Description	7. TBV/TBD Priority	8. TBV Due To		
2. Technical Product Input Source Title and Identifier(s) with Version		3. Section					Unqual.	From Uncontrolled Source	Un-confirmed
60.	Pickett, D.A. and Murphy, W.M. 1999. "Unsaturated Zone Waters from the Nopal I Natural Analog, Chihuahua, Mexico—Implications for Radionuclide Mobility at Yucca Mountain." *Scientific Basis for Nuclear Waste Management, XXII Symposium Proceedings, Boston, Massachusetts, November 30 – December 4, 1998 556*, 809-816. Warrendale, Pennsylvania: Materials Research Society. TIC: 246424.	Entire	N/A – Reference only	6.5.2.1.4.2.3	Composition of Nopal I waters	N/A	N/A	N/A	N/A

OFFICE OF CIVILIAN RADIOACTIVE WASTE MANAGEMENT
DOCUMENT INPUT REFERENCE SHEET

1. Document Identifier No./Rev.: ANL-NBS-HS-000007/Rev. 00			Change:	Title: Natural Analogs for the Unsaturated Zone					
Input Document			4. Input Status	5. Section Used in	6. Input Description	7. TBV/TBD Priority	8. TBV Due To		
2. Technical Product Input Source Title and Identifier(s) with Version		3. Section					Unqual.	From Uncontrolled Source	Un-confirmed
61.	Prikryl, J.D.; Pickett, D.A.; Murphy, W.M.; and Pearcy, E.C. 1997. "Migration Behavior of Naturally Occurring Radionuclides at the Nopal I Uranium Deposit, Chihuahua, Mexico." *Journal of Contaminant Hydrology, 26,* 61-69. New York, New York: Elsevier Science. TIC: 242381.	Entire	N/A – Reference only	6.5.2.1.4.1.1	U in secondary minerals at Nopal I - mineralogy	N/A	N/A	N/A	N/A
62.	Pruess, K. 1991. *TOUGH2—A General Purpose Numerical Simulator for Multiphase Fluid and Heat Flow.* Report LBL-29400. Berkeley, California: Lawrence Berkeley National Laboratory. ACC: NNA.19940202.0088.	Entire	N/A – Reference only	6.5.1.1	TOUGH2 reference.	N/A	N/A	N/A	N/A

OFFICE OF CIVILIAN RADIOACTIVE WASTE MANAGEMENT
DOCUMENT INPUT REFERENCE SHEET

1. Document Identifier No./Rev.: ANL-NBS-HS-000007/Rev. 00			Change:	Title: Natural Analogs for the Unsaturated Zone					
Input Document			4. Input Status	5. Section Used in	6. Input Description	7. TBV/TBD Priority	8. TBV Due To		
2. Technical Product Input Source Title and Identifier(s) with Version		3. Section					Unqual.	From Uncontrolled Source	Un-confirmed
63.	Pruess, K. 1998. "On Water Seepage and Fast Preferential Flow in Heterogeneous, Unsaturated Rock Fractures." *Journal of Contaminant Hydrology, 30* (3–4), 333–362. Amsterdam, The Netherlands: Elsevier Science. TIC: 238921.	Entire	N/A – Reference only	6.5.1.1.5.1	Description of water flow channeling in variably saturated rough walled fractures.	N/A	N/A	N/A	N/A
64.	Stockman, H.; Krumhansl, J.; Ho, C.; and McConnell, V. 1994. *The Valles Natural Analogue Project.* Report NUREG/CR-6221. Washington , D.C.: U.S. Nuclear Regulatory Commission. TIC: 246123.	Entire	N/A- Reference only	6.5.3.2	Study of contact alteration between obsidian and tuff, Valles Caldera.	N/A	N/A	N/A	N/A

OFFICE OF CIVILIAN RADIOACTIVE WASTE MANAGEMENT
DOCUMENT INPUT REFERENCE SHEET

1. Document Identifier No./Rev.: ANL-NBS-HS-000007/Rev. 00			Change:	Title: Natural Analogs for the Unsaturated Zone					
Input Document			4. Input Status	5. Section Used in	6. Input Description	7. TBV/TBD Priority	8. TBV Due To		
2. Technical Product Input Source Title and Identifier(s) with Version		3. Section					Unqual.	From Uncontrolled Source	Un-confirmed
65.	Su, G.W.; Geller, J.T.; Pruess, K.; and Wen, F. 1999. "Experimental Studies of Water Seepage and Intermittent Flow in Unsaturated, Rough-Walled Fractures." *Water Resources Research, 35* (4), 1019–1037. Washington, D.C.: American Geophysical Union. TIC: 245798.	Entire	N/A – Reference only	6.5.1.1.5.1	Description of water flow channeling in variably saturated rough walled fractures	N/A	N/A	N/A	N/A
66.	Tsang, Y.W. 1992. "Usage of 'Equivalent Apertures' for Rock Fractures as Derived from Hydraulic and Tracer Tests." *Water Resources Research, 28* (5), 1451-1455. Washington, D.C.: American Geophysical Union. TIC: 245891.	Entire	N/A – Reference only	5 6.5.1.1.5.1	Definition of average fracture aperture as measured by various methods	N/A	N/A	N/A	N/A

OFFICE OF CIVILIAN RADIOACTIVE WASTE MANAGEMENT
DOCUMENT INPUT REFERENCE SHEET

1. Document Identifier No./Rev.: ANL-NBS-HS-000007/Rev. 00			Change:	Title: Natural Analogs for the Unsaturated Zone					
Input Document			4. Input Status	5. Section Used in	6. Input Description	7. TBV/TBD Priority	8. TBV Due To		
2. Technical Product Input Source Title and Identifier(s) with Version		3. Section					Unqual.	From Uncontrolled Source	Un-confirmed
67.	Wallace, A.B. and Roper, M.W. 1981. "Geology and Ore Deposits Along the Northeastern Margin, McDermitt Caldera Complex, Oregon." *Uranium in Volcanic and Volcaniclastic Rocks: AAPG Studies in Geology, 13,* 73-80. Goodell, P.C. and Waters, A.C., eds. Tulsa, Oklahoma: American Association of Petroleum Geologists. TIC: 245898.	Entire	N/A – Reference only	6.5.2.2	Geology and ore deposits at northeast margin of McDermitt Caldera	N/A	N/A	N/A	N/A
68.	Wang, J.S.Y. 1991. "Propagation of Infiltration Pulses through Unsaturated Tuff Units." in *A Review of Rainier Mesa Tunnel and Borehole Data and Their Possible Implications to Yucca Mountain Site Study Plans.* LBL-32068. Berkeley, California: Lawrence Berkeley National Laboratory. ACC: NNA.19920506.0020	Entire	N/A – Reference only	6.5.1.2	Hydrogeology and structural features of Rainier Mesa	N/A	N/A	N/A	N/A

OFFICE OF CIVILIAN RADIOACTIVE WASTE MANAGEMENT
DOCUMENT INPUT REFERENCE SHEET

1. Document Identifier No./Rev.: ANL-NBS-HS-000007/Rev. 00			Change:	Title: Natural Analogs for the Unsaturated Zone					
Input Document			4. Input Status	5. Section Used in	6. Input Description	7. TBV/TBD Priority	8. TBV Due To		
2. Technical Product Input Source Title and Identifier(s) with Version		3. Section					Unqual.	From Uncontrolled Source	Un-confirmed
69.	Wang, J.S.Y. 1992. "Variations of Hydrological Parameters of Tuff and Soil." *High Level Radioactive Waste Management, Proceedings of the 3rd Annual International Conference, Las Vegas, Nevada, April 12-14, 1992*, 727-731. LaGrange Park, Illinois: American Nuclear Society. TIC: 208542.	Entire	N/A – Reference only	6.5.1.2	Flow parameters in Apache Leap Tuff	N/A	N/A	N/A	N/A

OFFICE OF CIVILIAN RADIOACTIVE WASTE MANAGEMENT
DOCUMENT INPUT REFERENCE SHEET

1. Document Identifier No./Rev.: ANL-NBS-HS-000007/Rev. 00			Change:	Title: Natural Analogs for the Unsaturated Zone					
Input Document			4. Input Status	5. Section Used in	6. Input Description	7. TBV/TBD Priority	8. TBV Due To		
2. Technical Product Input Source Title and Identifier(s) with Version		3. Section					Unqual.	From Uncontrolled Source	Un-confirmed
70.	Wang, J.S.Y.; Cook, N.G.W.; Wollenberg, H.A.; Carnahan, C.L.; Javandel, I.; and Tsang, C.F. 1993. "Geohydrologic Data and Models of Rainier Mesa and Their Implications to Yucca Mountain." *High Level Radioactive Waste Management, Proceedings of the 4th Annual International Conference, Las Vegas, Nevada, April 26-30, 1993*, 675-681. LaGrange Park, Illinois: American Nuclear Society. TIC: 208542.	Entire	N/A – Reference only	6.5.1.2	^{36}Cl measurements in Rainier Mesa tunnels; comparison of Rainier Mesa and YM hydrostratigraphy	N/A	N/A	N/A	N/A
71.	Whelan, J.A. and Reed, M.F. 1997. "Geostatistical Analysis of Regional Hydraulic Conductivity Variations in the Snake River Plain Aquifer, Eastern Idaho." *GSA Bulletin, 109* (7), 855-868. Boulder, Colorado: Geological Society of America. TIC: 246133.	Entire	N/A-Reference only	6.5.1.1.1	Geological description of Box Canyon site.	N/A	N/A	N/A	N/A

OFFICE OF CIVILIAN RADIOACTIVE WASTE MANAGEMENT
DOCUMENT INPUT REFERENCE SHEET

1. Document Identifier No./Rev.: ANL-NBS-HS-000007/Rev. 00			Change:	Title: Natural Analogs for the Unsaturated Zone					
Input Document			4. Input Status	5. Section Used in	6. Input Description	7. TBV/TBD Priority	8. TBV Due To		
2. Technical Product Input Source Title and Identifier(s) with Version		3. Section					Unqual.	From Uncontrolled Source	Un-confirmed
72.	WoldeGabriel, G.; Keating, G.N.; and Valentine, G.A. 1999. "Effects of Shallow Basaltic Intrusion into Pyroclastic Deposits, Grants Ridge, New Mexico, USA." *Journal of Volcanology and Geothermal Research, 92*, 389-411. Amsterdam, The Netherlands: Elsevier Science. TIC: 246037.	Entire	N/A – Reference only	6.5.3.2	Effects of basaltic intrusion on host rock TH-THC properties	N/A	N/A	N/A	N/A
73.	Wolery, T.J. and Daveler, S.A. 1992. *EQ6, A Computer Program for Reaction Path Modeling of Aqueous Geochemical Systems: Theoretical Manual, User's Guide, and Related Documentation (Version 7.0).* Report UCRL-MFA-110662, Pt. IV. Livermore, California: Lawrence Livermore National Laboratory. TIC: 205002.	Entire	N/A – Reference only	6.5.3.3	Example of reaction path code used by others for thermochemical modeling	N/A	N/A	N/A	N/A

OFFICE OF CIVILIAN RADIOACTIVE WASTE MANAGEMENT
DOCUMENT INPUT REFERENCE SHEET

1. Document Identifier No./Rev.: ANL-NBS-HS-000007/Rev. 00			Change:	Title: Natural Analogs for the Unsaturated Zone					
Input Document			4. Input Status	5. Section Used in	6. Input Description	7. TBV/TBD Priority	8. TBV Due To		
2. Technical Product Input Source Title and Identifier(s) with Version		3. Section					Unqual.	From Uncontrolled Source	Un-confirmed
74.	Wollenberg, H.A. and Flexser, S. 1986. "Contact Zones and Hydrothermal Systems as Analogues to Repository Conditions." *Chemical Geology 55*, 345-359. Amsterdam, The Netherlands: Elsevier Science Publishers. TIC: 246171.	Entire	N/A – Reference only	6.5.3.2	Transport of U and trace elements away from igneous contact zones	N/A	N/A	N/A	N/A
75.	Wong, V. 1998. *Gamma-Ray Characterization of Uranium-Series Nuclides and its Application to the Study of the Peña Blanca Natural Analog Site, Chihuahua, Mexico.* Ph.D. dissertation. El Paso, Texas: University of Texas at El Paso. TIC: 245933.	Entire	N/A – Reference only	6.5.2.1.4.1.2	U-series disequilibrium using gamma spectrometry	N/A	N/A	N/A	N/A

OFFICE OF CIVILIAN RADIOACTIVE WASTE MANAGEMENT
DOCUMENT INPUT REFERENCE SHEET

1. Document Identifier No./Rev.: ANL-NBS-HS-000007/Rev. 00			Change:	Title: Natural Analogs for the Unsaturated Zone					
Input Document			4. Input Status	5. Section Used in	6. Input Description	7. TBV/TBD Priority	8. TBV Due To		
	2. Technical Product Input Source Title and Identifier(s) with Version	3. Section					Unqual.	From Uncontrolled Source	Un-confirmed
76.	Wronkiewicz, D.J.; Bates, J.K.; Wolf, S.F.; and Buck, E.C. 1996. "Ten-Year Results from Unsaturated Drip Tests With UO^2 at 90°C: Implications for the Corrosion of Spent Nuclear Fuel." *Journal of Nuclear Materials, 238,* 78–95. Amsterdam, The Netherlands: Elsevier Science. TIC: 243361.	Entire	N/A – Reference only	6.5.2.1.3	Secondary U mineral phases formed in laboratory drip tests	N/A	N/A	N/A	N/A
77.	Xu, T. and Pruess, K. 1998. *Coupled Modeling of Non-Isothermal Multi-Phase Flow, Solute Transport and Reactive Chemistry in Porous and Fractured Media: 1. Model Development and Validation.* LBNL-42050. Berkeley, California: Lawrence Berkeley National Laboratory. TIC: 243735.	Entire	N/A-Reference only	7.1	Example reference of coupled process modeling code	N/A	N/A	N/A	N/A

OFFICE OF CIVILIAN RADIOACTIVE WASTE MANAGEMENT
DOCUMENT INPUT REFERENCE SHEET

1. Document Identifier No./Rev.: ANL-NBS-HS-000007/Rev. 00		Change:	Title: Natural Analogs for the Unsaturated Zone					
Input Document		4. Input Status	5. Section Used in	6. Input Description	7. TBV/TBD Priority	8. TBV Due To		
2. Technical Product Input Source Title and Identifier(s) with Version	3. Section					Unqual.	From Uncontrolled Source	Un-confirmed
78. YMP (Yucca Mountain Project) 1998. *Repository Safety Strategy: U.S. Department of Energy's Strategy to Protect Public Health and Safety after Closure of a Yucca Mountain Repository.* YMP/96-01, Rev. 2. Washington D.C.: DOE OCRWM. ACC: MOL.19980727.0001.	Entire	N/A - Reference only	7.1.1	Role of natural analogs in DOE/YMP safety strategy	N/A	N/A	N/A	N/A
79. Zyvoloski, G.A; Dash, Z.V.; and Kelkar, S. 1996. *FEHMN 1.0, Finite Element Heat and Mass Transfer Code.* Technical Report LA-12062-MS, Rev. 1. Albuquerque, New Mexico: Los Alamos National Laboratory. ACC: NNA.19910625.0038.	Entire	N/A – Reference only	6.5.3.2	Reference to code used by others in modeling hydrothermal processes	N/A	N/A	N/A	N/A
80. Software code: TOUGH2 V1.3. STN: 10061-1.3-00.	Entire	N/A–Q	6.5.1.1	Modeling code used in 6.5.1.1 of this report	N/A	N/A	N/A	N/A
81. Software macro: perm.for V1.0. ACC: MOL.19991011.0224.	Entire	N/A–Q	6.5.1.1	Software use	N/A	N/A	N/A	N/A

OFFICE OF CIVILIAN RADIOACTIVE WASTE MANAGEMENT
DOCUMENT INPUT REFERENCE SHEET

1. Document Identifier No./Rev.: ANL-NBS-HS-000007/Rev. 00			Change:	Title: Natural Analogs for the Unsaturated Zone					
Input Document			4. Input Status	5. Section Used in	6. Input Description	7. TBV/TBD Priority	8. TBV Due To		
2. Technical Product Input Source Title and Identifier(s) with Version		3. Section					Unqual.	From Uncontrolled Source	Un-confirmed
82.	Software macro: plot.for V1.0. ACC: MOL.19991011.0225.	Entire	N/A–Q	6.5.1.1	Software use	N/A	N/A	N/A	N/A
83.	Software macro: rocktype.for V1.0. ACC: MOL.19991011.0226.	Entire	N/A–Q	6.5.1.1	Software use	N/A	N/A	N/A	N/A
84.	Software macro: save2tec.for V1.0 ACC: MOL.19991011.0227.	Entire	N/A–Q	6.5.1.1	Software use	N/A	N/A	N/A	N/A
85.	Software macro: tough2tec.for V1.0. ACC: MOL.19991011.0228.	Entire	N/A–Q	6.5.1.1	Software use	N/A	N/A	N/A	N/A
86.	Software macro: trans_cal.for V1.0. ACC: MOL.19991011.0229.	Entire	N/A–Q	6.5.1.1	Software use	N/A	N/A	N/A	N/A
87.	Software macro: weight.for V1.0. ACC: MOL.19991011.0230.	Entire	N/A–Q	6.5.1.1	Software use	N/A	N/A	N/A	N/A

ATTACHMENT II.

LIST OF INPUT/OUTPUT FILES FOR BOX CANYON STUDY (SECTION 6.5.1.1)

The following files were used during the Box Canyon simulations and submitted to the TDMS under DTN: LB990930123122.002.

Pneumatic Injection Analysis

Parameter file for software routine rocktype.for used to create TOUGH2 (TOUGH2 V1.3, STN: 10061-1.3-00) input

C:\803D-74\FractureNetwork\grid\rocktype\rocktype_pneumatic.prm

TOUGH2 input and output files

C:\803D-74\results\pneumatic\pneumatic.zip

Infiltration Analysis

The following files were used for the 1-d infiltration calibration and are parameter files for software routine rocktype.for used to create TOUGH2 input.

C:\803D-74\FractureNetwork\grid\rocktype\rocktype_steady_e1.prm

\rocktype_trans_e1.prm

\obstimes_e1.dat

C:\803D-74\FractureNetwork\grid\rocktype\rocktype_steady_i1.prm

\rocktype_trans_i1.prm

\obstimes_i1.dat

C:\803D-74\FractureNetwork\grid\rocktype\rocktype_steady_i2.prm

\rocktype_trans_i2.prm

\obstimes_i2.dat

C:\803D-74\FractureNetwork\grid\rocktype\rocktype_steady_i3.prm

\rocktype_trans_i3.prm

\obstimes_i3.dat

C:\803D-74\FractureNetwork\grid\rocktype\rocktype_steady_t5.prm

\rocktype_trans_t5.prm

\obstimes_t5.dat

C:\803D-74\FractureNetwork\grid\rocktype\rocktype_steady_t6.prm

\rocktype_trans_t6.prm

\obstimes_t6.dat

C:\803D-74\FractureNetwork\grid\rocktype\rocktype_steady_t7.prm

\rocktype_trans_t7.prm

\obstimes_t7.dat

C:\803D-74\FractureNetwork\grid\rocktype\rocktype_steady_t8.prm

\rocktype_trans_t8.prm

\obstimes_t8.dat

C:\803D-74\FractureNetwork\grid\rocktype\rocktype_steady_t9.prm

\rocktype_trans_t9.prm

\obstimes_t9.dat

C:\803D-74\FractureNetwork\grid\rocktype\pond_96-1_97-1-4.dat

The "steady" file set up the steady-state conditions while the "trans" file sets up 96-1 to 97-1 to 97-4 infiltration conditions. The "obstimes" file set up TOUGH2 output times while the "pond" file was used to establish the infiltration rates.

Output from TOUGH2 after processing by software routine trans_cal.for is provided in the following directories:

C:\803D-74\FractureNetwork\grid\trans_cal\e1\trans_cal.dat

\i1\trans_cal.dat

\i2\trans_cal.dat

\i3\trans_cal.dat

\t5\trans_cal.dat

\t6\trans_cal.dat

\t7\trans_cal.dat

\t8\trans_cal.dat

\t9\trans_cal.dat

and the final Tecplot (a standard graphics program) input file created by plot.for using the above files is:

C:\803D-74\FractureNetwork\grid\trans_cal\plot\plot.dat

The following files were used in the 3-d infiltration simulations and are parameter files for software routine rocktype.for used to create TOUGH2 input.

C:\803D-74\FractureNetwork\grid\rocktype\rocktype_steady_3d.prm

\rocktype_trans_96-1_3d.prm

\pond_96-1.dat

\rocktype_trans_97-1-4_3d.prm

\pond_97-1_97-4.dat

\obstimes_3d.dat

The resulting TOUGH2 input/output is located in:

C:\803D-74\results\infiltration\steady\steady.zip

C:\803D-74\results\infiltration\96-1\96-1.zip

C:\803D-74\results\infiltration\97-1\97-1.zip

The software routine weight.for was used to create Tecplot input files to visualize the weighting factors used to condition the hydrogeological properties in the fracture continuum. All files are located in:

C:\803D-74\FractureNetwork\grid\WeightingFactor

The software routine perm.for was used to locate the packer centroid of each pneumatic test in the Box Canyon grid. All relevant files are located in:

C:\803D-74\FractureNetwork\grid\perm

The softare routine save2tec.for and tough2tec.for were used to extract output from TOUGH2 and reformat it for visualization using Tecplot. All relevant files are located in:

C:\803D-74\FractureNetwork\grid\save2tec

C:\803D-74\Fracture Network/grid/tough2tec

ATTACHMENT III.

PEÑA BLANCA NATURAL ANALOG BIBLIOGRAPHY

Alexander, W. and McKinley, I. 1992. "A Review of the Application of Natural Analogs in Performance Assessment: Improving Models of Radionuclide Transport in Groundwaters." *Journal of Geochemical Exploration, 46*, 83–115. Amsterdam, Netherlands.

Allard, T. and Muller, J.P. 1998. "Kaolinite as an In Situ Dosimeter for Past Radionuclide Migration at the Earth's Surface." *Applied Geochemistry, 13* (6), 751–765. Oxford, United Kingdom: Pergamon Press.

Bell, R. 1981. *Geology at Central Sierra Peña Blanca.* Masters Thesis. El Paso, Texas: University of Texas.

Cardenas-Flores, D. 1985. "Volcanic Stratigraphy and U-Mo Mineralization of the Sierra de Peña Blanca District, Chihuahua, Mexico." *Uranium Deposits in Volcanic Rocks, Proceedings of a Technical Committee Meeting on Volcanic Rocks, El Paso, Texas, April 2-5, 1984*, 125–136. IAEA-TC-490/31. Vienna, Austria: International Atomic Energy Agency.

Clark K.; Goodell. P.; and Lovejoy. E. 1983. "Geology and Mineral Resources of North Central Chihuahua." *Guidebook for the 1983 Field Conference, El Paso Geological Society, October 7-9, 1983.*

Finch, R.J. and Ewing, R. 1992. "The Corrosion of Uraninite Under Oxidizing Conditions." *Journal of Nuclear Materials, 190*, 133–156. Amsterdam, Netherlands: Elsevier Science Publishers.

George-Aniel, B.; Leroy, J.; and Poty, B. 1985. "Uranium Deposit of the Sierra Peña Blanca." *Uranium Deposits in Volcanic Rocks, Proceedings of a Technical Committee Meeting on Volcanic Rocks, El Paso, Texas, April 2-5, 1984*, 175–186. IAEA-TC-490/8. Vienna, Austria: International Atomic Energy Agency.

George-Aniel, B.; Leroy, J.; and Poty, B. 1991. "Volcanogenic Uranium Mineralizations in the Sierra Peña Blanca District, Chihuahua, Mexico: Three Genetic Models." *Economic Geology, 86* (2), 233–248.

Goodell P. 1980. "Geology of the Peña Blanca Uranium Deposits, Chihuahua, Mexico." *Uranium Deposits in Volcanic Rocks: Symposium Proceedings of the Annual Meeting of the Southwest Section of the American Association of Petroleum Geologists, El Paso, Texas, 1980, 13*, 275–292. Goodell, P. and Waters, A., eds. Tulsa, Oklahoma: American Association of Petroleum Geologist.

Goodell, P. 1985a. "Classification and Model of Uranium in Volcanic Deposits." *Uranium Deposits in Volcanic Rocks, Proceedings of a Technical Committee Meeting on Volcanic Rocks, El Paso, Texas, April 2-5, 1984*, 1–16. IAEATC-490/8. Vienna, Austria: International Atomic Energy Agency.

Goodell, P. 1985b. "Chihuahua City Uranium Province, Chihuahua, Mexico." *Uranium Deposits in Volcanic Rocks, Proceedings of a Technical Committee Meeting on Volcanic Rocks, El Paso, Texas, April 2-5, 1984*, 97–124. IAEATC-490/19. Vienna, Austria: International Atomic Energy Agency.

Green, R.; Rice, G.; and Meyer-James, K. 1995. *Hydraulic Characterization of Hydrothermally Altered Nopal Tuff.* NUREG/CR-6356, CNWRA 94-027. San Antonio, Texas: Center for Nuclear Waste Regulatory Analyses.

IAEA 1989. *Natural Analogs in Performance Assessment for the Disposal of Long-Lived Radioactive Wastes.* IAEA Technical Report Series No 304, 1–51. Vienna, Austria: International Atomic Energy Agency.

Ildefonse, P.; Muller, J.P.; Clozel, B.; and Calas, G. 1990a. "Study of Two Alteration Systems as Natural Analogues for Radionuclides Release and Migration." *Engineering Geology, 29* (4), 413–439.

Ildefonse, P.; Muller, J.P.; and Callas, G. 1990b. "Assessment of Radionuclide Migration in Natural Analogues by Radiation-Induced Centers in Kaolinite." *Symposium Proceedings of the Scientific Basis for Nuclear Waste Management XIV,* 212, 474. Abrajano, T. and Johnson, L., eds. Pittsburgh, Pennsylvania: Materials Research Society.

Ildefonse, P.; Muller, J.P.; Clozel, B.; and Calas, G. 1991. "Record of Past Contact Between Altered Rocks and Radioactive Solutions through Radiation-Induced Defects in Kaolinite." *Symposium Proceedings of the Scientific Basis for Nuclear Waste Management XV, 212,* 749. Pittsburgh, Pennsylvania: Materials Research Society.

Latham, A. and Schwarcz, H. 1989. "Review of the Modeling of Radionuclide Transport From U-Series Disequilibria and of Its Use in Assessing the Safe Disposal of Nuclear Waste in Crystalline Rock." *Applied Geochemistry, 4* (5), 527–537.

Leslie, B.; Pearcy, E.; and Prikryl, J. 1993a. *Geochemical Natural Analogs, in NRC High-Level Radioactive Waste Research at CNWRA, January-June 1992.* NUREG/CR-5817, CNWRA 92-01S, 3 (1), San Antonio, Texas: Center for Nuclear Waste Regulatory Analyses.

Leslie, B.; Pearcy, E.; and Prikryl, J. 1993b. "Oxidative Alteration of Uraninite at the Nopal I Deposit, Mexico." *Symposium Proceedings of the Scientific Basis for Nuclear Waste Management XVII, 294,* 505–512. Pittsburgh, Pennsylvania: Materials Research Society.

Leslie, B.; Pickett, D.A.; and Pearcy, E. 1999. "Vegetation-Derived Insights on the Mobilization and Potential Transport of Radionuclides from the Nopal I Natural Analog Site, Mexico." *Symposium Proceedings of the Scientific Basis for Nuclear Waste Management, XXII, Boston, Massachusetts, November 30-December 4, 1998.* Wronkiewicz, D. and Lee, J., eds. Pittsburgh, Pennsylvania: Materials Research Society.

Lueth, V. and Heizler, M. 1997. "Ar-40/Ar-39 Age and Origin of Jarosite Mineralization at the Ansonburg District, New Mexico." *Annual Meeting, New Mexico Geological Society, April 18, 1997.*

Lueth, V.; Goodell, P.; Heizler, M.; and Peters, L. 1998. "Geochemistry, Geochronology, and Tectonic Implications of Jarosite Mineralization in the Northern Franklin Mountains, Doña Ana County, New Mexico." *New Mexico Geological Guidebook, 309.* Las Cruces, New Mexico: New Mexico Geological Society.

Magonthier, M.C. 1985. "Caracteristicas Petrograficas y Geoquimicas de las Unidades Ignimbriticas Portadoras de Mineralizacion de Uranio de la Sierra Peña Blanca." *Uranium Deposits in Volcanic Rocks, Proceedings of a Technical Committee Meeting on Volcanic Rocks, El Paso, Texas, April 2-5, 1984*, 137–150. IAEATC-490/7. Vienna, Austria: International Atomic Energy Agency.

Magonthier, M.C. 1987. "Relations Entre Les Mineralisations D'uranium de la Sierra Peña Blanca (Mexique) et les Ignimbrites Porteuses." *Bulletin of Mineralogy, 110*, 305.

McKinley, I. and Alexander, W. 1993. "Assessment of Radionuclide Retardation: Uses and Abuses of Natural Analog Studies." *Journal of Contaminant Hydrology, 13* (1-4), 249–259. Amsterdam, Netherlands: Elsevier Science Publishers.

Meyer, K. 1995. *Hydraulic Characterization of Hydrothermally Altered Nopal Tuff.* Thesis Dissertation. San Antonio, Texas. The University of Texas.

Miranda, M.; Martinez, J.; and Olvera, L. 1985. "Emanometria de Radon en el Distrito Uranifero de Sierra Peña Blanca y en Ostras Areas Volcanicas de Chihuahua, Mexico." *Uranium Deposits in Volcanic Rocks, Symposium Proceedings of a Technical Committee Meeting on Volcanic Rocks, El Paso, Texas, April 2-5, 1984*, 151–160. IAEATC-490/21. Vienna, Austria: International Atomic Energy Agency.

Mitchell, S.; Goodell, P.; LeMone, D.; and Pingitore, N. 1980. "Uranium Mineralization of Sierra Gomez, Chihuahua, Mexico." *Uranium Deposits in Volcanic Rocks: Symposium Proceedings of the Southwest Section of the American Association of Petroleum Geologists, El Paso, Texas, 1980, 13*, 293–310. Goodell, P. and Waters, A., eds. Tulsa, Oklahoma: American Association of Petroleum Geologists.

Muller, J.P.; Ildefonse, P.; and Calas, G. 1990. "Paramagnetic Defect Centers in Hydrothermal Kaolinite from an Altered Tuff in the Nopal Uranium Deposit, Chihuahua, Mexico." *Clays and Clay Minerals, 38*, 600–608.

Murphy, W.; Pearcy, E.; and Goodell, P. 1991. "Possible Analog Research Sites for the Proposed High Level Nuclear Waste Repository in Hydrologically Unsaturated Tuff at Yucca Mountain, Nevada." *Nuclear Science and Technology: Proceedings of the Fourth Natural Analog Working Group Meeting and Poços de Caldas Project Final Workshop, June, 18-22, 1990, Pitlochry, Scotland,* 267–276. Report EUR-13014-EN. Luxembourg, Luxembourg: Commission of the European Communities.

Murphy, W. 1992. "Natural Analog Studies for Geological Disposal of Nuclear Waste." *Technology Today, June,* 16-21. San Antonio, Texas: Southwest Research Institute.

Murphy, W. and Pearcy, E. 1992. "Source-Term Constraints for the Proposed Repository at Yucca Mountain, Nevada, Derived from the Natural Analog at Peña Blanca, Mexico." *Symposium Proceedings from Scientific Basis for Nuclear Waste Management XV, 257,* 521–527. Sombret, C.G., ed. Pittsburgh, Pennsylvania: Materials Research Society.

Murphy, W.M. and Kovach, L.A. 1993. *The Role of Natural Analogs in Geologic Disposal of High-Level Nuclear Waste*, 1–113. Report CNWRA 93-020. San Antonio, Texas: Center for Nuclear Waste Regulatory Analyses.

Murphy, W.; Pearcy, E.; and Goodell, P. 1993. "Performance Assessment Significance of Natural Analog Studies at Peña Blanca, Mexico, and at Santorini, Greece." *Nuclear Science and Technology: Proceedings of the Fourth Natural Analog Working Group Meeting and Alligator River Analog Final Workshop, June 18-22, 1993, Pitlochry, Scotland,* 219–224. Côme, B. and Chapman, N.A., eds. Report EUR-13014-EN. Luxembourg, Luxembourg: Commission of the European Communities.

Murphy, W. and Pearcy, E. 1994. "Performance Assessment Significance of Natural Analog Studies at Peña Blanca , Mexico, and at Santorini, Greece." *Nuclear Science and Technology: Proceedings of the Fifth Analog Working Group Meeting, October 5-9, 1994, Toledo, Spain,* 219. Von Maravic, H. and Smellie, J.A.T., eds. Report EUR-15176-EN. Luxembourg, Luxembourg: Commission of the European Communities.

Murphy, W. 1995a. "Effects of Carbon System Geochemistry on Radionuclide Migration at the Proposed Nuclear Waste Repository at Yucca Mountain, Nevada, USA." *Migration Conference St. Malo, France, 1995*, 52.

Murphy, W. 1995b. "Natural Analogs for Yucca Mountain." *Radwaste Magazine, 2 (6)*, 45–50. La Grange Park, Illinois: American Nuclear Society.

Murphy, W. 1996. "Retrograde Solubilities of Source Term Phases." *Symposium Proceedings from Scientific Basis for Nuclear Waste Management XIX, 465*, 713. Pittsburgh, Pennsylvania: Materials Research Society.

Murphy, W.; Pearcy, E.; and Pickett, D. 1997a. "Natural Analog Studies at Peña Blanca and Santorini." *Nuclear Science and Technology: Proceedings from the Seventh Natural Analog Working Group Meeting, October 28-30, 1997, Stein am Rhein, Switzerland,* 105–112. Von Maravic, H. and Smellie, J.A.T., eds. Report EUR-17851-EN. Luxembourg, Luxembourg: Commission of the European Communities.

Murphy, W.; Pearcy, E.; and Pickett, D. 1997b. "Radionuclide Transport from Mined Uranium Ore at Peña Blanca." *Proceedings of the Fourth International Conference on Tailings and Mine Waste '97, Fort Collins, Colorado,* 401–404. Rotterdam, Netherlands: A.A. Balkema.

Murphy, W.; Pearcy, E.; Green, R.; Prikryl, J.; Mohanty, S.; Leslie, B.; Nedungadi, A. 1998. "A Test of Long-Term Predictive Geochemical Transport Modeling at the Akrotiri Archaeological Site." *Journal of Contaminant Hydrology, 29* (3), 245–279. Amsterdam, Netherlands: Elsevier Science Publishers.

Murphy, W. and Codell, R. 1999. "Alternate Source Term Models for Yucca Mountain Performance Assessment Based on Natural Analog Data and Secondary Mineral Solubility." *Proceedings from Scientific Basis for Nuclear Waste Management XXII, 556,* 713. Pittsburgh, Pennsylvania: Materials Research Society.

Pearcy, E. and Murphy, W. 1990a. *Geochemical Natural Analogs: Report on Research Activities for Calendar Year, 1990.* NUREG/CR-5817. San Antonio, Texas: Center for Nuclear Waste Regulatory Analyses.

Pearcy, E. 1990. *Geochemical Natural Analogs: Report on Research Activities for the Quarter April 1 through June 30, 1990.* Patrick, W., ed. CNWRA 90-02Q. San Antonio, Texas: Center for Nuclear Waste Regulatory Analyses.

Pearcy, E. 1991. "Oxidative Alteration of Uraninite in a Silicic Tuffaceous Environment." *Geological Society of America Abstracts with Program, 23*, A383. Denver, Colorado: Geological Society of America.

Pearcy, E. and Murphy, W. 1991. *Geochemical Natural Analogs: Report on Research Activities for the Quarter July 1 through September 30, 1991.* Patrick, W., ed. CNWRA 91-03Q. San Antonio, Texas: Center for Nuclear Waste Regulatory Analyses.

Pearcy, E.; Murphy, W.; Green, R.; Leslie, B.; Prikryl, J. 1991a. *NRC High-Level Radioactive Waste Research at CNWRA, Calendar Year 1991.* NUREG/CR-5817, CNWRA 91-01A. San Antonio, Texas: Center for Nuclear Waste Regulatory Analyses.

Pearcy, E.; Murphy, W.; Prikryl, J. 1991b. *Geochemical Natural Analogs: Report on Research Activities for the Quarter April 1 through June 30, 1991.* Patrick, W., ed. CNWRA 91-02Q. San Antonio, Texas: Center for Nuclear Waste Regulatory Analyses.

Pearcy, E. 1993. "Crystal Chemistry and Structures of Uraninite from the Nopal I Deposit, Peña Blanca District, Mexico." *Geological Society of America Abstracts with Program, 25,* A382. Denver, Colorado: Geological Society of America.

Pearcy, E. and Leslie, B. 1993. *Geochemical Natural Analog Research: NRC High-Level Radioactive Research at CNWRA, January through June 1993.* Sagar, B., ed. CNWRA 93-01S. San Antonio, Texas: Center for Nuclear Waste Regulatory Analyses.

Pearcy, E.; Murphy, W.; Green, R.; Leslie, B.; and Prikryl, J. 1993. *Geochemical Natural Analog Research: NRC High-Level Radioactive Research at CNWRA, Calendar Year 1991.* Patrick, W., ed. NUREG/CR-5817- Vol. 2, CNWRA 91-01A. San Antonio, Texas: Center for Nuclear Waste Regulatory Analyses.

Pearcy, E. 1994a. *Fracture Transport of Uranium at the Nopal I Analog Site.* CNWRA 94-011. San Antonio, Texas: Center for Nuclear Waste Regulatory Analyses.

Pearcy, E. 1994b. *Geochemical Natural Analog Research: NRC High-Level Radioactive Research at CNWRA, January through June 1994.* CNWRA 94-01S. San Antonio, Texas: Center for Nuclear Waste Regulatory Analyses.

Pearcy, E. and Manaktala, H. 1994. "Nuclear Fuel Corrosion over Millennia Interpreted Using Geologic Data." *Annual Conference of the National Association of Corrosion Engineers-Proceedings-Corrosion 94*, 129/1-129/8.

Pearcy, E.; Murphy, W.; Prikryl, J.; and Leslie, B. 1994. "Alteration of Uraninite from the Nopal I Deposit, Peña Blanca District, Chihuahua, Mexico, Compared to Degradation of Spent Nuclear Fuel in the Proposed U.S. High-Level Waste Repository at Yucca Mountain, Nevada." *Journal of Applied Geochemistry, 9*, 713–732. Amsterdam, Netherlands: Elsevier Science Publishers.

Pearcy, E.; Prikryl, J.; and Leslie, B. 1995. "Uranium Transport through Fractured Silicic Tuff and Relative Retention in Areas with Distinct Fracture Characteristics." *Journal of Applied Geochemistry, 10*, 685–704. Amsterdam, Netherlands: Elsevier Science Publishers.

Petit, J.C. 1990. "Migration of Radionuclides in the Geosphere: What Can We Learn from Natural Analogs?" *Radiochimica Acta, 51* (4), 181–188. Oxford, United Kingdom: Pergamon Press.

Pickett, D.; Prikryl, J.; Murphy, W.; and Pearcy, E. 1996. "Uranium-Series Disequilibria at the Nopal I Uranium Deposit, Peña Blanca District, Chihuahua, Mexico: Implications for Episodic Radionuclide Transport at a Geologic Repository for High Level Nuclear Waste." *EOS Transactions of the American Geophysical Union, 77* (17), 594. Washington, D.C.: American Geophysical Union.

Pickett, D. and Murphy, W. 1997. "Isotopic Constraints on Radionuclide Transport at Peña Blanca." *Nuclear Science and Technology: Proceedings of the Seventh Natural Analog Working Group Meeting, Stein am Rhein, Switzerland, October 28-30, 1996*, 113–122. EUR-17851-EN. Von Maravic, H. and Smellie, J., eds. Luxembourg: Commission of the European Communities.

Pickett, D. and Murphy, W. 1999. "Unsaturated Zone Waters from the Nopal I Natural Analog, Chihuahua, Mexico - Implications for Radionuclide Mobility at Yucca Mountain." *Symposium Proceedings of the Scientific Basis for Nuclear Waste Management, Boston, Massachusetts.* Pittsburgh, Pennsylvania: Materials Research Society. (in press).

Prikryl, J. 1994. "The Role of Secondary Mineral Formation on Uranium Retardation and Transport at the Nopal I Deposit, Peña Blanca District, Chihuahua, Mexico." *Geological Society of America Abstracts with Program, 26*, A441. Denver, Colorado: Geological Society of America.

Prikryl, J.; Pearcy, E.; and Pickett, D. 1995a. "Migration Behavior of Naturally Occurring Radionuclides at the Nopal I Uranium Deposit, Chihuahua, Mexico." *Chemistry and Migration*

Behaviour of Actinides and Fission Products in the Geosphere, 47. Migration Conference, St. Malo, France. Del Nero, M. and Fanghänel, eds. St. Malo, France: Institut de Physique Nucleaire and Forschungszentrum Karlsruhe.

Prikryl, J.; Pickett, D.; and Pearcy, E. 1995b. "Evidence for Uranium Mobilization and Retention on Fe-Oxides/Hydroxides at the Nopal I Uranium Deposit." *Geological Society of America, Abstracts with Program, 27,* A420. Denver, Colorado: Geological Society of America.

Prikryl, J.; Pickett, D.; and Pearcy, E. 1995c. *Geochemical Natural Analog Research: NRC High-Level Radioactive Research at CNWRA, January through June 1995.* CNWRA 95-01S. San Antonio, Texas: Center for Nuclear Waste Regulatory Analyses.

Prikryl, J.; Pickett, D.; and Pearcy, E. 1995d. *NRC High-Level Radioactive Waste Research at CNWRA, July through December 1995.* CNWRA 95-02S. San Antonio, Texas: Center for Nuclear Waste Regulatory Analyses.

Prikryl, J.; Pickett, D.; Murphy, W.; and Pearcy, E. 1997. "Migration Behavior of Naturally Occurring Radionuclides at the Nopal I Uranium Deposit Chihuahua, Mexico." *Journal of Contaminant Hydrology, 26* (1-4), 61–69. Amsterdam, Netherlands: Elsevier Science Publishers.

Reyes-Cortes, I.A. 1997. *Geologic studies in the Sierra de Peña Blanca, Chihuahua, Mexico.* Ph.D. Dissertation. El Paso, Texas: University of Texas.

Reyes-Cortes, I.A. 1985. "Deposito de Molibdeno Associado con Uranio en Peña Blanca, Mexico." *Uranium Deposits in Volcanic Rocks, Proceedings of a Technical Committee Meeting on Volcanic Rocks, El Paso, Texas, April 2-5, 1984,* 161–174. IAEATC-490/16. Vienna, Austria: International Atomic Energy Agency.

Wilson, C.N. 1991. "Results from Long-Term Dissolution Tests Using Oxidized Spent Fuel." *Symposium Proceedings of the Scientific Basis for Nuclear Waste Management XIV, 212,* 197. Pittsburgh, Pennsylvania: Materials Research Society.

Wong, V. 1994. *Nopal I Uranium at Peña Blanca District, Chihuahua, Mexico: A Study of Radionuclide Migration in a Natural Analog to Yucca Mountain, Nevada.* Masters Thesis. El Paso, Texas: University of Texas.

Wong, V.; Anthony, E.; and Goodell, P. 1996. "Nopal I Uranium Deposit: A Study of Radionuclide Migration." *High-Level Radioactive Waste Management, Proceedings of the Seventh Annual International Conference, April 29 – May 3, 1996, Las Vegas, Nevada,* 43–45. La Grange Park, Illinois: American Nuclear Society.

Wong, V.; Anthony, E.; and Goodell, P. 1997. "Application of Natural Analogs to Potential Radwaste Repositories." *Geological Society of America Abstracts with Program, 29,* 6. Denver, Colorado: Geological Society of America.

Wong, V. 1998. *Gamma-Ray Characterization of Uranium-Series Nuclides and its Application to the Study of the Peña Blanca Natural Analog Site, Chihuahua, Mexico.* Ph.D. Dissertation. El Paso, Texas: University of Texas.

Wronkiewicz, D.; Bates, J.; Gerding, T.; Veleckis, E.; and Tani, B. 1992. "Uranium Release and Secondary Phase Formation During Unsaturated Testing of UO_2 at 90°C." *Journal of Nuclear Materials, 190*, 107–127. Amsterdam, Netherlands: Elsevier Science Publishers.

Wronkiewicz, D.; Bates, J.; Wolf S.; and Buck, E. 1996. "Ten-Year Results from Unsaturated Drip Tests with UO_2 at 90°C: Implications for the Corrosion of Spent Nuclear Fuel." *Journal of Nuclear Materials, 238* (1), 78–95. Amsterdam, Netherlands: Elsevier Science Publishers.

ATTACHMENT IV.

DERIVATION OF FRACTURE CONTINUUM PROPERTIES

Figures IV-1a and IV-1b present an *x-y* view of a fracture continuum and discrete fracture representation of a single node in the Box Canyon model, respectively. This example only considers the case of fractures oriented perpendicular to the *y*-direction. The permeability of the fracture continuum is calculated by equating the volumetric flow of water through the node to that calculated using discrete fracture representation due to a gradient in potential gradient, ∇h, applied perpendicular to the *x-y* plane. Let Q_C and Q_D be the volumetric flow rate of water in the fracture continuum and discrete fracture representations in the *z*-direction only:

$$Q_C = \Delta x \Delta y \frac{k_C}{\mu} \nabla h \qquad \text{(Eq. IV.1)}$$

$$Q_D = n_f b \Delta x \frac{k_D}{\mu} \nabla h \qquad \text{(Eq. IV.2)}$$

where n_f is the number of fractures perpendicular to the *y*-direction within the node, b is the fracture aperture, μ is the viscosity of water, k_D and k_C are the permeability of the discrete fracture and fracture continuum representations, respectively, where:

$$n_f = \frac{\Delta y}{D} \qquad \text{(Eq. IV.3)}$$

$$k_D = \frac{b^2}{12} \qquad \text{(Eq. IV.4)}$$

Now, setting $Q_C = Q_D$ yields:

$$\Delta x \Delta y k_C \nabla h = \frac{\Delta y}{D} b \Delta x \frac{b^2}{12} \nabla h \qquad \text{(Eq. IV.5)}$$

$$k_C = \frac{b^3}{12D} \qquad \text{(Eq. IV.6)}$$

where D is the fracture spacing shown on Figure IV-1b

An identical derivation follows by analogy for fractures oriented in the x-direction.

To find the β_y scaling factor for this node with an observed water flow feature, set $n_f = 1$ to condition the node to contain a single discrete fracture (note: $D \geq \Delta y$ for all nodes in the Box Canyon model). Once again, setting $Q_C = Q_D$:

$$\Delta x \, \Delta y \, k_C^* \, \nabla h = b \, \Delta x \frac{b^2}{12} \nabla h \qquad \text{(Eq. IV.7)}$$

$$k_C^* = \frac{b^3}{12 \Delta y} \qquad \text{(Eq. IV.8)}$$

where k^*_C is the permeability of the conditioned fracture continuum node. Therefore, the scaling factor between this node and the background unconditioned nodes is:

$$\beta_y = \frac{k_C^*}{k_C} = \frac{\frac{b^3}{12 \Delta y}}{\frac{b^3}{12 D}} = \frac{D}{\Delta y} \qquad \text{(Eq. IV.9)}$$

The derivation of β_x follows by analogy.

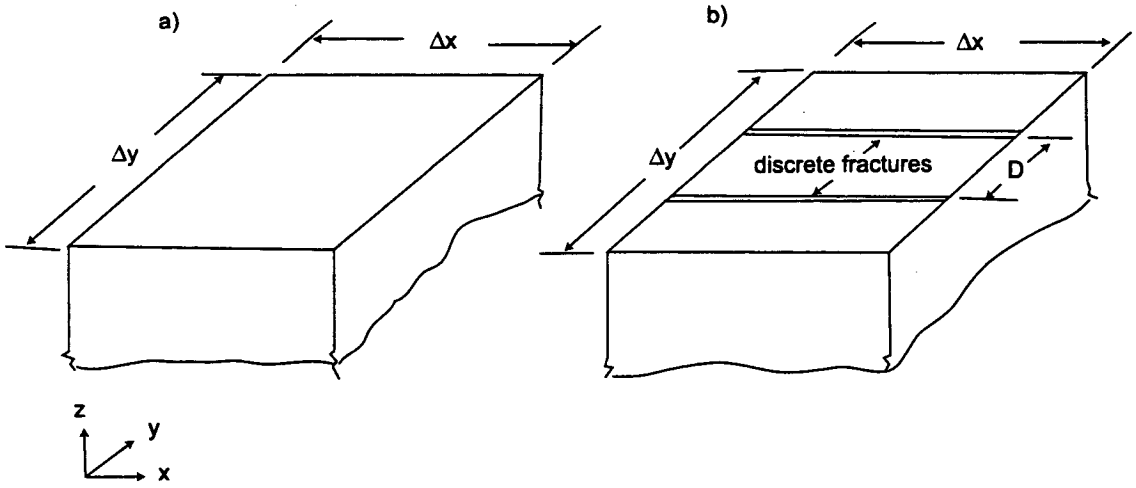

Figure IV-1. Plan view of node using a) fracture continuum and b) discrete fracture representations.

ATTACHMENT V

SOFTWARE ROUTINES

rocktype.for v1.0
Routine/Macro Documentation Form

The following information can be included in the scientific notebook. Attach and reference notebook pages and diskettes with files as needed when submitting routine/macro to records.

1. Name of routine/macro with version/OS/hardware environment :

   rocktype.for v1.0/Windows 98/Pentium III

2. Name of commercial software with version/OS/hardware used to develop routine/macro:

   Digital Visual Fortran V6.0/ Windows 98/Pentium III

3. **Test Plan.**

   - Explain whether this is a routine or macro and describe what it does:

     This routine develops input files for TOUGH2 representing the Box Canyon model. The routine converts input from a number of files to the input format required for TOUGH2.

   - Source code: (including equations or algorithms from software setup (LabView, Excel, etc.):

     Source code is printed on pp. 106-113 from S/N: YMP-LBNL-AMS-NA-AU-1 and is provided on accompanying CD entitled YMP-LBNL-AMS-NA-AU-1 (routines) in directory /rocktype.for/.

   - Description of test(s) to be performed (be specific):

     As explained on pp. 104-105, S/N: YMP-LBNL-AMS-NA-AU-1, the data will be verified by pausing the code execution and viewing the contents of all variables (pp.112-113, S/N: YMP-LBNL-AMS-NA-AU-1) to determine accuracy and consistency with expected values. The input files are processed by the routine, and the output is checked by hand calculation or visual inspection of the plotted results. The steps are:

     1. **Pause code after input control to verify correct values after each read from Rocktype.prn. Test will be considered successful if values agree.**
     2. **Pause code after completion of input to verify contents of arrays weight.dat, LayerElevGrid.data, ObsTimes.dat and Pend.dat by visual inspection against the ASCII input files. Test is successful if sample compared agrees with input files.**
     3. **Check the mapping of the zones to nodes has been performed correctly through visual inspection of a sample of the nodes. Successful completion of the test will be verified by visual inspection.**
     4. **Pause code after calculation of permeability and porosity values and compare to hand calculations from a sample of the input data. Test will be considered successful if hand calculations match generated values.**
     5. **Refer to pp. 105c-105e from S/N: YMP-LBNL-AMS-NA-AU-1 and is provided on accompanying CD entitled YMP-LBNL-AMS-NA-AU-1 (routines) in directory /rocktype.for/ for hydrogeological algorithms used in rocktype.for.**
     6. **Visually inspect a column of unconditioned nodes to identify a unique rock identifier. Compare the permeability and porosity of obtained from init.dat with values calculated by the routine. Test will be considered successful if permeability and porosity agree.**
     7. **Verify correct application of naming convention by visual inspection of CONNE in input.mesh. Successful inspection of the data will constitute a successful test.**

   - Specify the range of input values to be used and why the range is valid:

     The range of input is the input data files, rocktype.prm, weight.dat, LayerElevGrid.dat, obstimes.dat, pond.dat. These files are used for the test and for the eventual use of this single use routine. The portion of the test input that will be used for verifying mathematical equations is printed on pp.112-113, S/N: YMP-LBNL-AMS-NA-AU-1. The complete input

files are provided on accompanying CD entitled YMP-LBNL-AMS-NA-AU-1 (routines) in directory /rocktype.for/.

4. **Test Results.**

- Output from test (explain difference between input range used and possible input):

  The output data used for visual verification and for checking mathematical equations is printed on pp. 105c-105e, S/N: YMP-LBNL-AMS-NA-AU-1. Pages 105a and 105b are graphic images from TECPLOT and are hard copy images of the actual computer gernerated 3D images that were used to spot-check or verify the correct grid construction. See accompanying pages 105c-105e are example lines from the test output used to verify that the routine equations and reformatting were successful.

- Description of how the testing shows that the results are correct for the specified input:

  Several explicit hand calculations on pp. 105c-105e, S/N: YMP-LBNL-AMS-NA-AU-1 show that the input on pp. 112-113 match the output on pp. 105c-105e. The TECPLOT files (hard-copy examples plotted on pp. 105a-105b) verify correct grid construction by comparing specific XYZ coordinates visually. The routine Rocktype.for output produces TOUGH2 input files that are within acceptable ranges for inputs consistent with expectations. These files executed in TECPLOT without errors. A variable by variable inspection of the input file(s) and internal code blocks provided on the accompanying CD entitled YMP-LBNL-AMS-NA-AU-1 (routines) in directory /rocktype.for/. shows that the values agree as expected.

- List limitations or assumptions to this test case and code in general:

  Rocktype.for code is only tested to generate files for input to TOUGH2 for the specific 1D and 3D examples provided. The formatting and equations should be valid for other TOUGH2 output files however.

- Electronic files identified by name and location (include disc if necessary):

  All files used in the testing are provided on the accompanying CD entitled YMP-LBNL-AMS-NA-AU-1 (routines) in directory /rocktype.for/.

5. Supporting Information. Include background information, such as revision to a previous routine or macro, or explanation of the steps performed to run the software. Include listings of all electronic files and codes used. Attach Scientific Notebook pages with appropriate information annotated:

See attached pages for referenced Scientific Notebook pages and other supporting documentation.

Note: All relevant S/N pages are included in this package. In some instances, the included S/N pages cross-reference other pages that are not included here because these were not essential to the documentation of this routine.

MAINTAIN PAGES IN THIS ORDER:

1. **This rocktype.for v1.0 routine documentation form.**
2. **pp. 104-113 for S/N YMP-LBNL-AMS-NA-AU-1**
3. **Review forms**

Oct 7/99 entries from p. 104 to p. 126

Testing of rocktype.for v1.0

The function of this macro is to provide input files for TOUGH2 representing the Box Canyon model. Therefore, this macro processes data from various input files to condition hydrogeological parameters and convert them into a format required by TOUGH2. The acceptance criteria is that the macro correctly processes all sources of input and constructs a suitable series of files which allow TOUGH2 to perform a representative simulation. All relevant files are located in:

C:\803D-74\FractureNetwork\grid\rocktype

of computer LBL/DOE 6396546.

- rocktype_test_1d.prm p. 112
- rocktype_test_3d.prm p. 113

are examples of input control files used to generate the Box Canyon model.

1. Input control
   - Lines 109 to 166 consist of all input into **rocktype.for** through the input control file **rocktype.prm**. All input was verified by breaking the code after each read and checking the value of the parameters.
   - Lines 167 to 269 consist of input from various files:
     weight.dat – β weighting factors on pages 50 to 53
     LayerElevGrid.dat – elevation of each of the top of the seven basic units in the model
     obstimes.dat – output times for TOUGH2
     pond.dat – infiltration rates
     All of the above files are in ASCII format and correct input into **rocktype.for** was verified by breaking the code and checking the contents of the arrays.

2. Grid construction
   - Lines 271 to 359 determine the unit number (dimensionless depth zone of upper basalt, rubble zone or lower basalt) for which each node in the grid belongs. These units are constrained by the file **LayerElevGrid.dat** that defines the tops and bottoms of each zone.
   - Testing that the correct zones were mapped to the nodes is given by the figure on page 48. The blocky nature of the zones is due to the discretization of the mesh. These zones roughly coincide with the elevations in **LayerElevGrid.dat** and can also be checked by examining the figure on page 41 that shows the top ground surface elevation and the top of the rubble zone.

3. Hydrogeological property calculations
   - Lines 362 to 486 calculate the permeability and porosity values for each node in the grid based on in input fracture apertures. This was required during the pneumatic test calibration part where apertures from the table on page 65 in the "nodal parameters" and "background parameters" sections were used construct the model. Equations for the permeability and porosity are given on page 46 and 47.
   - Verification of permeability and porosity values was performed by breaking the code after these values were calculated and comparing them to hand calculations for aperture values input in **rocktype.prm**. The permeability values on page 65 only roughly coincide with those used in **rocktype.for** given that the aperture is

calculated differently from the permeability on page 65 than the by using the equations on pages 46 and 47. These values were verified by breaking the code and inspecting values with hand calculation.

- Lines 464 to 486 give the distance and interfacial area between the fracture and matrix continua at overlapping volumes within the grid. These values are given by equations on page 47 and were verified by hand calculation.

4. Rock type assembly
   - Lines 489 to 546 determine the number of unique rock types based on hydrogeological properties within the grid and build an index between the list of these properties and the nodes. This list is then used to in the ROCKS input of TOUGH2 given in **init.dat**.
   - Verification that the list of unique properties was constructed properly was performed by examining the TOUGH2 file **init.mesh**. By examining a column of unconditioned nodes along the edge of the model in ELEME, a unique rock identifier for nodes within the various zones was calculated. The permeability and porosity of these nodes was then obtained from the rock identifier in **init.dat** and compared to values calculated using the zonal background aperture from the **rocktype.prm**.

5. Node naming
   - Lines 548 to 694 involve providing a unique 5 symbol name for each node in the mesh. The first symbol is a letter and identifies the z location in the mesh where "a" represents the top node and "u" represents the bottom node. Symbols "v" and "w" identify the top and bottom boundary condition nodes respectively. Pond nodes are identified by the symbol "z". The second-third and fourth-fifth symbols give the x and y location, respectively. Values less than fifty are for fracture continuum nodes while values greater than fifty are for matrix continuum nodes.
   - Verification that the above node naming convention was followed was performed by examining the connection scheme in CONNE of **init.mesh**. The connection scheme between fracture and matrix continua nodes follows the description on page 46.

6. TOUGH2 input files
   - **rocktype.prm** creates input files for TOUGH2 called **init.dat**, **init.mesh** and **init.incon**. Sample input files for a 1-d and 3-d problem are provided in:
     C:\803D-74\FractureNetwork\grid\rocktype\rocktype_test_1d.prm
     C:\803D-74\FractureNetwork\grid\rocktype\rocktype_test_3d.prm
     and represent a steady state dual permeability variation of the model. These files can be easily used to construct and single permeability fracture continuum model.

Two Separate Views of the numerical model with zonal information

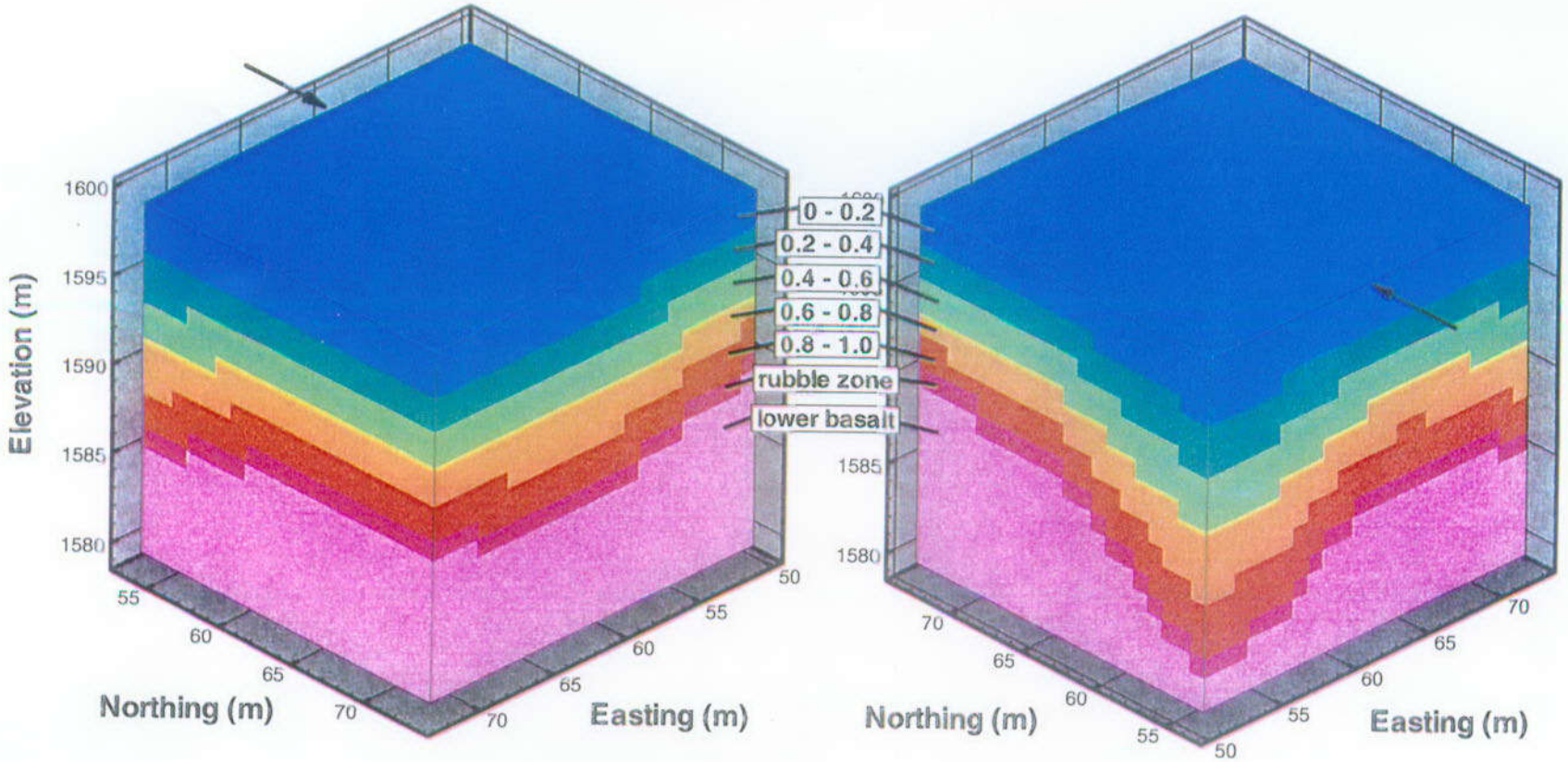

- verification that correct zones were mapped to nodes

(2. Grid Construction)

source file for figure: rocktype.dat

Elevation of (a) ground surface and (b) top of rubble zone with all well locations and perimeter of the infiltration pond.

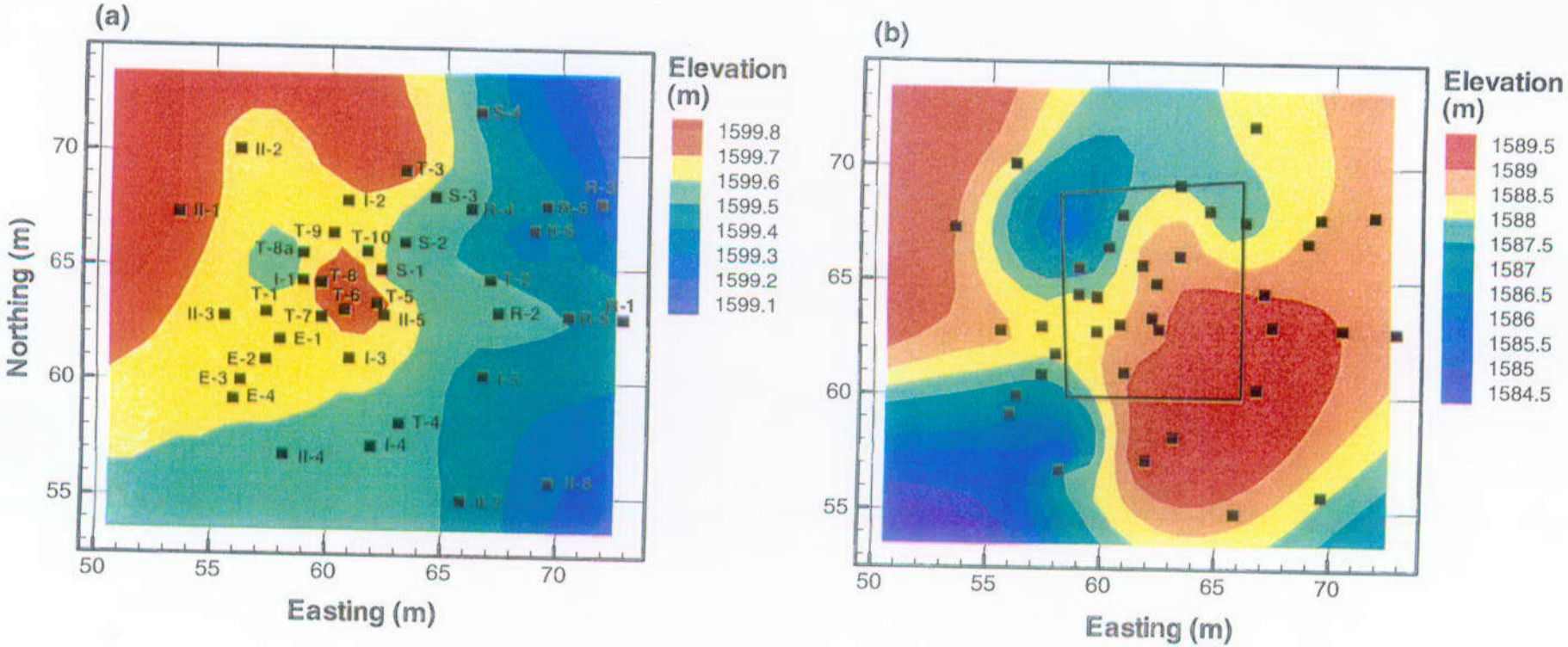

- verification that collect zones were mapped to nodes

(2. Grid Construction)

checking node (1,1,2)

ROCKS = r0001

```
Box Canyon
ROCKS
r0001    20.2400E+040.1281E-010.1038E-120.1038E-120.1038E-120.1730E+010.9358E+03
0.1000E-090.0000E+000.1730E+010.2500E+00
     3      0.1000E-010.0000E+00
     7      0.5000E+000.1000E-010.5000E-030.1000E+110.1000E+01
r0002    20.2400E+040.1388E-010.4052E-120.3715E-120.2364E-120.1730E+010.9358E+03
0.1000E-090.0000E+000.1730E+010.2500E+00
     3      0.1000E-010.0000E+00
     7      0.5000E+000.1000E-010.5000E-030.1000E+110.1000E+01
r0003    20.2400E+040.1665E-010.4052E-120.4728E-120.3377E-120.1730E+010.9358E+03
0.1000E-090.0000E+000.1730E+010.2500E+00
     3      0.1000E-010.0000E+00
     7      0.5000E+000.1000E-010.5000E-030.1000E+110.1000E+01
r0004    20.2400E+040.1480E-010.4052E-120.4052E-120.2701E-120.1730E+010.9358E+03
0.1000E-090.0000E+000.1730E+010.2500E+00
     3      0.1000E-010.0000E+00
     7      0.5000E+000.1000E-010.5000E-030.1000E+110.1000E+01
r0005    20.2400E+040.1295E-010.4052E-120.3377E-120.2026E-120.1730E+010.9358E+03
0.1000E-090.0000E+000.1730E+010.2500E+00
     3      0.1000E-010.0000E+00
     7      0.5000E+000.1000E-010.5000E-030.1000E+110.1000E+01
r0006    20.2400E+040.1850E-010.4052E-120.5403E-120.4052E-120.1730E+010.9358E+03
0.1000E-090.0000E+000.1730E+010.2500E+00
     3      0.1000E-010.0000E+00
     7      0.5000E+000.1000E-010.5000E-030.1000E+110.1000E+01
r0007    20.2400E+040.1665E-010.3377E-120.5403E-120.3377E-120.1730E+010.9358E+03
0.1000E-090.0000E+000.1730E+010.2500E+00
     3      0.1000E-010.0000E+00
     7      0.5000E+000.1000E-010.5000E-030.1000E+110.1000E+01
r0008    20.2400E+040.1110E-010.3377E-120.3377E-120.1351E-120.1730E+010.9358E+03
0.1000E-090.0000E+000.1730E+010.2500E+00
     3      0.1000E-010.0000E+00
     7      0.5000E+000.1000E-010.5000E-030.1000E+110.1000E+01
r0009    20.2400E+040.1388E-010.3715E-120.4052E-120.2364E-120.1730E+010.9358E+03
0.1000E-090.0000E+000.1730E+010.2500E+00
     3      0.1000E-010.0000E+00
     7      0.5000E+000.1000E-010.5000E-030.1000E+110.1000E+01
r0010    20.2400E+040.1665E-010.5403E-120.3377E-120.3377E-120.1730E+010.9358E+03
0.1000E-090.0000E+000.1730E+010.2500E+00
     3      0.1000E-010.0000E+00
     7      0.5000E+000.1000E-010.5000E-030.1000E+110.1000E+01
r0011    20.2400E+040.2220E-010.5403E-120.5403E-120.5403E-120.1730E+010.9358E+03
0.1000E-090.0000E+000.1730E+010.2500E+00
     3      0.1000E-010.0000E+00
     7      0.5000E+000.1000E-010.5000E-030.1000E+110.1000E+01
r0012    20.2400E+040.1665E-010.4728E-120.4052E-120.3377E-120.1730E+010.9358E+03
0.1000E-090.0000E+000.1730E+010.2500E+00
     3      0.1000E-010.0000E+00
     7      0.5000E+000.1000E-010.5000E-030.1000E+110.1000E+01
r0013    20.2400E+040.1474E-010.1583E-120.1583E-120.1583E-120.1730E+010.9358E+03
0.1000E-090.0000E+000.1730E+010.2500E+00
     3      0.1000E-010.0000E+00
     7      0.5000E+000.1000E-010.5000E-030.1000E+110.1000E+01
r0014    20.2400E+040.1111E-010.6781E-130.6781E-130.6781E-130.1730E+010.9358E+03
0.1000E-090.0000E+000.1730E+010.2500E+00
     3      0.1000E-010.0000E+00
     7      0.5000E+000.1000E-010.5000E-030.1000E+110.1000E+01
r0015    20.2400E+040.1295E-010.3715E-120.3715E-120.2026E-120.1730E+010.9358E+03
```

$$k_x = \beta_x \frac{b^3}{12 D_H} + \frac{b^3}{12 D_V}$$

$$k_y = \beta_y \frac{b^3}{12 D_H} + \frac{b^3}{12 D_V}$$

$$k_t = \beta_z \frac{b^3}{12 D_H}$$

$\beta_x = \beta_y = 1.0$

$\beta_z = 2.0$

(from weight.dat)

$$\phi = \beta_x \frac{b}{D_H} + \beta_y \frac{b}{D_H} + \frac{b}{D_V}$$

$$k_x = k_y = \frac{(1.0)(8.54\times10^{-5})^3}{(12)(1.0)} + \frac{(8.54\times10^{-5})^3}{(12)(1.0)}$$

$$= 1.038\times10^{-13}$$

$$k_t = \frac{(2.0)(8.54\times10^{-5})^3}{(12)(2.0)} = 1.038\times10^{-13}$$

$$\phi = \left[\frac{(1.0)(8.54\times10^{-5})}{1.0} + \frac{(1.0)(8.54\times10^{-5})}{1.0} + \frac{8.54\times10^{-5}}{1.0}\right]\lambda$$

$$= 0.0128$$

(note: see page 112 for parameters)

checking node (1,1,2)

```
ELEME
a 1 1          r00010.5400E+00                          1    1    1
b 1 1          r00010.1000E+01                          1    1    2
c 1 1          r00010.1000E+01                          1    1    3
d 1 1          r00010.1000E+01                          1    1    4
e 1 1          r00040.1000E+01                          1    1    5
f 1 1          r00040.1000E+01                          1    1    6
g 1 1          r00040.1000E+01                          1    1    7
h 1 1          r00330.1000E+01                          1    1    8
i 1 1          r00330.1000E+01                          1    1    9
j 1 1          r00330.1000E+01                          1    1   10
k 1 1          r00570.1000E+01                          1    1   11
l 1 1          r00570.1000E+01                          1    1   12
m 1 1          r00570.1000E+01                          1    1   13
n 1 1          r00570.1000E+01                          1    1   14
o 1 1          r00830.1000E+01                          1    1   15
p 1 1          r00830.1000E+01                          1    1   16
q 1 1          r00830.1000E+01                          1    1   17
r 1 1          r01030.1000E+01                          1    1   18
s 1 1          r01110.1000E+01                          1    1   19
t 1 1          r01110.1000E+01                          1    1   20
u 1 1          r01110.1000E+01                          1    1   21
v 1 1          topbd0.1000E+07                          1    1    1
w 1 1          botbd0.1000E+31                          1    1   21
a5151          mtrx10.5400E+00                          1    1    1
b5151          mtrx10.1000E+01                          1    1    2
c5151          mtrx10.1000E+01                          1    1    3
d5151          mtrx10.1000E+01                          1    1    4
e5151          mtrx20.1000E+01                          1    1    5
f5151          mtrx20.1000E+01                          1    1    6
g5151          mtrx20.1000E+01                          1    1    7
h5151          mtrx30.1000E+01                          1    1    8
i5151          mtrx30.1000E+01                          1    1    9
j5151          mtrx30.1000E+01                          1    1   10
k5151          mtrx40.1000E+01                          1    1   11
l5151          mtrx40.1000E+01                          1    1   12
m5151          mtrx40.1000E+01                          1    1   13
n5151          mtrx40.1000E+01                          1    1   14
o5151          mtrx50.1000E+01                          1    1   15
p5151          mtrx50.1000E+01                          1    1   16
q5151          mtrx50.1000E+01                          1    1   17
r5151          mtrx60.1000E+01                          1    1   18
s5151          mtrx70.1000E+01                          1    1   19
t5151          mtrx70.1000E+01                          1    1   20
u5151          mtrx70.1000E+01                          1    1   21

CONNE
b 1 1a 1 1     30.5000E+000.2700E+000.1000E+01-.1000E+01  1    1    2    1    1    1
c 1 1b 1 1     30.5000E+000.5000E+000.1000E+01-.1000E+01  1    1    3    1    1    2
d 1 1c 1 1     30.5000E+000.5000E+000.1000E+01-.1000E+01  1    1    4    1    1    3
e 1 1d 1 1     30.5000E+000.5000E+000.1000E+01-.1000E+01  1    1    5    1    1    4
f 1 1e 1 1     30.5000E+000.5000E+000.1000E+01-.1000E+01  1    1    6    1    1    5
g 1 1f 1 1     30.5000E+000.5000E+000.1000E+01-.1000E+01  1    1    7    1    1    6
h 1 1g 1 1     30.5000E+000.5000E+000.1000E+01-.1000E+01  1    1    8    1    1    7
i 1 1h 1 1     30.5000E+000.5000E+000.1000E+01-.1000E+01  1    1    9    1    1    8
j 1 1i 1 1     30.5000E+000.5000E+000.1000E+01-.1000E+01  1    1   10    1    1    9
k 1 1j 1 1     30.5000E+000.5000E+000.1000E+01-.1000E+01  1    1   11    1    1   10
l 1 1k 1 1     30.5000E+000.5000E+000.1000E+01-.1000E+01  1    1   12    1    1   11
m 1 1l 1 1     30.5000E+000.5000E+000.1000E+01-.1000E+01  1    1   13    1    1   12
```

$$D_{fm} = \frac{1}{3}\cdot\left[\frac{\beta_x \Delta x}{D_H} + \beta_y \frac{\Delta y}{D_H} + \frac{\Delta z}{D_V}\right]\cdot\frac{1}{10}$$

$$A_{fm} = 2\cdot\left[\beta_x \Delta y \Delta z \frac{\Delta x}{D_H} + \beta_y \Delta x \Delta z \frac{\Delta y}{D_H} + \beta_x \Delta y \Delta z \frac{\Delta z}{D_V}\right]\cdot X_{fm}$$

note: assume $\Delta x = \Delta y = \Delta z = 1.0$ (given)

$$D_{fm} = \frac{1}{3}\cdot\left[\frac{(1.0)(1.0)}{1.0} + \frac{(1.0)(1.0)}{1.0} + \frac{1.0}{1.0}\right]\cdot\frac{1}{10} = 0.1$$

$$A_{fm} = 2\cdot\left[\frac{(1.0)(1.0)(1.0)(1.0)}{1.0} + \frac{(1.0)(1.0)(1.0)(1.0)}{1.0} + \frac{(1.0)(1.0)(1.0)}{1.0}\right]\cdot 0.01$$

$= 0.06$

Next Page

fracture - fracture connection

fracture - matrix connection

n 1 1m 1 1	30.5000E+000.5000E+000.1000E+01-.1000E+01	1	1	14	1	1	13
o 1 1n 1 1	30.5000E+000.5000E+000.1000E+01-.1000E+01	1	1	15	1	1	14
p 1 1o 1 1	30.5000E+000.5000E+000.1000E+01-.1000E+01	1	1	16	1	1	15
q 1 1p 1 1	30.5000E+000.5000E+000.1000E+01-.1000E+01	1	1	17	1	1	16
r 1 1q 1 1	30.5000E+000.5000E+000.1000E+01-.1000E+01	1	1	18	1	1	17
s 1 1r 1 1	30.5000E+000.5000E+000.1000E+01-.1000E+01	1	1	19	1	1	18
t 1 1s 1 1	30.5000E+000.5000E+000.1000E+01-.1000E+01	1	1	20	1	1	19
u 1 1t 1 1	30.5000E+000.5000E+000.1000E+01-.1000E+01	1	1	21	1	1	20
v 1 1a 1 1	30.1000E-140.2700E+000.1000E+010.1000E+01	1	1	1	1	1	1
w 1 1u 1 1	30.1000E-140.5000E+000.1000E+01-.1000E+01	1	1	21	1	1	21
a5151a 1 1	10.1000E+000.5000E+000.6000E-010.0000E+00	1	1	1	1	1	1
b5151b 1 1	10.1000E+000.5000E+000.6000E-010.0000E+00	1	1	2	1	1	2
c5151c 1 1	10.1000E+000.5000E+000.6000E-010.0000E+00	1	1	3	1	1	3
d5151d 1 1	10.1000E+000.5000E+000.6000E-010.0000E+00	1	1	4	1	1	a41
e5151e 1 1	10.1667E+000.5000E+000.4000E-010.0000E+00	1	1	5	1	1	5
f5151f 1 1	10.1667E+000.5000E+000.4000E-010.0000E+00	1	1	6	1	1	6
g5151g 1 1	10.1667E+000.5000E+000.4000E-010.0000E+00	1	1	7	1	1	b41
h5151h 1 1	10.3000E+000.5000E+000.3000E-010.0000E+00	1	1	8	1	1	8
i5151i 1 1	10.3000E+000.5000E+000.3000E-010.0000E+00	1	1	9	1	1	9
j5151j 1 1	10.3000E+000.5000E+000.3000E-010.0000E+00	1	1	10	1	1	a01
k5151k 1 1	10.3000E+000.5000E+000.3000E-010.0000E+00	1	1	11	1	1	11
l5151l 1 1	10.3000E+000.5000E+000.3000E-010.0000E+00	1	1	12	1	1	12
m5151m 1 1	10.3000E+000.5000E+000.3000E-010.0000E+00	1	1	13	1	1	13
n5151n 1 1	10.3000E+000.5000E+000.3000E-010.0000E+00	1	1	14	1	1	14
o5151o 1 1	10.1667E+000.5000E+000.4000E-010.0000E+00	1	1	15	1	1	15
p5151p 1 1	10.1667E+000.5000E+000.4000E-010.0000E+00	1	1	16	1	1	16
q5151q 1 1	10.1667E+000.5000E+000.4000E-010.0000E+00	1	1	17	1	1	17
r5151r 1 1	10.1000E-010.5000E+000.6000E+000.0000E+00	1	1	18	1	1	18
s5151s 1 1	10.1667E+000.5000E+000.4000E-010.0000E+00	1	1	19	1	1	19
t5151t 1 1	10.1667E+000.5000E+000.4000E-010.0000E+00	1	1	20	1	1	20
u5151u 1 1	10.1667E+000.5000E+000.4000E-010.0000E+00	1	1	21	1	1	21
b5151a5151	30.5000E+000.2700E+000.1000E+01-.1000E+01	1	1	2	1	1	1
c5151b5151	30.5000E+000.5000E+000.1000E+01-.1000E+01	1	1	3	1	1	2
d5151c5151	30.5000E+000.5000E+000.1000E+01-.1000E+01	1	1	4	1	1	3
e5151d5151	30.5000E+000.5000E+000.1000E+01-.1000E+01	1	1	5	1	1	4
f5151e5151	30.5000E+000.5000E+000.1000E+01-.1000E+01	1	1	6	1	1	5
g5151f5151	30.5000E+000.5000E+000.1000E+01-.1000E+01	1	1	7	1	1	6
h5151g5151	30.5000E+000.5000E+000.1000E+01-.1000E+01	1	1	8	1	1	7
i5151h5151	30.5000E+000.5000E+000.1000E+01-.1000E+01	1	1	9	1	1	8
j5151i5151	30.5000E+000.5000E+000.1000E+01-.1000E+01	1	1	10	1	1	9
k5151j5151	30.5000E+000.5000E+000.1000E+01-.1000E+01	1	1	11	1	1	10
l5151k5151	30.5000E+000.5000E+000.1000E+01-.1000E+01	1	1	12	1	1	11
m5151l5151	30.5000E+000.5000E+000.1000E+01-.1000E+01	1	1	13	1	1	12
n5151m5151	30.5000E+000.5000E+000.1000E+01-.1000E+01	1	1	14	1	1	13
o5151n5151	30.5000E+000.5000E+000.1000E+01-.1000E+01	1	1	15	1	1	14
p5151o5151	30.5000E+000.5000E+000.1000E+01-.1000E+01	1	1	16	1	1	15
q5151p5151	30.5000E+000.5000E+000.1000E+01-.1000E+01	1	1	17	1	1	16
r5151q5151	30.5000E+000.5000E+000.1000E+01-.1000E+01	1	1	18	1	1	17
s5151r5151	30.5000E+000.5000E+000.1000E+01-.1000E+01	1	1	19	1	1	18
t5151s5151	30.5000E+000.5000E+000.1000E+01-.1000E+01	1	1	20	1	1	19
u5151t5151	30.5000E+000.5000E+000.1000E+01-.1000E+01	1	1	21	1	1	20

p.105d

matrix - matrix connection

10/02/90 at 2501

Connection scheme (dual-k)

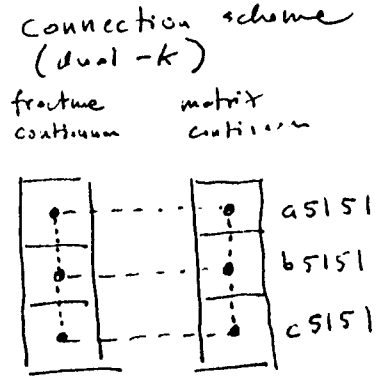

```
      program rocktype

      integer nx, ny, nz, nlayer, nrock, nzone, nlayer_plus_1,
     &        nsource, n_obs_times
      parameter (nx = 23, ny = 21, nz = 21, nlayer = 7,
     &           nlayer_plus_1 = 8, nrock = 1000,
     &           nzone = 1000, nsource = 100, n_obs_times = 100)

      integer model_type, pond_start, boundary_type, incon, transp,
     &        nx_min, ny_min, nx_max, ny_max, kr_type, obs_times,
     &        dual_k

      real xlayer(nx, ny, nlayer), ylayer(nx, ny, nlayer),
     &     zlayer(nx, ny, nlayer),
     &     xrock(nrock), yrock(nrock), zrock(nrock),
     &     xnode(nx, ny, nz), ynode(nx, ny, nz), znode(nx, ny, nz),
     &     layer_elev(nx, ny, nlayer_plus_1),
     &     xcoord(nx), ycoord(ny), zcoord(nz),
     &     volume(nx, ny, nz), ground_elev(nx, ny),
     &     qpond(nsource), qtpond(nsource), cpond(nsource),
     &     otime(n_obs_times)

      real frac_spacing(nlayer), aperture_zone(nzone),
     &     van_alpha_zone(nzone), van_m_zone(nzone),
     &     por_scale_zone(nzone), k_scale_zone(nzone),
     &     kx_prop(nrock), ky_prop(nrock), kz_prop(nrock),
     &     porosity_prop(nrock),
     &     van_alpha_prop(nrock), van_m_prop(nrock),
     &     infiltration,
     &     kx(nx, ny, nz), ky(nx, ny, nz), kz(nx, ny, nz),
     &     porosity(nx, ny, nz), van_alpha(nx, ny, nz),
     &     van_m(nx, ny, nz), frac_spacing_vert(nlayer),
     &     top_of_model, bottom_of_model, top_of_pond,
     &     aperture_layer(nlayer), van_alpha_layer(nlayer),
     &     van_m_layer(nlayer),
     &     por_scale_layer(nlayer), k_scale_layer(nlayer),
     &     avg_pond_elev, avg_pond_depth, pond_elev,
     &     Sw, Pw, Pg, top_elev, bottom_elev,
     &     kx_pond_liner, ky_pond_liner, kz_pond_liner,
     &     max_pond_elev, min_pond_elev, areaX_frac_mat,
     &     alphal, alphat, lambda, Kd, Dm

      real time_end, dtime_start

      real eps, eps_prop
      parameter (eps = 0.001, eps_prop = 1.0e-30)

      real kx_top_bnd, ky_top_bnd, kz_top_bnd,
     &     kx_bot_bnd, ky_bot_bnd, kz_bot_bnd,
     &     porosity_bot_bnd, porosity_top_bnd,
     &     van_alpha_top_bnd, van_alpha_bot_bnd,
     &     van_m_top_bnd, van_m_bot_bnd,
     &     D_top_bnd, D_bot_bnd,
     &     b_top_bnd, b_bot_bnd,
     &     Pg_init_top, Sg_init_top, T_init_top,
     &     Pg_init_bot, Sg_init_bot, T_init_bot,
     &     Pg_init, Sg_init, T_init,
     &     Pg_temp, Sg_temp, T_temp

      integer nad, irp, icp, isot, nk, neq, nph, nb

      real drok, cwet, spht, com, expan, cdry, tortx,
     &     mf, Slrf, Slsf, Ssrf, alphaf, Pmax, qinf, ex,
     &     d1, d2, areax, betax, vol

      real kx_mat(nlayer), ky_mat(nlayer), kz_mat(nlayer),
     &     porosity_mat(nlayer),
     &     van_alpha_mat(nlayer), van_m_mat(nlayer),
     &     D_mat_frac(nx, ny, nz), area_mat_frac(nx, ny, nz),
     &     Pg_init_mat, Sg_init_mat, T_init_mat

      character*80 line
      character*150 line150
```



```
      character*1 str1_ix, str1_iy, str1_iz, str1
      character*2 str2_ix, str2_iy, str2
      character*3 str3, str3_t, str3_b
      character*4 str4, type
      character*5 str5, str5_t, str5_b, node_label_temp

      character*5 rock_label(nrock), node_label(nx, ny, nz),
     &            top_bnd_rock_label, bot_bnd_rock_label,
     &            top_bnd_node_label(nx, ny),
     &            bot_bnd_node_label(nx, ny),
     &            matrix_label(nlayer), node_label_mat(nx, ny, nz),
     &            pond_node_label(9, 9, 10), pond_label,
     &            pond_liner_label

      integer rock_type(nx, ny, nlayer), rock_type_node(nx, ny, nz),
     &        rock_type_count, found_rock_type,
     &        rock_type_node_layer(nx, ny, nz),
     &        prop_type_count, found_prop_type,
     &        prop_type(nx, ny, nz)

      integer i1(nzone), i2(nzone), j1(nzone), j2(nzone),
     &        k1(nzone), k2(nzone)


      integer ix, iy, iz, irock, ilayer, i, nzone_in, izone, iprop,
     &        ixm1, iym1, izm1, pond_node, nsource_in, isource,
     &        n_obs_times_in, itime

      real dz, elev, xmin, xcentroid, xmax,
     &     ymin, ycentroid, ymax, zmin, zcentroid, zmax


      open (unit = 10, file = 'rocktype.out', status = 'unknown')

      open (unit = 8, file = 'rocktype.prm', status = 'unknown')

      read(8,*) nx_min, ny_min, nx_max, ny_max
      read(8,*) model_type
      read(8,*) dual_k
      read(8,*) transp
      read(8,*) incon
      read(8,*) infiltration
      read(8,*) obs_times
      read(8,*) time_end, dtime_start
      read(8,*) pond_start
      read(8,*) avg_pond_depth
      read(8,*) kx_pond_liner, ky_pond_liner, kz_pond_liner
      read(8,*) boundary_type
      read(8,*) b_top_bnd, D_top_bnd, van_alpha_top_bnd,
     &          van_m_top_bnd
      read(8,*) b_bot_bnd, D_bot_bnd, van_alpha_bot_bnd,
     &          van_m_bot_bnd
      read(8,*) Pg_init_top, Sg_init_top, T_init_top
      read(8,*) Pg_init_bot, Sg_init_bot, T_init_bot
      read(8,*) Pg_init, Sg_init, T_init
      read(8,*) Pg_init_mat, Sg_init_mat, T_init_mat
      read(8,*) areaX_frac_mat
      read(8,*) alphal, alphat, lambda, Kd, Dm
      read(8,*) kr_type
      do ilayer = 1, nlayer
         read(8,*) frac_spacing(ilayer), frac_spacing_vert(ilayer),
     &             aperture_layer(ilayer), van_alpha_layer(ilayer),
     &             van_m_layer(ilayer), por_scale_layer(ilayer),
     &             k_scale_layer(ilayer)
      end do
      do ilayer = 1, nlayer
         read(8,*) kx_mat(ilayer), ky_mat(ilayer), kz_mat(ilayer),
     &             porosity_mat(ilayer),
     &             van_alpha_mat(ilayer), van_m_mat(ilayer)
      end do
      read(8,*) nzone_in
      if (nzone_in .gt. nzone) then
```

```
            write(10,*) 'error: number of input zones cannot exceed 1000'
            stop
         end if
         do izone = 1, nzone_in
            read(8,*) i1(izone), j1(izone), k1(izone), i2(izone),
     [              j2(izone), k2(izone),
     [              aperture_zone(izone),
     [              van_alpha_zone(izone), van_m_zone(izone),
     [              por_scale_zone(izone), k_scale_zone(izone)
         end do
         kx_top_bnd = b_top_bnd**3 / (12.0 * D_top_bnd)
         ky_top_bnd = b_top_bnd**3 / (12.0 * D_top_bnd)
         kz_top_bnd = b_top_bnd**3 / (12.0 * D_top_bnd)
         kx_bot_bnd = b_bot_bnd**3 / (12.0 * D_bot_bnd)
         ky_bot_bnd = b_bot_bnd**3 / (12.0 * D_bot_bnd)
         kz_bot_bnd = b_bot_bnd**3 / (12.0 * D_bot_bnd)
         porosity_top_bnd = b_top_bnd / D_top_bnd
         porosity_bot_bnd = b_bot_bnd / D_bot_bnd

         close(8)


         if (model_type .eq. 3) then
            open (unit = 8, file = 'pond.dat', status = 'unknown')

            read(8,*) nsource_in
            if (transp .eq. 0) then
               do isource = 1, nsource_in
                  read(8,*) qtpond(isource), qpond(isource)
               end do
            else
               do isource = 1, nsource_in
                  read(8,*) qtpond(isource), qpond(isource), cpond(isource)
               end do
            end if
            close(8)
         end if


         if (obs_times .eq. 1) then
            open (unit = 8, file = 'obstimes.dat', status = 'unknown')

            read(8,*) n_obs_times_in
            do itime = 1, n_obs_times_in
               read(8,*) otime(itime)
            end do

            close(8)
         end if


         open (unit = 8, file = 'LayerElevGrid.dat', status = 'unknown')

         top_of_model = 1600.0
         bottom_of_model = 1579.0
         do iy = 1, ny
            do ix = 1, nx
               read(8,*) (layer_elev(ix, iy, ilayer),
     [                          ilayer = 1, nlayer)
            end do
         end do
         do iz = 1, nz
            do iy = 1, ny
               do ix = 1, nx
                  if (iz .eq. 1) then
                     volume(ix, iy, iz) =
     [                     max( layer_elev(ix, iy, 1)
     [                          - (top_of_model - 1.0),
     [                          0.1 )
                  else
                     volume(ix, iy, iz) = 1.0
                  end if
               end
```



```
            end do
         end do
         do iy = 1, ny
            do ix = 1, nx
               ground_elev(ix, iy) = layer_elev(ix, iy, 1)
               layer_elev(ix, iy, 1) = top_of_model
               layer_elev(ix, iy, nlayer_plus_1) = bottom_of_model
            end do
         end do


         close(8)


         open (unit = 8, file = 'weight.dat', status = 'unknown')

         do i = 1, 2
            read(8,1) line
    1       format(a80)
         end do

         do ilayer = 1, nlayer

            if (ilayer .eq. 1 .or.
     [          ilayer .eq. 6 .or.
     [          ilayer .eq. 7) then
               do iy = 1, ny
                  do ix = 1, nx
                     xlayer(ix, iy, ilayer) = 1.0
                     ylayer(ix, iy, ilayer) = 1.0
                     zlayer(ix, iy, ilayer) = 2.0
                  end do
               end do
            else
               read(8,1) line

               do iz = 1, 2
                  do iy = 1, ny
                     do ix = 1, nx
                        read(8,*) xcoord(ix), ycoord(iy), zcoord(iz),
     [                            xlayer(ix, iy, ilayer),
     [                            ylayer(ix, iy, ilayer),
     [                            zlayer(ix, iy, ilayer)
                     end do
                  end do
               end do
            end if
         end do

         close(8)

         xrock(1) = 1.0
         yrock(1) = 1.0
         zrock(1) = 2.0
         rock_type_count = 1
         do irock = 2, nrock
            xrock(irock) = 0.0
            yrock(irock) = 0.0
            zrock(irock) = 0.0
         end do

         do ilayer = 1, nlayer
            do iy = 1, ny
               do ix = 1, nx

                  found_rock_type = 0
                  do irock = 1, rock_type_count
                     if ((abs(xlayer(ix, iy, ilayer) - xrock(irock))
     [                                              .lt. eps) .and.
     [                   (abs(ylayer(ix, iy, ilayer) - yrock(irock))
     [                                              .lt. eps) .and.
     [                   (abs(zlayer(ix, iy, ilayer) - zrock(irock))
     [                                              .lt. eps)) then
```

```
                        found_rock_type = 1
                        rock_type(ix, iy, ilayer) = irock
                        goto 1000
                     end if
                  end do
     1000         continue

                  if (found_rock_type .eq. 0) then
                     rock_type_count = rock_type_count + 1

                     if (rock_type_count .gt. nrock) then
                        write(10,*) 'error: exceed number of rock types'
                        stop
                     end if

                     xrock(rock_type_count) = xlayer(ix, iy, ilayer)
                     yrock(rock_type_count) = ylayer(ix, iy, ilayer)
                     zrock(rock_type_count) = zlayer(ix, iy, ilayer)
                     rock_type(ix, iy, ilayer) = rock_type_count
                  end if

               end do
            end do
         end do


         dz = 1.0
         do iz = 1, nz
            zcoord(iz) = top_of_model + 0.5*dz - iz*dz
         end do

         do iy = 1, ny
            do ix = 1, nx

               do iz = 1, nz
                  rock_type_node(ix, iy, iz) = 0

                  do ilayer = 1, nlayer
                     if (layer_elev(ix, iy, ilayer) .ge.
                         zcoord(iz) .and.
                         layer_elev(ix, iy, ilayer+1) .lt.
                         zcoord(iz)) then
                        rock_type_node(ix, iy, iz) =
                         rock_type(ix, iy, ilayer)
                        xnode(ix, iy, iz) =
                                        xrock( rock_type_node(ix, iy, iz) )
                        ynode(ix, iy, iz) =
                                        yrock( rock_type_node(ix, iy, iz) )
                        znode(ix, iy, iz) =
                                        zrock( rock_type_node(ix, iy, iz) )
                        rock_type_node_layer(ix, iy, iz) = ilayer
                        goto 1010
                     end if
                  end do
     1010         continue

                  if (rock_type_node(ix, iy, iz) .eq. 0) then
                     write(10,*) 'error: could not find node in column'
                     write(10,*) 'ix = ',ix
                     write(10,*) 'iy = ',iy
                     write(10,*) 'iz = ',iz
                     stop
                  end if

               end do
            end do
         end do


         do iz = 1, nz
            do iy = 1, ny
               do ix = 1, nx
                  kx(ix, iy, iz) = -1.0
```



```
                  ky(ix, iy, iz) = -1.0
                  kz(ix, iy, iz) = -1.0
                  porosity(ix, iy, iz) = -1.0
               end do
            end do
         end do
         do iz = 1, nz
            do iy = 1, ny
               do ix = 1, nx
                  ilayer = rock_type_node_layer(ix, iy, iz)
                  kx(ix, iy, iz) = aperture_layer(ilayer)**3
     &                             / (12.0 * frac_spacing(ilayer))
     &                             * xnode(ix, iy, iz)
     &                           + aperture_layer(ilayer)**3
     &                             / (12.0 * frac_spacing_vert(ilayer))
                  ky(ix, iy, iz) = aperture_layer(ilayer)**3
     &                             / (12.0 * frac_spacing(ilayer))
     &                             * ynode(ix, iy, iz)
     &                           + aperture_layer(ilayer)**3
     &                             / (12.0 * frac_spacing_vert(ilayer))
                  kz(ix, iy, iz) = aperture_layer(ilayer)**3
     &                             / (12.0 * frac_spacing(ilayer))
     &                             * znode(ix, iy, iz)
                  kx(ix, iy, iz) = kx(ix, iy, iz) * k_scale_layer(ilayer)
                  ky(ix, iy, iz) = ky(ix, iy, iz) * k_scale_layer(ilayer)
                  kz(ix, iy, iz) = kz(ix, iy, iz) * k_scale_layer(ilayer)
                  porosity(ix, iy, iz) = (aperture_layer(ilayer)
     &                                    / frac_spacing(ilayer)
     &                                    * xnode(ix, iy, iz)
     &                                  + aperture_layer(ilayer)
     &                                    / frac_spacing(ilayer)
     &                                    * ynode(ix, iy, iz)
     &                                  + aperture_layer(ilayer)
     &                                    / frac_spacing_vert(ilayer))
     &                                  * por_scale_layer(ilayer)
                  porosity(ix, iy, iz) = min( porosity(ix, iy, iz),
     &                                        0.1 )
                  van_alpha(ix, iy, iz) = van_alpha_layer(ilayer)
                  van_m(ix, iy, iz) = van_m_layer(ilayer)
               end do
            end do
         end do
         do izone = 1, nzone_in
            do iz = k1(izone), k2(izone)
               do iy = j1(izone), j2(izone)
                  do ix = i1(izone), i2(izone)
                     ilayer = rock_type_node_layer(ix, iy, iz)
                     kx(ix, iy, iz) = aperture_zone(izone)**3
     &                                / (12.0 * frac_spacing(ilayer))
     &                                * xnode(ix, iy, iz)
     &                              + aperture_zone(izone)**3
     &                                / (12.0 * frac_spacing_vert(ilayer))
                     ky(ix, iy, iz) = aperture_zone(izone)**3
     &                                / (12.0 * frac_spacing(ilayer))
     &                                * ynode(ix, iy, iz)
     &                              + aperture_zone(izone)**3
     &                                / (12.0 * frac_spacing_vert(ilayer))
                     kz(ix, iy, iz) = aperture_zone(izone)**3
     &                                / (12.0 * frac_spacing(ilayer))
     &                                * znode(ix, iy, iz)
                     kx(ix, iy, iz) = kx(ix, iy, iz) * k_scale_zone(izone)
                     ky(ix, iy, iz) = ky(ix, iy, iz) * k_scale_zone(izone)
                     kz(ix, iy, iz) = kz(ix, iy, iz) * k_scale_zone(izone)
                     porosity(ix, iy, iz) = (aperture_zone(izone)
     &                                       / frac_spacing(ilayer)
     &                                       * xnode(ix, iy, iz)
     &                                     + aperture_zone(izone)
     &                                       / frac_spacing(ilayer)
     &                                       * ynode(ix, iy, iz)
     &                                     + aperture_zone(izone)
     &                                       / frac_spacing_vert(ilayer))
     &                                     * por_scale_zone(izone)
                     porosity(ix, iy, iz) = min( porosity(ix, iy, iz),
```

```
                                                    0.1 )
                  van_alpha(ix, iy, iz) = van_alpha_zone(izone)
                  van_m(ix, iy, iz) = van_m_zone(izone)
               end do
            end do
         end do
      end do
      do iz = 1, nz
         do iy = 1, ny
            do ix = 1, nx
               if (kx(ix, iy, iz) .lt. 0.0 .or.
     &             ky(ix, iy, iz) .lt. 0.0 .or.
     &             kz(ix, iy, iz) .lt. 0.0 .or.
     &             porosity(ix, iy, iz) .lt. 0.0) then
                  write(10,*) 'error: unset properties at node'
                  write(10,*) 'ix = ', ix
                  write(10,*) 'iy = ', iy
                  write(10,*) 'iz = ', iz
                  stop
               end if
            end do
         end do
      end do


      if (model_type .ge. 1) then
         do iz = 1, nz
            do iy = 1, ny
               do ix = 1, nx
                  ilayer = rock_type_node_layer(ix, iy, iz)
                  D_mat_frac(ix, iy, iz) = ((  frac_spacing(ilayer)
     &                                       / xnode(ix, iy, iz)
     &                                      + frac_spacing(ilayer)
     &                                       / ynode(ix, iy, iz)
     &                                      + frac_spacing_vert(ilayer)
     &                                     ) / 3.0) / 10.0
                  area_mat_frac(ix, iy, iz) = 2.0 * (
     &                                1.0 / (frac_spacing(ilayer)
     &                                 / xnode(ix, iy, iz))
     &                              + 1.0 / (frac_spacing(ilayer)
     &                                 / ynode(ix, iy, iz))
     &                              + 1.0 / frac_spacing_vert(ilayer)
     &                                    )
     &                              * areaX_frac_mat
               end do
            end do
         end do
      end if


      do iprop = 1, nrock
         kx_prop(iprop) = -1.0
         ky_prop(iprop) = -1.0
         kz_prop(iprop) = -1.0
         porosity_prop(iprop) = -1.0
         van_alpha_prop(iprop) = -1.0
         van_m_prop(iprop) = -1.0
      end do

      prop_type_count = 0
      do iz = 1, nz
         do iy = 1, ny
            do ix = 1, nx

               found_prop_type = 0
               do iprop = 1, prop_type_count
                  if ((abs(kx(ix, iy, iz) - kx_prop(iprop))
     &                                 .lt. eps_prop) .and.
     &                (abs(ky(ix, iy, iz) - ky_prop(iprop))
     &                                 .lt. eps_prop) .and.
     &                (abs(kz(ix, iy, iz) - kz_prop(iprop))
     &                                 .lt. eps_prop) .and.
     &                (abs(porosity(ix, iy, iz) - porosity_prop(iprop))
```



```
     &                                 .lt. eps_prop) .and.
     &                (abs(van_alpha(ix, iy, iz)
     &                     - van_alpha_prop(iprop))
     &                                 .lt. eps_prop) .and.
     &                (abs(van_m(ix, iy, iz) - van_m_prop(iprop))
     &                                 .lt. eps_prop)) then
                     found_prop_type = 1
                     prop_type(ix, iy, iz) = iprop
                     goto 1020
                  end if
               end do
 1020          continue

               if (found_prop_type .eq. 0) then
                  prop_type_count = prop_type_count + 1

                  if (prop_type_count .gt. nrock) then
                     write(10,*) 'error: prop exceeds number'
                     write(10,*) '       of rock types'
                     stop
                  end if

                  kx_prop(prop_type_count) = kx(ix, iy, iz)
                  ky_prop(prop_type_count) = ky(ix, iy, iz)
                  kz_prop(prop_type_count) = kz(ix, iy, iz)
                  porosity_prop(prop_type_count) = porosity(ix, iy, iz)
                  van_alpha_prop(prop_type_count) =
     &                                          van_alpha(ix, iy, iz)
                  van_m_prop(prop_type_count) = van_m(ix, iy, iz)
                  prop_type(ix, iy, iz) = prop_type_count
               end if

            end do
         end do
      end do

      top_bnd_rock_label = 'topbd'
      bot_bnd_rock_label = 'botbd'
      do iprop = 1, prop_type_count
         if (iprop .lt. 10) then
            write(str1,'(i1)') iprop
            rock_label(iprop) = 'r000'//str1
         else if (iprop .lt. 100) then
            write(str2,'(i2)') iprop
            rock_label(iprop) = 'r00'//str2
         else if (iprop .lt. 1000) then
            write(str3,'(i3)') iprop
            rock_label(iprop) = 'r0'//str3
         else if (iprop .lt. 10000) then
            write(str4,'(i4)') iprop
            rock_label(iprop) = 'r'//str4
         end if
      end do
      do iz = 1, nz
         do iy = 1, ny
            do ix = 1, nx
               if (iz .eq. 1) then
                  str1_iz = 'a'
               else if (iz .eq. 2) then
                  str1_iz = 'b'
               else if (iz .eq. 3) then
                  str1_iz = 'c'
               else if (iz .eq. 4) then
                  str1_iz = 'd'
               else if (iz .eq. 5) then
                  str1_iz = 'e'
               else if (iz .eq. 6) then
                  str1_iz = 'f'
               else if (iz .eq. 7) then
                  str1_iz = 'g'
               else if (iz .eq. 8) then
                  str1_iz = 'h'
               else if (iz .eq. 9) then
```

```
                  str1_iz = 'i'
               else if (iz .eq. 10) then
                  str1_iz = 'j'
               else if (iz .eq. 11) then
                  str1_iz = 'k'
               else if (iz .eq. 12) then
                  str1_iz = 'l'
               else if (iz .eq. 13) then
                  str1_iz = 'm'
               else if (iz .eq. 14) then
                  str1_iz = 'n'
               else if (iz .eq. 15) then
                  str1_iz = 'o'
               else if (iz .eq. 16) then
                  str1_iz = 'p'
               else if (iz .eq. 17) then
                  str1_iz = 'q'
               else if (iz .eq. 18) then
                  str1_iz = 'r'
               else if (iz .eq. 19) then
                  str1_iz = 's'
               else if (iz .eq. 20) then
                  str1_iz = 't'
               else if (iz .eq. 21) then
                  str1_iz = 'u'
               end if
               if (ix .lt. 10) then
                  write(str1_ix,'(i1)') ix
                  str3 = str1_iz//' '//str1_ix
               else if (ix .lt. 100) then
                  write(str2_ix,'(i2)') ix
                  str3 = str1_iz//str2_ix
               end if
               if (iy .lt. 10) then
                  write(str1_iy,'(i1)') iy
                  str5 = str3//' '//str1_iy
               else if (iy .lt. 100) then
                  write(str2_iy,'(i2)') iy
                  str5 = str3//str2_iy
               end if
               node_label(ix, iy, iz) = str5

               if (model_type .ge. 1) then
                  write(str2_ix,'(i2)') ix + 50
                  str3 = str1_iz//str2_ix
                  write(str2_iy,'(i2)') iy + 50
                  str5 = str3//str2_iy
                  node_label_mat(ix, iy, iz) = str5
               end if

            end do
         end do
      end do
      do iy = 1, ny
         do ix = 1, nx
            if (ix .lt. 10) then
               write(str1_ix,'(i1)') ix
               str3_t = 'v'//' '//str1_ix
               str3_b = 'w'//' '//str1_ix
            else if (ix .lt. 100) then
               write(str2_ix,'(i2)') ix
               str3_t = 'v'//str2_ix
               str3_b = 'w'//str2_ix
            end if
            if (iy .lt. 10) then
               write(str1_iy,'(i1)') iy
               str5_t = str3_t//' '//str1_iy
               str5_b = str3_b//' '//str1_iy
            else if (iy .lt. 100) then
               write(str2_iy,'(i2)') iy
               str5_t = str3_t//str2_iy
               str5_b = str3_b//str2_iy
            end if
```



```
               top_bnd_node_label(ix, iy) = str5_t
               bot_bnd_node_label(ix, iy) = str5_b

            end do
         end do
         if (model_type .eq. 2) then
            pond_node = 0
            do iz = 1, 10
               do iy = 8, 16
                  do ix = 9, 17
                     pond_node = pond_node + 1
                     if (pond_node .lt. 10) then
                        write(str1,'(i1)') pond_node
                        pond_node_label(ix-8, iy-7, iz) = 'z   '//str1
                     else if (pond_node .lt. 100) then
                        write(str2,'(i2)') pond_node
                        pond_node_label(ix-8, iy-7, iz) = 'z  '//str2
                     else if (pond_node .lt. 1000) then
                        write(str3,'(i3)') pond_node
                        pond_node_label(ix-8, iy-7, iz) = 'z '//str3
                     else if (pond_node .lt. 10000) then
                        write(str4,'(i4)') pond_node
                        pond_node_label(ix-8, iy-7, iz) = 'z'//str4
                     end if
                  end do
               end do
            end do
         end if
         matrix_label(1) = 'mtrx1'
         matrix_label(2) = 'mtrx2'
         matrix_label(3) = 'mtrx3'
         matrix_label(4) = 'mtrx4'
         matrix_label(5) = 'mtrx5'
         matrix_label(6) = 'mtrx6'
         matrix_label(7) = 'mtrx7'
         pond_label = 'pond1'
         pond_liner_label = 'pond2'


         open (unit = 8, file = 'rocktype.dat', status = 'unknown')
         open (unit = 9, file = 'grid.dat', status = 'unknown')

         write(8,100)
         write(8,101)
         write(8,102)
  100    format('TITLE = "Fracture Properties"')
  101    format('VARIABLES = "X", "Y", "Z", "Layer ID", ',
     [          '"Xscale", "Yscale", "Zscale", ',
     [          '"kx", "ky", "kz", ',
     c     [    '"log10(kx)", "log10(ky)", "log10(kz)", ',
     [          '"porosity"')
  102    format('ZONE T="grid", I=23, J=21, K=21, F=POINT')
         do iz = 1, nz
            do iy = 1, ny
               do ix = 1, nx
                  if (iz .eq. 1) then
                     elev = zcoord(2) + 0.5*dz + 0.5*volume(ix, iy, iz)
                  else
                     elev = zcoord(iz)
                  end if
                  write(8,10) xcoord(ix), ycoord(iy), elev,
     [                        rock_type_node_layer(ix, iy, iz),
     [                        xnode(ix, iy, iz), ynode(ix, iy, iz),
     [                        znode(ix, iy, iz),
     [                        kx(ix, iy, iz),
     [                        ky(ix, iy, iz),
     [                        kz(ix, iy, iz),
     c                  [     log10( kx(ix, iy, iz) ),
     c                  [     log10( ky(ix, iy, iz) ),
     c                  [     log10( kz(ix, iy, iz) ),
     [                  [     porosity(ix, iy, iz)
   10                   format(3(1pe14.6,1x),1(i5,1x),7(1pe14.6,1x))
```

```
                xmin = xcoord(ix) - 0.5
                xmax = xcoord(ix) + 0.5
                xcentroid = xcoord(ix)
                ymin = ycoord(iy) - 0.5
                ymax = ycoord(iy) + 0.5
                ycentroid = ycoord(iy)
                zmin = elev - 0.5*volume(ix, iy, iz)
                zmax = elev + 0.5*volume(ix, iy, iz)
                zcentroid = elev
                write(9,750) ix, iy, iz,
     [                       rock_type_node_layer(ix, iy, iz),
     [                       xmin, xcentroid, xmax,
     [                       ymin, ycentroid, ymax,
     [                       zmin, zcentroid, zmax,
     [                       xnode(ix, iy, iz), ynode(ix, iy, iz),
     [                       znode(ix, iy, iz)
  750           format(4(i5,1x),12(1pe14.6,1x))
              end do
           end do
        end do

        close(8)
        close(9)


        open (unit = 8, file = 'init.dat', status = 'unknown')

        write(8,2000)
  2000  format('*   Box Canyon')
        write(8,2001)
  2001  format('ROCKS')

        do iprop = 1, prop_type_count
           nad = 2
           drok = 2400.0
           cwet = 1.730
           spht = 935.8
           write(8,2002) rock_label(iprop), nad, drok,
     [                   porosity_prop(iprop), kx_prop(iprop),
     [                   ky_prop(iprop), kz_prop(iprop),
     [                   cwet, spht
  2002     format(a5,i5,7e10.4)

           com = 1.0e-10
           expan = 0.0e0
           cdry = 1.7300
           tortx = 0.2500
           write(8,2003) com, expan, cdry, tortx
  2003     format(4e10.4)

           if (transp .eq. 1) then
              write(8,2007) alphal, alphat, lambda, Kd, Dm
  2007        format(5e10.4)
           end if

           icp = 7
           Slrf = 0.01
           Slsf =  1.0
           Pmax = 1.0e10
           Ssrf = 0.0
           if (kr_type .eq. 1) then
              irp = 7
              write(8,2004) irp, van_m_prop(iprop), Slrf, Slsf
  2004        format(i5,5x,3e10.4)
           else
              irp = 3
              write(8,2004) irp, Slrf, Ssrf
           end if
           write(8,2005) icp, van_m_prop(iprop), Slrf,
     [                   van_alpha_prop(iprop), Pmax, Slsf
  2005     format(i5,5x,5e10.4)
        end do
        write(8,2
                  top_bnd_rock_label, nad, drok,
```



```
     [                porosity_top_bnd, kx_top_bnd,
     [                ky_top_bnd, kz_top_bnd,
     [                cwet, 1.0e30
        write(8,2003) com, expan, cdry, tortx
        if (transp .eq. 1) then
           write(8,2007) alphal, alphat, lambda, Kd, Dm
        end if
        write(8,2006) 3, 0.2, 0.3, 0.7, 0.8
  2006  format(i5,5x,5e10.4)
        write(8,2005) 1, 0.0, 0.0, 1.0
        write(8,2002) bot_bnd_rock_label, nad, drok,
     [                porosity_bot_bnd, kx_bot_bnd,
     [                ky_bot_bnd, kz_bot_bnd,
     [                cwet, 1.0e30
        write(8,2003) com, expan, cdry, tortx
        if (transp .eq. 1) then
           write(8,2007) alphal, alphat, lambda, Kd, Dm
        end if
        if (kr_type .eq. 1) then
           irp = 7
           write(8,2004) irp, van_m_bot_bnd, 0.0, Slsf
        else
           irp = 3
           write(8,2004) irp, Slrf, Ssrf
        end if
        write(8,2005) icp, van_m_bot_bnd, 0.0,
     [                van_alpha_bot_bnd, Pmax, Slsf
        if (model_type .ge. 1) then
           do ilayer = 1, nlayer
              write(8,2002) matrix_label(ilayer), nad, drok,
     [                      porosity_mat(ilayer),
     [                      kx_mat(ilayer), ky_mat(ilayer),
     [                      kz_mat(ilayer),
     [                      cwet, spht
              write(8,2003) com, expan, cdry, tortx
              if (transp .eq. 1) then
                 write(8,2007) alphal, alphat, lambda, Kd, Dm
              end if
              if (kr_type .eq. 1) then
                 irp = 7
                 write(8,2004) irp, van_m_mat(ilayer), 0.1, 1.0
              else
                 irp = 3
                 write(8,2004) irp, 0.1, 0.0
              end if
              write(8,2005) icp, van_m_mat(ilayer), 0.1,
     [                      van_alpha_mat(ilayer),
     [                      Pmax, 1.0
           end do
        end if
        if (model_type .eq. 2 .and. pond_start .eq. 1) then
           write(8,2002) pond_label, nad, drok,
     [                   1.0, 1.0e0, 1.0e0, 1.0e0,
     [                   cwet, 1.0e30
           write(8,2003) com, expan, cdry, tortx
           write(8,2006) 5
           write(8,2005) 1, 0.0, 0.0, 1.0
           write(8,2002) pond_liner_label, nad, drok,
     [                   1.0, kx_pond_liner, ky_pond_liner,
     [                   kz_pond_liner,
     [                   cwet, 1.0e30
           write(8,2003) com, expan, cdry, tortx
           if (transp .eq. 1) then
              write(8,2007) alphal, alphat, lambda, Kd, Dm
           end if
           write(8,2006) 5
           write(8,2005) 1, 0.0, 0.0, 1.0
        end if

        write(8,2109)
        write(8,2110)
        write(8,2111)
        write(8,2112) 0.0, time_end, dtime_start, 9.80665, 3.0
```

```
      write(8,2113)
      write(8,2114) Pg_init, Sg_init + 10.0, T_init
      write(8,2115)
      write(8,2116)
      if (obs_times .eq. 1) then
         write(8,2200) n_obs_times_in, n_obs_times_in
 2200    format(2i5)
         write(8,2201) (otime(itime), itime = 1, n_obs_times_in)
 2201    format(8(f10.1))
      else
         write(8,2117)
         write(8,2118) time_end
      end if
      write(8,2119)
      write(8,2120)
      write(8,2121)
      write(8,2122)
      write(8,2123)
      write(8,2124)
      if (transp .eq. 0) then
         nk = 2
         neq = 2
         nph = 2
         nb = 8
      else
         nk = 3
         neq = 3
         nph = 2
         nb = 8
      end if
      write(8,2125) nk, neq, nph, nb
      write(8,2126)
      write(8,2127)
      write(8,2128)
      write(8,2129)
 2109 format(' ')
 2110 format('PARAM            1234567890123456789012345678901234')
 2111 format(' 4 20150    01501000001000000000030    140    0.00e-05')
 2112 format(3e10.4,10x,'dummy',5x,2e10.4)
 2113 format(' 1.0000e-4')
 2114 format(3e20.6)
 2115 format(' ')
 2116 format('TIMES')
 2117 format('    1    1')
 2118 format(e10.4)
 2119 format(' ')
 2120 format('RTSOL prec       rtol info iplvl nitmx nort kacc  iredb')
 2121 format('    1.0e-6        0.1    0    1  250   15    2    0')
 2122 format('     1.e-5      1.e15      100.0      100.      ',
     [    '1.75       0.20        0.2    0')
 2123 format(' ')
 2124 format('MULTI')
 2125 format(4i5)
 2126 format(' ')
 2127 format('START')
 2128 format(' ')
 2129 format('GENER - Infiltration')

      do iy = ny_min, ny_max
         do ix = nx_min, nx_max
            if (model_type .le. 1 .or. pond_start .eq. 2) then
               qinf = infiltration
               ex = 1.0e4
               type = 'COM1'
               write(8,2130) node_label(ix, iy, 1), type,
     [                       qinf, ex
 2130          format(a5,30x,a4,1x,2e10.4)
            else if (model_type .eq. 2 .and. pond_start .eq. 1) then
               if (ix .lt. 9 .or. ix .gt. 17 .or.
     [             iy .lt. 8 .or. iy .gt. 16) then
                  qinf = infiltration
                  ex = 1.0e4
                  type = 'COM1'
```



```
                  write(8,2130) node_label(ix, iy, 1), type,
     [                          qinf, ex
               end if
            else if (model_type .eq. 3) then
               if (ix .lt. 9 .or. ix .gt. 17 .or.
     [             iy .lt. 8 .or. iy .gt. 16) then
                  qinf = infiltration
                  ex = 1.0e4
                  type = 'COM1'
                  write(8,2130) node_label(ix, iy, 1), type,
     [                          qinf, ex
               else
                  ex = 1.0e4
                  type = 'COM1'
                  write(8,2140) node_label(ix, iy, 1),
     [                          nsource_in, type, ex
 2140             format(a5,20x,i5,5x,a4,1ix,e10.4)
                  write(8,2141) (qtpond(isource),
     [                           isource = 1, nsource_in)
 2141             format(4e14.7)
                  write(8,2141) (qpond(isource),
     [                           isource = 1, nsource_in)
                  if (transp .eq. 1) then
                     ex = 1.0e4
                     type = 'COM3'
                     write(8,2140) node_label(ix, iy, 1),
     [                             nsource_in, type, ex
                     write(8,2141) (qtpond(isource),
     [                              isource = 1, nsource_in)
                     write(8,2141) (cpond(isource),
     [                              isource = 1, nsource_in)
                  end if
               end if
            end if
         end do
      end do

      write(8,2136)
 2136 format(' ')
      write(8,2135)
 2135 format('ENDCY')

      close(8)

      open (unit = 9, file = 'init.incon', status = 'unknown')

      if (model_type .eq. 0 .and. incon .eq. 1) then
         do iz = 1, nz
            do iy = ny_min, ny_max
               do ix = nx_min, nx_max
                  write(9,4502) node_label(ix, iy, iz)
                  write(9,4503) Pg_init, Sg_init + 10.0,
     [                          T_init
               end do
            end do
         end do
         do iy = ny_min, ny_max
            do ix = nx_min, nx_max
               write(9,4502) top_bnd_node_label(ix, iy)
               write(9,4503) Pg_init_top, Sg_init_top + 10.0,
     [                       T_init_top
               write(9,4502) bot_bnd_node_label(ix, iy)
               write(9,4503) Pg_init_bot, Sg_init_bot + 10.0,
     [                       T_init_bot
            end do
         end do

         write(9,4500) ' '
      end if

      if (model_type .eq. 1 .and. incon .eq. 2) then
         open (unit = 8, file = 'fracture.save', status = 'unknown')
```

```
      read(8,4500) line150
4500  format(a150)
      write(9,4501)
4501  format('INCON - initial condition for fracture ',
     [        'and matrix nodes')
      do i = 1, 23 !11109
         read(8,4502) node_label_temp
4502     format(a5)
         read(8,4503) Pg_temp, Sg_temp, T_temp
4503     format(3e20.6)
         write(9,4502) node_label_temp
         write(9,4503) Pg_temp, Sg_temp, T_temp
      end do

      do iz = 1, nz
         do iy = ny_min, ny_max
            do ix = nx_min, nx_max
               write(9,4502) node_label_mat(ix, iy, iz)
               write(9,4503) Pg_init_mat, Sg_init_mat + 10.0,
     [                       T_init_mat
            end do
         end do
      end do

      write(9,4500) ' '
      close(8)
   end if

   if (model_type .eq. 1 .and. incon .eq. 1) then
      do iz = 1, nz
         do iy = ny_min, ny_max
            do ix = nx_min, nx_max
               write(9,4502) node_label(ix, iy, iz)
               write(9,4503) Pg_init, Sg_init + 10.0,
     [                       T_init
               write(9,4502) node_label_mat(ix, iy, iz)
               write(9,4503) Pg_init_mat, Sg_init_mat + 10.0,
     [                       T_init_mat
            end do
         end do
      end do
      do iy = ny_min, ny_max
         do ix = nx_min, nx_max
            write(9,4502) top_bnd_node_label(ix, iy)
            write(9,4503) Pg_init_top, Sg_init_top + 10.0,
     [                    T_init_top
            write(9,4502) bot_bnd_node_label(ix, iy)
            write(9,4503) Pg_init_bot, Sg_init_bot + 10.0,
     [                    T_init_bot
         end do
      end do

      write(9,4500) ' '
   end if

   if (model_type .eq. 2 .and. incon .eq. 2) then
      if (pond_start .eq. 1) then
         open (unit = 8, file = 'fracmat.save', status = 'unknown')

         read(8,4500) line150
         write(9,4504)
4504     format('INCON - initial condition for fracture, ',
     [          'matrix and pond nodes')
         do i = 1, 21252
            read(8,4505) str1, ix, iy
4505        format(a1,i2,i2)
            read(8,4503) Pg_temp, Sg_temp, T_temp
            if (str1 .eq. 'v') then
               if (ix .ge. 9 .and. ix. le. 17 .and.
     [             iy .ge. 8 .and. iy .le. 16) then
                  write(9,4505) str1, ix, iy
                  write(9,4503) 100.0e3, 10.99, 20.0
               else
```



```
                  write(9,4505) str1, ix, iy
                  write(9,4503) Pg_temp, Sg_temp, T_temp
               end if
            else
               write(9,4505) str1, ix, iy
               write(9,4503) Pg_temp, Sg_temp, T_temp
            end if
         end do

         avg_pond_elev = 0.0
         max_pond_elev = -1.0e6
         min_pond_elev = 1.0e6
         do iy = 8, 16
            do ix = 9, 17
               avg_pond_elev = avg_pond_elev + ground_elev(ix, iy)
               max_pond_elev = max( ground_elev(ix, iy),
     [                              max_pond_elev )
               min_pond_elev = min( ground_elev(ix, iy),
     [                              min_pond_elev )
            end do
         end do
         avg_pond_elev = avg_pond_elev / 81.0
         pond_elev = avg_pond_elev + avg_pond_depth

         do iz = 1, 10
            do iy = 8, 16
               do ix = 9, 17
                  bottom_elev = ground_elev(ix, iy) + (iz-1)*0.05
                  top_elev = ground_elev(ix, iy) + iz*0.05
                  pond_elev_node = min( pond_elev,
     [                                  ground_elev(ix, iy) )
                  if (pond_elev .le. bottom_elev) then
                     Sw = 0.001
                     Pw = 100.0e3
                  else if (pond_elev .le. top_elev .and.
     [                     pond_elev .gt. bottom_elev) then
                     Sw = (pond_elev - bottom_elev) / 0.05
                     Pw = 100.0e3 + (pond_elev - ground_elev(ix, iy)
     [                               - (iz-1)*0.05 - 0.025) * 9807.0
                     Pw = min( Pw, 100.0e3 )
                  else if (pond_elev .gt. top_elev) then
                     Sw = 0.999
                     Pw = 100.0e3 + (pond_elev - ground_elev(ix, iy)
     [                               - (iz-1)*0.05 - 0.025) * 9807.0
                  end if
                  write(9,4502) pond_node_label(ix-8, iy-7, iz)
                  if (Sw .gt. 1.0e-10) then
                     write(9,4503) Pw, 11.0 - Sw, 20.0
                  else
                     write(9,4503) Pw, 0.9, 20.0
                  end if
               end do
            end do
         end do

      else if (pond_start .eq. 2) then

         open (unit = 8, file = 'pond.save', status = 'unknown')

         read(8,4500) line150
         write(9,4506)
4506     format('INCON - initial condition for fracture, ',
     [          'matrix nodes with pond removed')
         do i = 1, 54 !???
            read(8,4505) str1, ix, iy
            read(8,4503) Pg_temp, Sg_temp, T_temp
            if (str1 .eq. 'v') then
               Pg = 100.0e3 - (ground_elev(ix, iy) - bottom_of_model
     [                         * 9.8065 * 1.176
               write(9,4505) str1, ix, iy
               write(9,4503) Pg, 10.99, 20.0
            else if (str1 .ne. 'z') then
               write(9,4505) str1, ix, iy
```

```
                  write(9,4503) Pg_temp, Sg_temp, T_temp
               end if
            end do
         end if

         write(9,4500) ' '
         close(8)
      end if

      if (model_type .eq. 3) then
         open (unit = 8, file = 'fracmat.save', status = 'unknown')

         read(8,5500) line150
 5500    format(a150)
         if (transp .eq. 1) then
            write(9,5501)
            format('INCON - initial condition for fracture ',
     [           'and matrix nodes with transport')
         else
            write(9,5505)
            format('INCON - initial condition for fracture ',
     [           'and matrix nodes')
         end if
         do i = 1, 21171 !21252  !44
            read(8,4505) str1, ix, iy
            read(8,5503) Pg_temp, Sg_temp, T_temp
 5503       format(3e20.6)
            if (str1 .eq. 'v') then
               if (ix .lt. 9 .or. ix .gt. 17 .or.
     [             iy .lt. 8 .or. iy .gt. 16) then
                  write(9,4505) str1, ix, iy
                  if (transp .eq. 1) then
                     write(9,5504) Pg_temp, Sg_temp, 0.0, T_temp
                  else
                     write(9,5504) Pg_temp, Sg_temp, T_temp
                  end if
 5504             format(4e20.6)
               end if
            else
               write(9,4505) str1, ix, iy
               if (transp .eq. 1) then
                  write(9,5504) Pg_temp, Sg_temp, 0.0, T_temp
               else
                  write(9,5504) Pg_temp, Sg_temp, T_temp
               end if
            end if
         end do

         write(9,4500) ' '
         close(8)
      end if

      close(9)


      open (unit = 8, file = 'init.mesh', status = 'unknown')

      write(8,2210)
 2210 format('ELEME')

      do iz = 1, nz
         do iy = ny_min, ny_max
            do ix = nx_min, nx_max
               if (boundary_type .eq. 2) then
                  if (ix .eq. 1 .or. ix .eq. nx .or.
     [                iy .eq. 1 .or. iy .eq. ny) then
                     write(8,2211) node_label(ix, iy, iz),
     [                             rock_label( prop_type(ix, iy, iz) ),
     [                             1.0e7, ix, iy, iz
                  else
                     write(8,2211) node_label(ix, iy, iz),
     [                             rock_label( prop_type(ix, iy, iz) ),
     [                             volume(ix, iy, iz), ix, iy, iz
```



```
               end if
            else
               write(8,2211) node_label(ix, iy, iz),
     [                       rock_label( prop_type(ix, iy, iz) ),
     [                       volume(ix, iy, iz), ix, iy, iz
 2211          format(a5,10x,a5,e10.4,20x,3i5)
            end if
         end do
      end do
      do iy = ny_min, ny_max
         do ix = nx_min, nx_max
            iz = 1
            vol = 1.0e6
            if (model_type .eq. 3) then
               if (ix .lt. 9 .or. ix .gt. 17 .or.
     [             iy .lt. 8 .or. iy .gt. 16) then
                  write(8,2211) top_bnd_node_label(ix, iy),
     [                          top_bnd_rock_label,
     [                          vol, ix, iy, iz
               end if
            else
               write(8,2211) top_bnd_node_label(ix, iy),
     [                       top_bnd_rock_label,
     [                       vol, ix, iy, iz
            end if
            iz = nz
            vol = 1.0e30
            write(8,2211) bot_bnd_node_label(ix, iy),
     [                    bot_bnd_rock_label,
     [                    vol, ix, iy, iz
         end do
      end do
      if (model_type .ge. 1) then
         do iz = 1, nz
            do iy = ny_min, ny_max
               do ix = nx_min, nx_max
                  ilayer = rock_type_node_layer(ix, iy, iz)
                  write(8,2211) node_label_mat(ix, iy, iz),
     [                          matrix_label(ilayer),
     [                          volume(ix, iy, iz), ix, iy, iz
               end do
            end do
         end do
      end if
      if (model_type .eq. 2 .and. pond_start .eq. 1) then
         do iy = 8, 16
            do ix = 9, 17
               vol = 0.05
               write(8,2211) pond_node_label(ix-8, iy-7, 1),
     [                       pond_liner_label, vol,
     [                       ix, iy, 1
            end do
         end do
         do iz = 2, 10
            do iy = 8, 16
               do ix = 9, 17
                  vol = 0.05
                  write(8,2211) pond_node_label(ix-8, iy-7, iz),
     [                          pond_label, vol,
     [                          ix, iy, iz
               end do
            end do
         end do
      end if

      write(8,2212)
      write(8,2213)
 2212 format(' ')
 2213 format('CONNE')

      do iz = 1, nz
         do iy = ny_min, ny_max
```

```
1318              do ix = nx_min, nx_max
                     ixm1 = ix - 1
                     iym1 = iy - 1
                     izm1 = iz - 1

1320                 if (ixm1 .ge. nx_min) then
                        areax = (volume(ix, iy, iz)
     [                           + volume(ixm1, iy, iz)) / 2.0
                        d1 = 0.5
                        d2 = 0.5
1325                    betax = 0.0
                        isot = 1
                        write(8,2214) node_label(ix, iy, iz),
     [                                node_label(ixm1, iy, iz),
     [                                isot, d1, d2, areax, betax,
1330 [                                ix, iy, iz, ixm1, iy, iz
   2214                 format(2a5,15x,i5,4e10.4,10x,3i5,3x,3i5)
                     end if

                     if (iym1 .ge. ny_min) then
1335                    areax = (volume(ix, iy, iz)
     [                           + volume(ix, iym1, iz)) / 2.0
                        d1 = 0.5
                        d2 = 0.5
                        betax = 0.0
1340                    isot = 2
                        write(8,2214) node_label(ix, iy, iz),
     [                                node_label(ix, iym1, iz),
     [                                isot, d1, d2, areax, betax,
     [                                ix, iy, iz, ix, iym1, iz
1345                 end if

                     if (izm1 .ge. 1) then
                        areax = 1.0
                        d1 = volume(ix, iy, iz) / 2.0
1350                    d2 = volume(ix, iy, izm1) / 2.0
                        betax = -1.0
                        isot = 3
                        write(8,2214) node_label(ix, iy, iz),
     [                                node_label(ix, iy, izm1),
1355 [                                isot, d1, d2, areax, betax,
     [                                ix, iy, iz, ix, iy, izm1
                     end if

                  end do
1360           end do
               end do
               do iy = ny_min, ny_max
                  do ix = nx_min, nx_max
                     if (model_type .eq. 2 .and. pond_start .eq. 1) then
1365                    if (ix .ge. 9 .and. ix .le. 17 .and.
     [                      iy .ge. 8 .and. iy .le. 16) then
                           ixm1 = ix - 1
                           iym1 = iy - 1
                           if (ixm1 .ge. 9) then
1370                          iz = 1
                              d1 = 0.5
                              d2 = 0.5
                              areax = 0.05
                              betax = cos( 3.14159/2.0 -
1375 [                                atan( ground_elev(ix, iy)
     [                                      - ground_elev(ixm1, iy) ) )
                              isot = 1
                              write(8,2214) pond_node_label(ix-8, iy-7, iz),
     [                                      pond_node_label(ixm1-8, iy-7, iz),
1380 [                                      isot, d1, d2, areax, betax,
     [                                      ix, iy, iz, ix, iy, iz
                           end if
                           if (iym1 .ge. 8) then
                              iz = 1
1385                          d1 = 0.5
                              d2 = 0.5
                              areax = 0.05
```



```
                              betax = cos( 3.14159/2.0 -
     [                                atan( ground_elev(ix, iy)
1390 [                                      - ground_elev(ix, iym1) ) )
                              isot = 1
                              write(8,2214) pond_node_label(ix-8, iy-7, iz),
     [                                      pond_node_label(ix-8, iym1-7, iz),
     [                                      isot, d1, d2, areax, betax,
1395 [                                      ix, iy, iz, ix, iy, iz
                           end if

                           iz = 1
                           d1 = 0.025
1400                       d2 = volume(ix, iy, iz) / 2.0
                           areax = 1.0
                           betax = 1.0
                           isot = 3
                           write(8,2214) pond_node_label(ix-8, iy-7, iz),
1405 [                                   node_label(ix, iy, iz),
     [                                   isot, d1, d2, areax, betax,
     [                                   ix, iy, iz, ix, iy, iz
                           do iz = 1, 9
                              d1 = 0.025
1410                          d2 = 0.025
                              areax = 1.0
                              betax = 1.0
                              isot = 3
                              write(8,2214) pond_node_label(ix-8, iy-7, iz+1),
1415 [                                      pond_node_label(ix-8, iy-7, iz),
     [                                      isot, d1, d2, areax, betax,
     [                                      ix, iy, iz, ix, iy, iz+1
                           end do
                           iz = 10
1420                       d2 = 0.025
                           write(8,2214) top_bnd_node_label(ix, iy),
     [                                   pond_node_label(ix-8, iy-7, iz),
     [                                   isot, 1.0e-15, d2, areax, betax,
     [                                   ix, iy, iz, ix, iy, iz
1425
                        else
                           iz = 1
                           d2 = volume(ix, iy, iz) / 2.0
                           areax = 1.0
1430                       betax = 1.0
                           isot = 3
                           write(8,2214) top_bnd_node_label(ix, iy),
     [                                   node_label(ix, iy, iz),
     [                                   isot, 1.0e-15, d2, areax, betax,
1435 [                                   ix, iy, iz, ix, iy, iz
                        end if
                     else if (model_type .eq. 3) then
                        if (ix .lt. 9 .or. ix .gt. 17 .or.
     [                      iy .lt. 8 .or. iy .gt. 16) then
1440                       iz = 1
                           d2 = volume(ix, iy, iz) / 2.0
                           areax = 1.0
                           betax = 1.0
                           isot = 3
1445                       write(8,2214) top_bnd_node_label(ix, iy),
     [                                   node_label(ix, iy, iz),
     [                                   isot, 1.0e-15, d2, areax, betax,
     [                                   ix, iy, iz, ix, iy, iz
                        end if
1450                 else
                        iz = 1
                        d2 = volume(ix, iy, iz) / 2.0
                        areax = 1.0
                        betax = 1.0
1455                    isot = 3
                        write(8,2214) top_bnd_node_label(ix, iy),
     [                                node_label(ix, iy, iz),
     [                                isot, 1.0e-15, d2, areax, betax,
     [                                ix, iy, iz, ix, iy, iz
1460                 end if
```

```
            iz = nz
            d2 = volume(ix, iy, iz) / 2.0
            areax = 1.0
            betax = -1.0
            write(8,2214) bot_bnd_node_label(ix, iy),
     &                    node_label(ix, iy, iz),
     &                    isot, 1.0e-15, d2, areax, betax,
     &                    ix, iy, iz, ix, iy, iz
         end do
      end do
      if (model_type .ge. 1) then
         do iz = 1, nz
            do iy = ny_min, ny_max
               do ix = nx_min, nx_max
                  betax = 0.0
                  isot = 1
                  write(8,2214) node_label_mat(ix, iy, iz),
     &                          node_label(ix, iy, iz),
     &                          isot, D_mat_frac(ix, iy, iz), d2,
     &                          area_mat_frac(ix, iy, iz), betax,
     &                          ix, iy, iz, ix, iy, iz
               end do
            end do
         end do

         if (dual_k .eq. 1) then
            do iz = 1, nz
               do iy = ny_min, ny_max
                  do ix = nx_min, nx_max
                     ixm1 = ix - 1
                     iym1 = iy - 1
                     izm1 = iz - 1

                     if (ixm1 .ge. nx_min) then
                        areax = (volume(ix, iy, iz)
     &                          + volume(ixm1, iy, iz)) / 2.0
                        d1 = 0.5
                        d2 = 0.5
                        betax = 0.0
                        isot = 1
                        write(8,2214) node_label_mat(ix, iy, iz),
     &                                node_label_mat(ixm1, iy, iz),
     &                                isot, d1, d2, areax, betax,
     &                                ix, iy, iz, ixm1, iy, iz
                     end if

                     if (iym1 .ge. ny_min) then
                        areax = (volume(ix, iy, iz)
     &                          + volume(ix, iym1, iz)) / 2.0
                        d1 = 0.5
                        d2 = 0.5
                        betax = 0.0
                        isot = 2
                        write(8,2214) node_label_mat(ix, iy, iz),
     &                                node_label_mat(ix, iym1, iz),
     &                                isot, d1, d2, areax, betax,
     &                                ix, iy, iz, ix, iym1, iz
                     end if

                     if (izm1 .ge. 1) then
                        areax = 1.0
                        d1 = volume(ix, iy, iz) / 2.0
                        d2 = volume(ix, iy, izm1) / 2.0
                        betax = -1.0
                        isot = 3
                        write(8,2214) node_label_mat(ix, iy, iz),
     &                                node_label_mat(ix, iy, izm1),
     &                                isot, d1, d2, areax, betax,
     &                                ix, iy, iz, ix, iy, izm1
                     end if
                  end do
               end do
```



```
            end do
         end if
      end if

      write(8,2215)
 2215 format(' ')

      close(8)

      stop
      end
```

```
     1   1   1   1
_max, ny_max                                                    ! nx_min, ny_min, nx
1
 =1 fracture-matrix =2 f-m with pond nodes  =3 f-m with pond source terms
                                                                ! =0 fractures only,
1
=1 dual permeability                                            ! =0 dual porosity,
0
low + transport                                                 ! =0 flow only, =1 f
 1
 initialization, =2 restart                                     ! INCON: =1 complete
3.171e-6
s]  10 cm/yr x 1m3 = 3.171e-6 kg/s                              ! recharge rate [kg/
0
lation as observation time, =1 read in times                    ! =0 use end of simu
3.1536e13    1.0
 starting timestep: 1 day = 86400 sec, 1e6 years = 3.1536e13 sec, 37157040.0
                                                                ! end of simulation,
1
 pond, = 2 remove pond                                          ! pond start: =1 add
 0.0
ater in pond                                                    ! average depth of w
1.0e-15  1.0e-15  1.0e-15
terface between pond and aquifer                                ! permeability of in
1
 normal (impermeable) =2 large volme -1st type                  ! side boudaries: =1
0.001 1.0  5.0e-4  0.5
, van_alpha, van_m                                              ! top boundary: b, D
0.001 1.0  5.0e-4  0.5
, D, van_alpha, van_m                                           ! bottom boundary: b
100.0e3    0.999     20.0
it, Sg_init, T_init                                             ! top boundary Pg_in
100.0e3    0.9       20.0
it, Sg_init, T_init                                             ! bot boundary Pg_in
100.0e3    0.9       20.0
: Pg_init, Sg_init, T_init                                      ! interior fractures
100.0e3    0.01      20.0
g_init, Sg_init, T_init                                         ! interior matrix: P
0.01
 interfacial area between fractures and matrix                  ! scaling factor for
0.0  0.0  0.0  0.0  1.0e-10
disp, decay, Kd, molec diffu (for all nodes)                    ! long disp, transv
0
enuchten relative permeability function                         ! =0 Corey, =1 van G
1.0  1.0    8.54E-05  5.0e-4    0.5    50.0  1.0
D, van_alpha, van_m., porosity scale factor, k scale factor: 0.0 - 0.2
                                                                ! D horiz., D vert.
2.0  1.0    1.48E-04  5.0e-4    0.5    50.0  1.0
4.0  1.0    1.57E-04  5.0e-4    0.5    50.0  1.0                ! 0.2 - 0.4
4.0  1.0    1.22E-04  5.0e-4    0.5    50.0  1.0                ! 0.4 - 0.6
2.0  1.0    2.09E-04  5.0e-4    0.5    50.0  1.0                ! 0.6 - 0.8
0.1  0.1    8.59E-04  5.0e-4    0.5    50.0  1.0                ! 0.8 - 1.0
2.0  1.0    1.28E-03  5.0e-4    0.5     5.0  1.0                ! rubble zone
1.0e-14  1.0e-14  1.0e-14  0.2  5.0e-5 0.25                     ! lower basalt flow
, porosity, van_alpha, van_m: 0.0 - 0.2                         ! matrix: kx, ky, kz
1.0e-14  1.0e-14  1.0e-14  0.2  5.0e-5 0.25
1.0e-14  1.0e-14  1.0e-14  0.2  5.0e-5 0.25                     ! 0.2 - 0.4
1.0e-14  1.0e-14  1.0e-14  0.2  5.0e-5 0.25                     ! 0.4 - 0.6
1.0e-14  1.0e-14  1.0e-14  0.2  5.0e-5 0.25                     ! 0.6 - 0.8
1.0e-14  1.0e-14  1.0e-14  0.2  5.0e-5 0.25                     ! 0.8 - 1.0
1.0e-14  1.0e-14  1.0e-14  0.2  5.0e-5 0.25                     ! rubble zone
32                                                              ! lower basalt flow
nes                                                             ! number of input zo
  14  14   3  14  14   3  9.83E-05 5.0e-4  0.5    50.0  1.0    ! i1, j1, k1, i2, j2
, k2, b, van_alpha, van_m, porosity scale factor, k scale factor
  16  18   3  16  18   3  7.41E-05 5.0e-4  0.5    50.0  1.0    !
  13  10   4  13  10   4  1.65E-04 5.0e-4  0.5    50.0  1.0    !
  16  18   4  16  18   4  7.73E-05 5.0e-4  0.5    50.0  1.0    !
  13  10   5  13  10   5  9.08E-05 5.0e-4  0.5    50.0  1.0    !
  14  14   5  14  14   5  1.39E-04 5.0e-4  0.5    50.0  1.0    !
  16  17   5  16  17   5  4.82E-04 5.0e-4  0.5    50.0  1.0    !
  13  10   6  13  10   6  3.35E-04 5.0e-4  0.5    50.0  1.0    !
  13  13   6  13  13   6  1.14E-04 5.0e-4  0.5    50.0  1.0    !
  15  17   6  15  17   6  5.14E-05 5.0e-4  0.5    50.0  1.0    !
  16  17   6  16  17   6  4.31E-04 5.0e-4  0.5    50.0  1.0    !
  13  10   7  13  10   7  3.22E-04 5.0e-4  0.5    50.0  1.0    !
```



```
  13  13   7  13  13   7  6.40E-05 5.0e-4  0.5    50.0  1.0    !
  15  16   7  15  16   7  1.38E-04 5.0e-4  0.5    50.0  1.0    !
  13  10   8  13  10   8  3.99E-04 5.0e-4  0.5    50.0  1.0    !
  15  16   8  15  16   8  9.76E-05 5.0e-4  0.5    50.0  1.0    !
  13  10   9  13  10   9  5.90E-04 5.0e-4  0.5    50.0  1.0    !
  12  12   9  12  12   9  6.14E-05 5.0e-4  0.5    50.0  1.0    !
  13  12   9  13  12   9  9.84E-05 5.0e-4  0.5    50.0  1.0    !
  14  15   9  14  15   9  6.74E-05 5.0e-4  0.5    50.0  1.0    !
  15  15   9  15  15   9  6.91E-05 5.0e-4  0.5    50.0  1.0    !
  15  16   9  15  16   9  6.87E-05 5.0e-4  0.5    50.0  1.0    !
  12  11  10  12  11  10  4.64E-05 5.0e-4  0.5    50.0  1.0    !
  14  15  10  14  15  10  7.38E-04 5.0e-4  0.5    50.0  1.0    !
  12  11  11  12  11  11  3.16E-05 5.0e-4  0.5    50.0  1.0    !
  14  14  11  14  14  11  1.87E-03 5.0e-4  0.5    50.0  1.0    !
  13  10  12  13  10  12  8.59E-04 5.0e-4  0.5    50.0  1.0    !
  13  13  13  13  13  13  1.92E-03 5.0e-4  0.5    50.0  1.0    !
  13  13  14  13  13  14  4.26E-04 5.0e-4  0.5    50.0  1.0    !
  13  12  15  13  12  15  1.86E-03 5.0e-4  0.5    50.0  1.0    !
  12  12  16  12  12  16  4.69E-03 5.0e-4  0.5    50.0  1.0    !
  12  11  18  12  11  18  4.76E-04 5.0e-4  0.5    50.0  1.0    !

   9   8   1  17  16   1        1.0 5.0e-4  0.5  1.0    1.0  ! i1, j1, k1, i2, j2
, k2, b, van_alpha, van_m
```

permeabilities used in verification (pp 105c-105d)

```
      1   1  23  21
_max, ny_max                                                    ! nx_min, ny_min, nx
1
 =1 fracture-matrix =2 f-m with pond nodes  =3 f-m with pond source terms
1                                                               ! =0 fractures only,
=1 dual permeability
0                                                               ! =0 dual porosity,
low + transport
1                                                               ! =0 flow only, =1 f
 initialization, =2 restart
3.171e-6                                                        ! INCON: =1 complete
s]  10 cm/yr x 1m3 = 3.171e-6 kg/s
0                                                               ! recharge rate [kg/
lation as observation time, =1 read in times
3.1536e13    1.0                                                ! =0 use end of simu
 starting timestep: 1 day = 86400 sec, 1e6 years = 3.1536e13 sec, 37157040.0
1                                                               ! end of simulation,
 pond, = 2 remove pond
0.0                                                             ! pond start: =1 add
ater in pond
1.0e-15  1.0e-15  1.0e-15                                       ! average depth of w
terface between pond and aquifer
1                                                               ! permeability of in
 normal (impermeable) =2 large volme -1st type
0.001 1.0  5.0e-4  0.5                                          ! side boudaries: =1
, van_alpha, van_m
0.001 1.0  5.0e-4  0.5                                          ! top boundary: b, D
, D, van_alpha, van_m
100.0e3   0.999    20.0                                         ! bottom boundary: b
it, Sg_init, T_init
100.0e3   0.9      20.0                                         ! top boundary Pg_in
it, Sg_init, T_init
100.0e3   0.9      20.0                                         ! bot boundary Pg_in
: Pg_init, Sg_init, T_init
100.0e3   0.01     20.0                                         ! interior fractures
g_init, Sg_init, T_init
0.01                                                            ! interior matrix: P
 interfacial area between fractures and matrix
0.0  0.0  0.0  0.0  1.0e-10                                     ! scaling factor for
disp, decay, Kd, molec diffu (for all nodes)
0                                                               ! long disp, transv
enuchten relative permeability function
1.0  1.0   8.54E-05  5.0e-4   0.5   50.0  1.0                  ! =0 Corey, =1 van G
b, van_alpha, van_m., porosity scale factor, k scale factor:
2.0  1.0   1.48E-04  5.0e-4   0.5   50.0  1.0                  ! D horiz., D vert.
4.0  1.0   1.57E-04  5.0e-4   0.5   50.0  1.0                  ! 0.0 - 0.2
4.0  1.0   1.22E-04  5.0e-4   0.5   50.0  1.0                  ! 0.2 - 0.4
2.0  1.0   2.09E-04  5.0e-4   0.5   50.0  1.0                  ! 0.4 - 0.6
0.1  0.1   8.59E-04  5.0e-4   0.5    5.0  1.0                  ! 0.6 - 0.8
2.0  1.0   1.28E-03  5.0e-4   0.5    5.0  1.0                  ! 0.8 - 1.0
1.0e-14  1.0e-14  1.0e-14  0.2  5.0e-5 0.25                    ! rubble zone
, porosity, van_alpha, van_m: 0.0 - 0.2                         ! lower basalt flow
1.0e-14  1.0e-14  1.0e-14  0.2  5.0e-5 0.25                    ! matrix: kx, ky, kz
1.0e-14  1.0e-14  1.0e-14  0.2  5.0e-5 0.25                    ! 0.2 - 0.4
1.0e-14  1.0e-14  1.0e-14  0.2  5.0e-5 0.25                    ! 0.4 - 0.6
1.0e-14  1.0e-14  1.0e-14  0.2  5.0e-5 0.25                    ! 0.6 - 0.8
1.0e-14  1.0e-14  1.0e-14  0.2  5.0e-5 0.25                    ! 0.8 - 1.0
1.0e-14  1.0e-14  1.0e-14  0.2  5.0e-5 0.25                    ! rubble zone
32                                                              ! lower basalt flow
nes                                                             ! number of input zo
   14  14   3  14  14   3  9.83E-05 5.0e-4  0.5   50.0  1.0   ! i1, j1, k1, i2, j2
; k2, b, van_alpha, van_m, porosity scale factor, k scale factor
   16  18   3  16  18   3  7.41E-05 5.0e-4  0.5   50.0  1.0   !
   13  10   4  13  10   4  1.65E-04 5.0e-4  0.5   50.0  1.0   !
   16  18   4  16  18   4  7.73E-05 5.0e-4  0.5   50.0  1.0   !
   13  10   5  13  10   5  9.08E-05 5.0e-4  0.5   50.0  1.0   !
   14  14   5  14  14   5  1.39E-04 5.0e-4  0.5   50.0  1.0   !
   16  17   5  16  17   5  4.82E-04 5.0e-4  0.5   50.0  1.0   !
   13  10   6  13  10   6  3.35E-04 5.0e-4  0.5   50.0  1.0   !
   13  13   6  13  13   6  1.14E-04 5.0e-4  0.5   50.0  1.0   !
   15  17   6  15  17   6  5.14E-05 5.0e-4  0.5   50.0  1.0   !
   16  17   6  16  17   6  4.31E-04 5.0e-4  0.5   50.0  1.0   !
   13  10   7  13  10   7  3.22E-04 5.0e-4  0.5   50.0  1.0   !
```



```
   13  13   7  13  13   7  6.40E-05 5.0e-4  0.5   50.0  1.0   !
   15  16   7  15  16   7  1.38E-04 5.0e-4  0.5   50.0  1.0   !
   13  10   8  13  10   8  3.99E-04 5.0e-4  0.5   50.0  1.0   !
   15  16   8  15  16   8  9.76E-05 5.0e-4  0.5   50.0  1.0   !
   13  10   9  13  10   9  5.90E-04 5.0e-4  0.5   50.0  1.0   !
   12  12   9  12  12   9  6.14E-05 5.0e-4  0.5   50.0  1.0   !
   13  12   9  13  12   9  9.84E-05 5.0e-4  0.5   50.0  1.0   !
   14  15   9  14  15   9  6.74E-05 5.0e-4  0.5   50.0  1.0   !
   15  15   9  15  15   9  6.91E-05 5.0e-4  0.5   50.0  1.0   !
   15  16   9  15  16   9  6.87E-05 5.0e-4  0.5   50.0  1.0   !
   12  11  10  12  11  10  4.64E-05 5.0e-4  0.5   50.0  1.0   !
   14  15  10  14  15  10  7.38E-04 5.0e-4  0.5   50.0  1.0   !
   12  11  11  12  11  11  3.16E-05 5.0e-4  0.5   50.0  1.0   !
   14  14  11  14  14  11  1.87E-03 5.0e-4  0.5   50.0  1.0   !
   13  10  12  13  10  12  8.59E-04 5.0e-4  0.5   50.0  1.0   !
   13  13  13  13  13  13  1.92E-03 5.0e-4  0.5   50.0  1.0   !
   13  13  14  13  13  14  4.26E-04 5.0e-4  0.5   50.0  1.0   !
   13  12  15  13  12  15  1.86E-03 5.0e-4  0.5   50.0  1.0   !
   12  12  16  12  12  16  4.69E-03 5.0e-4  0.5   50.0  1.0   !
   12  11  18  12  11  18  4.76E-04 5.0e-4  0.5   50.0  1.0   !

    9   8   1  17  16   1        1.0 5.0e-4  0.5   1.0    1.0  ! i1, j1, k1, i2, j2
, k2, b, van_alpha, van_m
```

YMP-LBNL
REVIEW RECORD

1. QA: L
2. Page 1 of 1

3. Originator: Andre Unger
4. Document Title: Documentation for Routine rocktype.for v1.0 (Option 1 per AP-SI.1Q/Rev. 2/ICN4, Sec. 5.1)
5. Document Number: N/A
6. Revision/Mod.: N/A
7. Draft: N/A
8. Governing Procedure Number: AP-SI.1Q
9. Revision/Mod: 2/4

REVIEW CRITERIA

10. ☒ Standard Review Criteria: YMP-LBNL-QIP-6.1, Attch. 5, p. 18 Routine Review Criteria (One time use Option 1) (Taken from Attachment 5)

11. ☐ Specific Review Criteria:
☒ Source: AP-SI.1Q/Rev. 2/ICN4, Sec. 5.1.1 (One time use routine)
☐ Attached:

12. Comment Documentation:
☐ Comment Sheets
☐ Review Copy Mark-up

13. YMP-LBNL Project Manager (PM): Gudmundur S. Bodvarsson

☒ Scientific notebook/data associated with this review as noted on Attachment 3

14. Reviewer | Org./Discipline | Review Criteria

Reviewer	Org./Discipline	Review Criteria
Randall Hedegaard	LBNL/Hydrogeologist	Technical

Reviewer	Org./Discipline	Review Criteria

COMMENTS DUE:

15. Due Date: 1 MAR 2000

16. Originator/Review Coordinator: Andre Unger
Print Name

REVIEW BY:

17. Randall F. Hedegaard
Print Name

18. [signature] 1MAR00
Signature Date

19. Mandatory Comments: ☐ Yes ☒ No

ORIGINATOR/REVIEW COORDINATOR (After response completed):

20. Andre Unger [signature] 01/02/00
Print Name/Signature Date

CONCURRENCE:

21. Document Draft No: NA Date:

22. Reviewer: [signature] 1MAR00
Signature Date

23. PM: [signature] 3/3/00
Signature Date

DISPUTE RESOLUTION: (if applicable)

24. PM:
Signature Date

YMP-LBNL
REVIEW RECORD

1. QA: L
2. Page 1 of 1

3. Originator: Andre Unger
4. Document Title: Documentation for Routine rocktype.for v1.0 (Option 1 per AP-SI.1Q/Rev. 2/ICN4, Sec. 5.1)
5. Document Number: N/A
6. Revision/Mod.: N/A
7. Draft: N/A
8. Governing Procedure Number: AP-SI.1Q
9. Revision/Mod: 2/4

REVIEW CRITERIA

10. ☒ Standard Review Criteria: YMP-LBNL-QIP-6.1, Attch. 5, p. 18 Routine Review Criteria (One time use Option 1) (Taken from Attachment 5)

11. ☐ Specific Review Criteria:
☒ Source: AP-SI.1Q/Rev. 2/ICN4, Sec. 5.1.1 (One time use routine)
☐ Attached:

12. Comment Documentation:
☐ Comment Sheets
☐ Review Copy Mark-up

13. YMP-LBNL Project Manager (PM): Gudmundur S. Bodvarsson

☒ Scientific notebook/data associated with this review as noted on Attachment 3

14. Reviewer	Org./Discipline	Review Criteria	Reviewer	Org./Discipline	Review Criteria
Randall Hedegaard	LBNL/Hydrogeologist	Technical			

COMMENTS DUE:

15. Due Date: 1 MAR 2000

16. Originator/Review Coordinator:
Andre Unger
Print Name

REVIEW BY:

17. Randall F. Hedegaard
Print Name

18. [signature] 1MAR00
Signature Date

19. Mandatory Comments: ☐ Yes ☒ No

ORIGINATOR/REVIEW COORDINATOR (After response completed):

20. Andre Unger [signature] 01/02/00
Print Name/Signature Date

CONCURRENCE:

21. Document Draft No: NA Date:

22. Reviewer: [signature] 1MAR00
Signature Date

23. PM: [signature] 3/3/00
Signature Date

DISPUTE RESOLUTION: (if applicable)

24. PM:
Signature Date

YMP-LBNL
APPLICABLE REFERENCE INFORMATION

Document No.and Title: Routine Documentation for **rocktype.for v.1.0** per Option 1, AP-SI.1Q/Rev.2/ICN4, Sec. 5.5.1

Date of Document (or revision, draft revision number, as applicable):
NA

Pertinent sections of scientific notebook(s) or other backup documents and/or data DTN# are identified below, supporting the document which is the subject of this review. These documents/data shall be included in the scope of this review.

Document(s) Title/Data	Relevant Sections/Pages
Routine/Macro Documentation Form	pp. 1 and 2
YMP-LBNL-AMS-NA-AU-1 Scientific Notebook	pp. 104-113

STANDARD REVIEW CRITERIA

Routine/Macro Review Criteria, Option 1

NOTE: Where a checklist item does not apply to the software product, check "N/A".

	Yes	No	N/A	
R/M-1	X			**The information given below is to be documented in the technical product, in which the routine/macro is used to support. Does the routine/macro include:** Name of routine/macro with version/Operating System/hardware environment
R/M-2	X			Name of commercial software used to write the routine/macros with version/Operating System/hardware used to develop it
R/M-3	X			Test Plan • Explanation whether this is a routine or macro and a description of what it does • The source code (this section shall include equations or algorithms form software setup (Labview, Excel, etc.) • Description of test(s) to be performed (be specific) • Specified range of input values to be used and why the range is valid
R/M-4	X			Test Results • Output from test (explain difference between input range used and possib input) • Description of how the testing shows that the results are correct for the specified input • List of limitations or assumptions to this test case (s) and code in general • Electronic files identified by name and location (included if necessary to perform the tests)
R/M-5	X			Supporting Information. Include background information, such as revision to a previous routine or macro or explanation of the steps performed to run the software. Include listing of all electronic files and codes used. Attach Scientific Notebook pages with appropriate information annotated.

weight.for v1.0
Routine/Macro Documentation Form

The following information can be included in the scientific notebook. Attach and reference notebook pages and diskettes with files as needed when submitting routine/macro to records.

1. Name of routine/macro with version/OS/hardware environment :

   weight.for v1.0/Microsoft Windows 98/Pentium III

2. Name of commercial software with version/OS/hardware used to develop routine/macro:

   Digital Visual Fortran v6.0/Microsoft Windows 98/Pentium III.

3. Test Plan.

   - Explain whether this is a routine or macro and describe what it does:

     The function of this software routine is to reformat raw data weighting factors from four input files and create an output file in TECPLOT file format to visualize β weighting factors. The output file is saved to a new filename.

   - Source code: (including equations or algorithms from software setup (LabView, Excel, etc.):

     Source code is printed on pp. 114-115 from S/N: YMP-LBNL-AMS-NA-AU-1 and is provided on accompanying CD entitled YMP-LBNL-AMS-NA-AU-1 (routines) directory/weight.for/.

   - Description of test(s) to be performed (be specific):

     The four input files, X1.prn, X2.prn, X3.prn, X4.prn, containing raw weighting factor data will be read into the routine and reformatted into a TECPLOT format file. The output file will be saved to a new filename, weight.dat. See p. 114, S/N: YMP-LBNL-AMS-NA-AU-1 for a further explanation of the test. The routine test will be checked by visually comparing the spatial data output plots with the spatial data input file to verify that the reformatting is complete and correct. Furthermore, plotted figures will be used to verify that the weighting factors were correctly converted and placed in 3D space into the proper TECPLOT format.

   - Specify the range of input values to be used and why the range is valid:

     The range of input values is a representative sampling of the input files, printed on pp. 114-115, S/N YMP-LBNL-AMS-NA-AU-1 and shown on Figures printed on pp. 50-53, S/N YMP-LBNL-AMS-NA-AU-1. This test case input range is deemed valid because the routine's format conversion can be successfully inspected using only a small sampling of lines from very large input and output files which are acceptable and valid β weighting factors.

4. Test Results.

   - Output from test (explain difference between input range used and possible input):

     The TECPLOT output from the test is printed on pp. 50-53, S/N YMP-LBNL-AMS-NA-AU-1. The raw output file is provided on accompanying CD entitled YMP-LBNL-AMS-NA-AU-1 (routines) directory/weight.for/. For the purposes of this test (or the problem for which it was created) there is no difference between input range used and possible input.

   - Description of how the testing shows that the results are correct for the specified input:

The outputs of the code were manually inspected and are consistent with expectations. In addition, the file executed in TECPLOT without errors. A visual inspection of the fracture permeability factors (see pp. 114-115, S/N YMP-LBNL-AMS-NA-AU-1) versus the final plotted data shown on Figures on pp. 50-53, S/N YMP-LBNL-AMS-NA-AU-1 shows that the spatial data was correctly represented in the output.

- List limitations or assumptions to this test case and code in general:

  This software routine is valid for the identified input and output files on the accompanying CD and is intended to be used with TECPLOT.

- Electronic files identified by name and location (include disc if necessary):

  The routine weight.for is printed on pp. 114-115 from S/N: YMP-LBNL-AMS-NA-AU-1. All files used in the testing are provided on the accompanying CD entitled YMP-LBNL-AMS-NA-AU-1 (routines) in directory /weight.for/

5. Supporting Information. Include background information, such as revision to a previous routine or macro, or explanation of the steps performed to run the software. Include listings of all electronic files and codes used. Attach Scientific Notebook pages with appropriate information annotated:

See attached pages for referenced Scientific Notebook pages and other supporting documentation.

Note: All relevant S/N pages are included in this package. In some instances, the included S/N pages cross-reference other pages that are not included here because these were not essential to the documentation of this routine.

MAINTAIN PAGES IN THIS ORDER:

1. **This 2-page weight.for v1.0 routine documentation form.**
2. **pp. ~~114~~-115 and 50-53 from S/N YMP-LBNL-AMS-NA-AU-1**
3. **Review records**

113a
mc 3/7/00

Testing of routine weight.for v1.0

All files used for testing are located in:

D:\weight.for v1.0\Test

The following pages from scientific notebook YMP-LBNL-AMS-NA-AU-1 refer to testing of the routine: pp 114-115. Additional pages from this scientific notebook which support this testing include pp. 46, 47, 48, 50-53, 65

OS Type: Mcirosoft Windows 98

Compiler: Digitial Visual Fortran V6.0

Software compiled and executed on above OS and compiler on LBL/DOE 6396546 Pentium III.

Testing for weight.for v1.0

written in Fortran 77 routine

The function of this macro is to generate a Tecplot input file to visualize the β weighting factors on pages 46 and 47. The same Tecplot file is used as input to various other programs, such as **rocktype.for**, which require information on these weighting factors. The acceptance criteria for this macro is that it correctly processes all input files containing raw data on the weighting factors and converts them into a Tecplot file of acceptable format. All relevant files are located in:

C:\803D-74\FractureNetwork\grid\WeightingFactor

of computer LBL/DOE 6396546.

The range of input parameters is shown on figures on pp. 50 – 53 which show the values in these files 114e - 114h

1. Input control
   - Lines 13 to 51 read all the raw weighting factor data. This data is in the following files:
     X1.prn - β weighting factors for dimensionless depth zone 0.2 – 0.4 of the upper basalt. – see 114a, e
     X2.prn - β weighting factors for dimensionless depth zone 0.4 – 0.6 of the upper basalt. – see 114b, f
     X3.prn - β weighting factors for dimensionless depth zone 0.6 – 0.8 of the upper basalt. – see 114c, g
     X4.prn - β weighting factors for dimensionless depth zone 0.8 – 1.0 of the upper basalt. – see 114d, h
   - Verification that the raw data from the above files was read in correctly was performed by breaking the code and checking the contents of the arrays manually. Tecplot requires at least 2 data values in each of the three coordinate directions to use the 3-d visualization option. Therefore, the z direction consists of two identical layers of the β weighting factors to view each of the above layers in plan view.

2. Coordinate calculations
   - Lines 53 to 67 calculate the coordinates of the nodes in the grid. The x and y coordinates coincide with the conceptual model shown on page 48.
   - Verification of the coordinates was performed by breaking the code and checking the contents of the arrays. Note: can also compare page 114a – 114d with figures on pages (50-53) 114e - 114h

3. Output
   - Lines 69 to 119 output the weighting factors into Tecplot format in a file called **weight.dat**.
   - Verification that all aspects of the data conversion were performed correctly is given by pages 50 to 53. These figures indicate that the weighting factors were correctly converted into Tecplot format and organized for subsequent manipulation.

Fracture Permeability Factor for Dimensionless Depth 0 - 0.4

		1	2	3	4	5	6	7	8	9	10	11	12	13	14	15	16	17	18	19	20	21	22	23
21	k_x	1.00	1.00	1.00	1.00	1.00	1.00	1.00	1.00	1.00	1.00	1.00	1.00	1.00	1.00	1.00	1.00	1.00	1.00	1.00	1.00	1.00	1.00	1.00
	k_y	1.00	1.00	1.00	1.00	1.00	1.00	1.00	1.00	1.00	1.00	1.00	1.00	1.00	1.00	1.00	1.00	1.00	1.00	1.00	1.00	1.00	1.00	1.00
	k_z	2.00	2.00	2.00	2.00	2.00	2.00	2.00	2.00	2.00	2.00	2.00	2.00	2.00	2.00	2.00	2.00	2.00	2.00	2.00	2.00	2.00	2.00	2.00
20	k_x	1.00	1.00	1.00	1.00	1.00	1.00	1.00	1.00	1.00	1.00	1.00	1.00	1.00	1.00	1.00	1.00	1.00	1.00	1.00	1.00	1.00	1.00	1.00
	k_y	1.00	1.00	1.00	1.00	1.00	1.00	1.00	1.00	1.00	1.00	1.00	1.00	1.00	1.00	1.00	1.00	1.00	1.00	1.00	1.00	1.00	1.00	1.00
	k_z	2.00	2.00	2.00	2.00	2.00	2.00	2.00	2.00	2.00	2.00	2.00	2.00	2.00	2.00	2.00	2.00	2.00	2.00	2.00	2.00	2.00	2.00	2.00
19	k_x	1.00	1.00	1.00	1.00	1.00	1.00	1.00	1.00	1.00	1.00	1.00	1.00	1.00	1.00	1.00	1.00	1.00	1.00	1.00	1.00	1.00	1.00	1.00
	k_y	1.00	1.00	1.00	1.00	1.00	1.00	1.00	1.00	1.00	1.00	1.00	1.00	1.00	0.75	1.00	1.00	1.00	1.00	1.00	1.00	1.00	1.00	1.00
	k_z	2.00	2.00	2.00	2.00	2.00	2.00	2.00	2.00	2.00	2.00	2.00	2.00	2.00	1.75	2.00	2.00	2.00	2.00	2.00	2.00	2.00	2.00	2.00
18	k_x	1.00	1.00	1.00	1.00	1.00	1.00	1.00	1.00	1.00	1.00	1.00	1.00	1.00	1.00	1.00	1.00	1.00	1.00	1.00	1.00	1.00	1.00	1.00
	k_y	1.00	1.00	1.00	1.00	1.00	1.00	1.00	1.00	1.00	1.00	1.00	1.00	0.75	1.50	0.75	1.00	1.00	1.00	1.00	1.00	1.00	1.00	1.00
	k_z	2.00	2.00	2.00	2.00	2.00	2.00	2.00	2.00	2.00	2.00	2.00	1.75	2.50	1.75	2.00	2.00	2.00	2.00	2.00	2.00	2.00	2.00	2.00
17	k_x	1.00	1.00	1.00	1.00	1.00	1.00	1.00	1.00	1.00	1.00	1.00	1.00	1.00	1.00	1.00	1.00	1.00	1.00	1.00	1.00	1.00	1.00	1.00
	k_y	1.00	1.00	1.00	1.00	1.00	1.00	1.00	1.00	1.00	1.00	1.00	1.00	0.50	2.00	0.50	1.00	1.00	1.00	1.00	1.00	1.00	1.00	1.00
	k_z	2.00	2.00	2.00	2.00	2.00	2.00	2.00	2.00	2.00	2.00	2.00	1.50	3.00	1.50	2.00	2.00	2.00	2.00	2.00	2.00	2.00	2.00	2.00
16	k_x	1.00	1.00	1.00	1.00	1.00	1.00	1.00	1.00	0.75	0.75	0.50	0.75	0.75	0.75	1.00	1.00	1.00	1.00	1.00	1.00	1.00	1.00	1.00
	k_y	1.00	1.00	1.00	1.00	1.00	1.00	1.00	1.00	0.75	1.00	0.50	1.00	0.75	1.50	0.75	1.00	1.00	1.00	1.00	1.00	1.00	1.00	1.00
	k_z	2.00	2.00	2.00	2.00	2.00	2.00	2.00	2.00	1.50	1.75	1.00	1.75	1.50	2.25	1.75	2.00	2.00	2.00	2.00	2.00	2.00	2.00	2.00
15	k_x	1.00	1.00	1.00	1.00	1.00	1.00	1.00	0.75	1.50	1.50	2.00	1.50	1.50	1.50	0.75	1.00	1.00	1.00	1.00	1.00	1.00	1.00	1.00
	k_y	1.00	1.00	1.00	1.00	1.00	1.00	1.00	0.75	1.50	0.50	2.00	0.50	0.75	1.50	0.75	1.00	1.00	1.00	1.00	1.00	1.00	1.00	1.00
	k_z	2.00	2.00	2.00	2.00	2.00	2.00	2.00	1.50	3.00	2.00	4.00	2.00	2.25	3.00	1.50	2.00	2.00	2.00	2.00	2.00	2.00	2.00	2.00
14	k_x	1.00	1.00	1.00	1.00	1.00	1.00	1.00	1.00	0.75	0.75	0.50	0.75	0.75	0.75	1.00	1.00	1.00	1.00	1.00	1.00	1.00	1.00	1.00
	k_y	1.00	1.00	1.00	1.00	1.00	1.00	1.00	0.75	1.50	0.50	2.00	0.50	0.50	2.00	0.50	1.00	1.00	0.75	1.00	1.00	1.00	1.00	1.00
	k_z	2.00	2.00	2.00	2.00	2.00	2.00	2.00	1.75	2.25	1.25	2.50	1.25	1.25	2.75	1.50	2.00	2.00	1.75	2.00	2.00	2.00	2.00	2.00
13	k_x	1.00	1.00	1.00	1.00	1.00	1.00	1.00	1.00	1.00	1.00	1.00	1.00	1.00	1.00	1.00	1.00	1.00	1.00	1.00	1.00	1.00	1.00	1.00
	k_y	1.00	1.00	1.00	1.00	1.00	1.00	1.00	0.75	1.50	0.75	1.50	0.75	0.75	1.50	0.75	1.00	0.75	1.50	0.75	1.00	1.00	1.00	1.00
	k_z	2.00	2.00	2.00	2.00	2.00	2.00	2.00	1.75	2.50	1.75	2.50	1.75	1.75	2.50	1.75	2.00	1.75	2.50	1.75	2.00	2.00	2.00	2.00
12	k_x	1.00	1.00	1.00	1.00	1.00	1.00	0.75	0.75	0.50	0.50	0.50	0.50	0.50	0.75	1.00	1.00	1.00	1.00	1.00	1.00	1.00	1.00	1.00
	k_y	1.00	1.00	1.00	1.00	1.00	1.00	1.00	0.50	2.00	0.50	1.00	1.00	1.00	0.75	1.00	1.00	0.50	2.00	0.50	1.00	1.00	1.00	1.00
	k_z	2.00	2.00	2.00	2.00	2.00	2.00	1.75	1.25	2.50	1.00	1.50	1.50	1.50	1.50	2.00	2.00	1.50	3.00	1.50	2.00	2.00	2.00	2.00
11	k_x	1.00	1.00	1.00	1.00	1.00	0.75	1.50	1.50	2.00	2.00	2.00	2.00	2.00	1.50	0.75	1.00	1.00	1.00	1.00	1.00	1.00	1.00	1.00
	k_y	1.00	1.00	1.00	1.00	1.00	1.00	0.75	1.50	1.50	0.75	0.50	2.00	0.50	1.00	1.00	1.00	0.75	1.50	0.75	1.00	1.00	1.00	1.00
	k_z	2.00	2.00	2.00	2.00	2.00	1.75	2.25	3.00	3.50	2.75	2.50	4.00	2.50	2.50	1.75	2.00	1.75	2.50	1.75	2.00	2.00	2.00	2.00
10	k_x	1.00	1.00	1.00	1.00	1.00	1.00	0.75	0.75	0.50	0.50	0.50	0.50	0.50	0.75	1.00	1.00	1.00	1.00	1.00	1.00	1.00	1.00	1.00
	k_y	1.00	1.00	1.00	1.00	1.00	1.00	0.75	1.50	0.75	1.00	0.50	2.00	0.50	1.00	1.00	1.00	1.00	0.75	1.00	1.00	1.00	1.00	1.00
	k_z	2.00	2.00	2.00	2.00	2.00	2.00	1.50	2.25	1.25	1.50	1.00	2.50	1.00	1.75	2.00	2.00	2.00	1.75	2.00	2.00	2.00	2.00	2.00
9	k_x	1.00	1.00	1.00	1.00	1.00	1.00	0.75	0.50	1.00	1.00	1.00	1.00	1.00	1.00	1.00	1.00	1.00	1.00	1.00	1.00	1.00	1.00	1.00
	k_y	1.00	1.00	1.00	1.00	1.00	1.00	0.50	2.00	0.50	1.00	0.75	1.50	0.75	0.75	1.00	1.00	1.00	1.00	1.00	1.00	1.00	1.00	1.00
	k_z	2.00	2.00	2.00	2.00	2.00	2.00	1.25	2.50	1.50	2.00	1.75	2.50	1.75	1.75	2.00	2.00	2.00	2.00	2.00	2.00	2.00	2.00	2.00
8	k_x	1.00	1.00	1.00	1.00	1.00	1.00	1.50	2.00	0.50	1.00	1.00	1.00	1.00	1.00	1.00	1.00	1.00	1.00	1.00	1.00	1.00	1.00	1.00
	k_y	1.00	1.00	1.00	1.00	1.00	0.75	0.50	2.00	0.50	1.00	1.00	1.00	0.75	1.50	0.75	1.00	1.00	1.00	1.00	1.00	1.00	1.00	1.00
	k_z	2.00	2.00	2.00	2.00	2.00	1.75	2.00	4.00	1.00	2.00	2.00	2.00	1.75	2.50	1.75	2.00	2.00	2.00	2.00	2.00	2.00	2.00	2.00
7	k_x	1.00	1.00	1.00	1.00	1.00	1.00	0.75	0.50	1.00	1.00	1.00	1.00	1.00	1.00	1.00	1.00	1.00	1.00	1.00	1.00	1.00	1.00	1.00
	k_y	1.00	1.00	1.00	1.00	1.00	1.00	0.75	1.50	0.75	1.00	1.00	1.00	0.75	1.50	0.75	1.00	1.00	1.00	1.00	1.00	1.00	1.00	1.00
	k_z	2.00	2.00	2.00	2.00	2.00	2.00	1.50	2.00	1.75	2.00	2.00	2.00	1.75	2.50	1.75	2.00	2.00	2.00	2.00	2.00	2.00	2.00	2.00
6	k_x	1.00	1.00	1.00	1.00	1.00	1.00	1.00	1.00	1.00	1.00	1.00	1.00	1.00	1.00	1.00	1.00	1.00	1.00	1.00	1.00	1.00	1.00	1.00
	k_y	1.00	1.00	1.00	1.00	1.00	1.00	1.00	0.75	1.00	1.00	1.00	1.00	0.50	2.00	0.50	1.00	1.00	1.00	1.00	1.00	1.00	1.00	1.00
	k_z	2.00	2.00	2.00	2.00	2.00	2.00	2.00	1.75	2.00	2.00	2.00	2.00	1.50	3.00	1.50	2.00	2.00	2.00	2.00	2.00	2.00	2.00	2.00
5	k_x	1.00	1.00	1.00	1.00	1.00	1.00	1.00	1.00	1.00	1.00	1.00	1.00	1.00	1.00	1.00	1.00	1.00	1.00	1.00	1.00	1.00	1.00	1.00
	k_y	1.00	1.00	1.00	1.00	1.00	1.00	1.00	1.00	1.00	1.00	1.00	1.00	0.75	1.50	0.75	1.00	1.00	1.00	1.00	1.00	1.00	1.00	1.00
	k_z	2.00	2.00	2.00	2.00	2.00	2.00	2.00	2.00	2.00	2.00	2.00	1.75	2.50	1.75	2.00	2.00	2.00	2.00	2.00	2.00	2.00	2.00	2.00
4	k_x	1.00	1.00	1.00	1.00	1.00	1.00	1.00	1.00	1.00	1.00	1.00	1.00	1.00	1.00	1.00	1.00	1.00	1.00	1.00	1.00	1.00	1.00	1.00
	k_y	1.00	1.00	1.00	1.00	1.00	1.00	1.00	1.00	1.00	1.00	1.00	1.00	0.75	1.50	0.75	1.00	1.00	1.00	1.00	1.00	1.00	1.00	1.00
	k_z	2.00	2.00	2.00	2.00	2.00	2.00	2.00	2.00	2.00	2.00	2.00	1.75	2.50	1.75	2.00	2.00	2.00	2.00	2.00	2.00	2.00	2.00	2.00
3	k_x	1.00	1.00	1.00	1.00	1.00	1.00	1.00	1.00	1.00	1.00	1.00	1.00	1.00	1.00	1.00	1.00	1.00	1.00	1.00	1.00	1.00	1.00	1.00
	k_y	1.00	1.00	1.00	1.00	1.00	1.00	1.00	1.00	1.00	1.00	1.00	1.00	0.75	1.00	1.00	1.00	1.00	1.00	1.00	1.00	1.00	1.00	1.00
	k_z	2.00	2.00	2.00	2.00	2.00	2.00	2.00	2.00	2.00	2.00	2.00	1.75	2.00	2.00	2.00	2.00	2.00	2.00	2.00	2.00	2.00	2.00	2.00
2	k_x	1.00	1.00	1.00	1.00	1.00	1.00	1.00	1.00	1.00	1.00	1.00	1.00	1.00	1.00	1.00	1.00	1.00	1.00	1.00	1.00	1.00	1.00	1.00
	k_y	1.00	1.00	1.00	1.00	1.00	1.00	1.00	1.00	1.00	1.00	1.00	1.00	1.00	1.00	1.00	1.00	1.00	1.00	1.00	1.00	1.00	1.00	1.00
	k_z	2.00	2.00	2.00	2.00	2.00	2.00	2.00	2.00	2.00	2.00	2.00	2.00	2.00	2.00	2.00	2.00	2.00	2.00	2.00	2.00	2.00	2.00	2.00
1	k_x	1.00	1.00	1.00	1.00	1.00	1.00	1.00	1.00	1.00	1.00	1.00	1.00	1.00	1.00	1.00	1.00	1.00	1.00	1.00	1.00	1.00	1.00	1.00
	k_y	1.00	1.00	1.00	1.00	1.00	1.00	1.00	1.00	1.00	1.00	1.00	1.00	1.00	1.00	1.00	1.00	1.00	1.00	1.00	1.00	1.00	1.00	1.00
	k_z	2.00	2.00	2.00	2.00	2.00	2.00	2.00	2.00	2.00	2.00	2.00	2.00	2.00	2.00	2.00	2.00	2.00	2.00	2.00	2.00	2.00	2.00	2.00
		1	2	3	4	5	6	7	8	9	10	11	12	13	14	15	16	17	18	19	20	21	22	23

β_x
β_y
β_z

Fracture Permeability Factor for Dimensionless Depth 0 - 0.6

		1	2	3	4	5	6	7	8	9	10	11	12	13	14	15	16	17	18	19	20	21	22	23
21	k_x	1.00	1.00	1.00	1.00	1.00	1.00	1.00	1.00	1.00	1.00	1.00	1.00	1.00	1.00	1.00	1.00	1.00	1.00	1.00	1.00	1.00	1.00	1.00
	k_y	1.00	1.00	1.00	1.00	1.00	1.00	1.00	1.00	1.00	1.00	1.00	1.00	1.00	1.00	1.00	1.00	1.00	1.00	1.00	1.00	1.00	1.00	1.00
	k_z	2.00	2.00	2.00	2.00	2.00	2.00	2.00	2.00	2.00	2.00	2.00	2.00	2.00	2.00	2.00	2.00	2.00	2.00	2.00	2.00	2.00	2.00	2.00
20	k_x	1.00	1.00	1.00	1.00	1.00	1.00	1.00	1.00	1.00	1.00	1.00	1.00	1.00	1.00	1.00	1.00	1.00	1.00	1.00	1.00	1.00	1.00	1.00
	k_y	1.00	1.00	1.00	1.00	1.00	1.00	1.00	1.00	1.00	1.00	1.00	1.00	1.00	1.00	1.00	1.00	1.00	1.00	1.00	1.00	1.00	1.00	1.00
	k_z	2.00	2.00	2.00	2.00	2.00	2.00	2.00	2.00	2.00	2.00	2.00	2.00	2.00	2.00	2.00	2.00	2.00	2.00	2.00	2.00	2.00	2.00	2.00
19	k_x	1.00	1.00	1.00	1.00	1.00	1.00	1.00	1.00	1.00	1.00	1.00	1.00	1.00	1.00	1.00	1.00	1.00	1.00	1.00	1.00	1.00	1.00	1.00
	k_y	1.00	1.00	1.00	1.00	1.00	1.00	1.00	1.00	1.00	1.00	1.00	1.00	1.00	1.00	1.00	1.00	1.00	1.00	1.00	1.00	1.00	1.00	1.00
	k_z	2.00	2.00	2.00	2.00	2.00	2.00	2.00	2.00	2.00	2.00	2.00	2.00	2.00	2.00	2.00	2.00	2.00	2.00	2.00	2.00	2.00	2.00	2.00
18	k_x	1.00	1.00	1.00	1.00	1.00	1.00	1.00	1.00	1.00	1.00	1.00	1.00	1.00	1.00	1.00	1.00	1.00	1.00	1.00	1.00	1.00	1.00	1.00
	k_y	1.00	1.00	1.00	1.00	1.00	1.00	1.00	1.00	1.00	1.00	1.00	1.00	1.00	1.00	1.00	1.00	1.00	1.00	1.00	1.00	1.00	1.00	1.00
	k_z	2.00	2.00	2.00	2.00	2.00	2.00	2.00	2.00	2.00	2.00	2.00	2.00	2.00	2.00	2.00	2.00	2.00	2.00	2.00	2.00	2.00	2.00	2.00
17	k_x	1.00	1.00	1.00	1.00	1.00	1.00	1.00	1.00	0.75	0.75	0.25	0.75	0.75	0.75	1.00	1.00	1.00	1.00	1.00	1.00	1.00	1.00	1.00
	k_y	1.00	1.00	1.00	1.00	1.00	1.00	1.00	1.00	0.75	1.00	1.00	1.00	1.00	1.00	1.00	1.00	1.00	1.00	1.00	1.00	1.00	1.00	1.00
	k_z	2.00	2.00	2.00	2.00	2.00	2.00	2.00	2.00	1.50	1.75	1.25	1.75	1.75	1.75	2.00	2.00	2.00	2.00	2.00	2.00	2.00	2.00	2.00
16	k_x	1.00	1.00	1.00	1.00	1.00	1.00	1.00	0.75	0.75	0.75	0.25	0.75	0.75	0.75	0.75	1.00	1.00	1.00	1.00	1.00	1.00	1.00	1.00
	k_y	1.00	1.00	1.00	1.00	1.00	1.00	1.00	0.75	0.75	0.75	1.00	1.00	1.00	1.00	1.00	1.00	1.00	1.00	1.00	1.00	1.00	1.00	1.00
	k_z	2.00	2.00	2.00	2.00	2.00	2.00	2.00	1.50	1.50	1.50	1.25	1.75	1.75	1.75	1.75	2.00	2.00	2.00	2.00	2.00	2.00	2.00	2.00
15	k_x	1.00	1.00	1.00	1.00	1.00	1.00	0.75	0.75	2.00	2.00	4.00	2.00	2.00	2.00	0.75	0.75	1.00	1.00	1.00	1.00	1.00	1.00	1.00
	k_y	1.00	1.00	1.00	1.00	1.00	1.00	0.75	0.75	2.00	0.75	0.75	1.00	1.00	1.00	1.00	1.00	1.00	1.00	1.00	1.00	1.00	1.00	1.00
	k_z	2.00	2.00	2.00	2.00	2.00	2.00	1.50	1.50	4.00	2.75	4.75	3.00	3.00	3.00	1.75	1.75	2.00	2.00	2.00	2.00	2.00	2.00	2.00
14	k_x	1.00	1.00	1.00	1.00	1.00	1.00	1.00	0.75	0.75	0.75	0.25	0.75	0.75	0.75	0.75	1.00	1.00	1.00	1.00	1.00	1.00	1.00	1.00
	k_y	1.00	1.00	1.00	1.00	1.00	1.00	0.75	0.75	2.00	0.75	0.75	1.00	1.00	1.00	1.00	1.00	1.00	1.00	1.00	1.00	1.00	1.00	1.00
	k_z	2.00	2.00	2.00	2.00	2.00	2.00	1.75	1.50	2.75	1.50	1.00	1.75	1.75	1.75	1.75	2.00	2.00	2.00	2.00	2.00	2.00	2.00	2.00
13	k_x	1.00	1.00	1.00	1.00	1.00	1.00	0.75	0.75	0.25	0.25	0.25	0.75	0.75	0.75	1.00	1.00	1.00	1.00	1.00	1.00	1.00	1.00	1.00
	k_y	1.00	1.00	1.00	1.00	1.00	1.00	0.75	0.75	2.00	0.75	0.75	1.00	1.00	1.00	1.00	1.00	1.00	1.00	1.00	1.00	1.00	1.00	1.00
	k_z	2.00	2.00	2.00	2.00	2.00	2.00	1.50	1.50	2.25	1.00	1.00	1.75	1.75	1.75	2.00	2.00	2.00	2.00	2.00	2.00	2.00	2.00	2.00
12	k_x	1.00	1.00	1.00	1.00	1.00	0.75	0.75	0.75	0.25	0.25	0.25	0.25	1.00	1.00	1.00	1.00	1.00	1.00	1.00	1.00	1.00	1.00	1.00
	k_y	1.00	1.00	1.00	1.00	1.00	1.00	0.25	0.25	4.00	0.25	0.25	1.00	1.00	1.00	1.00	1.00	1.00	1.00	1.00	1.00	1.00	1.00	1.00
	k_z	2.00	2.00	2.00	2.00	2.00	1.75	1.00	1.00	4.25	0.50	0.50	1.25	2.00	2.00	2.00	2.00	2.00	2.00	2.00	2.00	2.00	2.00	2.00
11	k_x	1.00	1.00	1.00	1.00	0.75	0.75	2.00	2.00	4.00	4.00	4.00	0.25	0.25	1.00	1.00	1.00	1.00	1.00	1.00	1.00	1.00	1.00	1.00
	k_y	1.00	1.00	1.00	1.00	1.00	0.75	0.75	2.00	2.00	0.75	1.00	1.00	1.00	1.00	1.00	1.00	1.00	1.00	1.00	1.00	1.00	1.00	1.00
	k_z	2.00	2.00	2.00	2.00	1.75	1.50	2.75	4.00	6.00	4.75	5.00	1.25	1.25	2.00	2.00	2.00	2.00	2.00	2.00	2.00	2.00	2.00	2.00
10	k_x	1.00	1.00	1.00	1.00	1.00	0.75	0.75	0.75	0.25	0.25	0.25	0.25	1.00	1.00	1.00	1.00	1.00	1.00	1.00	1.00	1.00	1.00	1.00
	k_y	1.00	1.00	1.00	1.00	1.00	0.75	0.75	2.00	0.75	0.75	1.00	1.00	1.00	0.75	1.00	1.00	1.00	1.00	1.00	1.00	1.00	1.00	1.00
	k_z	2.00	2.00	2.00	2.00	2.00	1.50	1.50	2.75	1.00	1.00	1.25	1.25	2.00	1.75	2.00	2.00	2.00	2.00	2.00	2.00	2.00	2.00	2.00
9	k_x	1.00	1.00	1.00	1.00	1.00	1.00	0.75	0.75	0.25	0.25	0.25	1.00	1.00	1.00	1.00	1.00	1.00	1.00	1.00	1.00	1.00	1.00	1.00
	k_y	1.00	1.00	1.00	1.00	1.00	0.25	0.25	4.00	0.25	0.25	1.00	1.00	0.75	0.75	0.75	1.00	1.00	1.00	1.00	1.00	1.00	1.00	1.00
	k_z	2.00	2.00	2.00	2.00	2.00	1.25	1.00	4.75	0.50	0.50	1.25	2.00	1.75	1.75	1.75	2.00	2.00	2.00	2.00	2.00	2.00	2.00	2.00
8	k_x	1.00	1.00	1.00	1.00	1.00	1.00	1.00	1.00	1.00	1.00	1.00	1.00	1.00	1.00	1.00	1.00	1.00	1.00	1.00	1.00	1.00	1.00	1.00
	k_y	1.00	1.00	1.00	1.00	1.00	0.75	0.75	2.00	0.75	0.75	1.00	0.75	0.75	2.00	0.75	0.75	1.00	1.00	1.00	1.00	1.00	1.00	1.00
	k_z	2.00	2.00	2.00	2.00	2.00	1.75	1.75	3.00	1.75	1.75	2.00	1.75	1.75	3.00	1.75	1.75	2.00	2.00	2.00	2.00	2.00	2.00	2.00
7	k_x	1.00	1.00	1.00	1.00	1.00	1.00	1.00	1.00	1.00	1.00	1.00	1.00	1.00	1.00	1.00	1.00	1.00	1.00	1.00	1.00	1.00	1.00	1.00
	k_y	1.00	1.00	1.00	1.00	1.00	0.75	0.75	2.00	0.75	0.75	1.00	0.75	0.75	2.00	0.75	0.75	1.00	1.00	1.00	1.00	1.00	1.00	1.00
	k_z	2.00	2.00	2.00	2.00	2.00	1.75	1.75	3.00	1.75	1.75	2.00	1.75	1.75	3.00	1.75	1.75	2.00	2.00	2.00	2.00	2.00	2.00	2.00
6	k_x	1.00	1.00	1.00	1.00	1.00	1.00	1.00	1.00	1.00	1.00	1.00	1.00	1.00	1.00	1.00	1.00	1.00	1.00	1.00	1.00	1.00	1.00	1.00
	k_y	1.00	1.00	1.00	1.00	1.00	1.00	0.75	0.75	0.75	1.00	1.00	0.25	0.25	4.00	0.25	0.25	1.00	1.00	1.00	1.00	1.00	1.00	1.00
	k_z	2.00	2.00	2.00	2.00	2.00	2.00	1.75	1.75	1.75	2.00	2.00	1.25	1.25	5.00	1.25	1.25	2.00	2.00	2.00	2.00	2.00	2.00	2.00
5	k_x	1.00	1.00	1.00	1.00	1.00	1.00	1.00	1.00	1.00	1.00	1.00	1.00	1.00	1.00	1.00	1.00	1.00	1.00	1.00	1.00	1.00	1.00	1.00
	k_y	1.00	1.00	1.00	1.00	1.00	1.00	1.00	0.75	1.00	1.00	1.00	0.75	0.75	2.00	0.75	0.75	1.00	1.00	1.00	1.00	1.00	1.00	1.00
	k_z	2.00	2.00	2.00	2.00	2.00	2.00	2.00	1.75	2.00	2.00	2.00	1.75	1.75	3.00	1.75	1.75	2.00	2.00	2.00	2.00	2.00	2.00	2.00
4	k_x	1.00	1.00	1.00	1.00	1.00	1.00	1.00	1.00	1.00	1.00	1.00	1.00	1.00	1.00	1.00	1.00	1.00	1.00	1.00	1.00	1.00	1.00	1.00
	k_y	1.00	1.00	1.00	1.00	1.00	1.00	1.00	1.00	1.00	1.00	1.00	0.75	0.75	2.00	0.75	0.75	1.00	1.00	1.00	1.00	1.00	1.00	1.00
	k_z	2.00	2.00	2.00	2.00	2.00	2.00	2.00	2.00	2.00	2.00	2.00	1.75	1.75	3.00	1.75	1.75	2.00	2.00	2.00	2.00	2.00	2.00	2.00
3	k_x	1.00	1.00	1.00	1.00	1.00	1.00	1.00	1.00	1.00	1.00	1.00	1.00	1.00	1.00	1.00	1.00	1.00	1.00	1.00	1.00	1.00	1.00	1.00
	k_y	1.00	1.00	1.00	1.00	1.00	1.00	1.00	1.00	1.00	1.00	1.00	1.00	0.75	0.75	0.75	1.00	1.00	1.00	1.00	1.00	1.00	1.00	1.00
	k_z	2.00	2.00	2.00	2.00	2.00	2.00	2.00	2.00	2.00	2.00	2.00	2.00	1.75	1.75	1.75	2.00	2.00	2.00	2.00	2.00	2.00	2.00	2.00
2	k_x	1.00	1.00	1.00	1.00	1.00	1.00	1.00	1.00	1.00	1.00	1.00	1.00	1.00	1.00	1.00	1.00	1.00	1.00	1.00	1.00	1.00	1.00	1.00
	k_y	1.00	1.00	1.00	1.00	1.00	1.00	1.00	1.00	1.00	1.00	1.00	1.00	1.00	0.75	1.00	1.00	1.00	1.00	1.00	1.00	1.00	1.00	1.00
	k_z	2.00	2.00	2.00	2.00	2.00	2.00	2.00	2.00	2.00	2.00	2.00	2.00	2.00	1.75	2.00	2.00	2.00	2.00	2.00	2.00	2.00	2.00	2.00
1	k_x	1.00	1.00	1.00	1.00	1.00	1.00	1.00	1.00	1.00	1.00	1.00	1.00	1.00	1.00	1.00	1.00	1.00	1.00	1.00	1.00	1.00	1.00	1.00
	k_y	1.00	1.00	1.00	1.00	1.00	1.00	1.00	1.00	1.00	1.00	1.00	1.00	1.00	1.00	1.00	1.00	1.00	1.00	1.00	1.00	1.00	1.00	1.00
	k_z	2.00	2.00	2.00	2.00	2.00	2.00	2.00	2.00	2.00	2.00	2.00	2.00	2.00	2.00	2.00	2.00	2.00	2.00	2.00	2.00	2.00	2.00	2.00
		1	2	3	4	5	6	7	8	9	10	11	12	13	14	15	16	17	18	19	20	21	22	23

Fracture Permeability Factor for Dimensionless Depth 1 - 0.6

		1	2	3	4	5	6	7	8	9	10	11	12	13	14	15	16	17	18	19	20	21	22	23
21	k_x	1.00	1.00	1.00	1.00	1.00	1.00	1.00	1.00	1.00	1.00	1.00	1.00	1.00	1.00	1.00	1.00	1.00	1.00	1.00	1.00	1.00	1.00	1.00
	k_y	1.00	1.00	1.00	1.00	1.00	1.00	1.00	1.00	1.00	1.00	1.00	1.00	1.00	1.00	1.00	1.00	1.00	1.00	1.00	1.00	1.00	1.00	1.00
	k_z	2.00	2.00	2.00	2.00	2.00	2.00	2.00	2.00	2.00	2.00	2.00	2.00	2.00	2.00	2.00	2.00	2.00	2.00	2.00	2.00	2.00	2.00	2.00
20	k_x	1.00	1.00	1.00	1.00	1.00	1.00	1.00	1.00	1.00	1.00	1.00	1.00	1.00	1.00	1.00	1.00	1.00	1.00	1.00	1.00	1.00	1.00	1.00
	k_y	1.00	1.00	1.00	1.00	1.00	1.00	1.00	1.00	1.00	1.00	1.00	1.00	1.00	1.00	1.00	1.00	1.00	1.00	1.00	1.00	1.00	1.00	1.00
	k_z	2.00	2.00	2.00	2.00	2.00	2.00	2.00	2.00	2.00	2.00	2.00	2.00	2.00	2.00	2.00	2.00	2.00	2.00	2.00	2.00	2.00	2.00	2.00
19	k_x	1.00	1.00	1.00	1.00	1.00	1.00	1.00	1.00	1.00	1.00	1.00	1.00	1.00	0.75	0.75	0.25	0.75	0.75	1.00	1.00	1.00	1.00	1.00
	k_y	1.00	1.00	1.00	1.00	1.00	1.00	1.00	1.00	1.00	1.00	1.00	1.00	1.00	1.00	1.00	1.00	1.00	1.00	1.00	1.00	1.00	1.00	1.00
	k_z	2.00	2.00	2.00	2.00	2.00	2.00	2.00	2.00	2.00	2.00	2.00	2.00	2.00	1.75	1.75	1.25	1.75	1.75	2.00	2.00	2.00	2.00	2.00
18	k_x	1.00	1.00	1.00	1.00	1.00	1.00	1.00	1.00	1.00	1.00	1.00	1.00	0.75	0.75	0.75	0.25	0.75	0.75	0.75	1.00	1.00	1.00	1.00
	k_y	1.00	1.00	1.00	1.00	1.00	1.00	1.00	1.00	1.00	1.00	1.00	1.00	1.00	1.00	1.00	1.00	1.00	1.00	1.00	1.00	1.00	1.00	1.00
	k_z	2.00	2.00	2.00	2.00	2.00	2.00	2.00	2.00	2.00	2.00	2.00	2.00	1.75	1.75	1.75	1.25	1.75	1.75	1.75	2.00	2.00	2.00	2.00
17	k_x	1.00	1.00	1.00	1.00	1.00	1.00	1.00	1.00	1.00	1.00	1.00	0.75	0.75	2.00	2.00	4.00	2.00	2.00	0.75	0.75	1.00	1.00	1.00
	k_y	1.00	1.00	1.00	1.00	1.00	1.00	1.00	1.00	1.00	1.00	1.00	0.75	1.00	1.00	1.00	1.00	1.00	1.00	1.00	1.00	1.00	1.00	1.00
	k_z	2.00	2.00	2.00	2.00	2.00	2.00	2.00	2.00	2.00	2.00	2.00	1.50	1.75	3.00	3.00	5.00	3.00	3.00	1.75	1.75	2.00	2.00	2.00
16	k_x	1.00	1.00	1.00	1.00	1.00	1.00	1.00	1.00	1.00	1.00	1.00	1.00	0.75	0.75	0.75	0.25	0.75	0.75	0.75	1.00	1.00	1.00	1.00
	k_y	1.00	1.00	1.00	1.00	1.00	1.00	1.00	1.00	1.00	1.00	0.75	0.75	0.75	1.00	1.00	1.00	1.00	1.00	1.00	1.00	1.00	1.00	1.00
	k_z	2.00	2.00	2.00	2.00	2.00	2.00	2.00	2.00	2.00	2.00	1.75	1.75	1.50	1.75	1.75	1.25	1.75	1.75	1.75	2.00	2.00	2.00	2.00
15	k_x	1.00	1.00	1.00	1.00	1.00	1.00	1.00	1.00	1.00	1.00	1.00	1.00	1.00	0.75	0.75	0.25	0.75	0.75	1.00	1.00	1.00	1.00	1.00
	k_y	1.00	1.00	1.00	1.00	1.00	1.00	1.00	1.00	1.00	0.75	0.75	2.00	0.75	0.75	1.00	1.00	1.00	1.00	1.00	1.00	1.00	1.00	1.00
	k_z	2.00	2.00	2.00	2.00	2.00	2.00	2.00	2.00	2.00	1.75	1.75	3.00	1.75	1.50	1.75	1.25	1.75	1.75	2.00	2.00	2.00	2.00	2.00
14	k_x	1.00	1.00	1.00	1.00	1.00	1.00	1.00	0.75	0.75	0.25	0.75	0.25	0.75	0.75	1.00	1.00	1.00	1.00	1.00	1.00	1.00	1.00	1.00
	k_y	1.00	1.00	1.00	1.00	1.00	1.00	1.00	1.00	0.75	0.75	0.75	2.00	0.75	0.75	1.00	1.00	1.00	1.00	1.00	1.00	1.00	1.00	1.00
	k_z	2.00	2.00	2.00	2.00	2.00	2.00	2.00	1.75	1.50	1.00	1.50	2.25	1.50	1.50	2.00	2.00	2.00	2.00	2.00	2.00	2.00	2.00	2.00
13	k_x	1.00	1.00	1.00	1.00	1.00	1.00	0.75	0.75	0.75	0.25	0.75	0.25	0.75	0.75	1.00	1.00	1.00	1.00	1.00	1.00	1.00	1.00	1.00
	k_y	1.00	1.00	1.00	1.00	1.00	1.00	1.00	0.75	0.75	0.25	0.25	4.00	0.25	0.25	1.00	1.00	1.00	1.00	1.00	1.00	1.00	1.00	1.00
	k_z	2.00	2.00	2.00	2.00	2.00	2.00	1.75	1.50	1.50	0.50	1.00	4.25	1.00	1.00	1.75	2.00	2.00	2.00	2.00	2.00	2.00	2.00	2.00
12	k_x	1.00	1.00	1.00	1.00	1.00	0.75	0.75	2.00	2.00	4.00	2.00	4.00	2.00	2.00	0.75	0.75	1.00	1.00	1.00	1.00	1.00	1.00	1.00
	k_y	1.00	1.00	1.00	1.00	1.00	1.00	0.75	0.75	2.00	0.25	0.25	4.00	0.25	0.25	1.00	1.00	1.00	1.00	1.00	1.00	1.00	1.00	1.00
	k_z	2.00	2.00	2.00	2.00	2.00	1.75	1.50	2.75	4.00	4.25	2.25	8.00	2.25	2.25	1.75	1.75	2.00	2.00	2.00	2.00	2.00	2.00	2.00
11	k_x	1.00	1.00	1.00	1.00	1.00	1.00	0.75	0.75	0.75	0.25	0.75	0.25	0.75	0.75	0.75	1.00	1.00	1.00	1.00	1.00	1.00	1.00	1.00
	k_y	1.00	1.00	1.00	1.00	1.00	1.00	0.75	0.75	2.00	0.75	0.75	1.00	1.00	1.00	1.00	1.00	1.00	1.00	1.00	1.00	1.00	1.00	1.00
	k_z	2.00	2.00	2.00	2.00	2.00	2.00	1.50	1.50	2.75	1.00	1.50	1.25	1.75	1.75	1.75	2.00	2.00	2.00	2.00	2.00	2.00	2.00	2.00
10	k_x	1.00	1.00	1.00	1.00	1.00	1.00	1.00	0.75	0.75	0.25	0.75	0.25	0.75	0.75	1.00	1.00	1.00	1.00	1.00	1.00	1.00	1.00	1.00
	k_y	1.00	1.00	1.00	1.00	1.00	1.00	0.25	0.25	4.00	0.25	0.25	1.00	1.00	1.00	1.00	1.00	1.00	1.00	1.00	1.00	1.00	1.00	1.00
	k_z	2.00	2.00	2.00	2.00	2.00	2.00	1.25	1.00	4.75	0.50	1.00	1.25	1.75	1.75	2.00	2.00	2.00	2.00	2.00	2.00	2.00	2.00	2.00
9	k_x	1.00	1.00	1.00	1.00	1.00	1.00	1.00	1.00	1.00	1.00	1.00	1.00	1.00	1.00	1.00	1.00	1.00	1.00	1.00	1.00	1.00	1.00	1.00
	k_y	1.00	1.00	1.00	1.00	1.00	1.00	0.75	0.75	2.00	0.75	0.75	1.00	1.00	1.00	1.00	1.00	1.00	1.00	1.00	1.00	1.00	1.00	1.00
	k_z	2.00	2.00	2.00	2.00	2.00	2.00	1.75	1.75	3.00	1.75	1.75	2.00	2.00	2.00	2.00	2.00	2.00	2.00	2.00	2.00	2.00	2.00	2.00
8	k_x	1.00	1.00	1.00	1.00	1.00	1.00	1.00	1.00	1.00	1.00	1.00	1.00	1.00	1.00	1.00	1.00	1.00	1.00	1.00	1.00	1.00	1.00	1.00
	k_y	1.00	1.00	1.00	1.00	1.00	1.00	0.75	0.75	2.00	0.75	0.75	1.00	1.00	1.00	1.00	1.00	1.00	1.00	1.00	1.00	1.00	1.00	1.00
	k_z	2.00	2.00	2.00	2.00	2.00	2.00	1.75	1.75	3.00	1.75	1.75	2.00	2.00	2.00	2.00	2.00	2.00	2.00	2.00	2.00	2.00	2.00	2.00
7	k_x	1.00	1.00	1.00	1.00	1.00	1.00	1.00	1.00	1.00	1.00	1.00	1.00	1.00	1.00	1.00	1.00	1.00	1.00	1.00	1.00	1.00	1.00	1.00
	k_y	1.00	1.00	1.00	1.00	1.00	1.00	1.00	0.75	0.75	0.75	1.00	1.00	1.00	1.00	1.00	1.00	1.00	1.00	1.00	1.00	1.00	1.00	1.00
	k_z	2.00	2.00	2.00	2.00	2.00	2.00	2.00	1.75	1.75	1.75	2.00	2.00	2.00	2.00	2.00	2.00	2.00	2.00	2.00	2.00	2.00	2.00	2.00
6	k_x	1.00	1.00	1.00	1.00	1.00	1.00	1.00	1.00	1.00	1.00	1.00	1.00	1.00	1.00	1.00	1.00	1.00	1.00	1.00	1.00	1.00	1.00	1.00
	k_y	1.00	1.00	1.00	1.00	1.00	1.00	1.00	1.00	0.75	1.00	1.00	1.00	1.00	1.00	1.00	1.00	1.00	1.00	1.00	1.00	1.00	1.00	1.00
	k_z	2.00	2.00	2.00	2.00	2.00	2.00	2.00	2.00	1.75	2.00	2.00	2.00	2.00	2.00	2.00	2.00	2.00	2.00	2.00	2.00	2.00	2.00	2.00
5	k_x	1.00	1.00	1.00	1.00	1.00	1.00	1.00	1.00	1.00	1.00	1.00	1.00	1.00	1.00	1.00	1.00	1.00	1.00	1.00	1.00	1.00	1.00	1.00
	k_y	1.00	1.00	1.00	1.00	1.00	1.00	1.00	1.00	1.00	1.00	1.00	1.00	1.00	1.00	1.00	1.00	1.00	1.00	1.00	1.00	1.00	1.00	1.00
	k_z	2.00	2.00	2.00	2.00	2.00	2.00	2.00	2.00	2.00	2.00	2.00	2.00	2.00	2.00	2.00	2.00	2.00	2.00	2.00	2.00	2.00	2.00	2.00
4	k_x	1.00	1.00	1.00	1.00	1.00	1.00	1.00	1.00	1.00	1.00	1.00	1.00	1.00	1.00	1.00	1.00	1.00	1.00	1.00	1.00	1.00	1.00	1.00
	k_y	1.00	1.00	1.00	1.00	1.00	1.00	1.00	1.00	1.00	1.00	1.00	1.00	1.00	1.00	1.00	1.00	1.00	1.00	1.00	1.00	1.00	1.00	1.00
	k_z	2.00	2.00	2.00	2.00	2.00	2.00	2.00	2.00	2.00	2.00	2.00	2.00	2.00	2.00	2.00	2.00	2.00	2.00	2.00	2.00	2.00	2.00	2.00
3	k_x	1.00	1.00	1.00	1.00	1.00	1.00	1.00	1.00	1.00	1.00	1.00	1.00	1.00	1.00	1.00	1.00	1.00	1.00	1.00	1.00	1.00	1.00	1.00
	k_y	1.00	1.00	1.00	1.00	1.00	1.00	1.00	1.00	1.00	1.00	1.00	1.00	1.00	1.00	1.00	1.00	1.00	1.00	1.00	1.00	1.00	1.00	1.00
	k_z	2.00	2.00	2.00	2.00	2.00	2.00	2.00	2.00	2.00	2.00	2.00	2.00	2.00	2.00	2.00	2.00	2.00	2.00	2.00	2.00	2.00	2.00	2.00
2	k_x	1.00	1.00	1.00	1.00	1.00	1.00	1.00	1.00	1.00	1.00	1.00	1.00	1.00	1.00	1.00	1.00	1.00	1.00	1.00	1.00	1.00	1.00	1.00
	k_y	1.00	1.00	1.00	1.00	1.00	1.00	1.00	1.00	1.00	1.00	1.00	1.00	1.00	1.00	1.00	1.00	1.00	1.00	1.00	1.00	1.00	1.00	1.00
	k_z	2.00	2.00	2.00	2.00	2.00	2.00	2.00	2.00	2.00	2.00	2.00	2.00	2.00	2.00	2.00	2.00	2.00	2.00	2.00	2.00	2.00	2.00	2.00
1	k_x	1.00	1.00	1.00	1.00	1.00	1.00	1.00	1.00	1.00	1.00	1.00	1.00	1.00	1.00	1.00	1.00	1.00	1.00	1.00	1.00	1.00	1.00	1.00
	k_y	1.00	1.00	1.00	1.00	1.00	1.00	1.00	1.00	1.00	1.00	1.00	1.00	1.00	1.00	1.00	1.00	1.00	1.00	1.00	1.00	1.00	1.00	1.00
	k_z	2.00	2.00	2.00	2.00	2.00	2.00	2.00	2.00	2.00	2.00	2.00	2.00	2.00	2.00	2.00	2.00	2.00	2.00	2.00	2.00	2.00	2.00	2.00
		1	2	3	4	5	6	7	8	9	10	11	12	13	14	15	16	17	18	19	20	21	22	23

Fracture Permeability Factor for Dimensionless Depth 1 - 0.8

		1	2	3	4	5	6	7	8	9	10	11	12	13	14	15	16	17	18	19	20	21	22	23
21	k_x	1.00	1.00	1.00	1.00	1.00	1.00	1.00	1.00	1.00	1.00	1.00	1.00	1.00	1.00	1.00	1.00	1.00	1.00	1.00	1.00	1.00	1.00	1.00
	k_y	1.00	1.00	1.00	1.00	1.00	1.00	1.00	1.00	1.00	1.00	1.00	1.00	1.00	1.00	1.00	1.00	1.00	1.00	1.00	1.00	1.00	1.00	1.00
	k_z	2.00	2.00	2.00	2.00	2.00	2.00	2.00	2.00	2.00	2.00	2.00	2.00	2.00	2.00	2.00	2.00	2.00	2.00	2.00	2.00	2.00	2.00	2.00
20	k_x	1.00	1.00	1.00	1.00	1.00	1.00	1.00	1.00	1.00	1.00	1.00	1.00	1.00	1.00	1.00	1.00	1.00	1.00	1.00	1.00	1.00	1.00	1.00
	k_y	1.00	1.00	1.00	1.00	1.00	1.00	1.00	1.00	1.00	1.00	1.00	1.00	1.00	1.00	1.00	1.00	1.00	1.00	1.00	1.00	1.00	1.00	1.00
	k_z	2.00	2.00	2.00	2.00	2.00	2.00	2.00	2.00	2.00	2.00	2.00	2.00	2.00	2.00	2.00	2.00	2.00	2.00	2.00	2.00	2.00	2.00	2.00
19	k_x	1.00	1.00	1.00	1.00	1.00	1.00	1.00	1.00	1.00	1.00	1.00	1.00	1.00	1.00	1.00	1.00	1.00	1.00	1.00	1.00	1.00	1.00	1.00
	k_y	1.00	1.00	1.00	1.00	1.00	1.00	1.00	1.00	1.00	1.00	1.00	1.00	1.00	1.00	1.00	1.00	1.00	1.00	1.00	1.00	1.00	1.00	1.00
	k_z	2.00	2.00	2.00	2.00	2.00	2.00	2.00	2.00	2.00	2.00	2.00	2.00	2.00	2.00	2.00	2.00	2.00	2.00	2.00	2.00	2.00	2.00	2.00
18	k_x	1.00	1.00	1.00	1.00	1.00	1.00	1.00	1.00	1.00	1.00	1.00	1.00	1.00	0.75	0.75	0.50	0.75	0.75	1.00	1.00	1.00	1.00	1.00
	k_y	1.00	1.00	1.00	1.00	1.00	1.00	1.00	1.00	1.00	1.00	1.00	1.00	1.00	1.00	1.00	1.00	1.00	1.00	1.00	1.00	1.00	1.00	1.00
	k_z	2.00	2.00	2.00	2.00	2.00	2.00	2.00	2.00	2.00	2.00	2.00	2.00	2.00	1.75	1.75	1.50	1.75	1.75	2.00	2.00	2.00	2.00	2.00
17	k_x	1.00	1.00	1.00	1.00	1.00	1.00	1.00	1.00	1.00	1.00	1.00	1.00	0.75	1.50	1.50	2.00	1.50	1.50	0.75	1.00	1.00	1.00	1.00
	k_y	1.00	1.00	1.00	1.00	1.00	1.00	1.00	1.00	1.00	1.00	1.00	1.00	1.00	1.00	1.00	1.00	1.00	1.00	1.00	1.00	1.00	1.00	1.00
	k_z	2.00	2.00	2.00	2.00	2.00	2.00	2.00	2.00	2.00	2.00	2.00	2.00	1.75	2.50	2.50	3.00	2.50	2.50	1.75	2.00	2.00	2.00	2.00
16	k_x	1.00	1.00	1.00	1.00	1.00	1.00	1.00	1.00	1.00	1.00	1.00	1.00	1.00	0.75	0.75	0.50	0.75	0.75	1.00	1.00	1.00	1.00	1.00
	k_y	1.00	1.00	1.00	1.00	1.00	1.00	1.00	1.00	1.00	1.00	1.00	0.75	1.00	1.00	1.00	1.00	1.00	1.00	1.00	1.00	1.00	1.00	1.00
	k_z	2.00	2.00	2.00	2.00	2.00	2.00	2.00	2.00	2.00	2.00	2.00	1.75	2.00	1.75	1.75	1.50	1.75	1.75	2.00	2.00	2.00	2.00	2.00
15	k_x	1.00	1.00	1.00	1.00	1.00	1.00	1.00	1.00	1.00	1.00	1.00	1.00	1.00	1.00	1.00	1.00	1.00	1.00	1.00	1.00	1.00	1.00	1.00
	k_y	1.00	1.00	1.00	1.00	1.00	1.00	1.00	1.00	1.00	0.75	1.50	0.75	1.00	1.00	1.00	1.00	1.00	1.00	1.00	1.00	1.00	1.00	1.00
	k_z	2.00	2.00	2.00	2.00	2.00	2.00	2.00	2.00	2.00	1.75	2.50	1.75	2.00	2.00	2.00	2.00	2.00	2.00	2.00	2.00	2.00	2.00	2.00
14	k_x	1.00	1.00	1.00	1.00	1.00	1.00	1.00	1.00	1.00	1.00	1.00	1.00	1.00	1.00	1.00	1.00	1.00	1.00	1.00	1.00	1.00	1.00	1.00
	k_y	1.00	1.00	1.00	1.00	1.00	1.00	1.00	1.00	0.75	1.00	0.75	1.50	0.75	1.00	1.00	1.00	1.00	1.00	1.00	1.00	1.00	1.00	1.00
	k_z	2.00	2.00	2.00	2.00	2.00	2.00	2.00	2.00	1.75	2.00	1.75	2.50	1.75	2.00	2.00	2.00	2.00	2.00	2.00	2.00	2.00	2.00	2.00
13	k_x	1.00	1.00	1.00	1.00	1.00	1.00	1.00	0.75	0.75	0.50	0.75	0.50	0.75	0.75	1.00	1.00	1.00	1.00	1.00	1.00	1.00	1.00	1.00
	k_y	1.00	1.00	1.00	1.00	1.00	1.00	1.00	0.75	1.50	0.75	0.50	2.00	0.50	1.00	1.00	1.00	1.00	1.00	1.00	1.00	1.00	1.00	1.00
	k_z	2.00	2.00	2.00	2.00	2.00	2.00	2.00	1.50	2.25	1.25	1.25	2.50	1.25	1.75	2.00	2.00	2.00	2.00	2.00	2.00	2.00	2.00	2.00
12	k_x	1.00	1.00	1.00	1.00	1.00	1.00	0.75	1.50	1.50	2.00	1.50	2.00	1.50	1.50	0.75	1.00	1.00	1.00	1.00	1.00	1.00	1.00	1.00
	k_y	1.00	1.00	1.00	1.00	1.00	1.00	1.00	0.50	2.00	0.50	0.50	2.00	0.50	1.00	1.00	1.00	1.00	1.00	1.00	1.00	1.00	1.00	1.00
	k_z	2.00	2.00	2.00	2.00	2.00	2.00	1.75	2.00	3.50	2.50	2.00	4.00	2.00	2.50	1.75	2.00	2.00	2.00	2.00	2.00	2.00	2.00	2.00
11	k_x	1.00	1.00	1.00	1.00	1.00	1.00	1.00	0.75	0.75	0.50	0.75	0.50	0.75	0.75	1.00	1.00	1.00	1.00	1.00	1.00	1.00	1.00	1.00
	k_y	1.00	1.00	1.00	1.00	1.00	1.00	1.00	0.75	1.50	0.75	1.00	1.00	1.00	1.00	1.00	1.00	1.00	1.00	1.00	1.00	1.00	1.00	1.00
	k_z	2.00	2.00	2.00	2.00	2.00	2.00	2.00	1.50	2.25	1.25	1.75	1.50	1.75	1.75	2.00	2.00	2.00	2.00	2.00	2.00	2.00	2.00	2.00
10	k_x	1.00	1.00	1.00	1.00	1.00	1.00	1.00	1.00	1.00	1.00	1.00	1.00	1.00	1.00	1.00	1.00	1.00	1.00	1.00	1.00	1.00	1.00	1.00
	k_y	1.00	1.00	1.00	1.00	1.00	1.00	1.00	0.50	2.00	0.50	1.00	1.00	1.00	1.00	1.00	1.00	1.00	1.00	1.00	1.00	1.00	1.00	1.00
	k_z	2.00	2.00	2.00	2.00	2.00	2.00	2.00	1.50	3.00	1.50	2.00	2.00	2.00	2.00	2.00	2.00	2.00	2.00	2.00	2.00	2.00	2.00	2.00
9	k_x	1.00	1.00	1.00	1.00	1.00	1.00	1.00	1.00	1.00	1.00	1.00	1.00	1.00	1.00	1.00	1.00	1.00	1.00	1.00	1.00	1.00	1.00	1.00
	k_y	1.00	1.00	1.00	1.00	1.00	1.00	1.00	0.75	1.50	0.75	1.00	1.00	1.00	1.00	1.00	1.00	1.00	1.00	1.00	1.00	1.00	1.00	1.00
	k_z	2.00	2.00	2.00	2.00	2.00	2.00	2.00	1.75	2.50	1.75	2.00	2.00	2.00	2.00	2.00	2.00	2.00	2.00	2.00	2.00	2.00	2.00	2.00
8	k_x	1.00	1.00	1.00	1.00	1.00	1.00	1.00	1.00	1.00	1.00	1.00	1.00	1.00	1.00	1.00	1.00	1.00	1.00	1.00	1.00	1.00	1.00	1.00
	k_y	1.00	1.00	1.00	1.00	1.00	1.00	1.00	0.75	1.50	0.75	1.00	1.00	1.00	1.00	1.00	1.00	1.00	1.00	1.00	1.00	1.00	1.00	1.00
	k_z	2.00	2.00	2.00	2.00	2.00	2.00	2.00	1.75	2.50	1.75	2.00	2.00	2.00	2.00	2.00	2.00	2.00	2.00	2.00	2.00	2.00	2.00	2.00
7	k_x	1.00	1.00	1.00	1.00	1.00	1.00	1.00	1.00	1.00	1.00	1.00	1.00	1.00	1.00	1.00	1.00	1.00	1.00	1.00	1.00	1.00	1.00	1.00
	k_y	1.00	1.00	1.00	1.00	1.00	1.00	1.00	1.00	0.75	1.00	1.00	1.00	1.00	1.00	1.00	1.00	1.00	1.00	1.00	1.00	1.00	1.00	1.00
	k_z	2.00	2.00	2.00	2.00	2.00	2.00	2.00	2.00	1.75	2.00	2.00	2.00	2.00	2.00	2.00	2.00	2.00	2.00	2.00	2.00	2.00	2.00	2.00
6	k_x	1.00	1.00	1.00	1.00	1.00	1.00	1.00	1.00	1.00	1.00	1.00	1.00	1.00	1.00	1.00	1.00	1.00	1.00	1.00	1.00	1.00	1.00	1.00
	k_y	1.00	1.00	1.00	1.00	1.00	1.00	1.00	1.00	1.00	1.00	1.00	1.00	1.00	1.00	1.00	1.00	1.00	1.00	1.00	1.00	1.00	1.00	1.00
	k_z	2.00	2.00	2.00	2.00	2.00	2.00	2.00	2.00	2.00	2.00	2.00	2.00	2.00	2.00	2.00	2.00	2.00	2.00	2.00	2.00	2.00	2.00	2.00
5	k_x	1.00	1.00	1.00	1.00	1.00	1.00	1.00	1.00	1.00	1.00	1.00	1.00	1.00	1.00	1.00	1.00	1.00	1.00	1.00	1.00	1.00	1.00	1.00
	k_y	1.00	1.00	1.00	1.00	1.00	1.00	1.00	1.00	1.00	1.00	1.00	1.00	1.00	1.00	1.00	1.00	1.00	1.00	1.00	1.00	1.00	1.00	1.00
	k_z	2.00	2.00	2.00	2.00	2.00	2.00	2.00	2.00	2.00	2.00	2.00	2.00	2.00	2.00	2.00	2.00	2.00	2.00	2.00	2.00	2.00	2.00	2.00
4	k_x	1.00	1.00	1.00	1.00	1.00	1.00	1.00	1.00	1.00	1.00	1.00	1.00	1.00	1.00	1.00	1.00	1.00	1.00	1.00	1.00	1.00	1.00	1.00
	k_y	1.00	1.00	1.00	1.00	1.00	1.00	1.00	1.00	1.00	1.00	1.00	1.00	1.00	1.00	1.00	1.00	1.00	1.00	1.00	1.00	1.00	1.00	1.00
	k_z	2.00	2.00	2.00	2.00	2.00	2.00	2.00	2.00	2.00	2.00	2.00	2.00	2.00	2.00	2.00	2.00	2.00	2.00	2.00	2.00	2.00	2.00	2.00
3	k_x	1.00	1.00	1.00	1.00	1.00	1.00	1.00	1.00	1.00	1.00	1.00	1.00	1.00	1.00	1.00	1.00	1.00	1.00	1.00	1.00	1.00	1.00	1.00
	k_y	1.00	1.00	1.00	1.00	1.00	1.00	1.00	1.00	1.00	1.00	1.00	1.00	1.00	1.00	1.00	1.00	1.00	1.00	1.00	1.00	1.00	1.00	1.00
	k_z	2.00	2.00	2.00	2.00	2.00	2.00	2.00	2.00	2.00	2.00	2.00	2.00	2.00	2.00	2.00	2.00	2.00	2.00	2.00	2.00	2.00	2.00	2.00
2	k_x	1.00	1.00	1.00	1.00	1.00	1.00	1.00	1.00	1.00	1.00	1.00	1.00	1.00	1.00	1.00	1.00	1.00	1.00	1.00	1.00	1.00	1.00	1.00
	k_y	1.00	1.00	1.00	1.00	1.00	1.00	1.00	1.00	1.00	1.00	1.00	1.00	1.00	1.00	1.00	1.00	1.00	1.00	1.00	1.00	1.00	1.00	1.00
	k_z	2.00	2.00	2.00	2.00	2.00	2.00	2.00	2.00	2.00	2.00	2.00	2.00	2.00	2.00	2.00	2.00	2.00	2.00	2.00	2.00	2.00	2.00	2.00
1	k_x	1.00	1.00	1.00	1.00	1.00	1.00	1.00	1.00	1.00	1.00	1.00	1.00	1.00	1.00	1.00	1.00	1.00	1.00	1.00	1.00	1.00	1.00	1.00
	k_y	1.00	1.00	1.00	1.00	1.00	1.00	1.00	1.00	1.00	1.00	1.00	1.00	1.00	1.00	1.00	1.00	1.00	1.00	1.00	1.00	1.00	1.00	1.00
	k_z	2.00	2.00	2.00	2.00	2.00	2.00	2.00	2.00	2.00	2.00	2.00	2.00	2.00	2.00	2.00	2.00	2.00	2.00	2.00	2.00	2.00	2.00	2.00
		1	2	3	4	5	6	7	8	9	10	11	12	13	14	15	16	17	18	19	20	21	22	23

```
      program weight

      integer nx, ny, nz
      parameter (nx = 23, ny = 21, nz = 2, ndim = 3)

      real x1(ndim, nx, ny, nz), x2(ndim, nx, ny, nz),
     [     x3(ndim, nx, ny, nz), x4(ndim, nx, ny, nz),
     [     top_elev, bot_elev, x(nx), y(ny), z(nz),
     [     x_origin, y_origin, dx, dy

      integer ix, iy, iz, idim

      open (unit = 11, file = 'X1.prn', status = 'unknown')
      open (unit = 12, file = 'X2.prn', status = 'unknown')
      open (unit = 13, file = 'X3.prn', status = 'unknown')
      open (unit = 14, file = 'X4.prn', status = 'unknown')

      do iy = ny, 1, -1
         do idim = 1, ndim
            read(11,*) (x1(idim, ix, iy, 1), ix = 1, nx)
         end do
      end do

      do iy = ny, 1, -1
         do idim = 1, ndim
            read(12,*) (x2(idim, ix, iy, 1), ix = 1, nx)
         end do
      end do

      do iy = ny, 1, -1
         do idim = 1, ndim
            read(13,*) (x3(idim, ix, iy, 1), ix = 1, nx)
         end do
      end do

      do iy = ny, 1, -1
         do idim = 1, ndim
            read(14,*) (x4(idim, ix, iy, 1), ix = 1, nx)
         end do
      end do

      do iy = 1, ny
         do ix = 1, nx
            do idim = 1, ndim
               x1(idim, ix, iy, 2) = x1(idim, ix, iy, 1)
               x2(idim, ix, iy, 2) = x2(idim, ix, iy, 1)
               x3(idim, ix, iy, 2) = x3(idim, ix, iy, 1)
               x4(idim, ix, iy, 2) = x4(idim, ix, iy, 1)
            end do
         end do
      end do

      x_origin = 50.5
      y_origin = 53.5
      dx = 1.0
      dy = 1.0
      top_elev = 1577.0
      bot_elev = 1576.0
      z(1) = bot_elev
      z(2) = top_elev

      do ix = 1, nx
         x(ix) = x_origin + (ix - 1) * dx
      end do
      do iy = 1, ny
         y(iy) = y_origin + (iy - 1) * dy
      end do

      open (unit = 16, file = 'weight.dat', status = 'unknown')

      write(16,5)
      write(16,6)
    5 format('TITLE = "Fracture Propety Weighting Factors"')
```



```
    6 format('VARIABLES = "X", "Y", "Z", "Xx", "Xy", "Xz"')

      write(16,1)
    1 format('ZONE T="layer 1", I=23, J=21, K=2, F=POINT')
      do iz = 1, nz
         do iy = 1, ny
            do ix = 1, nx
               write(16,10) x(ix), y(iy), z(iz),
     [                      (x1(idim, ix, iy, iz), idim = 1, ndim)
   10          format(6(1pe10.4,1x))
            end do
         end do
      end do

      write(16,2)
    2 format('ZONE T="layer 2", I=23, J=21, K=2, F=POINT')
      do iz = 1, nz
         do iy = 1, ny
            do ix = 1, nx
               write(16,10) x(ix), y(iy), z(iz),
     [                      (x2(idim, ix, iy, iz), idim = 1, ndim)
            end do
         end do
      end do

      write(16,3)
    3 format('ZONE T="layer 3", I=23, J=21, K=2, F=POINT')
      do iz = 1, nz
         do iy = 1, ny
            do ix = 1, nx
               write(16,10) x(ix), y(iy), z(iz),
     [                      (x3(idim, ix, iy, iz), idim = 1, ndim)
            end do
         end do
      end do

      write(16,4)
    4 format('ZONE T="layer 4", I=23, J=21, K=2, F=POINT')
      do iz = 1, nz
         do iy = 1, ny
            do ix = 1, nx
               write(16,10) x(ix), y(iy), z(iz),
     [                      (x4(idim, ix, iy, iz), idim = 1, ndim)
            end do
         end do
      end do

      stop
      end
```

Fracture continuum weighting factors (a) β_x, (b) β_y and (c) β_z for dimensionless depth interval of 0.2 – 0.4

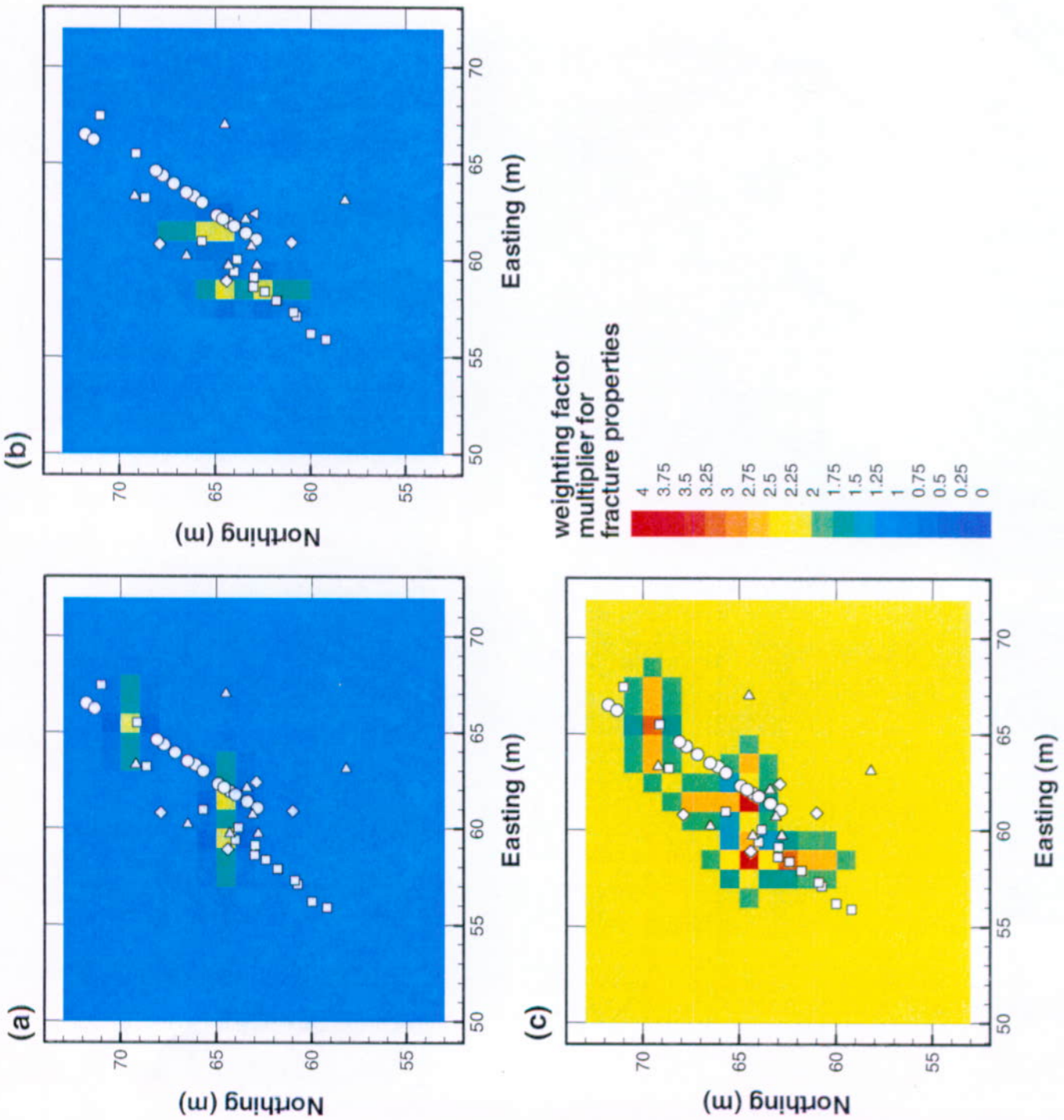

Fracture continuum weighting factors (a) β_x, (b) β_y and (c) β_z for dimensionless depth interval of 0.4 to 0.6

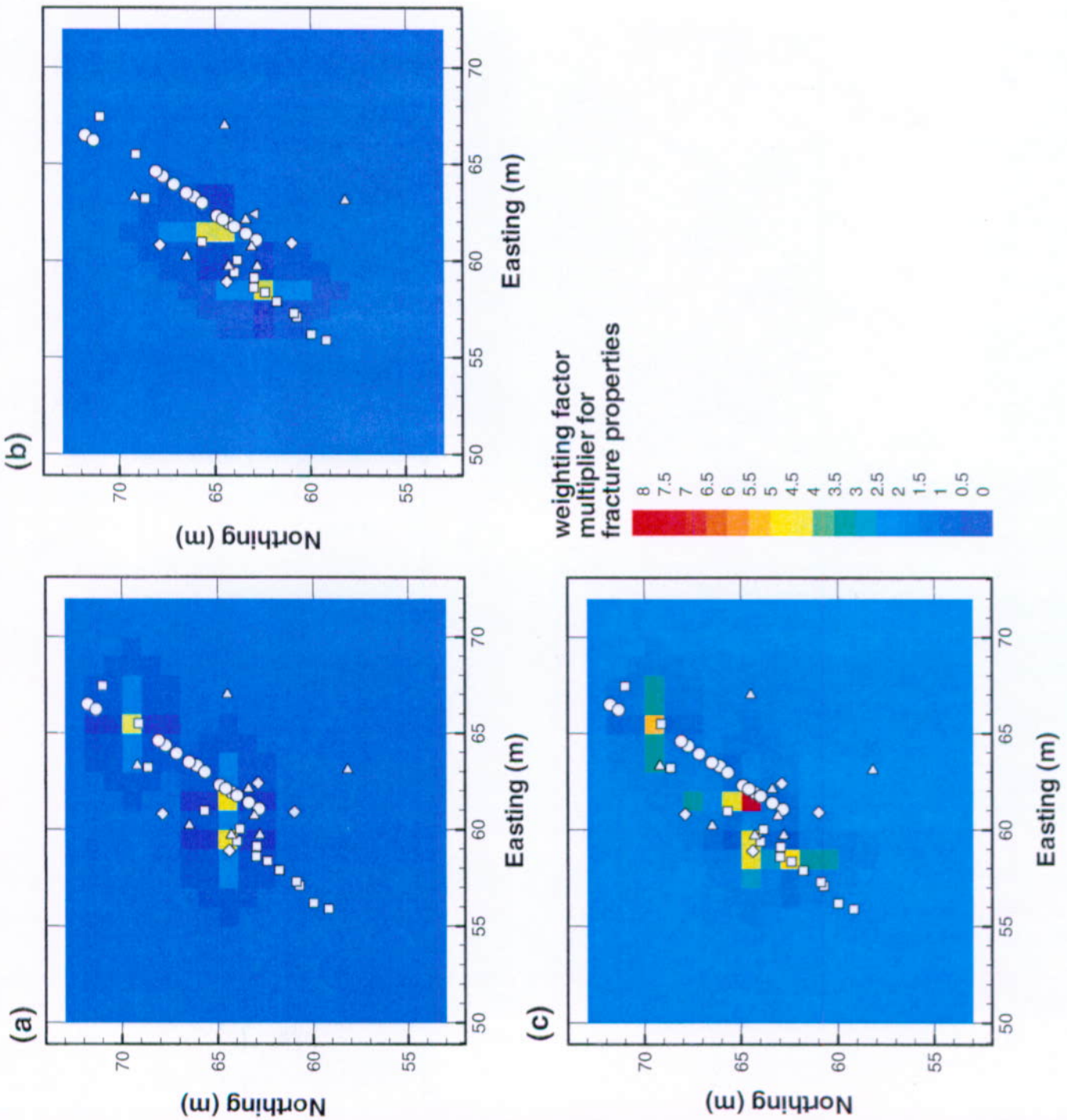

Fracture continuum weighting factors (a) β_x, (b) β_y and (c) β_z for dimensionless depth interval of 0.6 to 0.8.

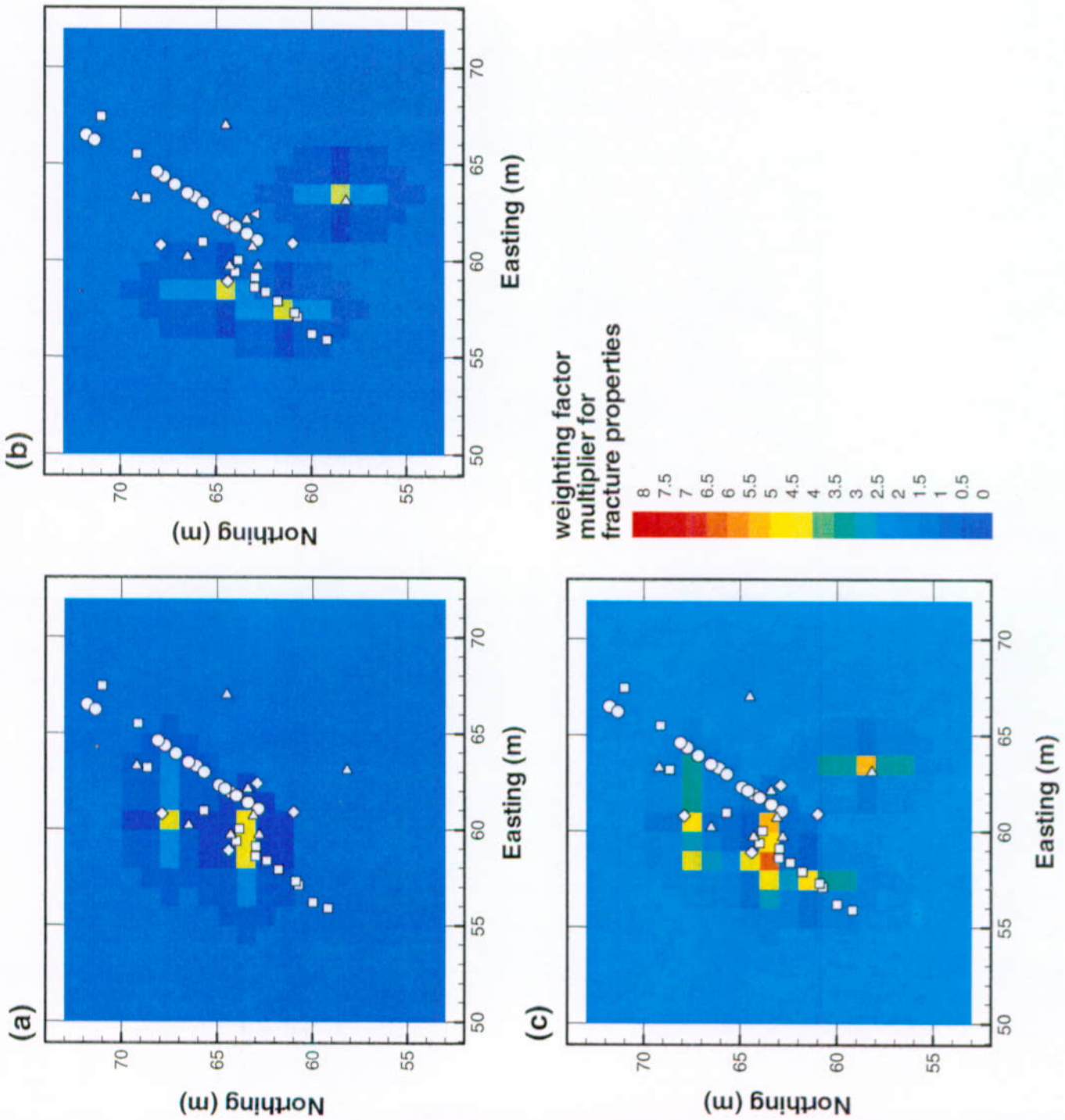

Fracture continuum weighting factors (a) β_x, (b) β_y and (c) β_z for dimensionless depth interval of 0.8 to 1.0

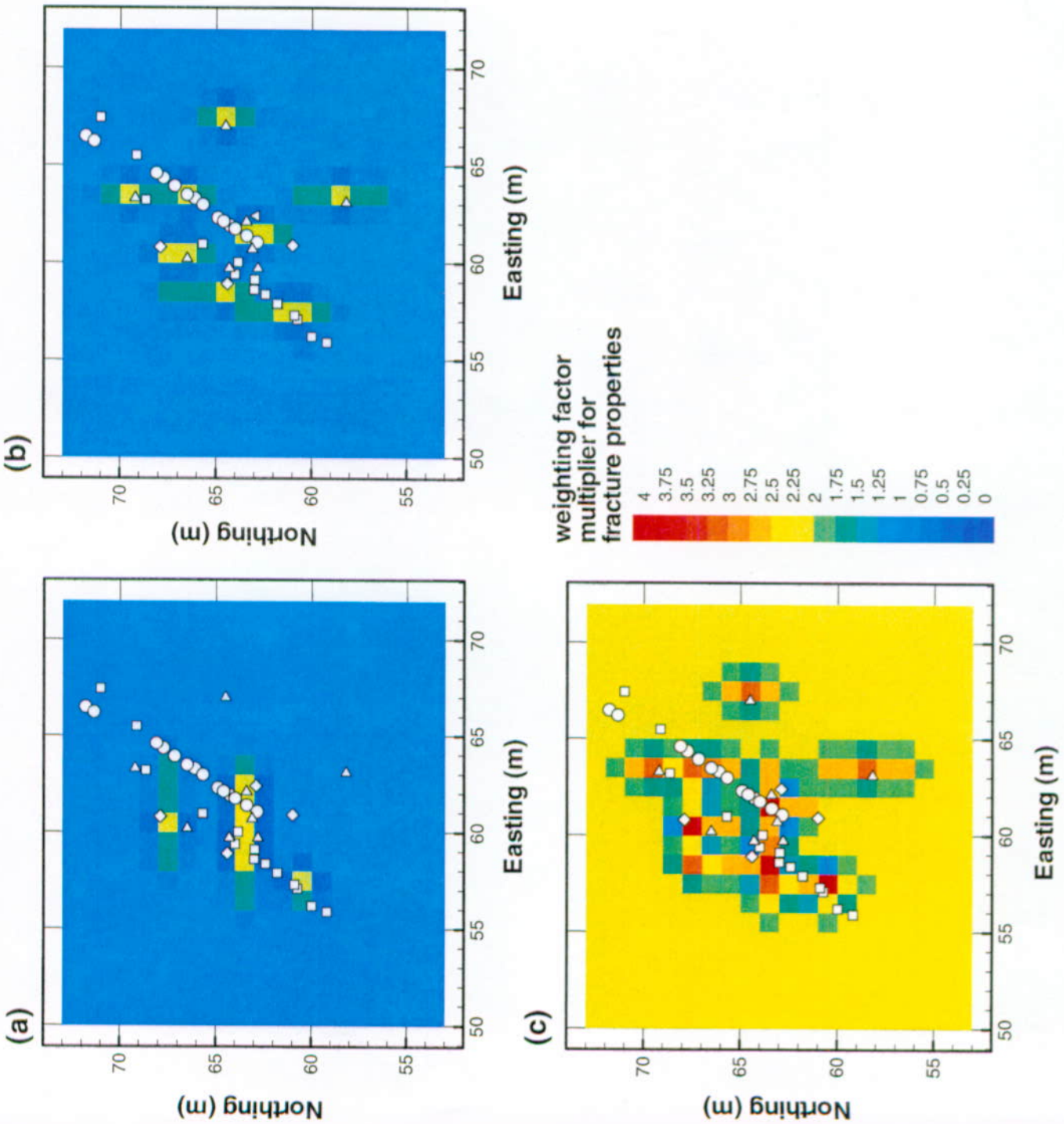

```
      program weight

      integer nx, ny, nz
      parameter (nx = 23, ny = 21, nz = 2, ndim = 3)

      real x1(ndim, nx, ny, nz), x2(ndim, nx, ny, nz),
     [     x3(ndim, nx, ny, nz), x4(ndim, nx, ny, nz),
     [     top_elev, bot_elev, x(nx), y(ny), z(nz),
     [     x_origin, y_origin, dx, dy

      integer ix, iy, iz, idim

      open (unit = 11, file = 'X1.prn', status = 'unknown')
      open (unit = 12, file = 'X2.prn', status = 'unknown')
      open (unit = 13, file = 'X3.prn', status = 'unknown')
      open (unit = 14, file = 'X4.prn', status = 'unknown')

      do iy = ny, 1, -1
         do idim = 1, ndim
            read(11,*) (x1(idim, ix, iy, 1), ix = 1, nx)
         end do
      end do

      do iy = ny, 1, -1
         do idim = 1, ndim
            read(12,*) (x2(idim, ix, iy, 1), ix = 1, nx)
         end do
      end do

      do iy = ny, 1, -1
         do idim = 1, ndim
            read(13,*) (x3(idim, ix, iy, 1), ix = 1, nx)
         end do
      end do

      do iy = ny, 1, -1
         do idim = 1, ndim
            read(14,*) (x4(idim, ix, iy, 1), ix = 1, nx)
         end do
      end do

      do iy = 1, ny
         do ix = 1, nx
            do idim = 1, ndim
               x1(idim, ix, iy, 2) = x1(idim, ix, iy, 1)
               x2(idim, ix, iy, 2) = x2(idim, ix, iy, 1)
               x3(idim, ix, iy, 2) = x3(idim, ix, iy, 1)
               x4(idim, ix, iy, 2) = x4(idim, ix, iy, 1)
            end do
         end do
      end do

      x_origin = 50.5
      y_origin = 53.5
      dx = 1.0
      dy = 1.0
      top_elev = 1577.0
      bot_elev = 1576.0
      z(1) = bot_elev
      z(2) = top_elev

      do ix = 1, nx
         x(ix) = x_origin + (ix - 1) * dx
      end do
      do iy = 1, ny
         y(iy) = y_origin + (iy - 1) * dy
      end do

      open (unit = 16, file = 'weight.dat', status = 'unknown')

      write(16,5)
      write(16,6)
    5 format('TITLE = "Fracture Propety Weighting Factors"')
```



```
    6 format('VARIABLES = "X", "Y", "Z", "Xx", "Xy", "Xz"')

      write(16,1)
    1 format('ZONE T="layer 1", I=23, J=21, K=2, F=POINT')
      do iz = 1, nz
         do iy = 1, ny
            do ix = 1, nx
               write(16,10) x(ix), y(iy), z(iz),
     [                      (x1(idim, ix, iy, iz), idim = 1, ndim)
   10          format(6(1pe10.4,1x))
            end do
         end do
      end do

      write(16,2)
    2 format('ZONE T="layer 2", I=23, J=21, K=2, F=POINT')
      do iz = 1, nz
         do iy = 1, ny
            do ix = 1, nx
               write(16,10) x(ix), y(iy), z(iz),
     [                      (x2(idim, ix, iy, iz), idim = 1, ndim)
            end do
         end do
      end do

      write(16,3)
    3 format('ZONE T="layer 3", I=23, J=21, K=2, F=POINT')
      do iz = 1, nz
         do iy = 1, ny
            do ix = 1, nx
               write(16,10) x(ix), y(iy), z(iz),
     [                      (x3(idim, ix, iy, iz), idim = 1, ndim)
            end do
         end do
      end do

      write(16,4)
    4 format('ZONE T="layer 4", I=23, J=21, K=2, F=POINT')
      do iz = 1, nz
         do iy = 1, ny
            do ix = 1, nx
               write(16,10) x(ix), y(iy), z(iz),
     [                      (x4(idim, ix, iy, iz), idim = 1, ndim)
            end do
         end do
      end do

      stop
      end
```

OFFICE OF CIVILIAN RADIOACTIVE WASTE MANAGEMENT
SPECIAL INSTRUCTION SHEET

1. QA: QA

Page: 1 of: 1

Complete Only Applicable Items

This is a placeholder page for records that cannot be scanned or microfilmed

2. Record Date EFFECTIVE DATE OF DOCUMENT 04/24/2000	3. Accession Number ATT-10: MOL. 19990721.0524
4. Author Name(s) ARDYTH SIMMONS	5. Author Organization N/A

6. Title
NATURAL ANALOGS FOR THE UNSATURATED ZONE

7. Document Number(s) ANL-NBS-HS-000007	8. Version REV. 00
9. Document Type CD KLQ 4.28.00 Report; AMR	10. Medium CD-ROM / OPTIC

11. Access Control Code
Pub

12. Traceability Designator
DC #21789

13. Comments
THIS IS A ONE OF A KIND DOCUMENT DUE TO THE CD ENCLOSED, SEE THE RPC FOR MORE DETAILS

THIS SPECIAL PROCESS DISK CAN BE
LOCATED THROUGH THE RECORDS
PROCESSING CENTER